

DISSERTATION

Macromolecular Design of Inks for
Two-Photon Laser Printing



**UNIVERSITÄT
HEIDELBERG**
ZUKUNFT
SEIT 1386

Samantha Olivia Catt

2024

DISSERTATION

zur

Erlangung der Doktorwürde (Dr. rer. nat.)

der

Gesamtfakultät für Mathematik, Ingenieur- und Naturwissenschaften

der

Ruprechts-Karls-Universität Heidelberg

vorgelegt von

Samantha Olivia Catt

aus Hornsby

Tag der mündlichen Prüfung: 18. Oktober 2024

Macromolecular Design of Inks for Two-Photon Laser Printing

Gutachter

Prof. Dr. Eva Blasco

Jun.-Prof. Dr. Franziska Thomas

“Up ahead they's a thousan' lives we might live,
but when it comes it'll on'y be one.”

— John Steinbeck, *Grapes of Wrath*

Acknowledgements

Eva, I need to thank you for your confidence in me throughout this whole experience. Your unwavering support and guidance over the last years even when, or rather especially when, I believed there was no way forward, made this once daunting journey another task that I knew I could achieve. As a mentor, you were exactly the kind that I needed, allowing me to grow and adapt, to challenge myself, while listening, guiding, and providing me with many opportunities. It has been my pleasure to work with you, and I hope to one day be the kind of mentor you were and are for me.

I would never have made it this far without all of the mentors I have had over the past years, who somehow saw something in me that I may not have seen in myself at the time, and provided unending support and countless opportunities. Prof. Jürgen Groll, Prof. Paul Dalton, Prof. Tim Dargaville, Prof. James Blinco, I have thanked you once before, but I think that a second round is in order. I know without a doubt that I would not be where I am today without all of you. Prof. Groll, you gave me many pieces of advice, which still help me to this day whenever I need to make difficult decisions.

I would like to thank Prof. Müllner and the group at USYD, in particular Chenyou, who welcomed me ‘home’ and into their lab for the weeks I was there—I look forward to seeing you again shortly. I would also like to thank Dr. Maximilian Hackner and Prof. Joachim Spatz, firstly for the initial collaboration for my first project, as well as ongoing assistance with the nanoindenter. Additionally, the staff at Bruker, particularly Dr. Ude Hangen and Dr. Jaroslav Lukes for the ongoing support as we transitioned the instrument to Heidelberg. I also would like to thank Sebastian Lindenthal and Prof. Jana Zaumseil for access, training, and support with the Raman spectrometer. Martina and Fabian, thank you for all of the support you have brought to the group. Additionally, I would like to express my gratitude to Pia, Victoria, Britta, Jessica, Amanda, and Clara for their expert copyediting and proofreading skills, and Britta and Pia in particular for the abstract translation.

To the past and present members of the Blasco group, thank you for making coming to work each day that little bit easier. Firstly, I want to thank the ‘Blasco girls’.

Li Yun, my first office buddy, thank you for your warm welcome to the group and all the nice snacks throughout the years—I still think about that matcha tiramisu. Although we were brought together mostly by our differences to the others, being so far away from home, our conversations always made me feel a bit less alone and for that I am grateful. Britta, 402 will always be our lab. I stand by it. It is rare to get to spend the entire PhD with one lab buddy, and I am very glad it was you. You supported me from the very beginning, without judgement, both in and out of the lab, and I have learned a lot from you. I look forward to the next chapter of our friendship.

Clara, your joining the group was a light that never went out. Although we are from places that quite literally could not be further apart, somehow we share much more in common than I could have expected. I am in awe of your capacity to help and care for others, scientifically and personally. Your passion for research has reminded me many times why I began this journey.

Pia, it has been a great joy to watch your transition from student, through the master thesis, and now into the PhD. You have always impressed me with your ideas and problem solving, and I have enjoyed all of the evenings spent crafting or swimming together, as well as countless coffee breaks that helped me keep my sanity in the process.

The other students I supervised: Julius, thank you for being so passionate about the project and not giving up after every mass spec gone wrong, I am sure your next endeavors will be successful. Moritz, I think you have done more polymerisations in the master thesis than I managed in the whole PhD. Thank you for always being up to chat about Taylor Swift conspiracies, gym weirdos, music and books, and of course the scientific discussions—I look forward to seeing you flourish in the PhD!

Christoph, thank you also for the welcome into the group and being the go to for all things Nanoscribe. Marcus, with similar timelines I think we have had similar experiences throughout, thank you for letting me vent during the stressful times, and not being offended when I got way too invested in beating you at board games or pub quizzes. Philipp, thank you for being my office buddy for (almost) the entire time, and for the good bar recommendations around Heidelberg. Finn, thank you for all of the coffee break chats, swim trips, and occasional bouldering excursions (und Deutsche Dienstags

auch...). Silas and Duc, thank you for the nice coffee break and gym chats, Duc in particular thank you for letting me vent my stress by being a literal punching bag in boxing class. Christian, thank you for your calming presence and positive vibes you bring to the group. Niklas, as well as the others of the Thomas group, thank you for being our first CAM lab mates and for various equipment loaning and help throughout.

So many people have contributed to the group over the years, to whom I would like give thanks. To the visitors, students, PhDs, and post docs, past and present, that are not named here, I wish I could thank each and every one of you. Suffice to say I am eternally grateful for every moment in the last three years that has made this experience what it was.

Choosing to move my life 16,000 km away from my home and family was a decision that did not come easily, but was made that much easier by the friends who became like family along the way. Amanda and Olli, thank you for letting me be a part of your life here, it's been amazing to watch you and your family grow over the years. I take my role as Aunt Samantha very seriously, Harrison don't forget your promise to get a tattoo with me when you turn 18. Jessica, Victoria, Andrew, and Patrick, never have I met more kind and generous people, thank you for supporting me and all of the fun together. Although working at Wiley for two years means finishing the PhD on the brink of 30, it brought me such an amazing and supportive group of friends, I wouldn't change a thing. Dylan, thank you for your friendship and support over these long 12 years; if the bachelor was level 99, I guess this is 120.

Last and certainly not least, I need to thank my family, especially Mum, Dad, and Rachael, who I know still have absolutely no bloody idea what I am doing no matter how many times I try to explain it, but support me unquestioningly nevertheless.

If this rollercoaster of a journey has taught me one thing, that I have seen evidenced time and time again in not only my colleagues but also my friends, and dare I say in myself—you are capable of so much more than you may believe. All you have to do is show up.

Abstract

Over recent decades 3D printing, or additive manufacturing, has become an invaluable fabrication method, making a significant impact across many sectors of society. With the development of new printing techniques and printable materials, great progress has been made, particularly on the macroscale. However, as a result of key technological advances, 3D printing on the micro and nanoscale has also become more accessible. To that end, two-photon laser printing (2PLP) has emerged as one of the most suitable and useful methods for fabricating complex objects with arbitrary geometries and fine features. As these technologies progress, the need for more advanced and functional materials becomes evident. With further developments in synthetic methods, new and advanced macromolecular architectures once unattainable have become more readily available. The current library of materials typically used as inks for 2PLP fall into the category of multifunctional small molecules or functionalised polymers containing a distribution of crosslinkable groups. Despite developments toward functional inks with novel properties for 2PLP, the underlying relationships between the properties of the macromolecules used as inks and their behaviour during printing, as well as the effects on the resultant printed structures, remain underexplored.

To that end, the work herein examines the rational design of macromolecular inks for 2PLP with precise control and previously unexplored architectures, to investigate the effects of the (macro)molecular architecture on the printability and subsequently, in the printed microstructures. Three overarching concepts are explored in this regard: firstly, the design of pre-polymer inks with tailored comonomer composition, with varied physicochemical properties such as glass transition temperature and molecular weight. Secondly, an approach to determine the effect of molecular sequence, whereby sequence-defined oligomers are printed for the first time. With identical composition, varying only in the sequence of crosslinkable groups, clear differences in properties are observed. Lastly, leveraging the potential afforded by synthetic advances in polymer architecture design, novel macromolecular bottlebrushes are developed as inks for 2PLP.

The common thread throughout these chapters, is the investigation of relationships between synthetic design, 3D printing, and material properties, highlighting the benefits of rationally designing macromolecular inks toward the goal of fabricating objects with specific and tailorable properties. Understanding and exploring these relationships becomes particularly relevant in the rapidly expanding field of functional material development for future 2PLP applications.

Kurzfassung

Der 3D Druck, auch additive Fertigung genannt, hat sich in den vergangenen Jahrzehnten als eine sehr wertvolle Fertigungsmethode mit erheblichem Einfluss auf viele Bereiche der Gesellschaft hervorgetan. Dabei konnten durch die Etablierung neuer Druckmethoden und druckbarer Materialien große Fortschritte, insbesondere auf der Makroskala, erzielt werden. Darüber hinaus haben diese Entwicklungen auch den 3D-Druck auf der Mikro- und Nanoskala leichter zugänglich gemacht. Hierbei hat sich der Zwei-Photonen-Laserdruck als eine besonders geeignete Methode für die Herstellung komplexer und detailreicher Objekte mit beliebigen Geometrien auf der Mikro- und Nanoskala erwiesen. Die kontinuierliche Weiterentwicklung dieser Technologien erfordert jedoch neue funktionale Materialien. Die Erforschung neuer Synthesemethoden ermöglicht dabei die Herstellung von zuvor unzugänglichen komplexen makromolekularen Architekturen. Das Spektrum an Materialien für die Fertigung von Tinten für den Zwei-Photonen-Laserdruck bewegt sich aktuell meist im Rahmen multifunktionaler kleiner Moleküle oder funktionalisierter Polymere mit vernetzbaren Gruppen. Trotz der stetigen Entwicklung funktioneller Tinten mit neuartigen Eigenschaften für den Zwei-Photonen-Laserdruck, sind die zugrundeliegenden Beziehungen zwischen den Eigenschaften der als Tinten verwendeten Makromoleküle und ihrem Verhalten während des Druckprozesses, sowie dem daraus resultierenden Einfluss auf die Eigenschaften der gedruckten Strukturen noch nicht ausreichend erforscht. Dem zufolge behandelt die vorliegende Arbeit das rationale Design makromolekularer Tinten mit präziser Kontrolle und zuvor unerforschten Architekturen, um die Auswirkung der (makro)molekularen Architekturen auf die Druckbarkeit und die daraus resultierend gedruckten Mikrostrukturen zu untersuchen.

In diesem Zusammenhang werden drei übergreifende Konzepte betrachtet: Erstens, das Design von Prä-Polymerintinten mit maßgeschneiderter Co-Monomerkomposition und variierenden physiochemischen Eigenschaften wie Glasübergangstemperatur und Molekulargewicht. Zweitens, ein Ansatz, um den Effekt molekularer Sequenzen zu bestimmen, wobei sequenz-definierte Oligomere erstmals gedruckt werden. Durch deren identische Zusammensetzung, welche sich nur in der Sequenz der Monomere

unterscheidet, können klare Unterschiede der Eigenschaften beobachtet werden. Zuletzt, die erstmalige Verwendung makromolekulare Bottlebrushes als Tinten für den Zwei-Photonen-Laserdruck, um das Potential komplexer Polymerarchitekturen, ermöglicht durch den synthetischen Fortschritt, auszuschöpfen.

Der rote Faden, welcher diese Kapitel verbindet, ist die Untersuchung der Zusammenhänge zwischen synthetischem Design, 3D-Druck und den resultierenden Materialeigenschaften. Dabei werden die Vorteile von rationalem Design makromolekularer Tinten mit dem Ziel der Herstellung von Objekten mit spezifischen und anpassbaren Eigenschaften hervorgehoben. Das Verständnis dieser Zusammenhänge ist in dem sich schnell entwickelnden Feld funktioneller Materialien für zukünftige Anwendung im Zwei-Photonen-Laserdruck von besonderer Bedeutung.

List of Abbreviations

2PA	two-photon absorption
2PLP	two-photon laser printing
AFM	atomic force microscopy
AM	additive manufacturing
ATR	attenuated total reflectance
ATRP	atom transfer radical polymerisation
BA	butyl acrylate
BAPO	phenylbis(2,4,6-trimethylbenzoyl)phosphine oxide)
BHT	butylated hydroxytoluene
CARS	coherent anti-Stokes Raman spectroscopy
CLIP	continuous liquid interface production
CPDB	2-cyanoprop-2-yl dithiobenzoate
CPDT	2-cyano-2-propyl dodecyl trithiocarbonate
CSIRO	Commonwealth Scientific and Industrial Research Organisation
CTA	chain transfer agent
CTBPA	4-cyano-4-(phenylcarbonothioylthio)pentanoic acid
DCM	dichloromethane
DETC	7-diethylamino 3-thenoylcoumarin
DIW	direct ink writing
DLP	digital light processing
DMAc	N,N-dimethylacetamide
DMF	N,N-dimethylformamide
DoC	degree of conversion
DP	degree of polymerisation
DSC	differential scanning calorimetry
E-BiBB	ethyl α -bromoisobutyrate
EBM	electron beam machining
EEA	1-ethoxyethyl acrylate
Er	reduced elastic modulus

Et ₂ O	diethyl ether
FDM	fused deposition modelling
FRP	free-radical polymerisation
FTIR	Fourier-transform infrared
HEA	2-hydroxyethyl acrylate
HEMA	2-hydroxyethyl methacrylate
HMTETA	1,1,4,7,10,10-hexamethyltriethylenetetramine
IBA	isobornyl acrylate
IEG	iterative exponential growth
ISG	iterative stepwise growth
LED	light-emitting diode
MA	methyl acrylate
MADIX	macromolecular design via the interchange of xanthates
MALDI	matrix-assisted laser desorption/ionisation
MMA	methyl methacrylate
MPB	molecular polymer bottlebrush
MS	mass spectroscopy
NIR	near infrared
NMP	nitroxide-mediated polymerisation
NP	nanoparticle
pBIEM	poly(2-(2-bromoisobutyryloxy)ethyl methacrylate)
PDMS	poly(dimethylsiloxane)
PE	polyethylene
PEG	poly(ethylene glycol)
PEGDA	poly(ethylene glycol) diacrylate
PETA	pentaerythritol triacrylate
pHEMA	poly(2-hydroxyethyl methacrylate)
PP	polypropylene
PTFE	polytetrafluoroethylene
RAFT	reversible addition-fragmentation chain transfer
RT	room temperature

RDRP	reversible-deactivation radical polymerisation
ROMP	ring opening metathesis polymerization
SEC	size exclusion chromatography
SEM	scanning electron microscopy
SLA	stereolithography
SLS	selective laser sintering
SUMI	single unit monomer insertion
TEMPO	2,2,6,6-tetramethylpiperidin-1-oxyl
TFA	trifluoroacetic acid
T _g	glass transition temperature
TIPS	triisopropylsilyl
TMS	trimethylsilyl
TPO	bis(2,4,6-trimethylbenzoyl)-phenylphosphineoxide
UV	ultraviolet
wt%	weight percent
α-BiBB	α-bromoisobutyryl bromide

Table of Contents

Acknowledgements	i
Abstract	v
Kurzfassung	vii
List of Abbreviations	ix
Table of Contents	xiii
List of Publications and Conference Contributions	xv
1 Introduction and Outline	1
2 Theoretical Background	5
2.1 Polymers: from discovery to design and control.....	5
2.2 Sequence-defined macromolecules: beyond control toward precision	20
2.3 Molecular polymer bottlebrushes: advanced architectures	23
2.4 3D Printing	30
2.5 Vat photopolymerisation	32
3 Pre-polymers as 2PLP inks	43
3.1 Motivation and aims	44
3.2 Synthesis of pre-polymers	45
3.3 Pre-polymer inks for 2PLP: structure–property relationships	58
3.4 Summary	66
4 Sequence-defined oligomers as 2PLP inks	69
4.1 Motivation and aims	70
4.2 Synthesis of sequence-defined oligomers	71
4.3 Sequence-defined inks for 2PLP: structure–property relationships.....	82
4.4 Summary	92
5 Molecular polymer bottlebrush architectures as novel 2PLP inks	93

5.1	Motivation and aims	94
5.2	Synthesis of molecular polymer bottlebrushes	95
5.3	Molecular polymer bottlebrush inks for 2PLP: advanced architectures	111
5.4	Summary	116
6	Conclusion and Outlook	119
7	Experimental.....	125
7.1	Materials.....	125
7.2	Synthesis	125
7.3	Methods	133
8	Appendices	137
8.1	Appendix A: synthetic characterisation	137
8.2	Appendix B: material characterisation	145
	Bibliography.....	149
	Eidesstattliche Versicherung	155

List of Publications and Conference Contributions

Journal Articles (from the current PhD thesis):

- **S. O. Catt**, M. Hackner, J. P. Spatz, E. Blasco*, Macromolecular Engineering: From Precise Macromolecular Inks to 3D Printed Microstructures, *Small*, 2023, 19, 2300844
- **S. O. Catt**, C. Vazquez-Martel, E. Blasco*, Investigation of pre-polymer design on material properties for two-photon laser printing, 2024, *submitted*.
- **S. O. Catt**, E. Blasco*, *Two-photon 3D printing of responsive molecular polymer bottlebrushes*, 2024, *in preparation*.

Journal Articles (other contributions):

- Y. Hou, G. Zhu, **S. O. Catt**, Y. Yin, J. Xu, E. Blasco*, and N. Zhao*, Closed-Loop Recyclable Silica-Based Nanocomposites with Multifunctional Properties and Versatile Processability, *Advanced Science*, 2023, 10, 2304147.
- X. Lopez de Pariza, O. Varela, **S. O. Catt**, T. E. Long, E. Blasco, and H. Sardon*, Loop 3D printing: recyclable photoresins for light-mediated additive manufacturing, *Nature Communications*, 2023, 14, 5504
- H.B. Duc Tran, C. Vazquez-Martel, **S. O. Catt**, Y. Jia, M. Tsotsalas, C. A. Spiegel*, E. Blasco*, 4D printing of adaptable “living” materials based on alkoxyamine chemistry, 2023, *Advanced Functional Materials*, 2024, 34, 2315238.

Conferences

- **S. O. Catt**, E. Blasco, “3D Laser Printing of Sequence-Defined Oligomers”, Macromolecular Colloquium Freiburg 2023, February 2023, Freiburg, Germany, oral presentation.
- **S. O. Catt**, M. Hackner, J. P. Spatz, E. Blasco, “Molecular Engineering: From Precise Macromolecular Inks to 3D Printed Microstructures”, Bayreuth

Polymer Symposium, September 2023, Bayreuth, Germany, poster presentation.

- **S. O. Catt**, B. Weidinger, E. Blasco, “Designing precise materials for two-photon 3D laser printing”, SPIE Photonics West 2024, California, USA, January 2024, oral presentation.
- C. Vazquez-Martel, **S. O. Catt**, E. Blasco, “Structure-Property Relationships of 3D/4D Printed Microstructures”, Nanobrücken 2024, Lyon, France, May 2024.
- C. Spiegel, **S. O. Catt**, E. Blasco, “Functional materials for 4D (micro)printing”, European Symposium of Photopolymer Science 2024, Stresa, Italy, June 2024.

1 Introduction and Outline

Since the beginning of humankind, materials have shaped our lives. Not only the resources naturally available to us, but the way in which we interact with and shape these materials, has defined human progress over millennia. Beyond natural materials and composites, the discovery of synthetic materials and in particular soft matter and polymeric materials, has advanced society in leaps and bounds in recent decades. These advancements have been led in no small part by the scientists who developed and optimized pathways toward the synthesis of polymers with a wide variety of compositions. This made it not only possible to synthesise polymers with great control over their composition and dispersity, but the capability to pick and choose the architecture to fabricate polymers of various shapes, sizes, and compositions has allowed the field of soft materials to bloom. By controlling the architecture of (macro)molecules—and oligomers and polymers in particular—it is possible to influence a number of physicochemical properties, leading to materials with new and intriguing properties. As advancements have been made in the way we create and synthesise these macromolecular architectures, developments have also been made in the way we shape them i.e. how the macromolecules can be formed and applied into useful and functional materials.

Notably, additive manufacturing, or 3D printing, has emerged as one of the most useful tools for fabricating objects from polymeric materials. At the macroscale, extrusion-based printers, such as fused deposition modelling printers, are available for almost any household. In many cases, light is used as a trigger to afford greater spatial and temporal control, as in the case of digital light projection or stereolithography techniques. These and other macroscopic 3D printing methods have allowed many research fields to expand, from optics and electronics, to tissue engineering and medicine. When moving to the microscale of light-based 3D printing, two-photon laser printing (2PLP) emerges as one of the most useful precision tools for the fabrication of micro- to nanoscale objects, such as optical lenses, biological scaffolds, or microelectronics, to name a few. Despite

progress in both the synthesis of materials and the fabrication of resultant products, few attempts have been made to understand and investigate the relationships between the two. In particular, the effect of molecular structure design and architecture on the properties and printability of microscale structures using 2PLP. Using controlled radical polymerisation methods, it is possible to create a library of polymers that are suitable as inks for 2PLP with varied physical properties such as molecular weight, T_g , and comonomer compositions. This allows relationships to be drawn between the physical properties and comonomer choice with printing range and the mechanical properties of resultant printed structures. Toward an even deeper understanding of the effect of macromolecular control, sequence-defined molecules as inks, identical in composition apart from the sequence of crosslinkable groups, allow for the precise relationships to be determined between the sequence and resulting properties. Beyond precise macromolecular composition, even more advanced architectures such as molecular polymer bottlebrushes show promise for novel inks due to their unique and tuneable characteristics, including high entanglement molecular weights and super soft elastomeric properties.

To that end, this thesis is comprised of three overarching research chapters that can be summarized as an investigation into how (macro)molecular design can aid in and influence the properties of inks and printed structures fabricated using two-photon laser printing, including the relationship to printability of each ink. After an introduction of the underlying and current literature in **Chapter 2**, we begin the investigation with a systematic study of pre-polymeric inks in **Chapter 3**. Here, controlled-radical polymerisation is used to synthesise three ‘pre-polymer’ inks allowing the effect of molecular composition, such as choice of comonomer, on the two-photon polymerisation process, to be examined. In **Chapter 4**, more control is introduced to the molecular architecture through the rational design of three sequence-defined oligomers as inks. The step-by-step synthesis of these oligomers allows complete control over the monomer sequence, and thus, the positioning of the crosslinkable group within the molecular architecture, allowing a correlation to be drawn between molecular sequence, network formation, printability, and material properties of printed structures. In the last

research chapter, **Chapter 5**, this macromolecular design is expanded into new architectures beyond linear polymers with the synthesis of photoreactive molecular bottlebrush polymer inks. By incorporating crosslinkable moieties into brush-like polymers, new properties and functionalities are envisioned for 2PLP structures. **Chapters 3 and 4** follow the same format, whereby the molecular components are synthesised and formulated into a printable ink, followed by an investigation into the window of printability for each individual formulation. The printed structures are then investigated for their chemical properties i.e. the degree of acrylate conversion, as well as their mechanical properties, i.e. the reduced elastic modulus. The correlation between these properties with the varied molecular compositions is examined and conclusions drawn. **Chapter 5** examines the development and optimisation of bottlebrush polymers as inks for two-photon laser printing for the first time. **Chapter 6** provides conclusions to the body of work, along with the outlook and potential subsequent areas of research.

2 Theoretical Background

2.1 POLYMERS: FROM DISCOVERY TO DESIGN AND CONTROL

The world of polymer and macromolecular science has developed exponentially since its conception in the early 20th century with the pioneering works of Hermann Staudinger.^[1-3] Today, it is difficult to imagine a world that is not centred around polymers. In fact, humankind has exploited polymers for millennia through the advantageous use of naturally-derived polymer-based materials. However, it was the discovery and determination of the molecular structure and synthesis mechanisms of such polymers that has allowed us to develop the field into what it is today, allowing us to quite literally shape these (macro)molecules to our will. With the development of new and more advanced technologies for additive manufacturing combined with the possibilities for the controlled synthesis of various macromolecular architectures, the capacity for fabrication of precise materials for various applications is increasing rapidly.

2.1.1 Composition and Characterisation

As proposed by Staudinger, polymers are macromolecules comprised of repeating monomer units, covalently connected to form large chains. The commonly encountered architecture of polymers is linear, however through synthetic design it is possible to create a multitude of different structural variations such as linear, star, branched, hyperbranched, dendritic and networks, to name a few (Figure 1).

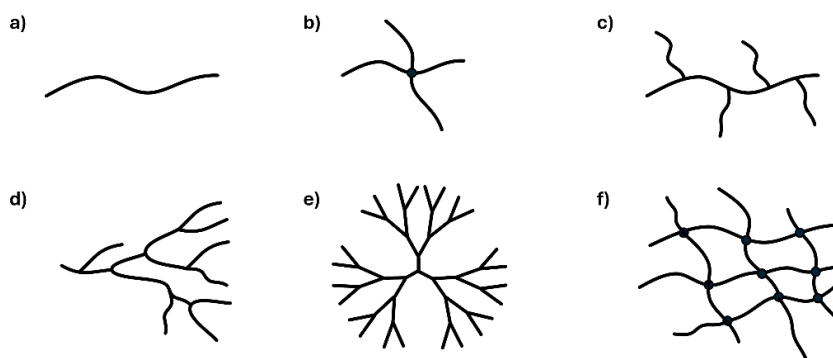


Figure 1: Schematic representation of various common polymer forms. a) linear, b) star, c) branched, d) hyperbranched, e) dendritic, f) network.

For the characterisation of polymers, two properties are commonly considered: the molecular weight and the dispersity. Typical polymerisations lead to linear chains comprising one or more monomer units. The number of monomer units incorporated is commonly referred to as the degree of polymerisation (DP). Considering the molecular weight of each monomer, as well as the DP, the molecular weight of a given polymer species can be calculated using Equation 1:

$$M = DP * M_{ru} \quad \text{Equation 1}$$

where M is the molecular weight, DP is the average degree of polymerisation and M_{ru} is the mass of the monomer repeat unit. However, as polymerisation is a statistical process, each individual polymer species has a different DP i.e. not every chain will be identical, and thus, there is a dispersity between the chain lengths. This can be characterised either by the number average (M_n) or weight average (M_w). M_n is the statistical average molecular weight calculated by:

$$M_n = \frac{\sum N_i M_i}{\sum N_i} \quad \text{Equation 2}$$

where M_i is the molecular weight of a specific chain, and N_i is the number of chains possessing that molecular weight. Alternatively, M_w , the weighted average is defined by:

$$M_w = \frac{\sum N_i M_i^2}{\sum N_i M_i} \quad \text{Equation 3}$$

Unlike the M_n of a polymer, M_w considers the molecular weight of a chain in the contribution to the result. Since larger molecules weigh more than small molecules the M_w is skewed to higher values and is always larger than M_n in a polydisperse sample. The ratio of these two values, termed dispersity \mathcal{D} , is calculated by:

$$\mathcal{D} = \frac{M_w}{M_n} \quad \text{Equation 4}$$

with values closer to 1 for the narrower dispersity of the polymer (Figure 2).

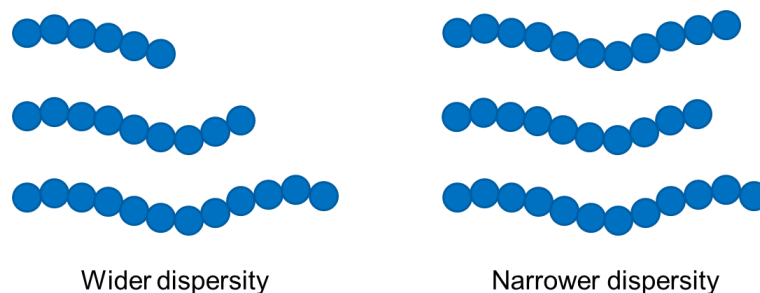


Figure 2: Representation of the difference between a polymer with wide or narrow dispersity.

In the case that these two values are identical, for example, as aimed for in sequence-defined polymers, it is said to be monodisperse. Lower dispersity polymers can be obtained through control over the synthesis, a goal that has become increasingly successful in the past decades. For the determination of molecular weight, multiple methods are commonly employed, and can be classified as either absolute, such as group analysis, mass spectrometry, osmometry and static light scattering, or relative, such as viscometry and size exclusion chromatography (SEC). The dominant method for determination of molecular weight is SEC, also known as gel phase chromatography, and is capable of determination of both M_n and M_w .^[4] This method involves the use of one or more columns packed with a porous crosslinked gel through which the mobile phase containing the dilute polymer solution flows. The separation mechanism is based on the differences in size of the macromolecules, where larger chains interact less and elute faster while smaller chains elute last as they enter and interact with the pores more easily. The amount of polymer eluting from the column is measured with an appropriate detector, such as refractive index, viscosity, or light scattering. Despite the straightforward set up, SEC presents limitations, such as the necessity for calibration with standard samples of known molecular weight for accurate measurements.^[5]

In addition to molecular weight, polymers can also be classified by their monomer composition (Figure 3), particularly when more than one monomer is involved.^[4] In this way, it is not enough to know the overall monomer content of a given polymer, but also the distribution of these monomers in relation to one another. A linear polymer comprised of single a monomer type is referred to as a homopolymer. However, when considering more than one monomer, multiple distribution patterns can be obtained: statistical, alternating, and block being the typical examples.

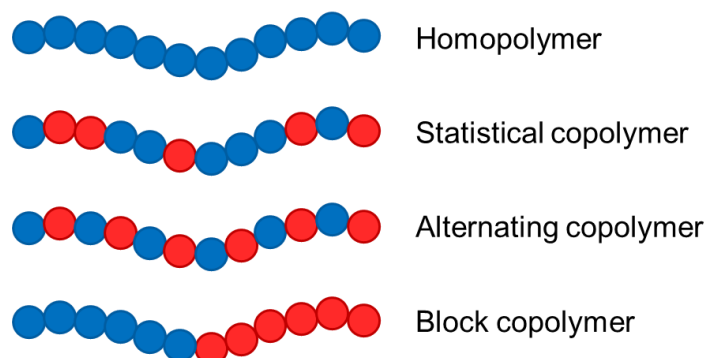


Figure 3: Representation of the commonly encountered copolymer distribution patterns comprised of two monomer types.

A statistical copolymer, also referred to as random copolymer, is formed when two monomers are introduced concurrently, resulting in a statistical distribution of both monomers governed by the relative abundance and type of monomers, as well as polymerisation technique. When the two monomers are distributed in regular and repeating fashion, the polymer is termed alternating—this is typically achieved by reversibly linking the monomers during polymerisation in a way that can be then cleaved after polymerisation to give the resultant alternating pattern. Lastly, block copolymers are formed from two homopolymers, typically through the formation of a single telechelic polymer that is then polymerised a second time. When a third polymerisation is performed, a triblock polymer is formed. It should be noted that the mentioned distributions are not limited to two monomers, but can be formed through the use of multiple different monomers. Thus, it is clear that through monomer choice, synthetic design, and polymerisation method, the number of available polymer compositions is expansive.

2.1.2 Polymers in bulk

Aside from the local structure, i.e. linear, star-like, branched, etc., polymers can be also considered globally as bulk materials with unique physical and mechanical properties. Unlike typical organic small molecules that exist as liquids or crystalline solids, polymers exist in many forms and are classified in many ways: from hard or soft to brittle or elastic, as liquids or solids or gels, as amorphous or crystalline. These properties are in part determined by the underlying molecular structure, intermolecular interactions, and crosslinking degree. In simplified terms, typical linear or uncrosslinked polymer chains in a solid or molten state interact with one another through physical forces such as van der

Waals or hydrogen bonding, and the properties of these materials depend on the strength of these interactions as well as the primary molecular structure. These forces can be disrupted in a reversible manner, for example by heating, allowing the polymer materials to be processed at high temperatures and reset with cooling—typically referred to as thermoplastics. Polyethylene (PE), polypropylene (PP), and polytetrafluoroethylene (PTFE) are some examples. When considering crosslinked polymers, where the linear chains are linked intermolecularly through chemical bonds, two classes are typically defined: elastomers and thermosets. Elastomers have a low degree of chemical crosslinking, typically leading to glass transition temperatures (T_g) below room temperature. This results in insoluble, viscoelastic materials that remain flexible at normal operating temperatures and can be swollen in suitable solvents. For amorphous polymers, T_g is defined as the temperature at which a transition from the hard/glassy to ductile/rubbery state, or vice versa, occurs. Thermosets, on the other hand, are highly chemically-crosslinked, resulting in low-swelling, insoluble materials, that do not flow upon heating.^[5]

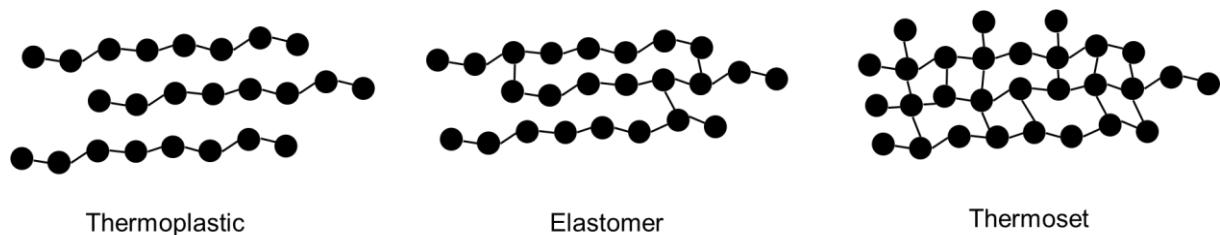


Figure 4: Graphical representation of the conformation of polymer materials: thermoplastic, elastomer, thermoset.

2.1.3 Polymerisation techniques

The synthesis of different polymer classes can be achieved through various methods, typically categorized by either step-growth or chain-growth polymerisation. Step-growth includes polycondensation and polyaddition reactions, where complimentary starting materials containing two or more functional groups participate in the formation of new bonds in a stepwise manner (Figure 5), i.e. dimers or oligomers that then undergo subsequent reactions.

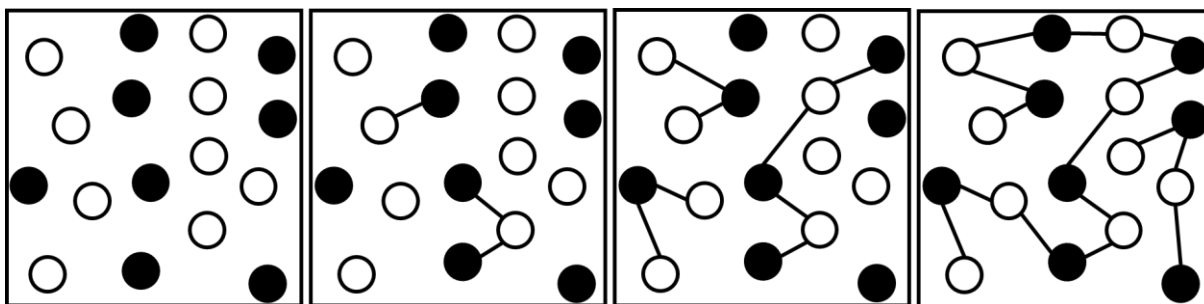


Figure 5: Graphical representation of the step growth polymerisation mechanism. Monomer units rapidly form many short chains that react stepwise, combining to high degrees of polymerisation only with high conversion.

Alternatively, chain-growth is the class of ionic (cationic and anionic) and free-radical-based polymerisations and offers the most control over the polymerisation process. Chain-growth polymerisation is characterised by an initiation process that leads to the formation of ‘active’ chains to which monomers are added consecutively (Figure 6).

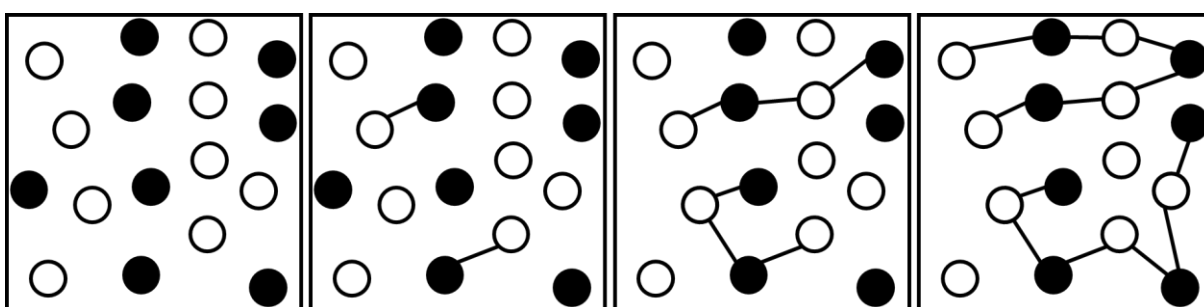


Figure 6: Graphical representation of the chain growth polymerisation mechanism. Monomer units are introduced to active species, growing active polymer chains at an equal rate, resulting in high degrees of polymerisation even at low conversion.

The result of stepwise growth is small chains that grow exponentially as the reaction progresses; thus, even at a relatively high monomer conversion, the DP remains relatively low. Conversely, in chain-growth polymerisation with low conversion the average molecular weight is relatively high and reaches a plateau. Chain-growth methods are typically characterised by initiation, propagation, and termination steps. In cases where side reactions and termination steps are not present, the polymerisation is termed ‘living’. In these cases, there will be a constant growth of polymer chains toward low dispersity products where, without external influence such as air or moisture, the reaction is dependent on the monomer feed, and chain growth will continue linearly until the monomers are entirely depleted or termination is deliberately employed. The first

living polymerisation system described by Michael Szwarc in 1956 was an anionic polymerisation.^[6] However, ‘livingness’ has been subsequently incorporated into other polymerisation methods such as cationic, ring-opening metathesis, and free-radical polymerisation (FRP).^[7] The desire to employ control over polymerisation mechanisms has been typically driven by the prospect of material development.^[8] In this context, free-radical polymerisations have been the subject of extensive research due to the versatility, improved control, and ease of industrialization. As the main method used throughout this thesis the following paragraphs focus on FRP, with emphasis on introducing control as a controlled living polymerisation, more recently referred to as reversible-deactivation radical polymerisation methods.

2.1.3.1 Free-radical polymerisation (FRP)

Although FRP and ionic polymerisations are similar in mechanism, the precise requirements of ionic processes—such as specific and controlled reaction conditions, intolerance to impurities, and limited monomer suitability—have led to free-radical polymerisation being employed as the more typical method for the development of novel materials.

FRP, as a chain-growth type reaction, is characterised by initiation, propagation and termination steps (Figure 7). In the initiation step, free radicals are generated through an external stimulus—for example heat or light—providing the initial point at which chains are grown by sequential addition of monomer units. With a high concentration of free radicals, the monomer units are consumed at a fast rate in the beginning of the polymerisation. Additionally, each active chain has a relatively short lifetime with a high potential for recombination and termination, leading to a large dispersity of polymer chains in standard FRP.

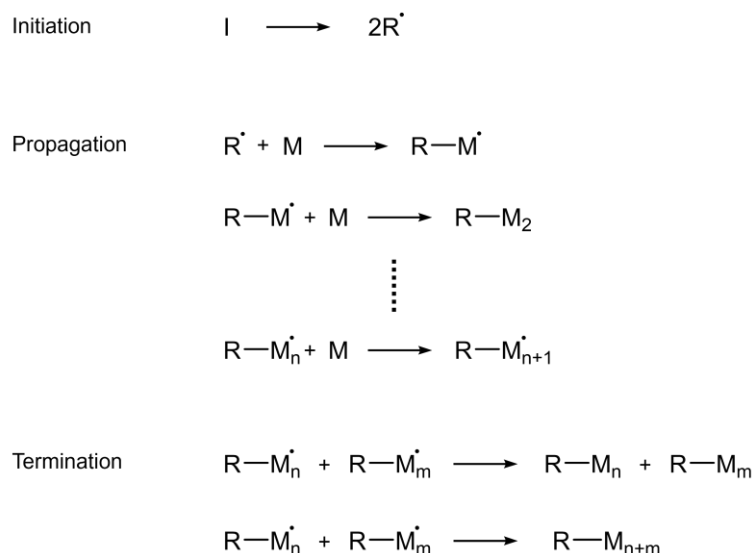


Figure 7: Standard mechanism of free-radical polymerisation.^[5]

2.1.3.2 Reversible-deactivation radical polymerisation

The years since the initial reporting of living polymerisation have seen many developments toward even greater control over polymerisation methods. In the 1990's this led to the development of one of today's most commonly employed techniques for the synthesis of highly-controlled polymers with a diverse range of architectures and properties: reversible-deactivation radical polymerisation (RDRP), which was previously also referred to as controlled living polymerisation. RDRP methods allow a similar 'livingness' through the reversible deactivation of active chains, reducing the probability of irreversible termination, and allowing the propagating species to exist in a dormant state. One feature of RDRP is internal first-order kinetics, where the logarithmic monomer concentration, $\ln([M_0]/[M])$, is linear with respect to time, assuming fast initiation. This is due to the constant concentration of propagating radicals, due to a rapid equilibrium between the activation and deactivation processes, allowing the rate of initiation to be greater than the rate of propagation. The second feature is a linear growth of polymerisation degree with monomer conversion, due to the constant number of chains throughout the polymerisation. The latter requires that initiation is sufficiently fast, allowing all chains to grow simultaneously, and that no chain transfer occurs to increase the total number of chains.^[9]

RDRP reactions can be categorised into three distinct mechanisms (Figure 8): radical-mediated systems for example, nitroxide-mediated polymerisation (NMP), atom transfer

radical polymerisation (ATRP), and degenerative-transfer radical polymerisation for example reversible addition-fragmentation chain transfer (RAFT).^[10]

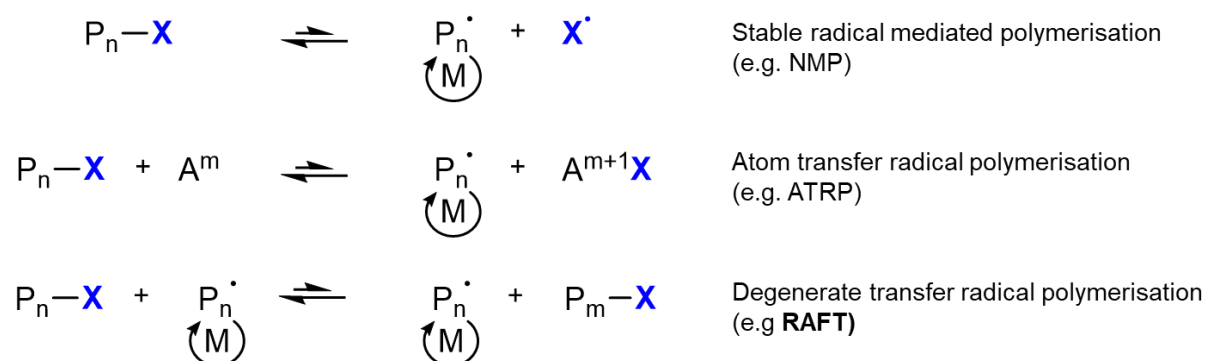


Figure 8: Typical mechanisms of RDRP based polymerisations (e.g. NMP, ATRP, RAFT). Adapted with permission.^[10] Copyright 2020.

NMP: Nitroxide-Mediated Polymerisation

NMP was discovered in the Commonwealth Scientific and Industrial Research Organisation (CSIRO) in Australia in the 1980's.^[11] As seen in Figure 8, NMP is a stable radical-mediated polymerisation method, based on the reversible deactivation of the growing propagating chain with a nitroxide moiety to form a dormant alkoxyamine species. Initial studies favoured the nitroxide containing 2,2,6,6-tetramethylpiperidin-1-oxyl (TEMPO), however, due to limitations such as the requirement of high reaction temperatures and compatibility with only select monomers, 2nd and 3rd generation nitroxides, such as 2,2,5-trimethyl-4-phenyl-3-azahexane-3-nitroxide (TIPNO) and N-tert-butyl-1-diethylphosphono-2,2-dimethylpropyl nitroxide (DEPN), were quickly developed (Figure 9).

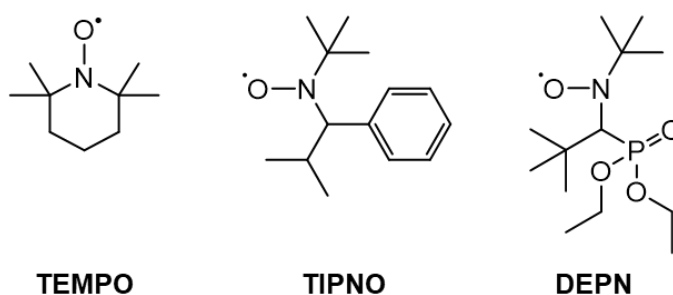


Figure 9: Example chemical structures of nitroxide molecules employed in NMP.

Although NMP was the first RDRP method to be developed, research on alternative mechanisms—ATRP and RAFT—has surpassed NMP in recent years due to advantages such as a wider range of controllable monomers, polymerisation temperatures, or chain-end functionalisation potential.^[12]

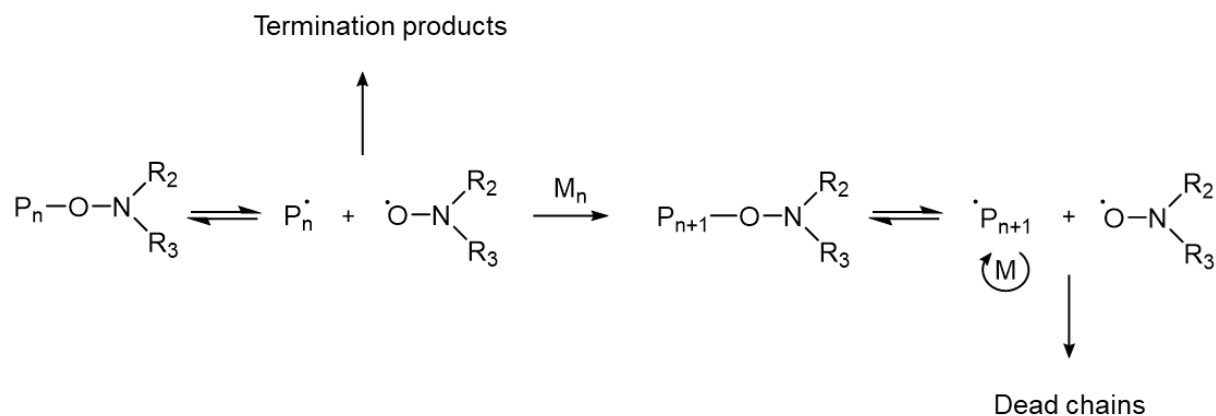


Figure 10: Scheme of the general mechanism of NMP. ^[12]

ATRP: Atom-Transfer Radical Polymerisation

The first instances of RDRP through metal-catalysed atom-transfer radical addition processes were presented by Wang and Matyjaszewski^[9] and Sawamoto's team^[13] independently in 1995, and has expanded drastically in subsequent years. The reversible deactivation typically follows the same pattern, despite a wide variety of catalytic systems and reagents. The mechanism involves the initiation of an alkyl halide ($\text{P}_n\text{-X}$) in the presence of a low oxidation state transition metal species (Mt^m), which is most often copper based (Figure 11).

Although following a similar concept as NMP and ATRP processes, RAFT polymerisation does not rely on persistent radical effects to establish control but, the equilibrium between active and dormant chains, in a degenerative transfer process. The key feature is thiocarbonylthio compounds, often referred to as RAFT agents or chain transfer agents (CTAs) with the typical form $Z-C(=S)S-R$, where the R group initiates polymer chains and the Z group stabilises the intermediate species, giving polymer chains predominantly with the form $R-M_n-S(S=)C-Z$, where M_n is the number of monomers added. The mechanism, as shown in Figure 12, begins with the generation of free radicals, typically through the light- or heat-induced fragmentation of a free radical initiator, such as AIBN, which reacts with one or more monomers forming active chains P_n . These active chains can then add to the CTA and form an intermediate radical species in a pre-equilibrium step, also referred to as reversible chain transfer or initialisation. The intermediate radical species can then restabilize through the fragmentation of the R group, giving the thiocarbonylthio group and an R group radical which can initiate and propagate more polymer chains in a step called reinitiation. The next step is the main equilibrium, or chain equilibrium stage, where growing polymer chains reversibly attach and detach from the CTA while also reacting with monomers, increasing the chain length at a stable rate across all polymer chains.

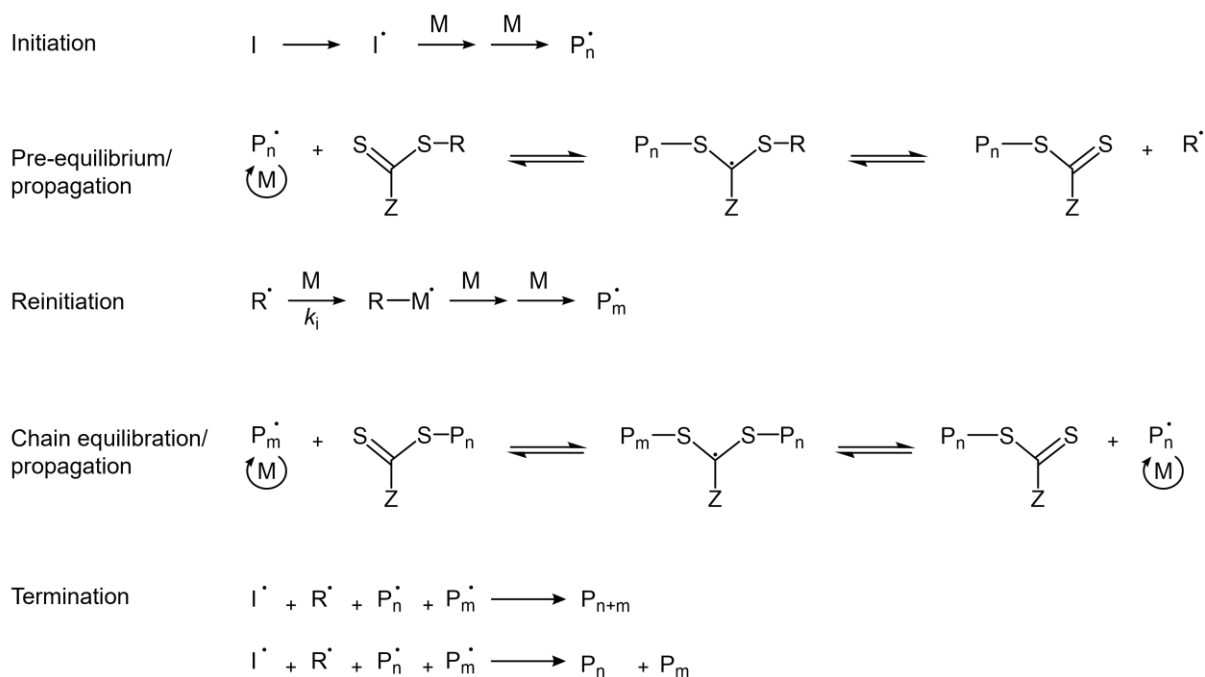


Figure 12: Scheme for the general mechanism of RAFT polymerisation.^[18]

As the number of radical species is constant throughout the reaction process, the number of radical species generated is equal to the number of initiated chains, which additionally is equal to the number of dead chains at the end of the reaction—assuming termination only through disproportionation. The resultant polymer chains typically have the R- and the Z-C(=S)S-groups of the CTA forming the α and ω ends. However, termination through recombination is also possible, and side products such as the chain initiated by the initiator species rather than the R group, as well as so called ‘dead’ polymer chains that terminate with an end group that cannot undergo further chain extension (Figure 13).

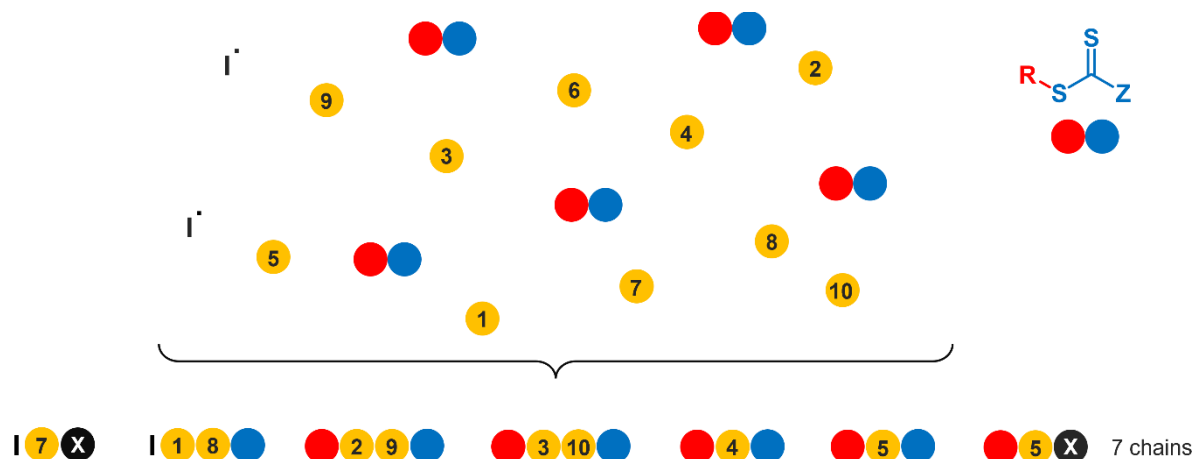


Figure 13: Schematic representation of RAFT chain formation. Whereby two radicals (I) are present in a system of 10 monomers (yellow) and five CTA's comprised of an R group (red) and Z-C(=S)-S group (blue). During polymerisation, 7 chains are formed. Living chains are formed with ω ends of Z-C(=S)-S and α -ends of either I or R. Dead chains (black) contain no Z-C(=S)-S group, and either I or R groups at the α -end. Adapted under the terms and conditions of ACS Authors Choice license.^[19] Copyright 2017, American Chemical Society.

2.1.3.3 Complex polymer architectures through RDRP

RDRP is a great synthetic tool to access new and intricate polymer architectures. In particular, RAFT and ATRP methods have been used prolifically in recent years to generate a wide range of macromolecular and polymer architectures and topologies. Between RAFT and ATRP methods, there are a host of available monomers as well as CTAs, initiators, and ligands for their controlled polymerisation. Through rational experimental design, controlled polymers can be synthesised under various conditions using both techniques (Figure 14).

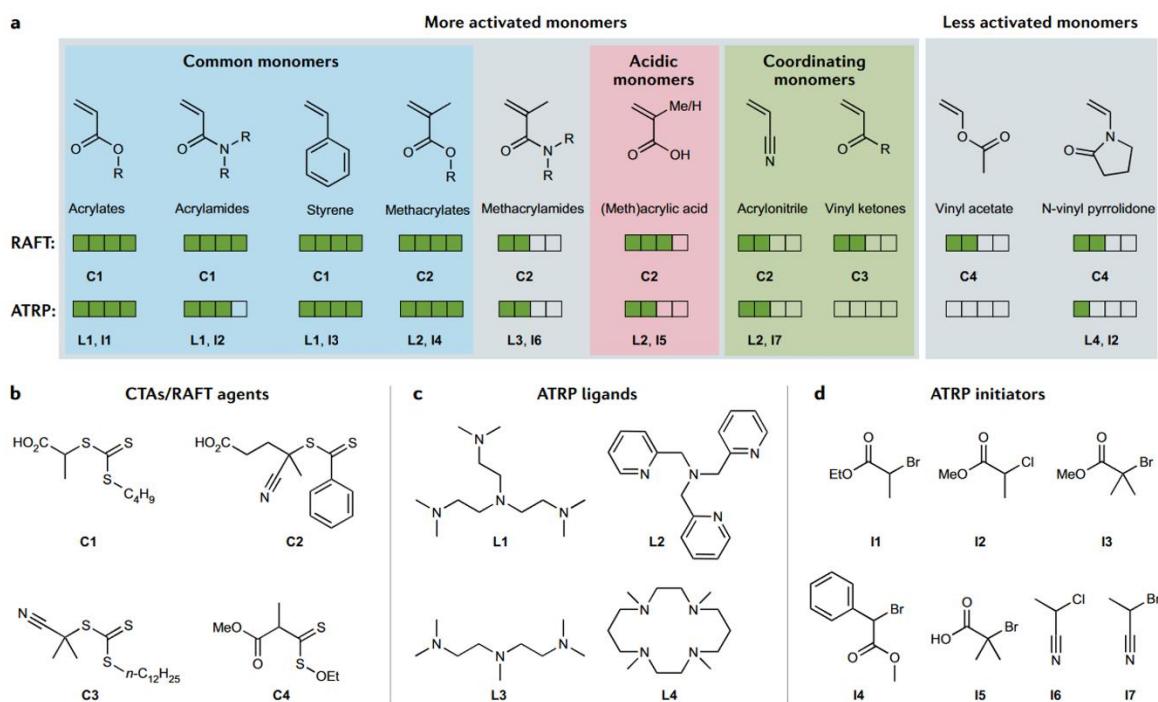


Figure 14: Overview of a) typical monomers and b) control agents for RAFT, c) ligands, and d) initiators ATRP polymerisations, where the higher rating indicates higher control and more numerous literature examples. Adapted with permission.^[20] Copyright 2021, Springer Nature.

The reversible-deactivation of the control agent on dormant chains and degenerative chain transfer in RDRP polymerisations leads high end-group fidelity and produces telechelic products, giving a multitude of options for post modifications and expanding the achievable structural architectures, including but not limited to those shown in Figure 15.

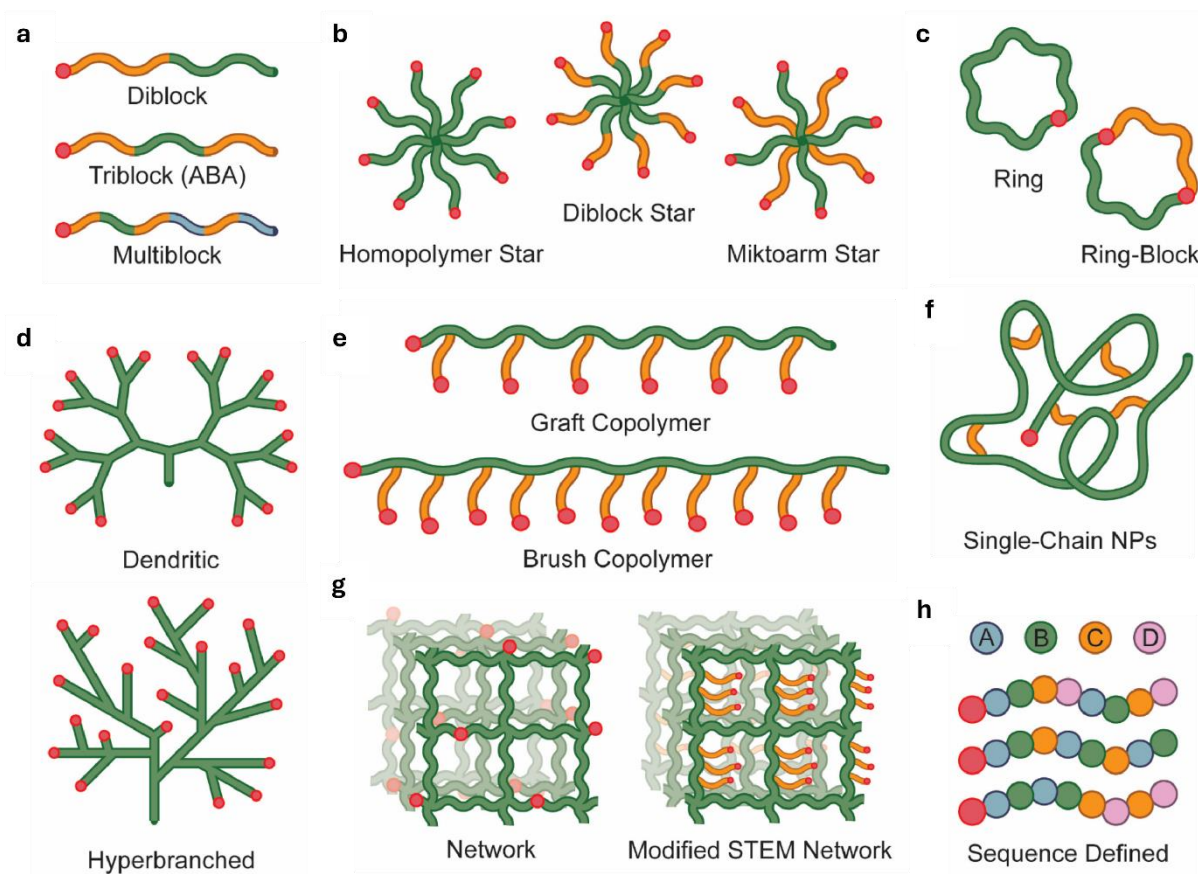


Figure 15: Architectures synthesised through RDRP methods. a) block copolymers, b) star copolymers, c) ring copolymers, d) branched and dendritic copolymers, e) graft and brush copolymers, f) single chain nanoparticles (NPs), g) networks, h) sequence-defined copolymers. Adapted with permission.^[10] Copyright 2020, Elsevier.

Most simplistically, RDRP can be used for the synthesis of almost any conceivable linear composition from homopolymers and copolymers to di-, tri- and multi-block (Figure 15a). By introducing this linear synthesis protocol to a multifunctional starting point, star shaped polymers of many compositions can be achieved (Figure 15b). Taking linear polymers with complimentary α - and ω -chain end groups and reacting them in dilute solutions can lead to closure forming ring-like, circular architectures (Figure 15c). Dendritic or hyperbranched structures can be synthesised through methods such as sequential polymerisation and grafting procedures (Figure 15d). Graft copolymers or brush copolymers are an interesting architecture comprised of linear backbones with secondary polymer side chains (Figure 15e), which can be formed through multiple synthetic pathways. Their unique structure gives way to many unique properties, which will be discussed in more detail in the subsequent Chapter 2.3. Single chain

nanoparticles (NPs) are formed from intramolecular reactions or interactions, such as crosslinking or folding, through pendant functionalities leading to collapsed single polymeric chains (Figure 15f). When these molecules and molecular architectures interact either through physical or chemical crosslinking, networks can be formed (Figure 15g). The final example here is sequence-defined macromolecules (Figure 15h). As opposed to the previous examples, where the polymer sequence is formed of monomers adding to one another in a statistical manner, leading to a disperse but controlled product, sequence-defined molecules introduce monomers in a defined manner with the goal of monodispersity, i.e. every polymer chain with a single uniform length. Sequence-defined macromolecules can be synthesised through RDRP techniques,—examples of which can be found in the work of Junkers^[21,22] and Boyer^[23]. However alternative methods such as those used for peptide synthesis are most common.

2.2 SEQUENCE-DEFINED MACROMOLECULES: BEYOND CONTROL TOWARD PRECISION

Until now, the previous chapters have explored polymers and macromolecules as synthetic products, and attempts made by scientists to develop materials where a great degree of control is afforded. However, when we turn our attention toward nature, it is clear that this is where the greatest control is already found. For example, the precise polymer code required for human life is contained within our DNA. In most cases, natural polymers are so-called ‘sequence-defined’ macromolecules—each molecule is identical with a dispersity of 1. Taking this inspiration from nature, the synthesis of natural biopolymers such as peptides and proteins has been targeted by researchers in past decades. However, the application of this precision approach toward non-natural polymer products has gained attention in fields such as material science in recent years.^[24–26]

2.2.1 Synthesis and characteristics

For the precision synthesis of sequence-defined or sequence-controlled (macro)molecules, multiple strategies have been developed (Figure 16). Compared to polymerisation methods discussed previously, where products are controlled but still disperse, the common factor for sequence-defined methods is the introduction of

monomer units in a precise manner toward the goal of products with a defined molecular structure and a dispersity of 1.

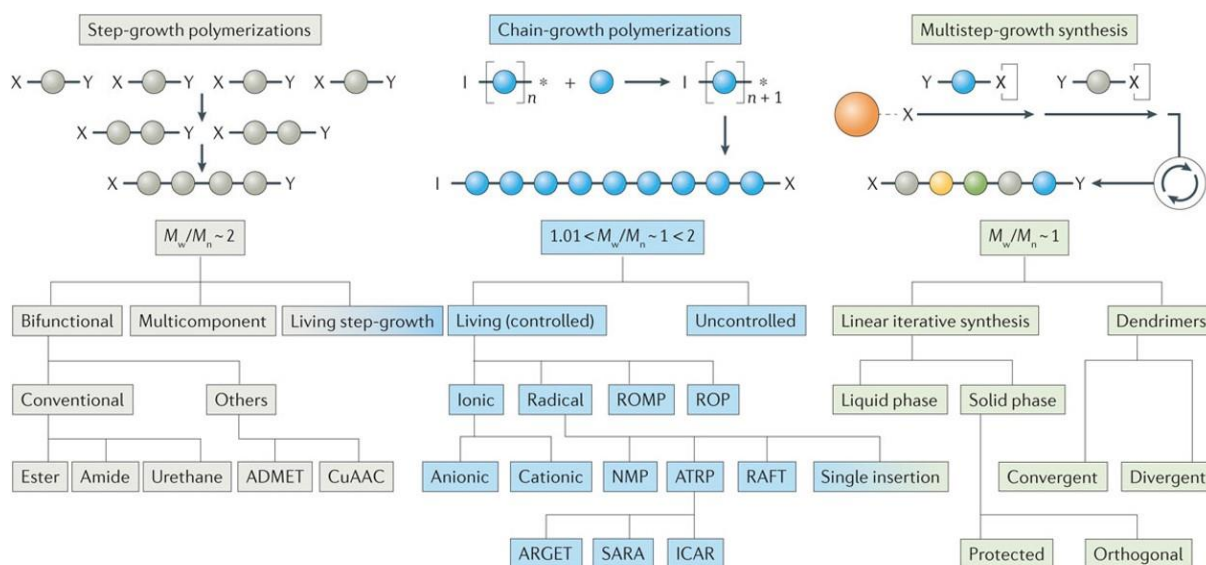
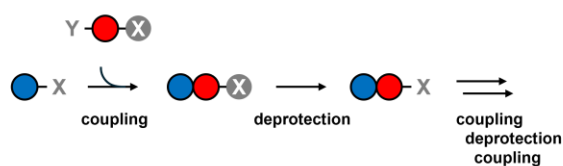


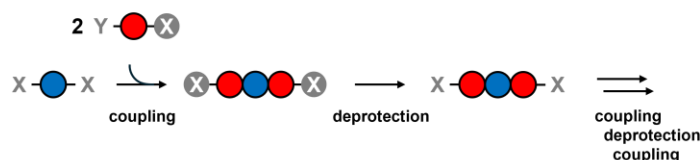
Figure 16: Synthesis strategies commonly employed for polymerisations with increasing levels of control from standard step-growth polymerisations to chain-growth polymerisations and multi-step growth synthesis. Reproduced with permission.^[24] Copyright 2016, Macmillan Publishers Limited.

Initial methods for the synthesis of sequence-defined polymers were based on classical organic small molecule chemistry protocols, and can be classified into three categories: iterative stepwise growth (ISG) (either monodirectional or bidirectional) iterative exponential growth (IEG) (Figure 17), and single unit monomer insertion (SUMI).^[27] These methods can be advantageous in that they allow facile reaction monitoring and good purification and characterisation of intermediates and products. However, the synthetic demand is high, with tedious and time-consuming procedures making medium to long chain polymers difficult.^[28]

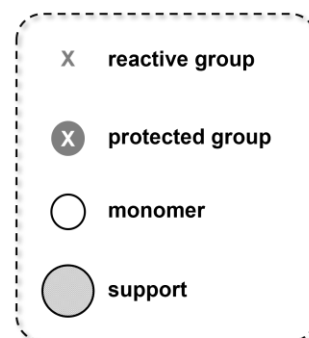
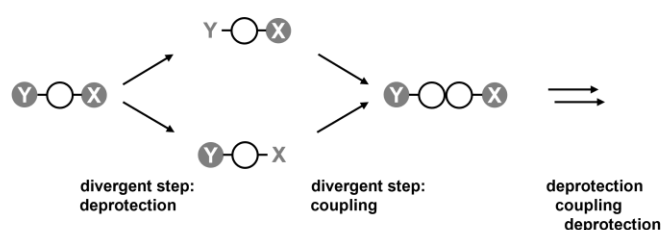
a) linear monodirectional growth



b) linear bidirectional growth



c) exponential growth



d) support-based iterative growth

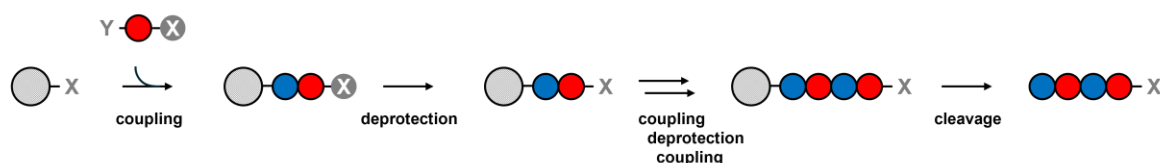


Figure 17: Synthesis strategies of sequence-defined polymers with iterative stepwise growth both a) monodirectional and b) bidirectional growth, c) exponential growth and d) support-based iterative growth methods. Adapted under the terms and conditions of the CC BY 4.0 license.^[29] Copyright 2021, The Authors.

Another method that is becoming increasingly common, known as support-based iterative synthesis, takes inspiration from the strategies most well known in peptide synthesis. Similar to ISG methods, support-based iterative synthesis methods rely on the covalent attachment of monomer units in a stepwise manner. However, unlike ISG, this method involves either a soluble (liquid) or insoluble (solid) phase support. Monomers are ‘grown’ from the support material to generate the desired sequence-defined product, which can then be removed from the support (Figure 17).^[30] As opposed to solution-based synthesis, this strategy facilitates simplified purification through methods such as filtration for the solid-state support or precipitation for liquid-phase support. The use of

these support-based synthesis methods has allowed for increasingly large sequence-defined molecules to be formed, typically in oligomeric length scales (<50 units).

2.2.2 Sequence-defined macromolecules in bulk

The applications of sequence-defined oligomers and polymers are typically afforded by their precise sequence, leading to unique and tuneable properties. For example, taking advantage of the precise sequence allows for biomimetic properties typically only afforded by nature, such as folding and self-assembly.^[31–33] These properties may give rise to potential applications in catalysis or even artificial enzymes. Another interesting field where precision molecules have been shown to have promise is cryptography and data storage.^[34] It has been seen that the sequence of a macromolecule or polymer can also affect the resultant physical properties. For example, Norris et al. saw an influence of sequence on the electronic and optical properties of conjugated *p*-phenylene–vinylene polymer materials.^[35] More recently, studies have been conducted using sequence-defined oligomers to examine the effect of sequence on thermal properties such as T_g in oligomeric materials. For example, in a study by Liu and coworkers in 2022, the monomer sequence in pentameric cyclic vinyl oligomers, where one unit was replaced by acrylic acid monomer, was shown to have a distinct effect on T_g .^[36] Alternatively, Haven and colleagues investigated the effect of discrete (meth)acrylate and di(ethylene glycol) ethyl ether acrylate oligomers with lengths from 1 to 10 units on T_g , showing a trend of increasing T_g with increasing molecular weight.^[37] A few investigations have also been conducted on the effect of sequence-defined macromolecules in network topology and the effect of molecular structure on crosslinked materials. For example, Alabi et al. looked at crosslinked thiol-ene films formed from oligomers with differing sequences, showing that both thermal and mechanical properties are affected by monomer sequence.^[38,39]

2.3 MOLECULAR POLYMER BOTTLEBRUSHES: ADVANCED ARCHITECTURES

Molecular polymer bottlebrushes (MPBs) are polymers with a unique polymeric architecture, which have been gaining traction in the field of materials science for their distinctive and tuneable properties. The origin of bottlebrush polymers can be traced

back to the work of Yamashita et al. in 1989 with initial studies stemming from the concept of graft polymers, and the polymerisation of so-called ‘macromonomers’.^[40] Therein, ‘macromonomers’ are defined as higher molecular weight monomers or polymers with further polymerisable functionality. While there are many similarities between graft and brush polymers, the main distinction is grafting density, i.e. the number of side chains per initiation point along the backbone—where bottlebrush polymers aim for high density side chains toward to goal of one side chain unit per monomer unit of the backbone. This high grafting density of side chains gives rise to steric repulsions, resulting in the distinct conformation and physical properties of bottlebrush polymers.^[41]

2.3.1 Synthesis and characteristics

The synthesis of MPBs is typically achieved through common and well-established grafting synthesis techniques. There are three general methods that can be categorised based on the approach used to generate or attach the side chains to the polymer backbone: namely grafting ‘from’, grafting ‘through’, or grafting ‘to’ (Figure 18).^[42,43] Each method offers strengths and limitations; typically the method is chosen in each use case to leverage these toward the desired product. Each method effectively results in the synthesis of a polymeric bottlebrush architecture composed of a linear backbone with a length defined as N_{BB} and side chains with length defined by N_{SC} .

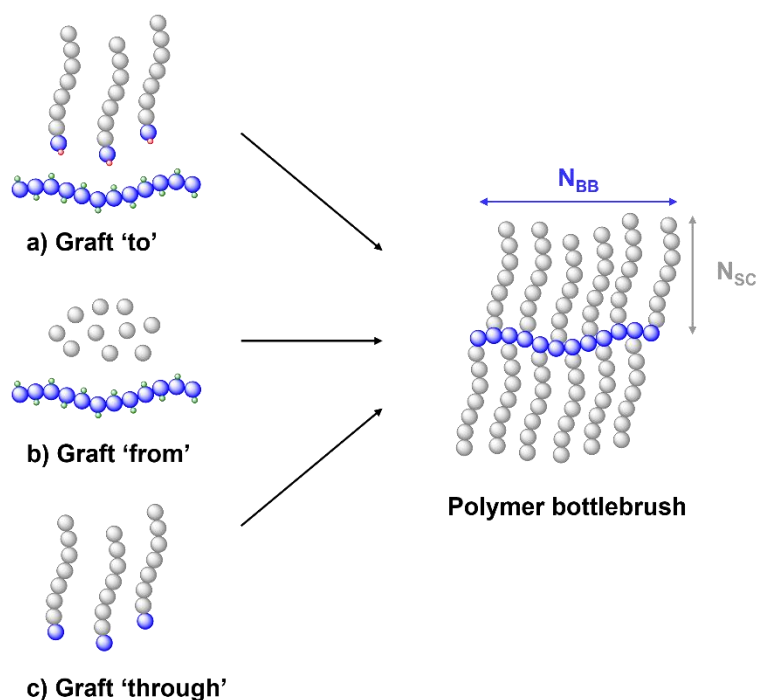


Figure 18: Graphical representation of synthesis strategies for the formation of molecular polymer bottlebrushes: a) grafting 'to', b) grafting 'from', c) grafting 'through' resulting in polymer bottlebrushes with a backbone length of N_{BB} and side chain length of N_{SC} . Adapted with permission.^[42] Copyright 2022, American Chemical Society.

Grafting 'to': For the grafting 'to' method, both backbone and side chains are pre-formed, where the side chains are telechelic or semi-telechelic polymers, and the backbone is a polymer comprised of monomers with complimentary functionality. By grafting these preformed side chains 'to' the backbone through complimentary functional groups, the bottlebrush is formed. The coupling reactions typically chosen to attach the side chains to the backbone are robust and high yielding, such as click chemistry, Diels–Alder cycloaddition, nucleophilic substitution, or thiol-ene/thiol-yne reactions. Unique to this approach is the capability for precise characterisation due to the possibility to characterise the backbone and side chains independently of one another before forming the brush architecture. However, the bulkiness of the side chains leads to steric hindrance and limits the achievable grafting potential, making this technique more suitable for low density architectures, such as comb-like polymers.

Grafting 'from': Similar to grafting 'to', grafting 'from' involves a pre-synthesised backbone. However, in this case, the side chains are formed through the polymerisation of monomer units directly from a 'preinstalled' initiation site or CTA on the backbone, for

example, through standard RDRP techniques such as RAFT or ATRP. ATRP is the most common due to the simplicity of synthesising a defined backbone and introduction of the initiation sites, as well as the large variety of compatible monomers for these polymerisation methods. RAFT is used less frequently due to the less straightforward possibility of introducing CTA to the backbone as initiation points. Grafting ‘from’, overall, is a powerful choice for the synthesis of bottlebrushes with high DP backbones and side chains, and also allows for more densely grafted side chains. By controlling the composition of the backbone, i.e. by copolymerising one functional monomer with one non-functional monomer, it is also possible to control the grafting density using this method. Additionally, advanced architectures, such as core–shell bottlebrushes, are attainable through sequential polymerisations of different monomers in block copolymer, like polymerisations of the side chains. However, this method also has some drawbacks. For instance, there are limits to the synthetic precision, such as the necessity for protection and deprotection of functional groups for more complex compositions, as well as the potential for dispersity in the side chains.

Grafting ‘through’: the grafting ‘through’ method differs from grafting ‘from’ whereby the side chains are essentially pre-synthesised. Here, bottlebrushes are formed through the polymerisation of side chains that have been modified to contain a reactive and polymerisable pendant group—a ‘macromonomer’. In this way, the bottlebrushes created using grafting ‘through’ methods have perfect grafting density as the side chains are the monomers used for the formation of the backbone. The backbone length is determined by the relative ratio of macromonomer feedstock to catalyst and initiator. Here, again, the polymerisation is limited by the reactivity of a sterically hindered and bulky macromonomer to an already large and growing backbone. At even moderate macromonomer concentrations, solution viscosities can be high. Thus, for this technique, highly active catalysts are needed to achieve higher conversion and controlled polymerisation. Due to these limitations one of the most effective polymerisation methods has been ring opening metathesis polymerisation (ROMP) of norbornyl macromonomers using Grubbs’ third generation catalyst.^[44–49] The need for high macromonomer conversion for significant backbone lengths can also result in difficulty in purifying any residual macromonomer from the product.

It is clear that depending on the desired product, a number of factors need to be considered when deciding the chosen technique for the synthesis of MBPs. Additionally, the synthesis and resultant architecture affects the properties of the resultant polymer brush, and can be finely tuned accordingly. When the degree of polymerisation of the backbone is shorter than the side chains ($N_{BB} \ll N_{SC}$), the polymer takes on a star-like confirmation; however, as the length of the backbone approaches that of the side chains ($N_{BB} \approx N_{SC}$), the bottlebrush has a more rigid conformation where the backbone is hindered from movement by the densely grafted side chains. Beyond this, when the backbone length exceeds the side chain length ($N_{BB} \gg N_{SC}$), the polymer begins to exhibit more typical linear polymer behaviour, where there is backbone flexibility relatively unhindered by side chain density allowing movement such as coiling (Figure 19).

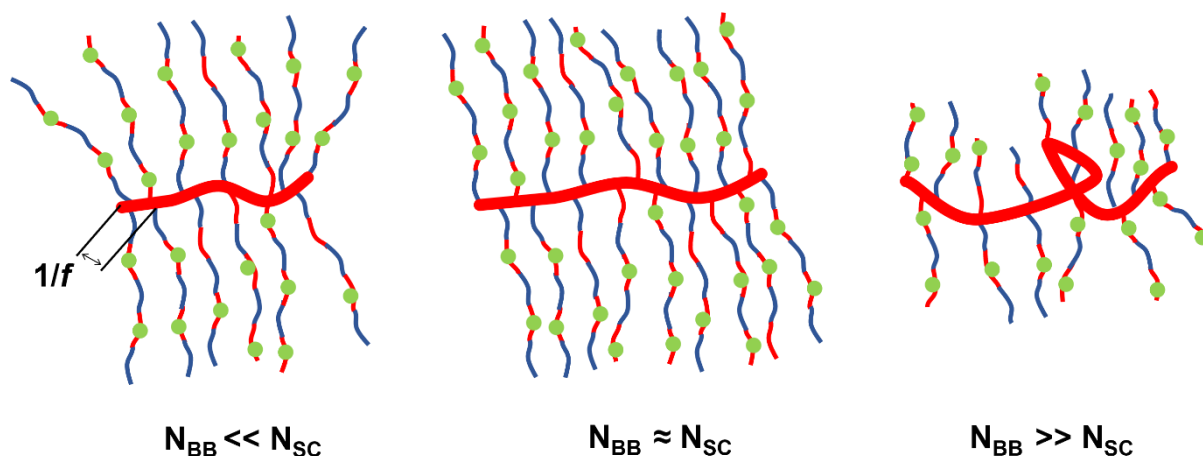


Figure 19: Typical confirmations of MPBs, resulting from the ratio of backbone length N_{BB} to side chain length N_{SC} , as well as grafting density ($1/f$).

In addition to the synthesis of linear backbones and side chains, a number of more advanced architectures with interesting topologies can be formed through the strategic design of the synthetic pathway and control of the monomer composition (Figure 20). For example, core-shell, random, di- and multi-block copolymer brushes, and even cyclic brushes.

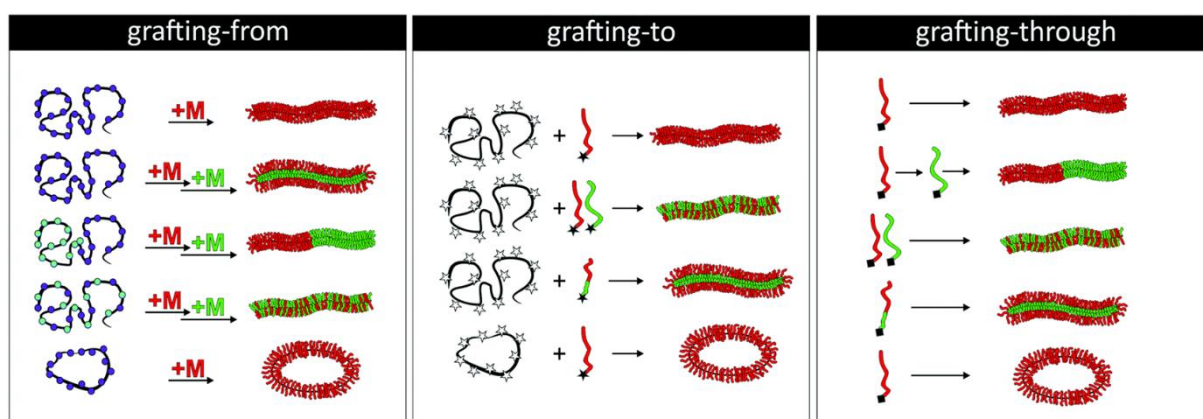


Figure 20: Different bottlebrush compositions, architectures and topologies achievable through the three commonly used synthetic approaches: grafting from, grafting to, and grafting through. Reproduced with permission.^[50] Copyright 2022, The Royal Society of Chemistry.

In dilute solutions, MPBs can be characterised as cylindrical objects with persistence length l_p and a brush diameter D . Light scattering techniques, such as dynamic light scattering (DLS) or neutron scattering, as well as other methods such as atomic force microscopy (AFM) or size exclusion chromatography, have been used to gain insight into the properties of bottlebrushes in solution.^[41] The conformation can be characterised additionally on surfaces, through visualisation techniques such as AFM, providing intermolecular resolution, or in combination with the Langmuir–Blodgett technique, to provide molecular weight distribution.^[51–53]

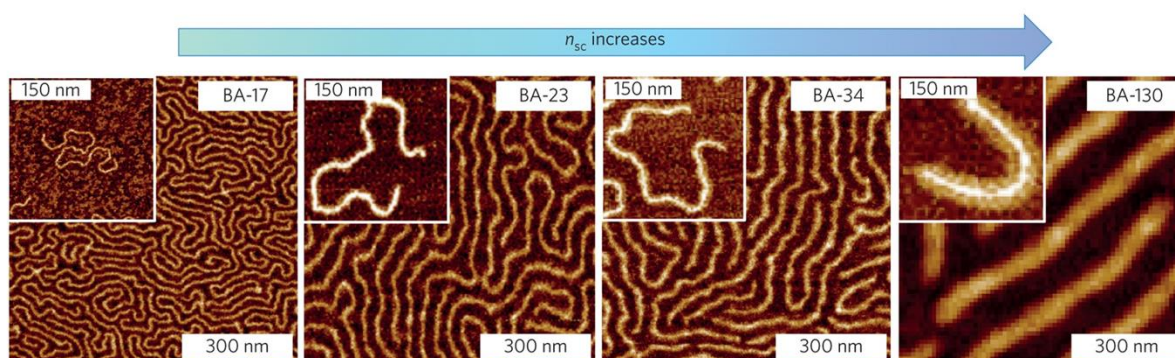


Figure 21: pBA bottlebrushes imaged through AFM, showing the effect of increasing side-chain DP (left to right) with constant backbone DP on a mica substrate. Inserts show single molecules, prepared by spin casting. Reproduced with permission.^[53] Copyright 2015, Springer Nature Limited.

2.3.2 Polymer bottlebrushes in bulk

The unique properties of MPBs have lent to their exploration in many applications, particularly in materials. One particularly interesting avenue is for soft elastomers. As mentioned previously, elastomeric polymer materials are typically entangled linear polymers with low crosslinking degrees. It is desirable in many instances to form soft elastomers, for example, to mimic biological materials. For linear polymers, the achievable properties are limited by the density of crosslinks and entanglement degree, thus limiting the potential softness that can be achieved with this type of architecture. For MPBs however, the architecture with densely grafted side chains, can prevent entanglement, resulting in elastomers with mechanical properties below the threshold achievable for linear counterparts, even without the addition of solvents (Figure 22).

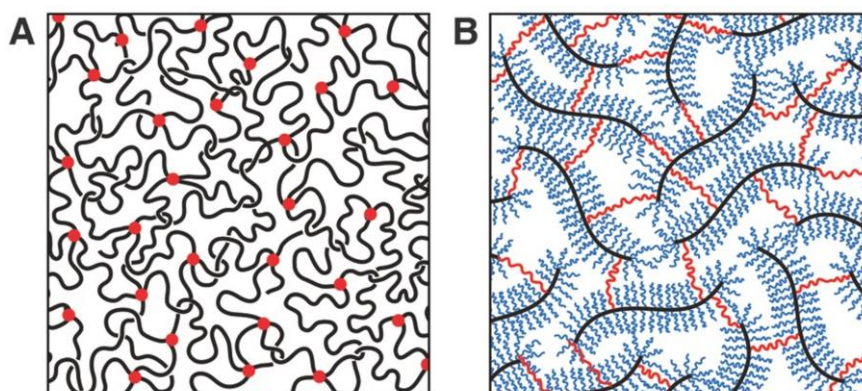


Figure 22: Schematic interpretation of elastomeric network formation of a) crosslinked linear polymers versus b) crosslinked bottlebrush polymers. Reproduced with permission.^[54] Copyright 2015, Wiley-VCH.

For example, in 2015, Cai et al. reported poly(dimethylsiloxane) (PDMS) bottlebrush elastomers with moduli in the range of 1 – 100 kPa.^[54] Similarly, in 2021 Dashtimoghadam and colleagues explored functionalised poly(ethylene glycol) (PEG)-*co*-PDMS bottlebrush melts that could be crosslinked spontaneously upon addition of a crosslinker with compatible chemistry, resulting in a solvent free elastomer with tuneable Young's modulus between 1 – 1000 kPa.^[55] Besides crosslinking, MPBs also show unique self-assembly behaviour in thin films and bulk. As first demonstrated by Runge et al. in 2005, the assembled bottlebrush copolymers form much larger domains (100 – 200 nm) than those typically observed for linear block copolymers.^[56] They also observed domains

ranging from 100 – 300 nm with lamellar, cylindrical or spherical morphologies depending on the relative block lengths of brush-linear diblock copolymers.^[57,58]

2.4 3D PRINTING

Additive manufacturing (AM), sometimes interchangeably referred to as 3D printing, refers to the fabrication of 3D objects of arbitrary geometry based on a digital model. First presented in the 1980's with the introduction of stereolithography (SLA), 3D printing was born from the need for rapid prototyping for complex objects. Since then, this technology has expanded exponentially, and is now indispensable to many fields from medicine^[59] and biomaterials^[60], to aerospace^[61,62] and (micro)robotics^[63]. This is due to the rapidly expanding library of available materials being developed for various 3D printing technologies, encompassing metals, ceramics, and glass, as well as all kinds of polymeric materials, including thermoplastics, thermosets, elastomers, hydrogels, and even biological systems.^[64] 3D printing technologies can be categorized into seven standardised categories, initially designated by the ASTM International Committee F42 on Additive Manufacturing Technology ISO/ASTM 52900 standard, developed in 2009 and revised in 2012.^[64,65]

Binder jetting: Utilises a powder bed to which a liquid binder is selectively introduced in a layer-by-layer fashion to bind the powder particles. Common powder materials include metals, ceramics, biomaterials and polymers while the liquid binder can be water or organic binders. This technique allows for complex 3D structures, such as overhangs, due to the self-supportive nature of the unbound powder bed.^[66]

Directed energy deposition: Utilises focused thermal energy, such as a laser, electron beam, or plasma, to melt materials as they are deposited through a nozzle, similar to material extrusion. This technique is unique in the degree of freedom afforded by 4 and 5 axis machines, allowing for material deposition in multiple directions. Thus, this technique is often applied for repairing and adding to existing components is currently limited to metals and alloys.^[67]

Material extrusion: Utilises a nozzle through which materials are selectively deposited. Numerous techniques have been developed that fall into this category, notably fused deposition modelling (FDM) whereby polymer thermoplastics are heated and extruded as a melt onto a moving platform. Direct ink writing (DIW) and 3D dispensing or bioplotting also fall into this category. A diverse variety of materials, particularly polymers, can be applied to these 3D printing methods such as thermoplastics, thermosets, biomaterials and hydrogels.^[68,69]

Material jetting: Utilises selective deposition of droplets onto a surface, in either a continuous or 'drop on demand' manner, where it solidifies, and objects are built in a layer-by-layer fashion. Within this category are methods such as inkjet printing, which allows printing of photopolymer or thermoplastic materials.^[70]

Powder bed fusion: Utilises thermal energy to selectively fuse regions of a powder bed, using sources such as laser, electron, or infrared beams. Typical methods include selective laser sintering (SLS) and electron beam machining (EBM). Materials range from polymer-based to metals and ceramics.^[71]

Sheet lamination: Utilises thin sheets of polymers or paper sequentially stacked and bound together with adhesive or laminated in a layer-by-layer manner, to form the final 3D geometry.^[72]

Vat photopolymerisation: Utilises selective curing of a liquid or solid photosensitive species through light-activated polymerisation. There are multiple examples of vat photopolymerisation techniques such as SLA, digital light processing (DLP), and multiphoton laser printing or 2PLP. Typical materials include photopolymerisable monomers and polymers, as well as ceramics or glass.^[73-75]

The use of light in 3D printing, such as with vat photopolymerisation, is advantageous due to the versatility, high degree of spatiotemporal control afforded, and wide variety of

applicable materials. Herein, vat photopolymerisation is the main focus of this thesis, with particular emphasis on 2PLP.

2.5 VAT PHOTOPOLYMERISATION

As discussed, vat photopolymerisation 3D printing involves the projection of a light source into a vat to generate 3D structures. The vat contains a photosensitive ink (sometimes referred to as a resin or resist), while the light source is typically light-emitting diodes (LEDs) or a laser with wavelengths ranging from ultraviolet (UV) to visible, as well as near infrared (NIR). Various types of inks exist; however most commercial inks are comprised of acrylate- or epoxy-based monomers along with a photoinitiator to initiate polymerisation when irradiated. This initiation can occur in two ways: through either one-photon or two-photon absorption processes. One photon-based printing methods include SLA, DLP, and continuous liquid interface production (CLIP). The following section will explore the theory of two-photon-based fabrication as the base of the experimental work in this thesis.

2.5.1 Two-photon laser printing (2PLP)

Where the previously mentioned one-photon processes are typically used for macroscale 3D printing, 2PLP is a two-photon absorption (2PA)-based method. 2PLP is suited for the fabrication of objects from the micro- to nanoscale. Here, a laser is focused through an objective lens into a liquid ink, where polymerisation occurs only at the focal point or 'voxel' of the laser—this is where the photon density is highest (Figure 23). The desired 3D object is formed by scanning the laser in a layer-by-layer fashion through the liquid ink. After the object is fabricated, excess unreacted ink is washed away.

Fabrication using two-photon absorption was pioneered by Maruo et al. in 1997 with the use of a Ti:sapphire NIR (790 nm) 200 fs pulsed laser.^[76] 3D microstructures were printed using an ink composed of photoinitiators, urethane acrylate monomers, and urethane acrylate oligomers. Leveraging two-photon absorption, a nonlinear process as explained in the following paragraph, complex and arbitrary geometries can be fabricated.

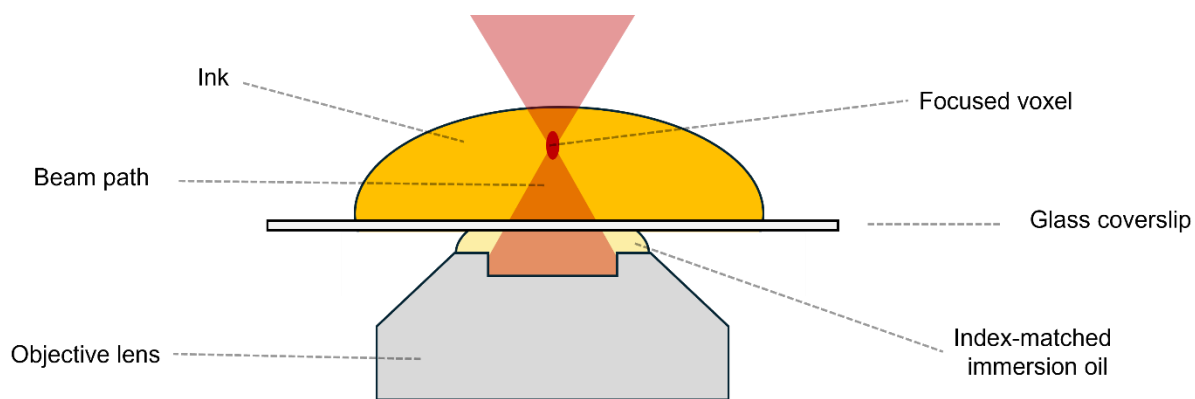


Figure 23: Schematic for the general set up of two-photon laser printing in oil immersion mode where the beam path travels from the objective lens through an index matched immersion oil and glass coverslip into the liquid ink where it is focused into a voxel at which point polymerisation occurs.

Two-photon absorption (2PA)

2PA was first described by Maria Göppert-Mayer in 1931 in her doctoral thesis, and later validated experimentally in the 1960's after the emergence of the laser.^[77,78] By the 1980's technological advances provided solid-state femtosecond (fs) pulsed lasers that had sufficient enough light intensities for 2PA in the laboratory. 2PA occurs when two photons are absorbed simultaneously by a molecule or atom to excite it from the ground state, S_0 , to an excited singlet manifold, S_1 , through a short-lived (fs) virtual state (Figure 24).

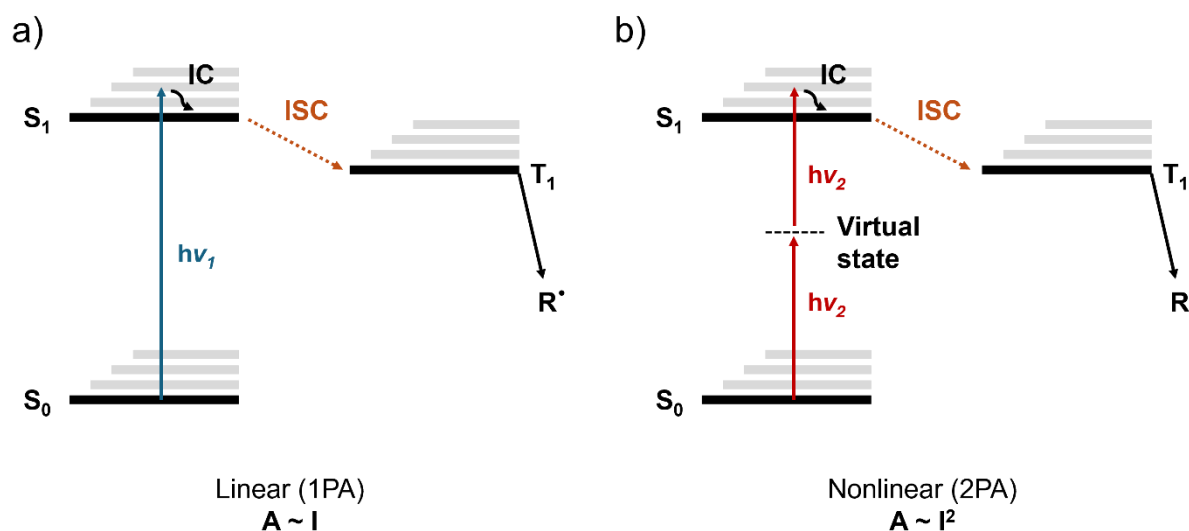


Figure 24: Simplified Jablonski diagram for absorption (A) and radical formation in the case of a) linear one-photon absorption (1PA) and b) nonlinear two-photon absorption (2PA).

From the excited state, the system relaxes to the lowest S_1 state through internal conversion (IC). From there it undergoes intersystem crossing (ISC) to the lowest triplet excited state followed by decay through the α -cleavage of bonds to give radical species.^[79] Due to the very low probability of simultaneous absorption of two photons, high photon flux densities in the range of 10^{31} photons $s^{-1} cm^{-2}$, achievable only by pulsed laser sources, are required to produce enough radical species to initiate two-photon polymerisation at a sufficient degree for solid network formation. The low probability of 2PA is not just advantageous in this instance, but a necessity, as it is this property that allows for printing of fine resolution structures at small length scales afforded by 2PLP. This is due to the second order dependence of absorption ($N = 2$) with respect to the intensity I , giving a relationship to radical concentration $[R\bullet]$ and optical dose D :

$$[R\bullet] \propto D \propto I^N$$

One-photon processes result in a nonlinearity exponent $N = 1$, leading to severe dose accumulation and therefore resulting in difficulty confining the polymerisation. The reaction-diffusion kinetics are complex and not fully understood. However, two assumptions can be used to describe the polymerisation behaviour of (negative-tone, as elaborated on in Chapter 2.5.2) inks or photoresists in 2PLP: the threshold dose or the accumulation model.^[80]

Threshold dose model: When considering the potential for generating stable 3D printed structures during 2PLP, the threshold model can be considered a binary model. Focusing on the irradiated voxel, the threshold dose model describes a certain energy dosage, E_{th} , that results in sufficient polymerisation or crosslinking for the resultant material to withstand development. Below this threshold dose, the material is not sufficiently crosslinked and will be solubilised and removed during development. In this way, when considering the ink itself, the voxels that are exposed to a dose above the threshold react, and everything outside of this does not. There is no ‘memory’ within the material below this threshold i.e. the ink ‘forgets’ any exposure below this threshold—effectively resulting in a ‘material’ or ‘no material’ binary system. Within this model, no limit is imposed by the diffraction of light, and arbitrary geometries and small features can be printed. In theory, two lines could be printed side by side, with no fundamental limitation to the distance achievable between them.^[81] However, this assumption is oversimplified,

and in practice, printed structures display a lack of the previously mentioned features (arbitrarily small gaps between linewidths, for example) that should be seemingly afforded by this model. This can be described by incorporating the accumulation model.

Accumulation model: In contrast to the threshold model, where a material ‘forgets’ any exposure below a certain threshold exposure, the accumulation model describes the accumulative effect of two or more point exposures at the same or different locations. Within this model, there is residual ‘memory’ of exposure at each point, regardless of whether above or below the exposure threshold, leading to dose accumulation over multiple point exposures. Within this model it is possible to print complex 3D architectures using 2PA but not with 1PA, as seen in Figure 25. The minimal separation distance between two features is defined by the Sparrow criterion, where the resolvable distance between two voxels is diffraction limited. Here, voxels are broadened by diffusion, but are resolvable as long as a local minimum occurs at the center overlap of the two signals.^[81]

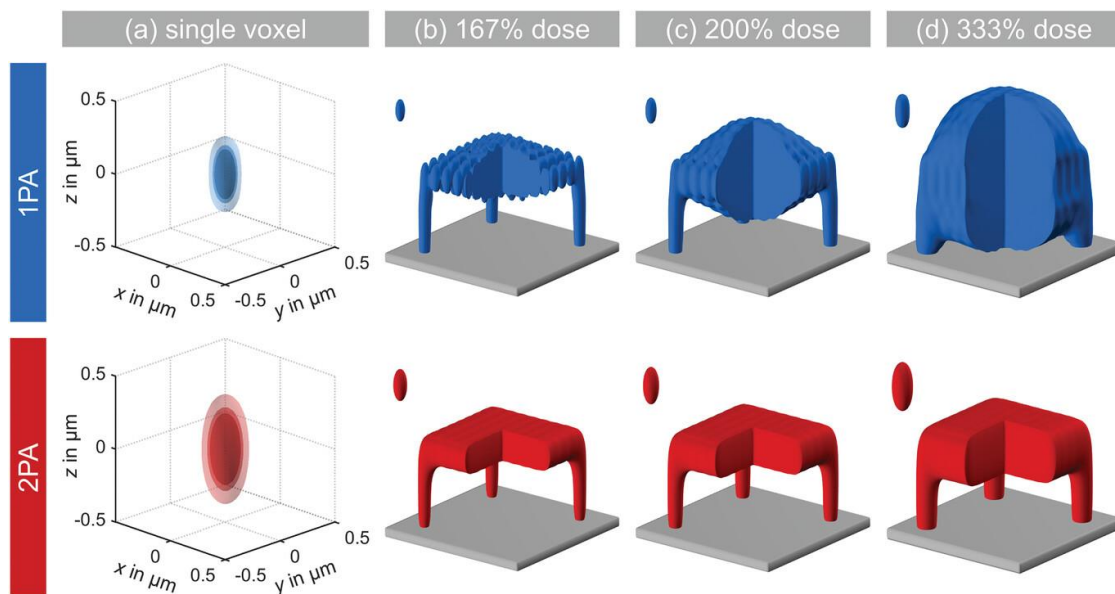


Figure 25: Illustration of 3D laser nanoprinting (also known as 2PLP) comparing 1PA and 2PA effects with increasing exposure dose. In this study, the simulation was carried out using an objective with a numerical aperture of $NA = 1.4$, with a printing wavelength of 400 nm for 1PA and exposure dose proportional to the intensity of light ($D_{\text{exp}} \propto I$) and 800 nm for 2PA with an exposure dose proportional to the squared intensity ($D_{\text{exp}} \propto I^2$). The single voxels (a) were defined using the threshold model, and the resulting printed structures were produced by increasing the exposure dose to b) 167%, c) 200%, and d) 333%, based on the accumulation model. Reproduced under the terms and conditions of the Creative Commons CC BY 4.0 license.^[80] Copyright 2020, The Authors.

2.5.2 Inks for 2PLP

As briefly mentioned previously, materials used in 2PLP are generally termed inks, resins or resists. For simplicity, the term ink is used throughout. The versatility of 2PLP inks has led to diverse applications from microrobots and microfluidics, to optics, photonics and life sciences.^[82] Inks can be classified into two categories: positive- or negative-tone. For negative tone resists, printing involves irradiation with a specific dose within a focused voxel to initiate polymerisation and network formation. After printing, the sample is washed with solvent in a step termed ‘development’, leaving the printed structures and removing any remaining insufficiently reacted ink. Alternatively, with positive-tone inks, the two-photon absorption leads to degradation or breaking of bonds. Typically, the ink is coated onto a surface and selectively irradiated, through a photomask or direct printing methods. The irradiated areas are washed away during development, leaving the desired structure.^[83,84] Positive-tone inks are used in applications such as microchip fabrication, and less commonly in 2PLP.^[85] The following chapters focus on negative-tone resists.

Ink composition

For the formulation of negative-tone inks for 2PLP, the basic requirements include a two-photon photoinitiator that is suitable for the wavelength of the laser, as well as a material consisting of photopolymerisable or crosslinkable units. In cases where the components are highly viscous or insoluble, a high boiling point solvent or additive may be also included. The chosen system can range from acrylate and methacrylate-based, utilising FRP, epoxide-based through cationic polymerisation, or thiol-ene systems. In the case of (meth)acrylate-based inks, a radical photoinitiator is used to initiate the polymerisation. On the other hand, for epoxide-based inks that react through cationic polymerisation, the initiating species is a photoacid generator, such as onium salts, which form acids upon exposure to light to initiate the polymerisation.^[86–88]

The work herein utilizes free-radical-based ink systems, which are most commonly employed due to their fast cure speed and high sensitivity, as well as a wide range of available functionalities.^[89] Generally, free-radical photoinitiators can be classified as Norrish type I or type II. Norrish type I photoinitiators are single molecules that homolytically cleave into radical species with exposure to light of a suitable wavelength,

two commonly used examples are bis(2,4,6-trimethylbenzoyl)-phenylphosphineoxide (BAPO) and bis(2,4,6-trimethylbenzoyl)-phenylphosphineoxide (TPO). On the other hand, Norrish type II photoinitiators are two-component systems comprised of a light absorbing molecule (sensitiser) along with a co-initiator (synergist). Typical sensitisers are benzophenones or thioxanthenes. Upon irradiation with a suitable wavelength the excited triplet state of the sensitiser abstracts hydrogen from the synergist, which is typically a tertiary amine, generating radicals that can then initiate FRP.^[64,90] An interesting case for one of the most commonly used photoinitiators, and the photoinitiator used predominantly throughout this thesis, is the absorption behaviour of 7-diethylamino 3-thenoylcoumarin (DETC). Owing to its chemical structure, DETC behaves as a Norrish type II photoinitiator, showing $N = 2$ photon absorption dependence in the presence of a co-initiator, with femtosecond lasers of around 800 nm. However, it is well documented that DETC can also initiate polymerisation in 2PLP without the use of a co-initiator.^[91] Recently, Mauri et al. investigated this phenomenon and report possible pathways for the FRP initiation of DETC in 2PLP.^[92] Herein, DETC was used in all cases without a co-initiator.

Macromolecular design in 2PLP inks

Within the context of this thesis, which looks at the macromolecular design of precise inks and advanced architectures for 2PLP such as sequence-defined or macromolecular polymer bottlebrush inks, the current literature is limited. A number of studies have investigated the relationship of 2PLP parameters such as laser power and scan speed on material properties, showing expected trends, for example increasing acrylate conversion and thus Young's modulus with increasing laser power (and therefore increased dosage). However, the materials used in these studies until now are limited to multifunctional molecules such as pentaerythritol triacrylate (PETA) and poly(ethylene glycol) diacrylate (PEGDA), and commercial materials with undefined composition—leading to a lack of information for generating structure–property relationships. 3D printing of sequence-defined inks was demonstrated for the first time by our group in 2023^[93], as demonstrated in Chapter 4: Sequence-defined oligomers as 2PLP inks. Following this, Barner-Kowollik et al. investigated how molecular architecture affects

photoreactivity in 2PLP through the synthesis and microprinting of macromolecules with controlled spacer lengths.^[94] The unique properties of MPBs have been leveraged in the field of additive manufacturing, where bottlebrush polymers have been 3D printed using extrusion-based^[95–99] or VAT polymerisation methods^[100]. The materials fabricated through 3D printing of these bottlebrush materials have overall modulus in the 100 – 1000 kPa range, and allow for interesting applications such as tuneable structural colour based on deposition conditions (Figure 26).^[96] However, until now, 2PLP of molecular polymer bottlebrushes remains unexplored.

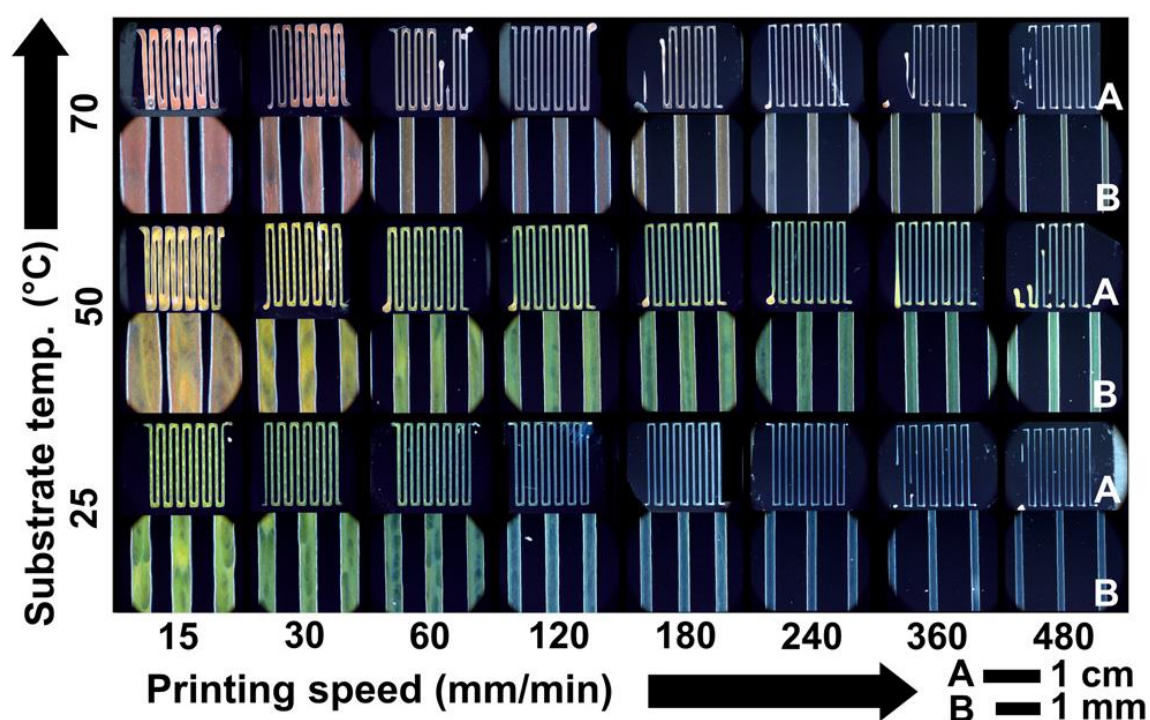


Figure 26: Optical microscopy images of 3D printed poly(dimethylsiloxane)-block-poly(lactic acid) (PDMS-b-PLA) brushes, tuning the optical properties through deposition conditions. Images shown are at a) low magnification and b) high magnification. Reproduced under the terms and conditions of the Creative Commons Attribution Non-Commercial License CC BY-NC 4.0.^[96] Copyright 2020, The American Association for the Advancement of Science.

2.5.3 Characterisation of 2PLP microstructures

For the characterisation of 2PLP microstructures, the methods chosen depend on the material, as well as the desired information. Herein, three main techniques are utilised to gain insight into the properties of the printed structures: scanning electron microscopy (SEM), vibrational spectroscopy and nanoindentation.

Scanning electron microscopy (SEM)

For characterisation of the topological properties of structures such as surface defects, shrinkage, or minimum feature resolution, SEM is an ideal choice as a fast and non-destructive imaging technique, which requires little sample preparation. In SEM, a focused beam of high-energy electrons is scanned over the sample surface, interacting with atoms to produce various signals that are collected by detectors to generate high resolution images of the sample surface.^[101] Due to the high depth of focus of SEM, compared to standard light microscopy, it is possible to retrieve a 3D impression of imaged samples. For 2PLP structures, SEM is particularly useful due to the tilting and rotating capabilities, allowing the topology of complex 3D structures to be captured. For further surface information such as surface roughness, techniques such as AFM are also suitable.^[102]

Vibrational spectroscopy

It can be useful to determine the degree of conversion (DoC) of reactive moieties for the characterisation of 2PLP structures for various reasons. In the case of free-radical polymerisation of acrylates, the DoC is determined by measuring the conversion of acrylate double bonds as they are incorporated into the network during polymerisation. The DoC can therefore be a useful indication of the polymerisation behaviour and network stability, and can be correlated to the laser power and scan speed used during 2PLP. In previous investigations, it has been shown that the DoC can provide information regarding physical properties of a material, where increased DoC typically correlates to increased stiffness.^[103] In particular, different degrees of conversion can result in material properties within microstructures that vary significantly from properties measured in the bulk material. Additionally, some methods typically used to characterise the curing kinetics and conversion in one-photon based inks such as photorheology or differential scanning calorimetry (DSC), cannot be correlated to two-photon processes.^[104] Therefore, methods for characterising these properties on the microscale are required.^[105] To that end, Raman and Fourier-transform infrared spectroscopy, commonly used for characterisation of photoresists, can be combined with light microscopy to allow chemical and structural information determination down to the

micron scale. For the micro- to nanoscale size of 2PLP structures, this is particularly advantageous. Spectroscopic methods such as Raman spectroscopy^[106], tip-enhanced Raman spectroscopy^[107], coherent anti-Stokes Raman spectroscopy (CARS)^[105], or Fourier-transform infrared (FTIR) spectroscopy, have been used to determine the degree of monomer conversion with respect to power or scan speed of the laser. Typically, the relationship between the DoC and the resolution of the printed structures is investigated.

Nanoindentation

Nanoindentation is a measurement technique that uses a hard probe to deform a sample surface in order to measure local mechanical properties at nano- and micro-length-scales. Load–displacement curves are measured by performing indentation on samples either in a force- or displacement-controlled manner. From these curves, models exist to retrieve information, such as elastic modulus and hardness. In particular, utilising the method introduced by Oliver and Pharr in 1992.^[108,109] This model is useful for materials with non-linear unloading behaviour, where Oliver and Pharr suggest few, if any, materials display perfectly linear unloading.^[108] The prevalent method for analysing indentation data estimates the first derivative of the fitted function of the unloading curve at maximum displacement (Figure 27).^[110]

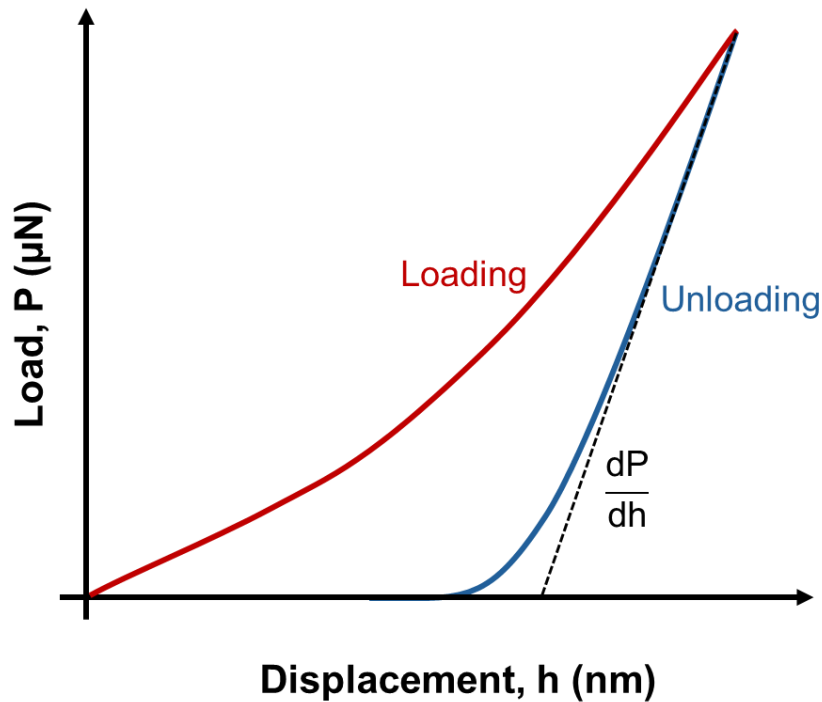


Figure 27: Example load-displacement curve of a triangular load-controlled measurement showing loading, unloading, and the slope of the unloading curve (dP/dh) where P is the indentation load and h is the displacement. Adapted with permission.^[108] Copyright 2011, The Materials Research Society.

Originally, the focus of nanoindentation development was toward linearly elastic, isotropic and homogeneous materials such as metals and ceramics. Recently, interest in nanoindentation as a tool to characterise material properties of polymers and soft materials, such as biological tissues, has increased due to being particularly useful for samples with limited dimensions or complex microstructures. In standard measurements, a triangular measurement profile is used, as seen in Figure 28a. However, a number of challenges arise during the measurement of viscoelastic materials, such as polymers, such as ‘creep’ related artifacts. In this case, instead of the ideal unloading curve, a ‘nose’-like artifact is present when the material continues to increase in displacement from the loading force during the unloading segment, making it difficult to extrapolate the slope of the unloading curve (Figure 28d). To circumvent this, typically a trapezoidal profile is used for viscoelastic materials (Figure 28b). In the case of very soft materials or to characterise probe-sample adhesion a ‘lift-off’ segment may be included (Figure 28c).

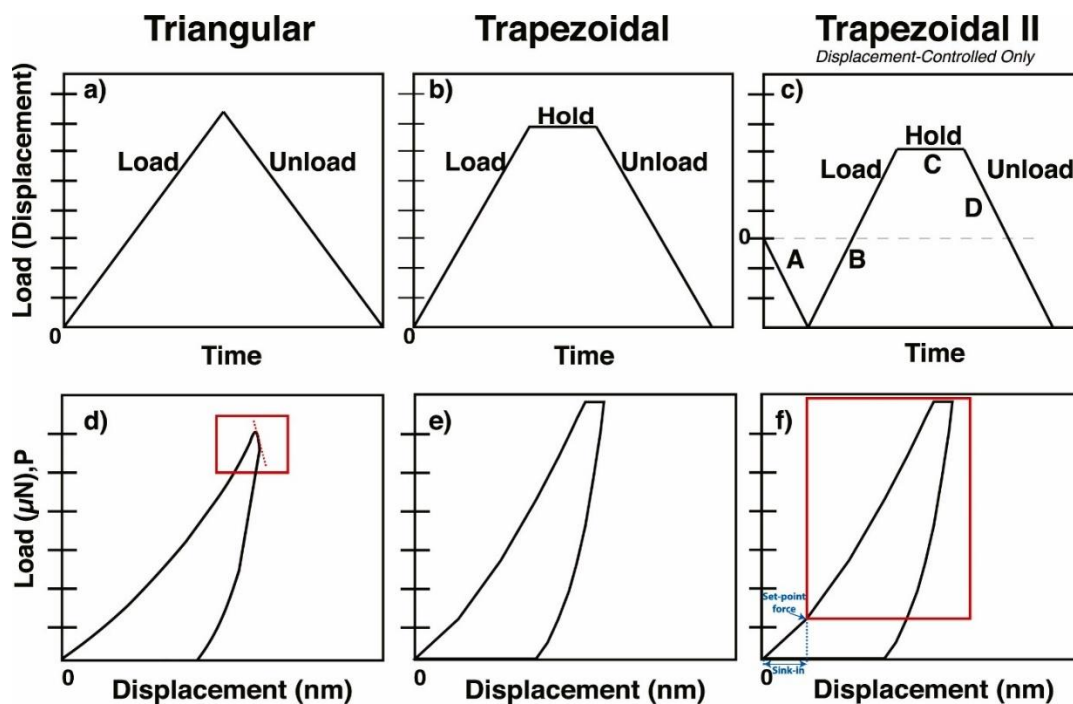
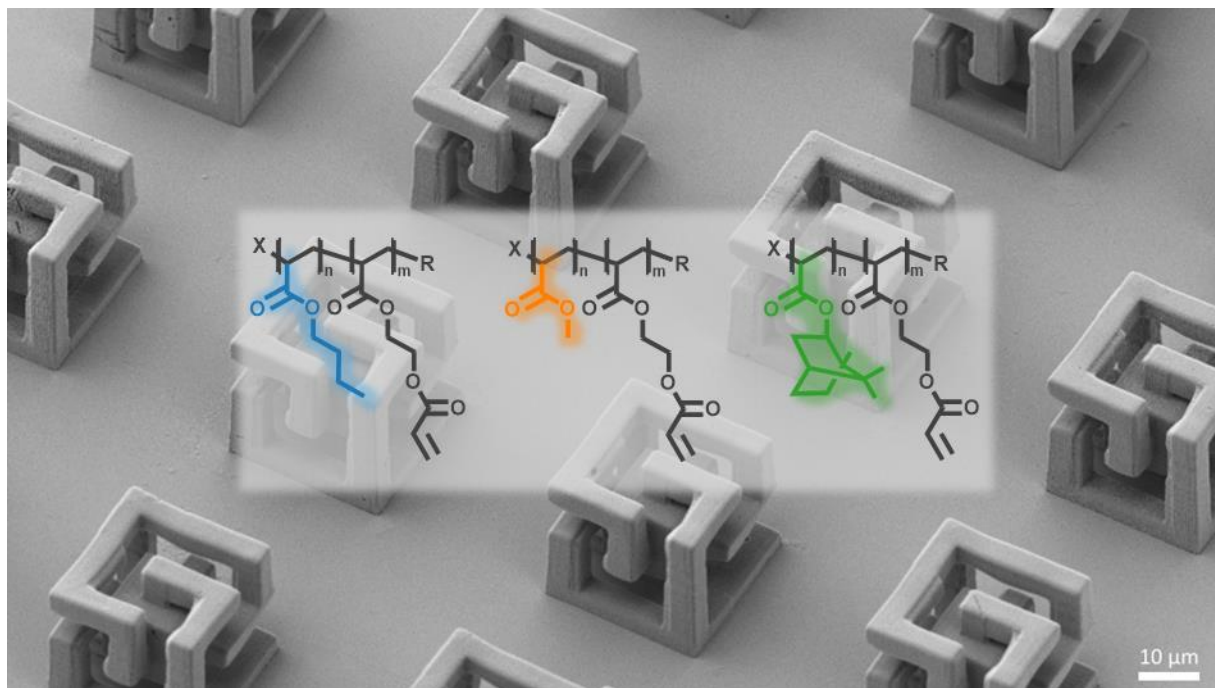


Figure 28: Load (displacement)-time profiles for a) triangular, b) trapezoidal, and c) trapezoidal II measurement set ups. d-f) Resultant load-displacement response of viscoelastic materials for profiles a-c, respectively. Reproduced with permission.^[110] Copyright 2022, Elsevier.

Other research has looked at mechanical characterisation of 2PLP structures fabricated with different materials, through various methods such as nanoindentation^[111,112], bending and torsion vibration of cantilevers^[113], microbending of cantilevers^[114], or nanowire tensile testing^[115]. When considering the relationship between mechanical properties of 2PLP structures with the chemical properties such as degree of conversion, some investigations combine both vibrational spectroscopy and nanoindentation simultaneously to characterise 2PLP structures.^[103,116-121]

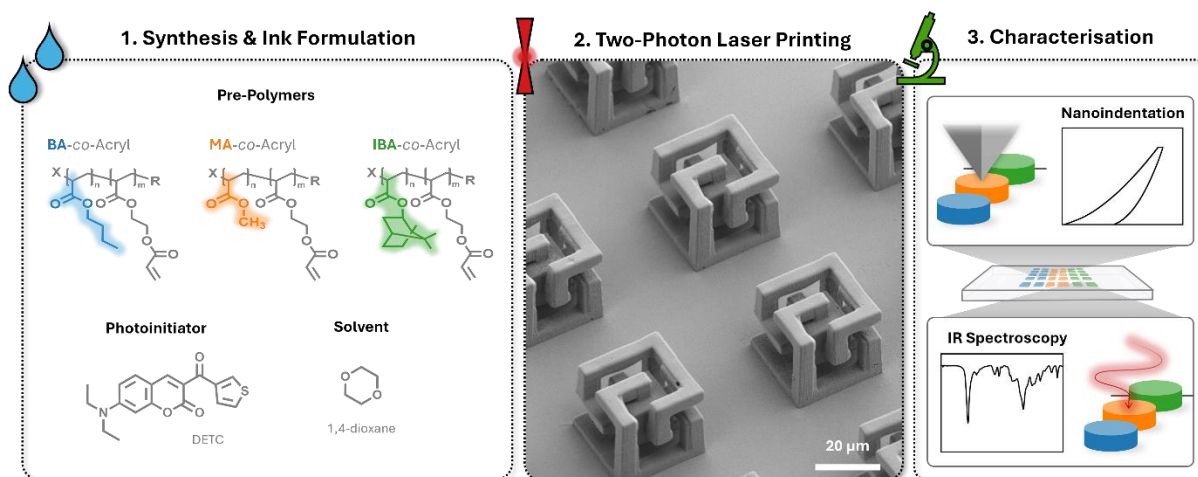
3 Pre-polymers as 2PLP inks



The results described in this chapter have been submitted for publication:
S. O. Catt, C. Vazquez-Martel, E. Blasco*, *Investigation of pre-polymer design on material properties for two-photon laser printing*, 2024, submitted.

3.1 MOTIVATION AND AIMS

2PLP has emerged as a versatile method for additive manufacturing of micro- to nano-scale objects in a variety of fields. Due to the increasing number of applications, the range of available inks is increasing in quantity and versatility with a trend toward functional or responsive materials. To incorporate functionality into 2PLP materials, one approach that is yet to be comprehensively exploited, is the use of a ‘pre-polymer’ ink containing photoreactive monomers which are covalently incorporated into the polymer. However, the synthetic design of pre-polymer inks for 2PLP often relies on arbitrary choice rather than systematic design, despite evidence that the polymer properties affect resultant material properties. Additionally, some studies have made efforts to determine the influence of printing parameters, for example the influence of laser power and scan speed, as well as the effects of photoinitiator choice, on printability and resultant properties. However, all of the current studies are limited to either commercial materials (e.g. PETA, PEGDA) or commercial inks (e.g. Nanoscribe: IP-DIP, IP-S etc.) typically comprised from small monomers, resulting in a lack of discernible correlation between the macromolecular composition of an ink with the resultant printability and structure properties. Despite clear indications that a structure–property relationship exists, the effect of physical properties on the printability, processability, and resultant material characteristics of 2PLP inks has not yet been studied in detail. Herein, a library of three pre-polymer inks with varied properties, such as molecular weight, glass transition temperature, and comonomer composition, is synthesised and formulated into inks for 2PLP. Structures are fabricated and characterised with scanning electron microscopy to determine printability as well as infrared spectroscopy and nanoindentation to determine acrylate conversion and reduced elastic modulus (E_r), respectively (Scheme 1). Correlations between the macromolecular design and chemical or physical properties are observed for all three inks.



Scheme 1: General outline of Chapter 3 in three steps: synthesis and formulation of the ink, printing characterisation with 2PLP, and mechanical and chemical characterisation.

3.2 SYNTHESIS OF PRE-POLYMERS

RAFT polymerisation was chosen for the synthesis of a small library of low molecular weight copolymers. The overall synthetic pathway was designed with the goal of incorporating the crosslinkable printing group into the polymer after the polymerisation in a post functionalisation step; thus, a synthetic handle must be available. Based on previous expertise within the group using the esterification of an alcohol and acyl halide to introduce acrylates to polymer backbones, an alcohol was chosen as the synthetic handle. The general schematic of the proposed synthetic pathway can be seen in Figure 29.

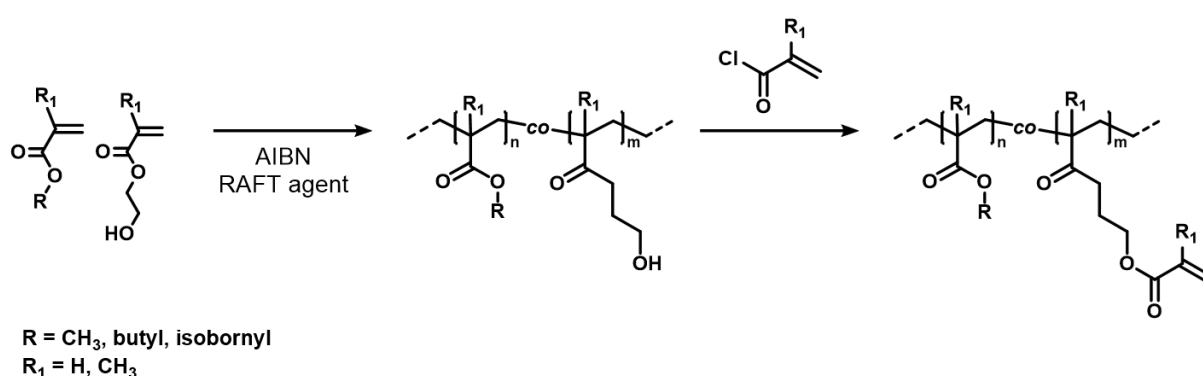


Figure 29: General reaction scheme employed for the synthesis of RAFT controlled copolymers and subsequent functionalisation with an acyl halide. R = methyl, butyl, isobornyl groups and R₁ = hydrogen or methyl group.

3.2.1 Methacrylate backbone

The first synthetic attempts were made using methacrylate monomers, as methacrylates are of the most common materials used in 3D printing and polymerisations. To that end, polymerisations of monomers 2-hydroxyethyl methacrylate (HEMA) and methyl methacrylate (MMA) were investigated, targeting low molecular weight products based on previous literature (Figure 30).^[18,122] The CTA 2-cyanoprop-2-yl dithiobenzoate (CPDB) was chosen due to its reported suitability for the polymerisation of methacrylate monomers.^[18]

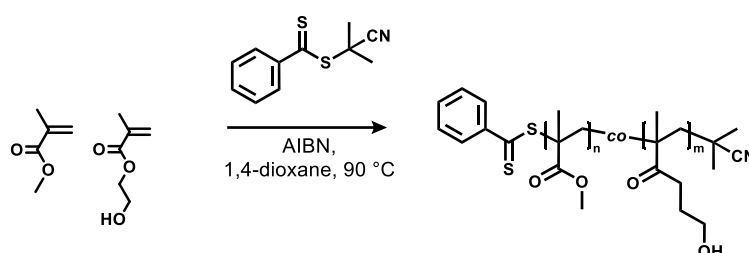


Figure 30: Exemplary copolymerisation reaction conditions of MMA and HEMA used for the synthesis of HEMA-co-MMA, using CPDB CTA.

The reaction progress was monitored and characterised with ^1H NMR spectroscopy, calculating the acrylate conversion based on the decrease of the $\text{CH}=\text{CH}_2$ protons at 5.5 and 6.0 ppm, referenced to the aromatic protons of the end group in a standard end group analysis method (Figure 31).

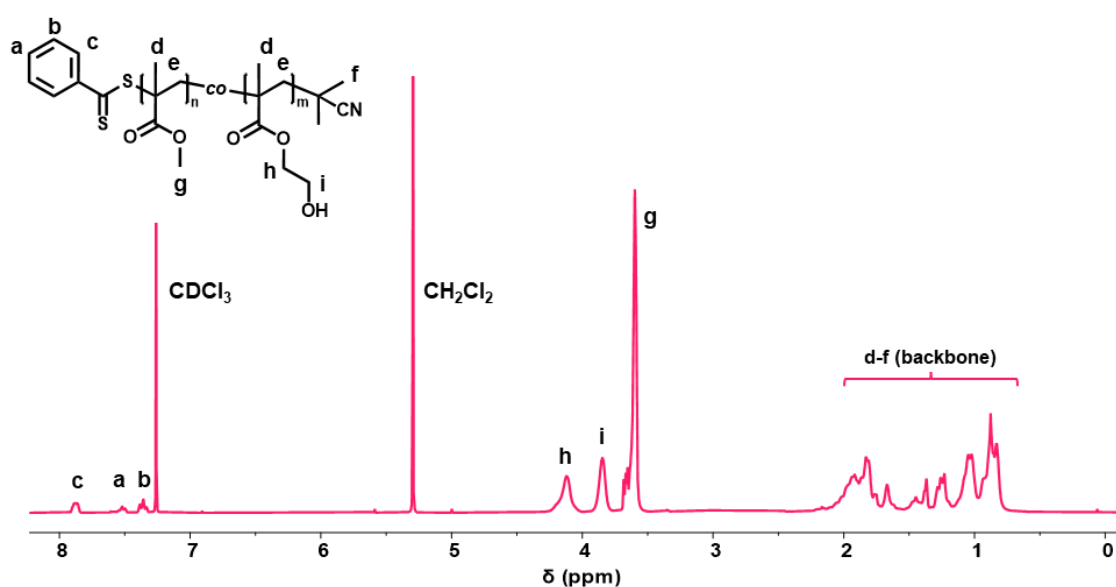


Figure 31: ^1H NMR spectrum (CDCl_3 , 300 MHz) of the polymer MMA-co-HEMA.

As seen in Figure 32, after 30 min the monomer conversion reached approx. 45% (left), with a M_n of 4700 g mol^{-1} , maintaining a dispersity of around 1.2 (right) as the reaction progressed.

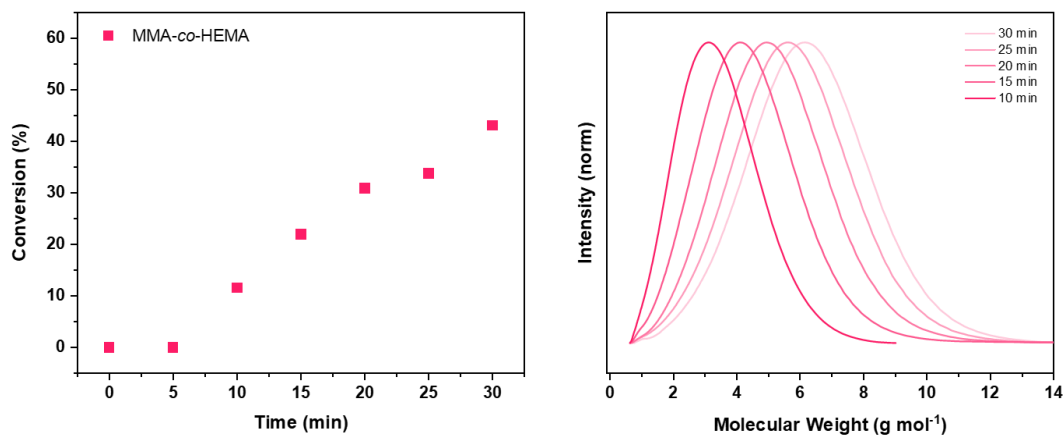


Figure 32: Monomer conversion as determined via ^1H NMR spectroscopy over the first 30 minutes of the reaction (left) and SEC traces of kinetic samples taken between 10 and 30 min (right) for the synthesis of MMA-co-HEMA.

Despite linear reaction kinetics (Figure 33) and a low molecular weight polymer, the purified product was a brittle pink solid.

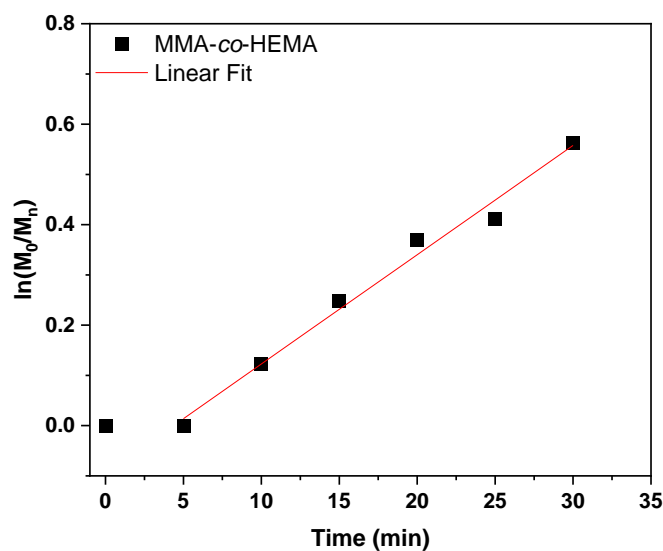


Figure 33: Graph of $\ln([M]_0/[M]_t)$ vs. time for MMA-co-HEMA the corresponding linear fits with $y = 0.022x$ with $R^2_{\text{corr}} = 0.984$

Ideally, the product would be liquid at room temperature to facilitate printing. Thus, the reaction conditions were modified from a methacrylate to acrylate backbone, using acrylate monomers, as acrylates and their polymers have lower T_g than the methacrylate analogues.

3.2.2 Acrylate backbone

For the synthesis of RAFT polymers using acrylate monomers the CTA was varied as the previous CPDB is more suited for methacrylates. Thus, for further reactions, 2-cyano-2-propyl dodecyl trithiocarbonate (CPDT) was used, and the monomers were switched to their acrylate analogues methyl acrylate (MA) and 2-hydroxyethyl acrylate (HEA) (Figure 34).

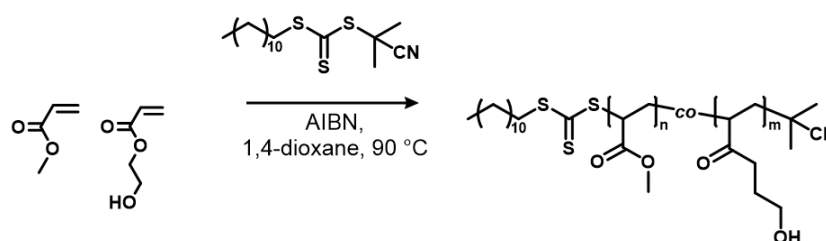


Figure 34: Reaction conditions used for synthesis of MA-co-HEA in 1,4-dioxane, using CPDT CTA.

The reaction progression was monitored over the first 30 minutes, reaching a monomer conversion of approx. 80% (left), with a M_n 6000 g mol^{-1} and a dispersity of around 1.2 (right).

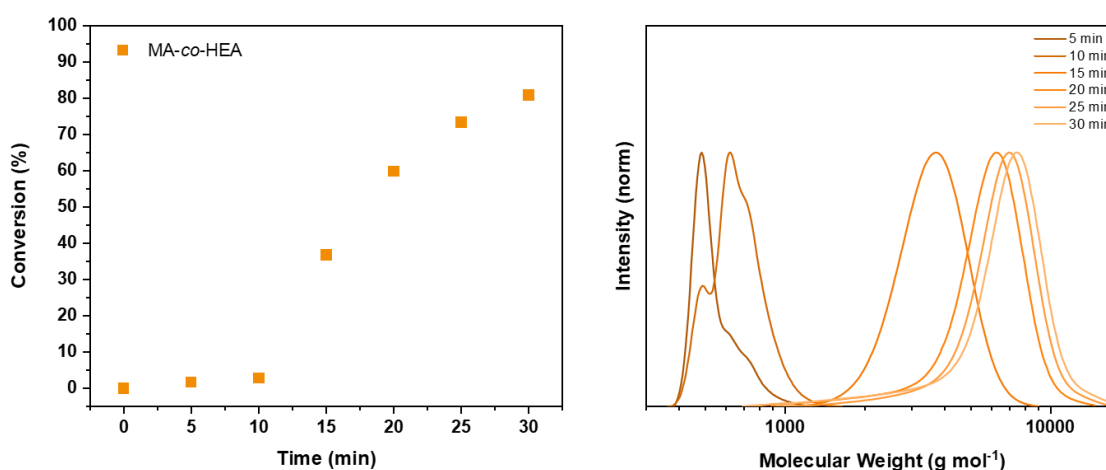


Figure 35: Monomer conversion as determined via ^1H NMR spectroscopy over the first 30 minutes of the reaction (left) and SEC traces of kinetic samples taken between 5 and 30 min (right) for the synthesis of MA-co-HEA.

Here, within the first 10 minutes, a negligible degree of polymerisation has occurred, with conversion approximately 3%—enough to allow size exclusion chromatography SEC measurements which show multimodal and low molecular weight products. However as further propagation takes place, the conversion increases and a linear behaviour is observed after the first 10 min (Figure 36).

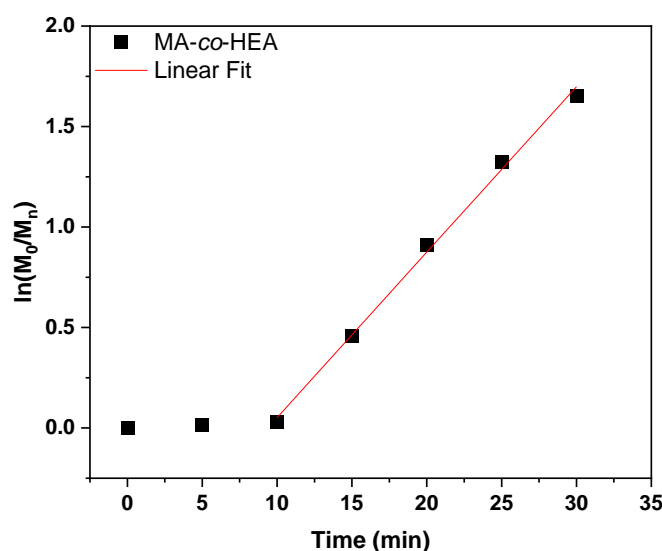


Figure 36: Graph of $\ln([M]_0/[M]_t)$ vs. time for MA-co-HEA the corresponding linear fit with $y = 0.082x$ with $R^2_{\text{corr}} = 0.996$

For simplicity of end group analysis, the solvent was changed from 1,4-dioxane to toluene, previously avoided due to the overlapping signals of this solvent with the CPDB protons that were to be used for end group analysis. With identical reaction conditions, using toluene as the solvent, the reaction reached approximately 85% conversion after 25 min (Figure 37), with a calculated molecular weight of 5300 g mol^{-1} , with 16 HEA units and 36 MA units incorporated, determined by end group analysis. The ^1H NMR spectrum of the purified product can be seen in Figure 38.

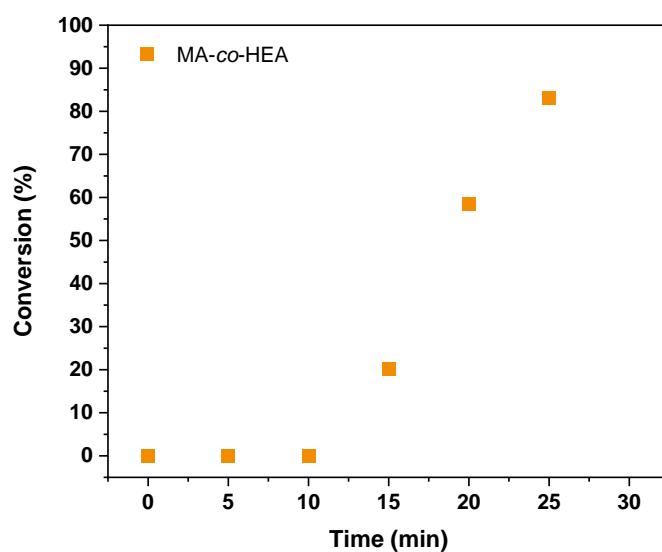


Figure 37: Monomer conversion as determined via ^1H NMR spectroscopy over the first 25 min of the reaction for the synthesis of MA-co-HEA.

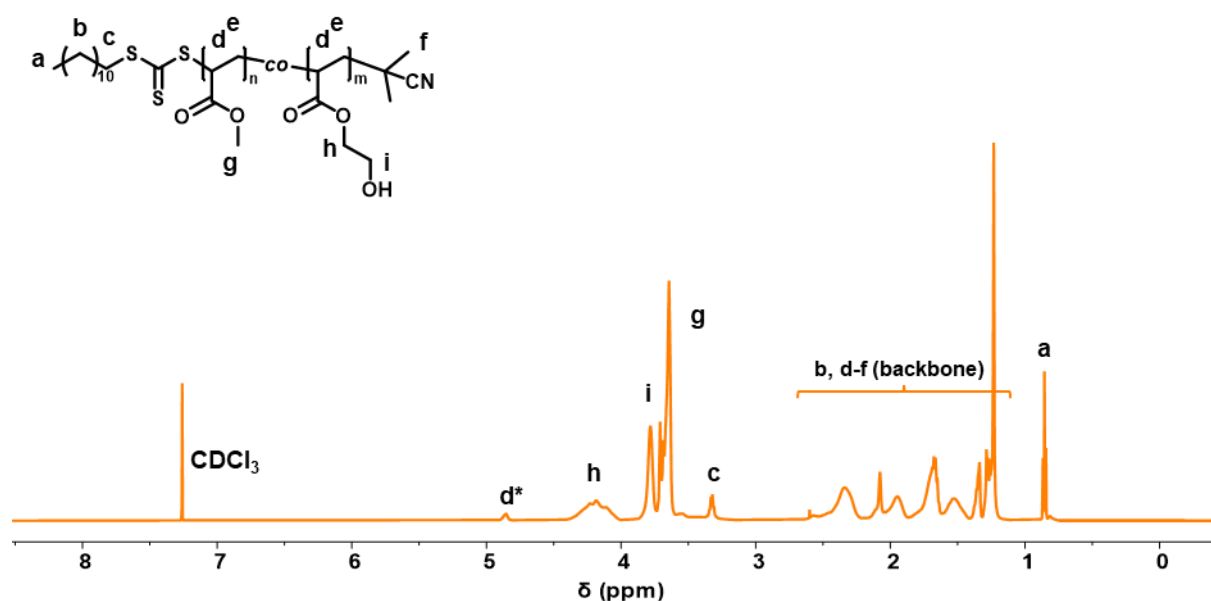


Figure 38: ^1H NMR spectrum (CDCl_3 , 300 MHz) of the polymer MA-co-HEA, d^* represents the proton of the monomer directly adjacent to the S of the CTA.

However, the overall goal was the reduce the molecular weight of the final product and ensure reproducibility of the reaction conditions. Taking inspiration from literature, where the CPDT CTA was used for the synthesis of short chain poly(methacrylate) oligomers^[21] the reaction conditions were altered slightly. With these parameters (Figure 39), and reducing the monomer equivalents, reproducible reaction conditions were achieved with

98% conversion giving a product with monomodal distribution, a dispersity of 1.1, and M_n between 2400-2500 g mol^{-1} (Figure 40). The monomer units incorporated were calculated to be an average of 5 units HEA and 9 units MA.

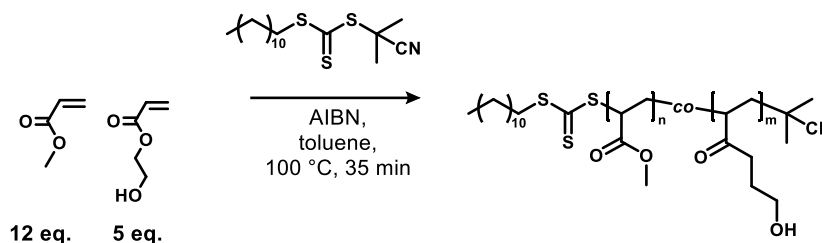


Figure 39: Reaction conditions used for the copolymerisation of MA and HEMA monomers in toluene using CPDT CTA, to give MA-co-HEA.

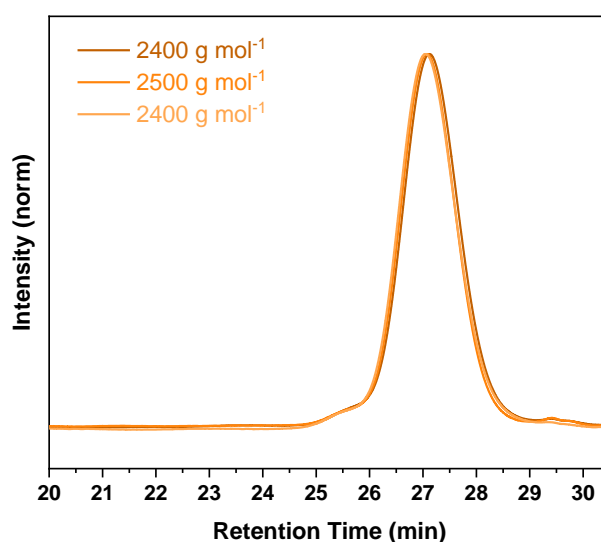


Figure 40: SEC traces of the product MA-co-HEA, demonstrating the reproducible synthesis of low molecular weight low dispersity polymer.

Following these reaction parameters, modifying slightly the monomer feed ratio, the three copolymers with the general formula **X-co-HEA** were synthesised as summarised in Table 1, where X is the comonomer either butyl acrylate (BA), methyl acrylate (MA) or isobornyl acrylate (IBA). The monomers were chosen to give a range of polymers with different T_g and molecular structure. For BA-co-HEA the monomer feed ratio was 6:4 HEA:BA (Figure 41), and the reaction success was determined through ^1H NMR spectroscopy (Figure 42).

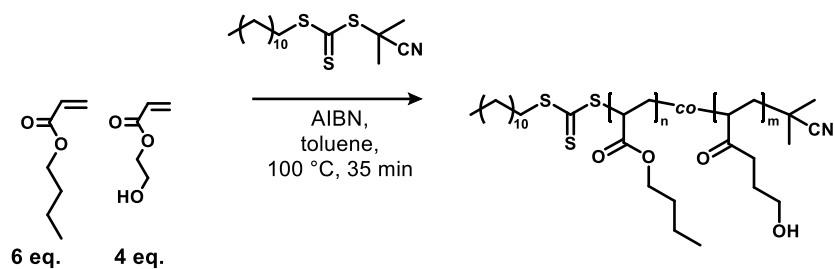


Figure 41: Reaction conditions used for copolymerisation of BA and HEA monomers in toluene using CPDT CTA, to give of BA-co-HEA.

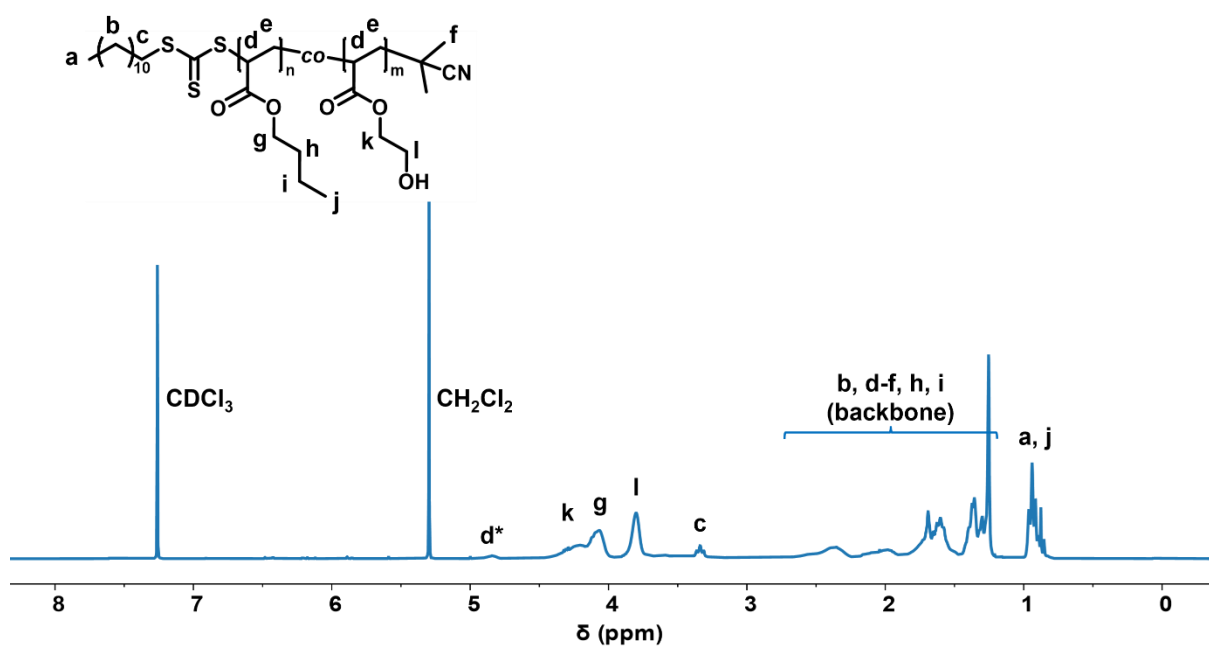


Figure 42: ^1H NMR spectrum (CDCl₃, 300 MHz) of the polymer BA-co-HEA. d* represents the proton of the monomer directly adjacent to the S of the CTA.

Conversion over the first 35 min was also measured for BA-co-HEA polymerisation (Figure 43). Here, the reaction reached approximately 65% after 35 minutes, giving a polymer with M_n of 1500 g mol⁻¹ and dispersity of 1.1. Although multiple peaks are visible in the SEC trace, the dispersity is low. This is due to the sensitivity of the SEC at very low molecular weights, in this case very slight differences in monomer unit incorporation are visible due to the specific columns used; i.e. while the product is not monomodal, the distribution varies by only a few repeat units.

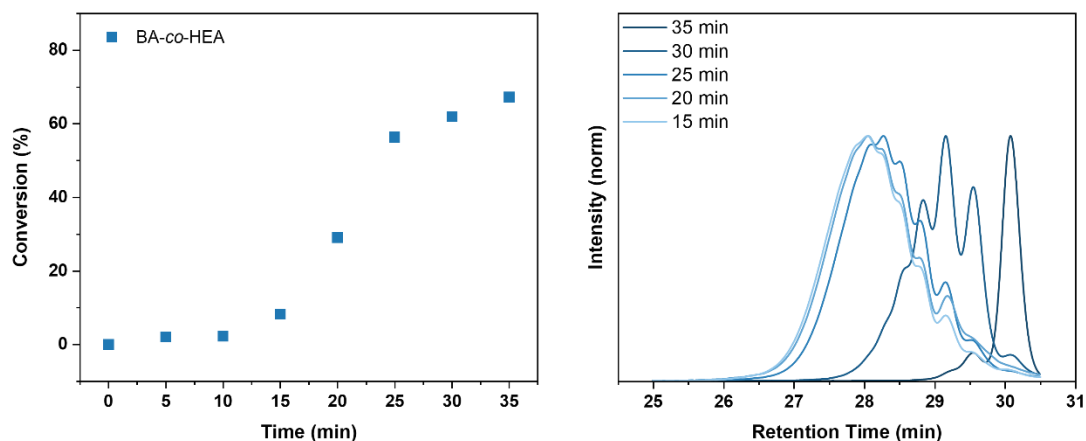


Figure 43: Monomer conversion as determined via ^1H NMR spectroscopy over the first 35 min of the reaction (left) and SEC traces of kinetic samples taken between 15 and 35 minutes (right) for the synthesis of BA-co-HEA.

The reaction kinetics were calculated as seen in Figure 44. As with MA-co-HEA, the conversion before 15 minutes was negligible.

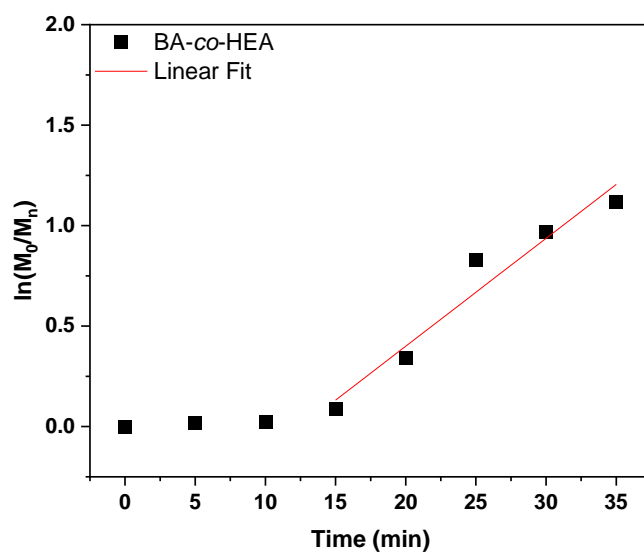


Figure 44: Graph of $\ln([M]_0/[M]_t)$ vs. time for BA-co-HEA the corresponding linear fit with $y = 0.054x$ with $R^2_{\text{corr}} = 0.930$.

The reaction was performed in triplicate, using 6 eq. of BA and 4 eq. of HEA, as per Figure 41. Again, the reproducibility was high, giving a product with a M_n of approximately 1800 g mol^{-1} , and dispersity of 1.1 (Figure 45).

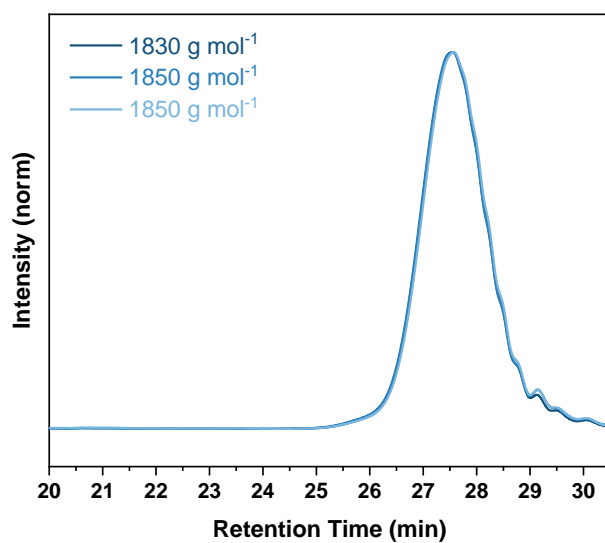


Figure 45: SEC traces of the product BA-co-HEA, demonstrating the reproducible synthesis of a low molecular weight, low dispersity polymer.

Using the same conditions, altering the comonomer feed slightly (Figure 46), the reaction was performed using IBA as a third comonomer, giving the polymer IBA-co-HEA, with an average of 7.5 units of IBA and 12.7 units of HEA as determined by ^1H NMR spectroscopy (Figure 47).

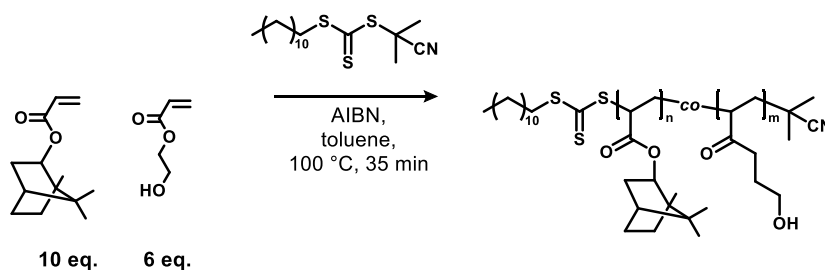


Figure 46: Reaction conditions used for copolymerisation of IBA and HEA monomers in toluene using CPDT CTA, to give of IBA-co-HEA.

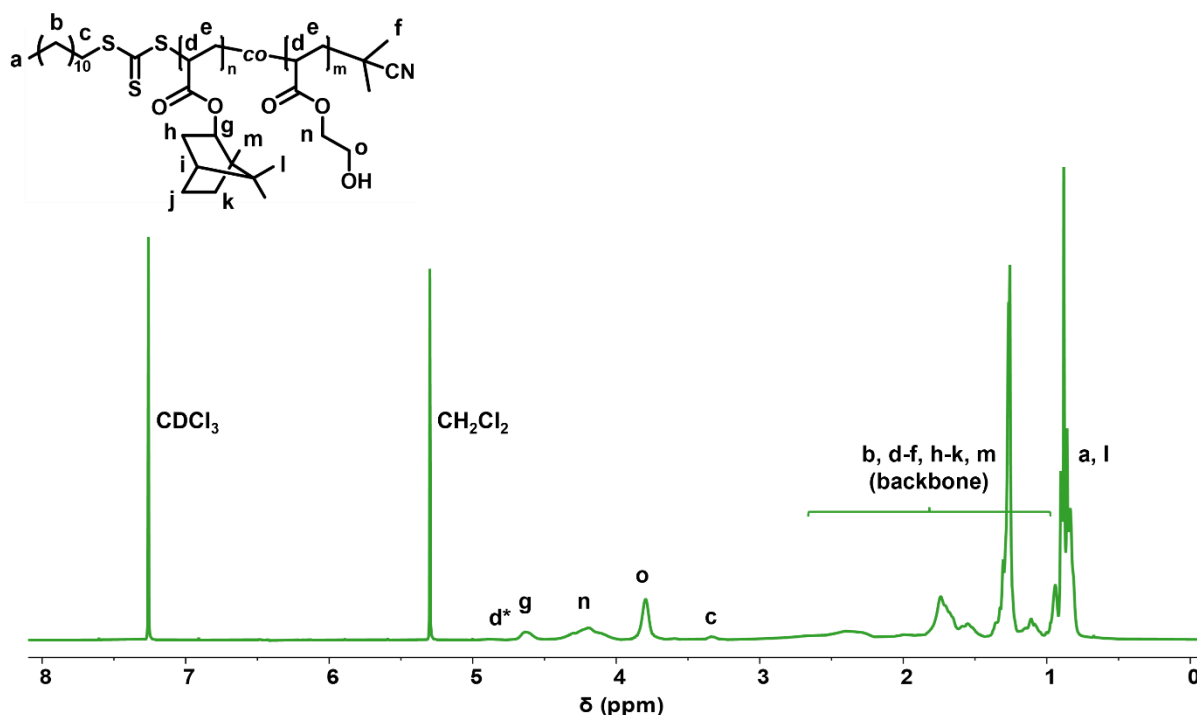


Figure 47: ^1H NMR spectrum (CDCl_3 , 300 MHz) of the polymer IBA-co-HEA.

A summary of the final resultant polymers can be seen in Table 1, along with their chemical structures in Figure 48. where d^* represents the proton of the monomer directly adjacent to the S of the CTA.

Table 1: Composition and characteristics of the three synthesised polymers: X-co-HEA.

Comonomer (X)	X	HEA	M_{nSEC} (g mol^{-1})	\bar{D}	T_g ($^{\circ}\text{C}$)
BA	4.2	4.7	1500	1.05	-44
MA	5.3	7.3	1600	1.08	-42
IBA	7.5	12.7	2900	1.07	-5

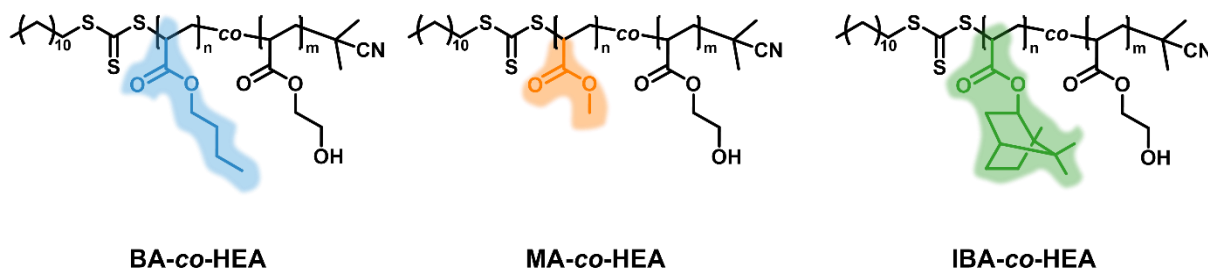


Figure 48: Chemical structure of the synthesised polymers before post functionalisation. Left to right: BA-co-HEA, MA-co-HEA, and IBA-co-HEA.

The T_g temperature was measured using differential scanning calorimetry (DSC), showing differences between the three polymers. The T_g for BA-co-HEA was the lowest at -44°C , similar to MA-co-HEA with -42°C , while IBA-co-HEA had the highest with -5°C (Figure 49a). Additionally, all products were monomodal, with BA-co-HEA again showing the lowest M_n of 1500 g mol^{-1} , MA-co-HEA with 1600 g mol^{-1} , and IBA-co-HEA the highest with a M_n of 2900 g mol^{-1} (Figure 49b). This trend is expected as the T_g typically increases with increasing molecular weight, and additionally, the T_g of IBA homopolymers is higher than that of BA and MA counterparts.^[21,123]

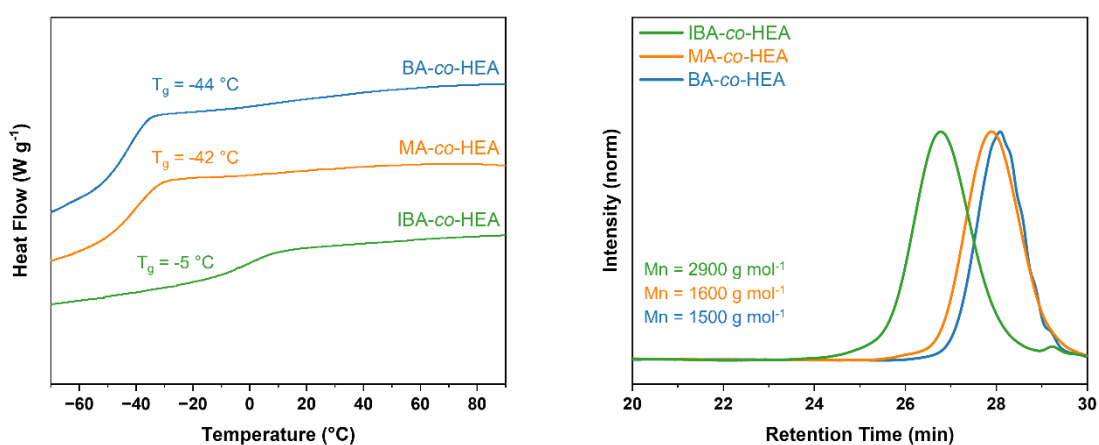


Figure 49: a) DSC and b) SEC traces for the characterisation of the three polymers BA-co-HEA, MA-co-HEA, and IBA-co-HEA, showing T_g and monomodal dispersity for the three materials.

The three polymers were functionalised to introduce an acrylate group for crosslinking during the 2PLP process. A typical reaction involved the reaction between the alcohol of the polymer with an acrylate acyl halide, resulting in an ester with the conformation X-co-Acryl (Figure 50). Excess reagents were used to ensure full conversion of the hydroxy group.

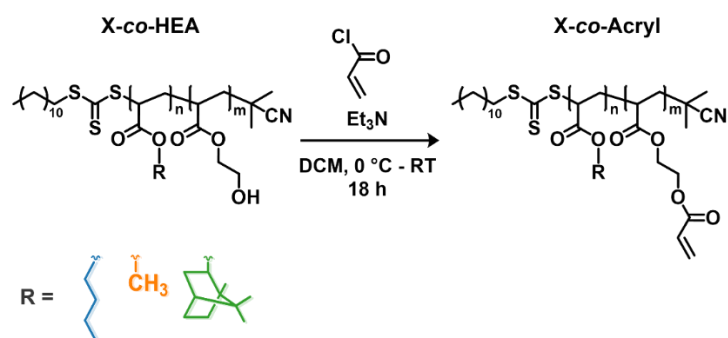


Figure 50: Reaction conditions used for the post functionalisation with acryloyl chloride of the three polymers synthesised.

The successful functionalisation was confirmed using ^1H NMR spectroscopy. It was observed previously that the purification through precipitation can also cause the separation of lower molecular weight polymers from the bulk of the product, and therefore, the final polymer repeat unit composition varies between X-co-HEA and X-co-Acryl. Thus, after purification, the composition of the final products was determined through end group analysis using ^1H NMR spectroscopy (Figure 51).

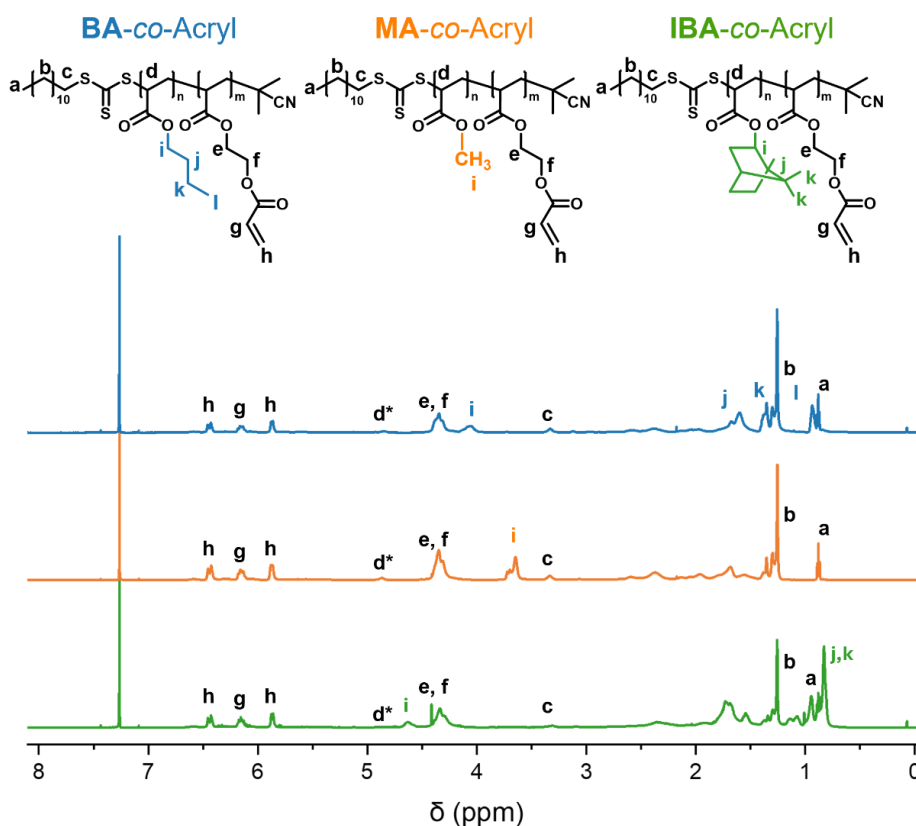


Figure 51: Chemical structure and ^1H NMR spectra (CDCl_3 , 600 MHz) of the three acrylate functionalised polymers BA-co-Acryl, MA-co-Acryl and IBA-co-Acryl (top to bottom).

The final composition of the three polymers is summarised in Table 2. Each polymer contains approximately 55% acrylate units compared to the comonomer (X), with a ratio of 1:0.8 Acryl:X. It should be noted here that the DSC (T_g) and SEC (M_n and \bar{M}_w) data refer to the unfunctionalised polymer X-co-HEA; however, the trend should remain after functionalisation.

Table 2: Chemical and physical properties of polymers with varied comonomer composition determined from a) unfunctionalized pre-polymer or b) functionalized pre-polymer.

Comonomer (X)	^{a)} M_{nSEC} ($g\ mol^{-1}$)	^{a)} \bar{M}_w	^{a)} T_g ($^{\circ}C$)	^{b)} Acrylate (%)	^{b)} Acrylate Units	^{b)} Comonomer (X) Units	^{b)} Ratio Acryl:X
BA	1500	1.05	-44	55.1	5.4	4.4	1 : 0.8
MA	1600	1.08	-42	56.3	6.3	4.9	1 : 0.8
IBA	2900	1.07	-5	54.7	8.1	6.7	1 : 0.8

3.3 PRE-POLYMER INKS FOR 2PLP: STRUCTURE-PROPERTY RELATIONSHIPS

3.3.1 Ink formulation

A typical ink formulation for 2PLP contains the crosslinkable species and the photoactive species that will initiate the reaction. For this purpose, an efficient and well known 2PLP photoinitiator DETC was chosen. To solubilise the photoinitiator within the polymer components, a solvent was added. In this case, the initial solvent chosen was N,N-dimethylacetamide (DMAc). The composition of polymer 66 weight percent (wt%) with 0.5 wt% DETC in DMAc proved successfully printable; however, after further investigation it was determined that after development of the unreacted polymer material, some DMAc remained in within the printed structures. This resulted in unreliable and nonreproducible results during characterisation of the printed structures, for example, as the carbonyl stretch is used as a reference band when measuring IR spectroscopy any remaining DMAc influences the intensity of this band. Thus, another high boiling point solvent, 1,4-dioxane, was used for further printing, keeping the composition otherwise constant. Using this formulation, high resolution structures with fine features and overhangs could be fabricated using the three inks (Figure 52).

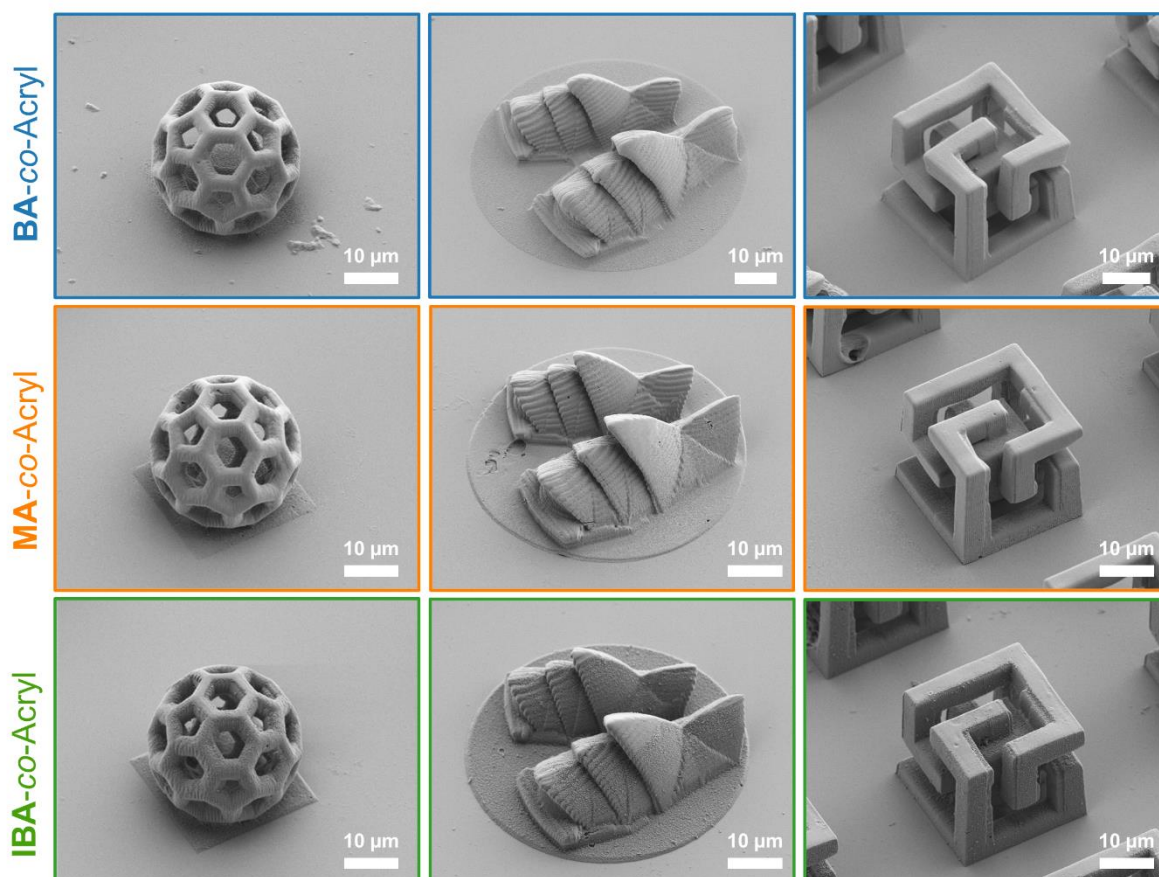


Figure 52: SEM images of 3D structures with high resolution and fine features (left to right: fullerene Buckyball, Sydney Opera House, and a geometrical bridge structure) printed using all three inks with the printing parameters 32.5 mW and 15 mm s⁻¹.

3.3.2 Printability window

With the previously optimised formulation, each of the three inks were investigated to determine their printability. Here, two parameters are scanned based on the 2PLP method. First, it is possible to vary the laser power dosage within each voxel, from 0 to 50 mW, 50 being the maximum laser intensity available for the printer. The second parameter is the scan speed; the speed at which the laser focus is moved throughout the ink, in this case in the range of μm to mm s^{-1} . The Buckminster C60 fullerene ‘buckyball’, was chosen as the standard structure to determine printability, due to the complex shape and hollow centre. After printing an array of this structure with varied laser power (15 – 40 mW) and scan speed (10, 15 and 20 mm s⁻¹), the window of printability can be easily determined visually through SEM images (Figure 53). The window of printability is defined

as the laser power and scan speed parameters for each ink whereby free standing structures with defined pores are clearly visible, as seen in the highlighted structures on the left of Figure 53. Above this window, the dosage becomes too high leading to localised ‘microexplosions’ and overexposure, resulting in uncontrolled polymerisation and undefined printed structures. Below the threshold of printability, the dosage is too low, leading to insufficient polymerisation and structure deformation and insufficient crosslinking, where the buckyball has either collapsed, or is not fully formed.

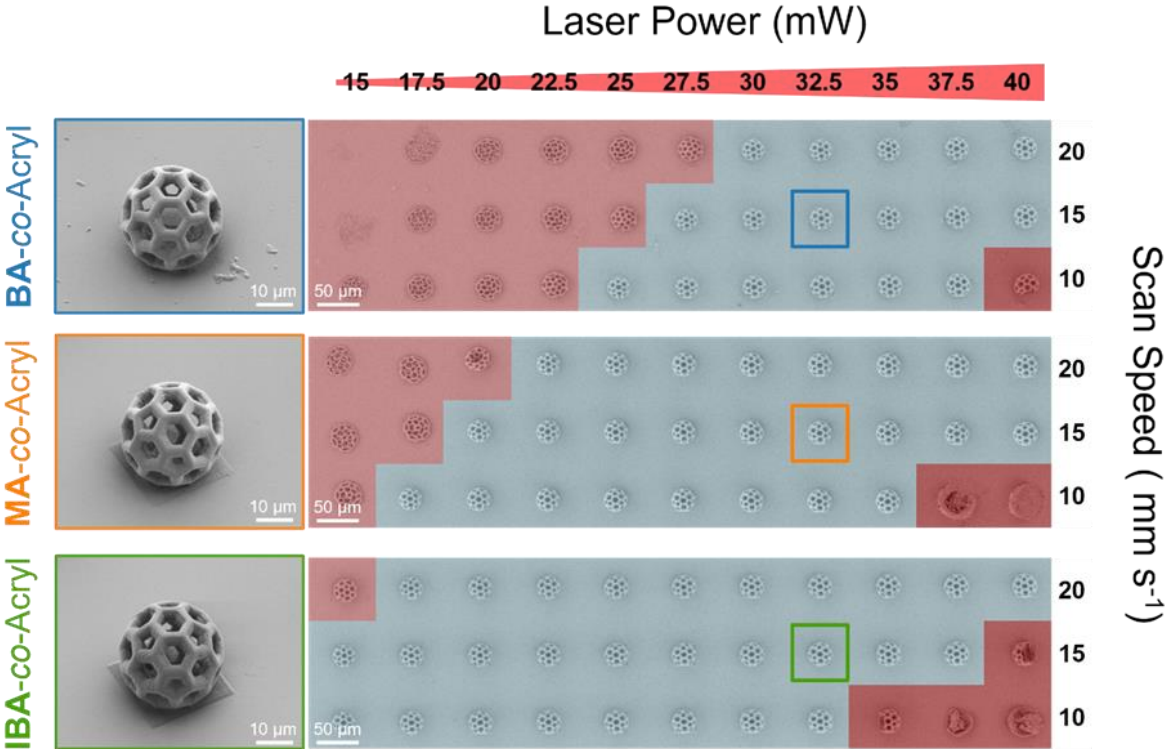


Figure 53: SEM images of buckyballs printed with the three polymer inks with varied laser power (15 – 40 mW) and scan speed (10, 15, 20 mm s⁻¹) showing the determined printability range of each ink. The window of printability is determined as the laser power and scan speed parameters where the structures remained stable (blue), above and below this range under or overexposure occurred (red). Representative SEM images of structures printed with parameters within the printing window with the three inks BA-co-Acryl, MA-co-Acryl and IBA-co-Acryl are highlighted.

Increasing the scan speed effectively lowers the laser power dosage, thus increasing scan speed results in a shift of the printability window to higher laser powers. This trend was observed for all three polymer inks. Comparing the three inks, specifically when printed at 15 mm s⁻¹, the BA-co-Acryl ink shows the smallest printing window, beginning

at 27.5 mW, requiring the highest laser power to form stable structures. The MA-co-Acryl ink had a printing window beginning at approximately 20 mW, compared to IBA-co-Acryl where stable structures were already realised at 15 mW. However, at the higher laser power range, IBA-co-Acryl displayed overexposure when printing with 40 mW, which was not the case for the two other inks. As each ink was formulated with identical composition of polymer, photoinitiator, and solvent, it is likely that the differences in printability arise due to the macromolecular composition i.e. the comonomer, as well as the molecular weight and T_g . BA-co-Acryl and MA-co-Acryl have similar T_g and M_n ; however, BA-co-Acryl has slightly fewer acrylate units overall (5.4) compared to MA-co-Acryl (6.3), lowering the minimum printability threshold. This is further supported by the larger range of 15 – 37.5 mW, observed for IBA-co-Acryl, which has even more acrylate units (8.1). However, when considering the effect of comonomer, the IBA polymer additionally has a higher T_g and M_n , which may also increase the printability range.

3.3.3 Structure–property relationships

Chemical conversion: Infrared microscopy

To gain deeper insight into the relationship between the network formation and what is happening at the molecular level during the printing, with the goal of relating that to the ink composition and printing window, infrared spectroscopy was measured for all three inks. Here, cubic structures of $40 \times 40 \times 10 \mu\text{m}^3$ were fabricated over the same printing window as used for the printability study, and IR spectra were recorded for each parameter. Two distinct bands are observed, characteristic of carbonyl stretching (C=O) at 1725 cm^{-1} , as well as bending at 808 (C=C) (Figure 54).

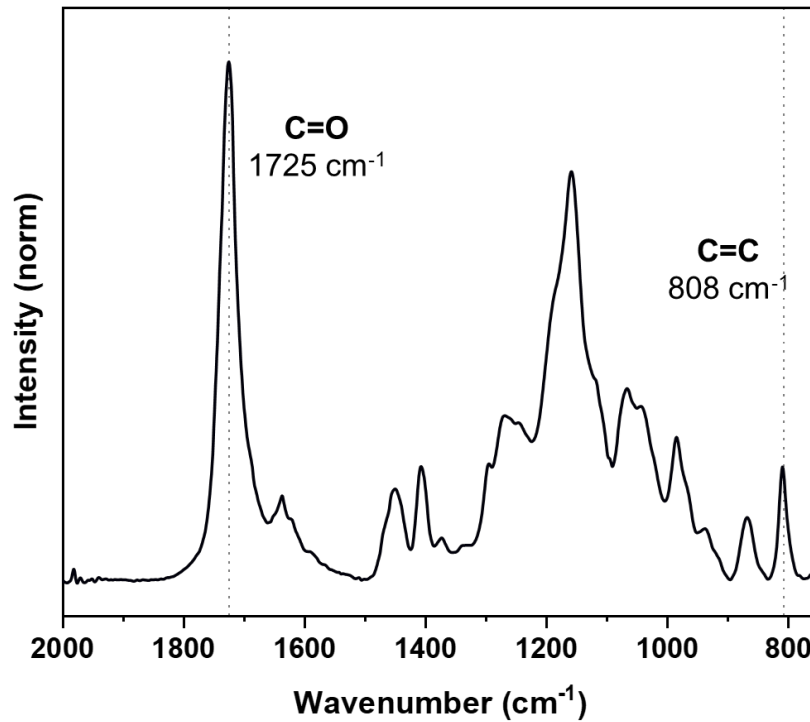


Figure 54: Exemplary FT-IR spectra of BA-co-Acryl, with distinct bands corresponding to the acrylate double bond (C=C) at 808 cm⁻¹ and carbonyl stretch (C=O) at 1725 cm⁻¹.

The carbonyl does not participate in the reaction, while the C=C of the acrylate reacts to form new carbon-carbon bonds. Thus, using Equation 5, it is possible to calculate the degree of acrylate conversion by comparing integrated spectra of printed structures to the reference spectrum of the unprinted ink, assuming the carbonyl remains constant throughout the reaction.^[102,105,120]

$$DoC \% = \frac{(A_{C=C} / A_{O-C=O})}{(A_{C=C}^{resin} / A_{O-C=O}^{resin})} \times 100 \quad \text{Equation 5}$$

After analysing the range of printed structures for all three inks, the DoC of acrylate over the laser power range is seen in Figure 55, where the scan speed was kept constant at 15 mm s⁻¹.

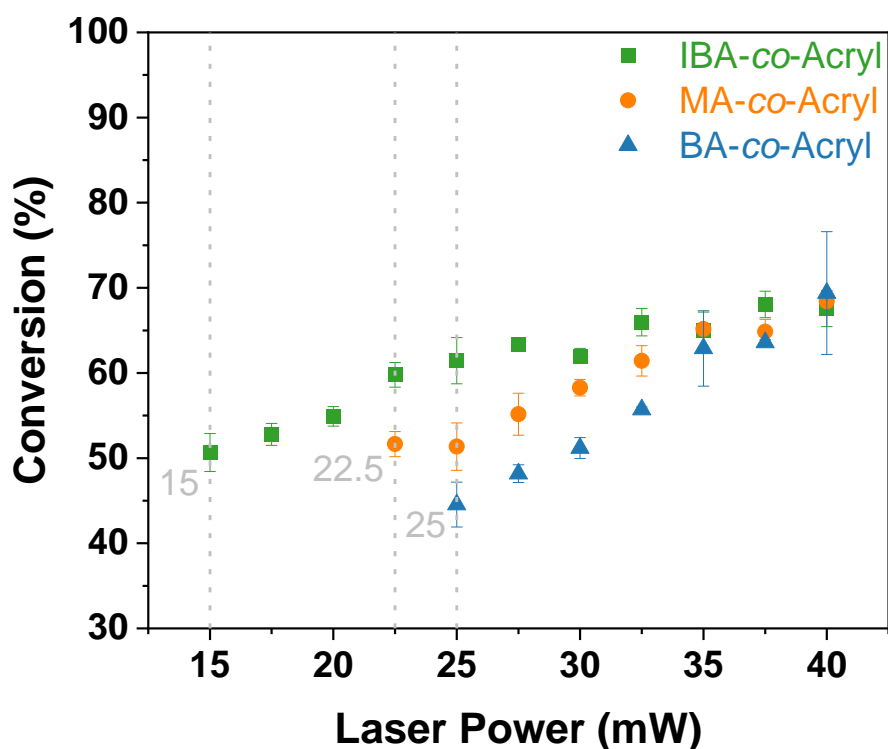


Figure 55: Degree of acrylate conversion, calculated from FT-IR spectroscopy, showing an increase in conversion with increasing laser powers for structures printed with IBA-co-Acryl, MA-co-Acryl and BA-co-Acryl inks. Annotations indicate the laser power minimum threshold for measurement.

As expected, increasing the laser power in turn increases the acrylate conversion. In Figure 55, a grey dashed line indicates the minimum measurable laser power. Below this value, structures could be printed; however, they could not be measured. Likely in the case of Fourier-transform infrared (FTIR) microscopy measurements, the pressure of the attenuated total reflectance (ATR) diamond tip was too high, and the structures too soft, leading to the interference of the glass slide underneath as the structure was completely crushed. Interestingly, all three inks showed a similar DoC over the printable range, beginning at 45-50% for the minimum, up to approximately 70% before overexposure occurred. Despite similar overall range of DoC, each ink required different laser power doses to achieve this lower threshold. For example, the BA-co-Acryl ink required much higher laser power to reach the same DoC as IBA-co-Acryl, and slightly higher laser power than MA-co-Acryl. All three inks reach a similar DoC at the highest laser power around 70%.

Mechanical properties: Nanoindentation

To examine the mechanical properties of the printed structures and investigate any correlation between mechanical and chemical properties as well as printability, nanoindentation was performed on printed nanopillars with a diameter of 60 μm and a height of 15 μm . In particular, by calculating the slope of the tangent of the elastic unloading curve from the load–displacement curve, it was possible to determine the reduced elastic modulus, E_r , which represents the elastic deformation in the microstructures, as well as the hardness.^[108] E_r was measured over a range of laser powers for each ink. A similar trend is observed here for the lower threshold, as was seen for the printability window and IR spectroscopy; approximately 15-17.5 mW for IBA-co-Acryl, 20-22.5 mW for MA-co-Acryl, and 25-25.7 mW for BA-co-Acryl, as seen by the grey dashed lines in Figure 56. This supports the idea that below this threshold value the structural integrity is too low for accurate measurements, and unable to form a stable network for printing.

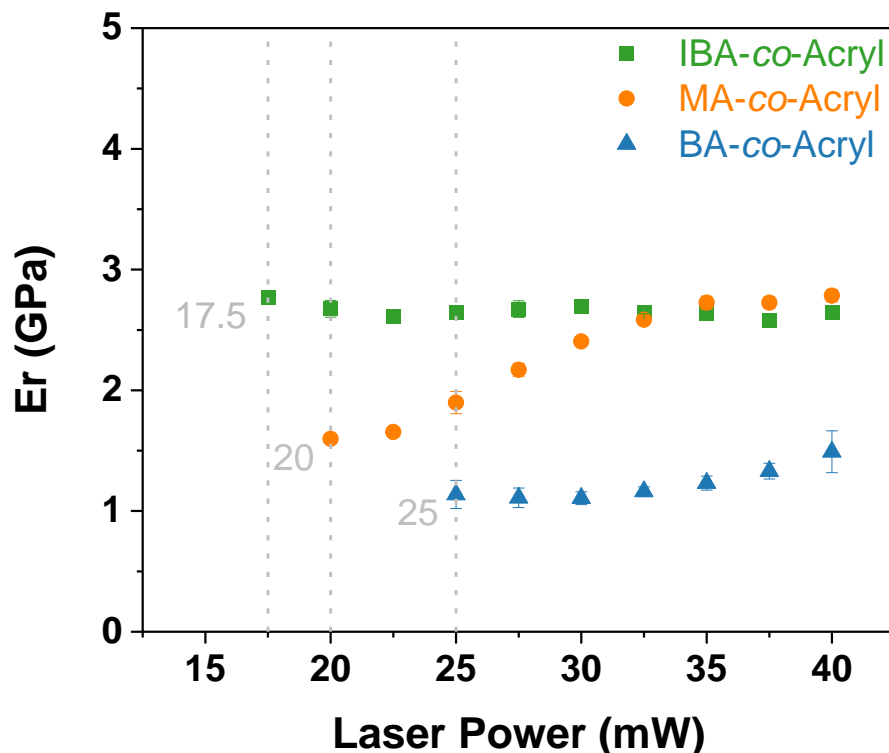


Figure 56: Nanoindentation measurements for structures printed with IBA-co-Acryl, MA-co-Acryl and BA-co-Acryl inks giving reduced elastic modulus over increasing laser powers. Annotations indicate the laser power minimum threshold for measurement.

Above this lower threshold laser power the pillars appear similar to the desired geometry with a diameter of 60 μm , whereas below this threshold deviation is observed, for example as shown in the SEM images of pillars used to measure nanoindentation for BA-co-Acryl in Figure 57. This effect may contribute to the unrealistic E_r values obtained for measurements below this threshold.

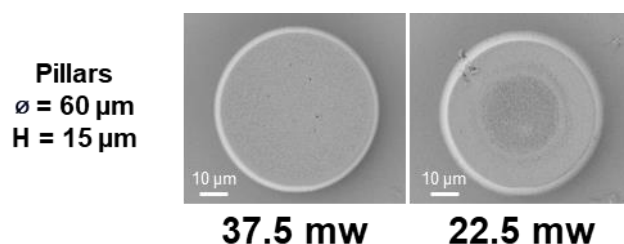


Figure 57: SEM images of representative 2PLP printed micropillars printed at higher (37.5 mW) and lower (22.5 mW) laser powers, showing the shrinkage and deformation at lower laser power.

Overall, IBA-co-Acryl showed the highest reduced elastic modulus over the laser power range, seemingly independent of the degree of acrylate conversion with a consistent modulus of approximately 2.6 GPa. For MA-co-Acryl a slight increase from 1.6 GPa at 20 mW to 2.8 GPa at 40 mW was observed, reaching a similar E_r as IBA-co-Acryl at 40 mW. The BA-co-Acryl ink displayed the lowest modulus overall, from 1.1 – 1.5 GPa for 25 – 40 mW, respectively. Despite the increase in acrylate conversion for BA-co-Acryl from 44.5 to 69.4% over the laser power range, the increase in E_r is not as significant when compared to the increase observed for MA-co-Acryl of 1.2 GPa over a similar DoC range (51.7 – 68.5%). A similar trend is seen for all pre-polymers when measuring hardness (Figure B1). When considering the effect of molecular composition of polymers and the topology of the network formed, it has been previously shown that alkyl chains, such as the butyl groups in BA-co-Acryl, can have a plasticising effect on the crosslinked network, softening the material.^[38,93] The plasticising effect of butyl groups as dangling chains within the BA-co-Acryl printed structures, may account for the lowered reduced modulus, in particular when compared to the MA-co-Acryl ink which has a similar molecular weight, glass transition temperature, and number of acrylate groups. On the other hand, the isobornyl groups in IBA-co-Acryl, as well as the increased molecular

weight, increase the T_g which may contribute to the increased printability and higher reduced elastic modulus of the printed structures.

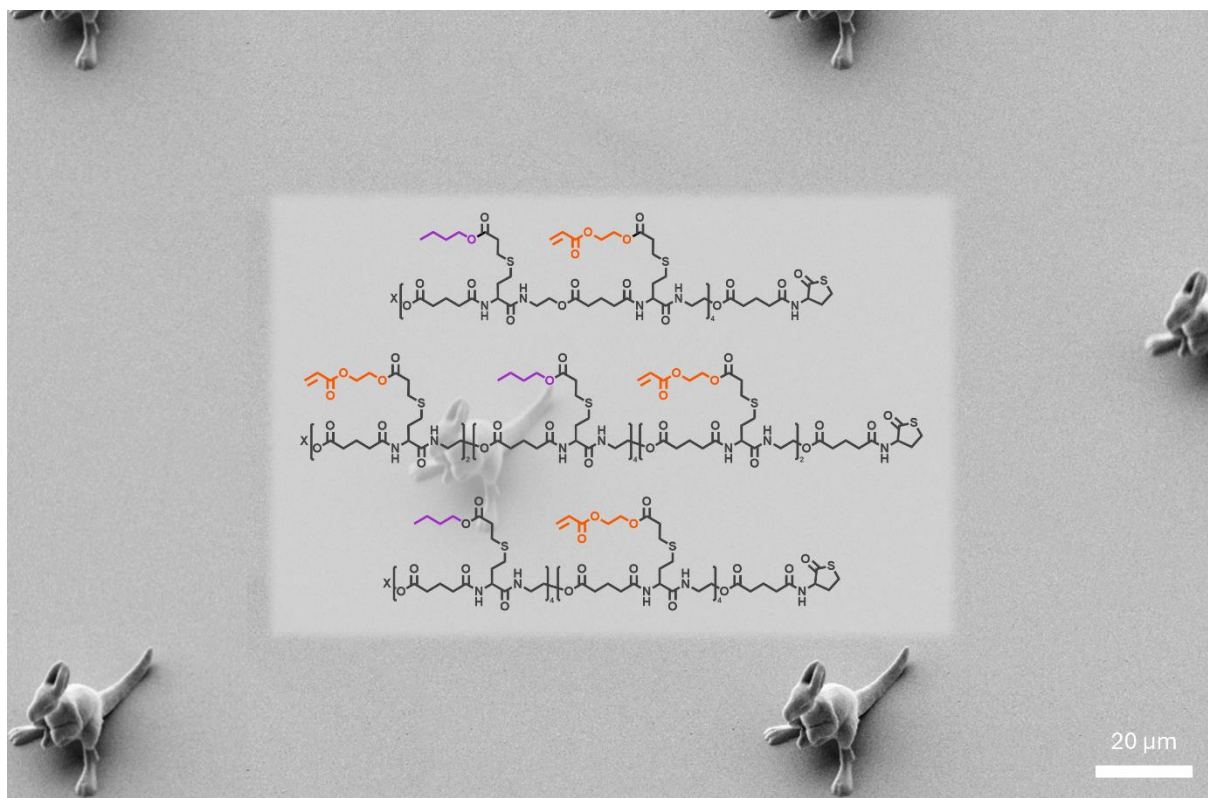
3.4 SUMMARY

A library of three pre-polymers with varied comonomer compositions was fabricated, formulated into inks for 2PLP, and characterised, allowing relationships between molecular composition, printing properties, and mechanical and chemical properties to be investigated. The three 'pre-polymer' inks were synthesised through controlled RAFT copolymerisation of the hydroxy group containing monomer HEA and three comonomers: either butyl, methyl or isobornyl acrylate (BA, MA, and IBA, respectively). The resultant low molecular weight polymers (BA-co-HEA, MA-co-HEA, and IBA-co-HEA) were characterised via SEC and DSC to determine their molecular weight and dispersity, and glass transition temperature, respectively. The BA-co-HEA pre-polymer had a molecular weight of 1500 g mol^{-1} , similar to that of MA-co-HEA with 1600 g mol^{-1} , the molecular weight of IBA-co-HEA was higher at 2900 g mol^{-1} ; however, all three had a low dispersity of approximately 1.1. The T_g followed a similar trend, with BA, MA, and IBA pre-polymers having transition temperatures of -44 , -42 , and $-5 \text{ }^\circ\text{C}$, respectively. Each pre-polymer was then functionalised through the hydroxy groups to introduce crosslinkable acrylate moieties for 2PLP, resulting in a ratio of 1:1 acrylate (Acryl) to comonomer, as determined by ^1H NMR spectroscopy. Using optimized ink formulations containing a suitable two-photon photoinitiator (DETC, 0.5 wt%), and a percentage of solvent to solubilise each component (1,4-dioxane, 33.5 wt%), various structures were printed with 2PLP and characterised for their chemical and mechanical properties.

The printability range was determined by printing and imaging structures with SEM. Across varying laser powers, the DoC of acrylate for the printed structures was examined via FTIR microscopy, and the mechanical properties, such as reduced elastic modulus and hardness, were determined using nanoindentation. When considering a single scan speed (15 mm s^{-1}), it was found that each ink displayed a different minimum laser power for printing stable structures. This laser power was lowest for IBA-co-Acryl, followed by MA-co-Acryl and BA-co-Acryl with 15, 20, and 27.5 mW, respectively. The degree of acrylate conversion was measured within this range for each ink using FTIR microscopy.

For all three inks, the DoC at the lower threshold was between 45 – 50 %, reaching 70 % at the maximum. Thus, although the DoC required for printing of stable structures was similar for each ink, the laser power required to reach this threshold differs depending on the pre-polymer. When considering the mechanical properties of the printed structures for each ink, the same lower laser power threshold trend is observed. Additionally, IBA-co-Acryl exhibited the highest E_r (around 2.6 GPa), which was consistent across different laser powers, regardless of DoC. MA-co-Acryl showed an increase in modulus from 1.6 GPa at 20 mW to 2.8 GPa at 40 mW, reaching a similar modulus as IBA-co-Acryl at the highest laser power. BA-co-Acryl had the lowest modulus overall, ranging from 1.1 to 1.5 GPa between 25 and 40 mW. Although the DoC of BA-co-Acryl increased significantly, the rise in modulus was less pronounced compared to MA-co-Acryl. It is proposed that this may be due to effects of the macromolecular structure, for example, through differences in the network topology. In the case of BA-co-Acryl, which displayed the lowest E_r and required the highest laser power, the butyl side chains may act similarly to a plasticiser to lower the E_r of the printed structures, despite the similar DoC to the other inks. On the other hand, the increased number of acrylate groups in the IBA-co-Acryl ink may contribute to the lower laser power requirement, while the high E_r may be influenced by the higher T_g and molecular weight. Overall, a clear correlation between the comonomer choice, as well as physical and molecular properties, and their influence on the printing behavior and resultant properties of 2PLP structures, was observed. It is shown that through careful consideration of pre-polymer design, it is possible to create tailored material properties in 2PLP microstructures.

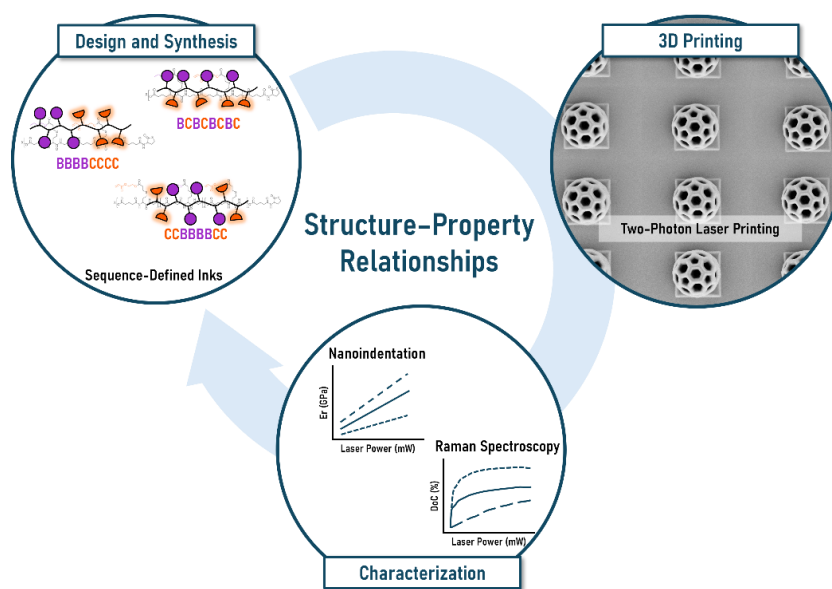
4 Sequence-defined oligomers as 2PLP inks



The results described in this chapter have been published:^[93]
S. O. Catt, M. Hackner, J. P. Spatz, E. Blasco*, *Macromolecular Engineering: From Precise Macromolecular Inks to 3D Printed Microstructures*, Small, 2023, 19, 2300844

4.1 MOTIVATION AND AIMS

This chapter takes the molecular control of inks to a higher degree, through the synthesis of precise oligomers with varied side chain sequences for 2PLP. Although sequence-defined materials have been used in various applications, few examples of covalent crosslinking of sequence-defined molecules have been demonstrated. Herein, we present the first example of 3D printing of sequence-defined inks. In this chapter, three sequence-defined polymer inks are designed, consisting of two monomers—either non-functional (B) or crosslinkable (C)—in varied patterns termed alternating (BCBCBCBC), triblock (CCBBBBCC) or block (BBBBCCCC). The three oligomers are formulated into inks for the printing of structures through 2PLP, and the properties of these structures are characterised chemically and mechanically, through Raman spectroscopy and nanoindentation, respectively. Due to the precise control of the molecular structure, in particular the positioning of the crosslinkable monomer group, it is possible to determine relationships between the macromolecular sequence and the network formation of the printed structures as well as how these characteristics affect the crosslinking and mechanical properties (Scheme 2).



Scheme 2: Overview and relationship of the steps explored in the following work: design and synthesis of the three crosslinkable oligomers with controlled monomer sequence, 2PLP of 3D microstructures from the formulated inks, chemical and mechanical characterisation of the 3D microstructures, and the relationships from macromolecular control to printed microstructures.

4.2 SYNTHESIS OF SEQUENCE-DEFINED OLIGOMERS

Several approaches exist for the synthesis of sequence-defined macromolecules, as discussed in Chapter 2.2, most often using a multistep growth method. Here, for the preparation of precise oligomers, a solid-phase linear iterative synthesis method was chosen, inspired by and originally developed for the synthesis of peptides. This method uses iterative steps of chemical reactions of monomer units to build oligomeric or polymeric chains in a linear fashion, where the often labour intensive and time-consuming purification step is facilitated by a solid (or insoluble) support. An example of how this methodology was adapted for the synthesis of sequence-defined oligomers herein is shown in Figure 58.

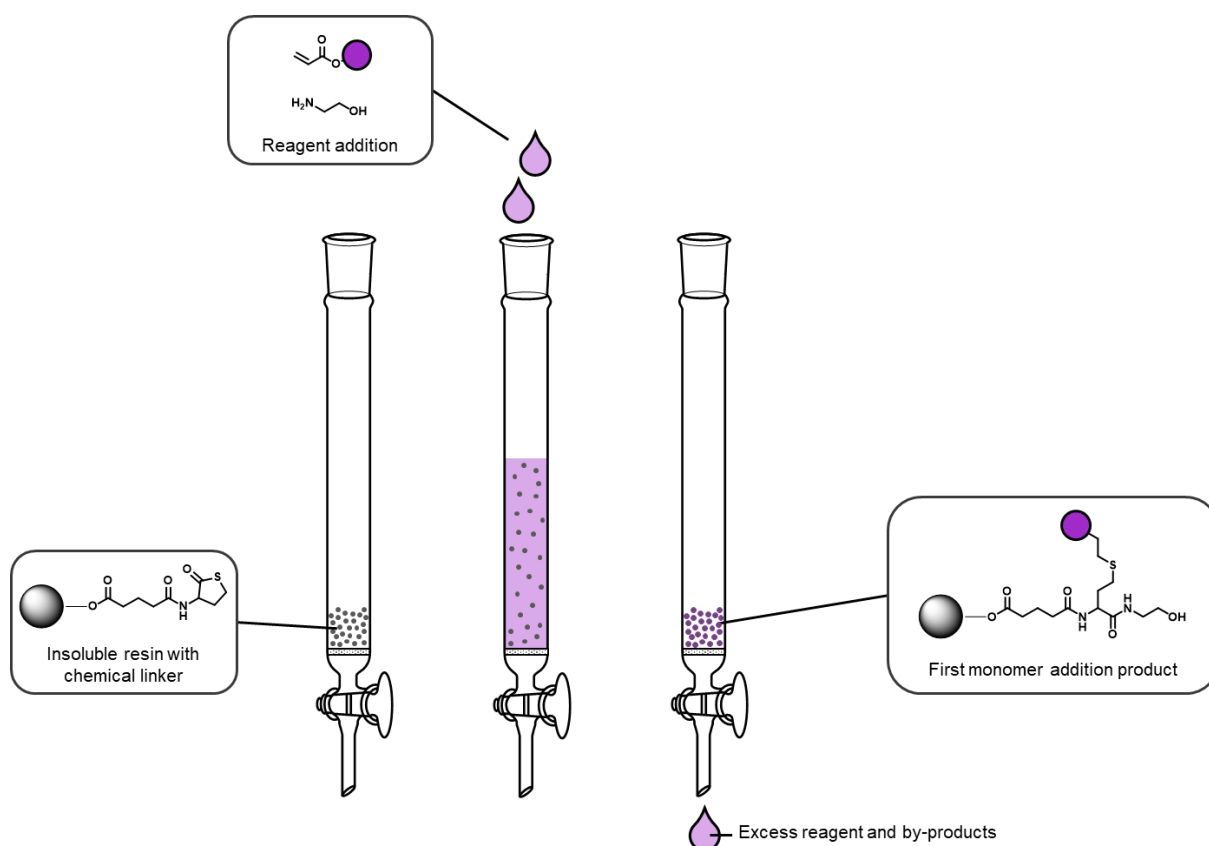


Figure 58: General reaction set up for solid-supported synthesis with an insoluble resin, whereby resin and reagents are added to the vessel, shaken, and then excess is washed out after reaction is complete. The first monomer addition step is shown as an example.

As the multistep growth synthesis pathway typically involves a reaction between two functional moieties, it is necessary to ensure selectivity when planning the synthetic

protocol, i.e. monomers and products should not contain functional handles that are able to participate in the reaction in an undesired manner, therefore leading to side-products. This has led to the development of sequence-defined polymers with either ‘non-functional’ monomers, or the requirement to protect any functional groups that should not react in situ. Using this solid-supported synthesis method, three oligomers with eight-unit length were targeted: alternating (BCBCBCBC), triblock (CCBBBBCC) or block (BBBBCCCC) (Figure 59). This specific design of the three oligomers was chosen as it allows precise positioning of the crosslinkable acrylate group along the backbone.

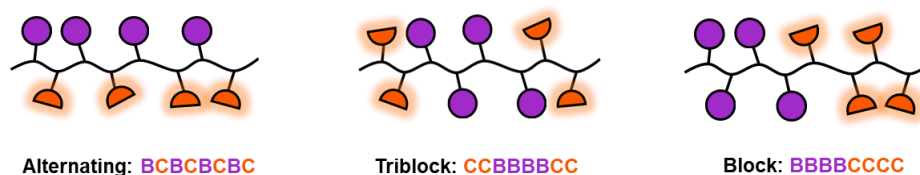


Figure 59: Schematic representation of the three oligomers targeted in this project from left to right: alternating, triblock, or block, where B (purple) represents the non functional monomer and C (orange) represents the functional/crosslinkable monomer.

Herein, after optimisation, solid supported iterative monomer/linker addition synthesis methods were used, adapted from previous literature.^[124–126] For forming the oligomers on the solid resin generally involved three steps: **i)** functionalisation of the resin with a linker molecule, which in all cases was a thiolactone, **ii)** introduction of the chosen monomer, and **iii)** extension of the chain with the linker molecule. **iv)** After the formation of the desired sequence, it is cleaved from the solid support and **v)** the crosslinkable group is introduced in the last step after the solid support is removed. A schematic of the general optimized synthesis procedure with five steps can be seen in Figure 60. To achieve defined oligomers with the most straightforward synthetic route, two types of linker molecules were investigated (4.2.1: Optimized choice of linker molecule). It was also necessary to introduce the monomer that will be used for the introduction of the crosslinkable molecule, which required a functional moiety to be protected during the iterative synthesis steps and therefore different protecting groups were also investigated (4.2.2: A study of protecting groups for controlled reaction conditions).

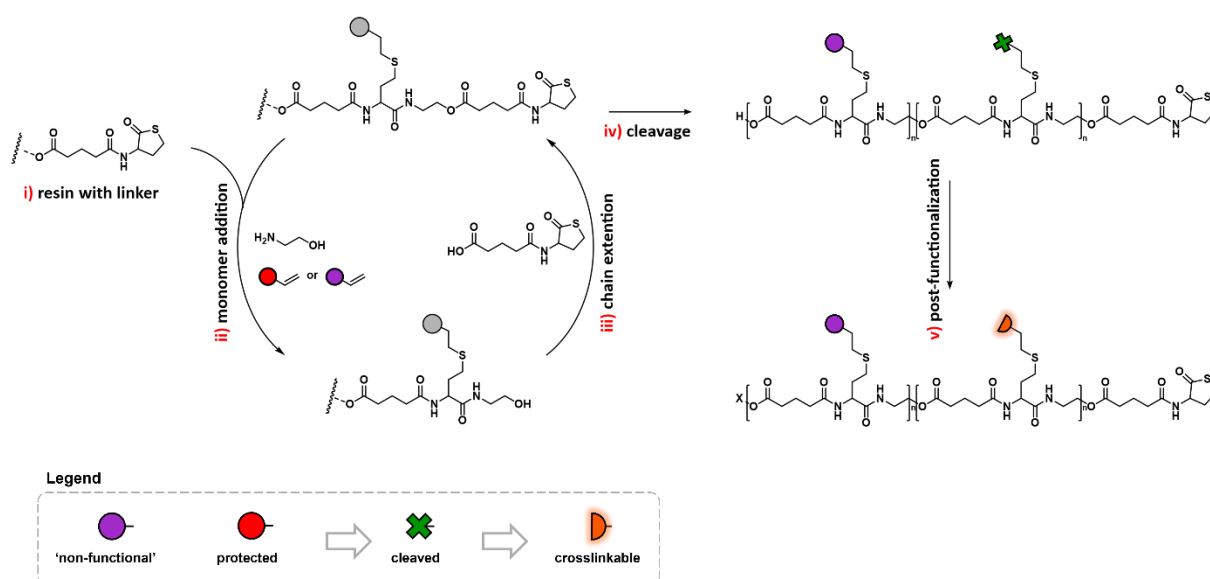


Figure 60: Simplified schematic of the iterative solid resin phase synthesis procedure with four steps: i) introduction of the linker to the insoluble resin, ii) introduction of the monomer of choice, iii) chain extension, i.e. reintroduction of the linker molecule, and iv) cleavage of the insoluble resin.

4.2.1 Optimized choice of linker molecule

As shown in Figure 60, after each monomer addition step, it is necessary to reintroduce the linker molecule (in this case a thiolactone) in order to allow the next monomer addition. Here, two types of linker molecules were synthesised and characterised by ^1H NMR spectroscopy: isocyanate (Figure A1) containing or carboxylic acid containing thiolactone (Figure A2). The reaction conditions can be seen in Figure 61.

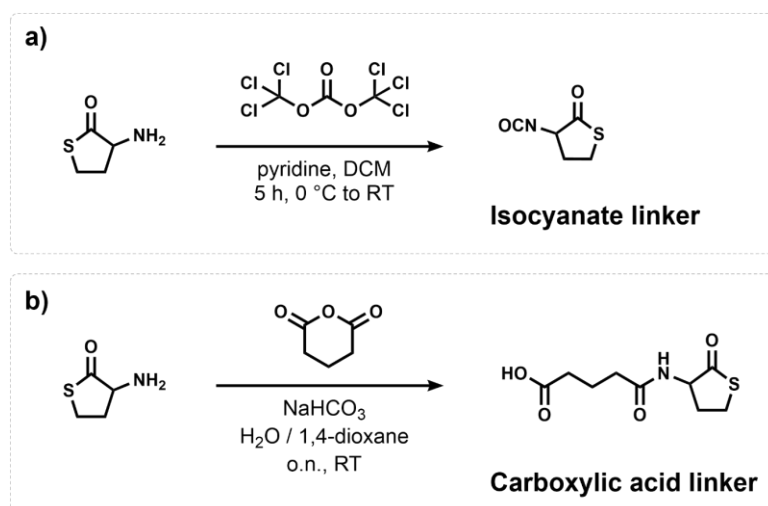


Figure 61: Reaction scheme of the two types of linker molecules examined for reintroduction of the thiolactone moiety for iterative sequence-defined synthesis, either a) isocyanate containing or b) carboxylic acid containing.

Both linker molecules were examined for suitability, and although both proved successful, the synthesis of isocyanates requires reagents that are generally considered high risk. To ensure full conversion at every step, a large excess of the linker molecule is required, and therefore the synthesis is necessary in large quantities or multiple repetitions and therefore the carboxylic acid linker was chosen for further investigations.

4.2.2 A study of protecting groups for controlled reaction conditions

As mentioned, the requirements of this iterative synthesis is for each step to only have the potential for one product, and to achieve complete conversion. In all instances, the monomer addition step involved the linker containing a thiolactone moiety undergoing ring opening to give a free thiol (SH) group, and consecutively the thiol-Michael addition between the thiol and acrylate of the monomer. Figure 60 shows the schematic of the final synthetic protocol that was developed, with the introduction of each monomer in an iterative process, followed by the removal of the solid resin, and finally the introduction of the crosslinkable group—in this case an acrylate.

From this schematic it is clear that the monomer that will contain the acrylate group to be used for 3D printing cannot be introduced during the initial synthesis, as it would compete during the thiol-Michael addition. Therefore, the synthesis was designed to introduce the acrylate moiety after cleaving the sequence-defined oligomers from the solid support, to be functionalised in a final ‘post functionalisation’ step. Thus, the chosen ‘functional’ monomer required a synthetic handle that can be used to introduce the acrylate in a final step. The initial synthetic design included a hydroxy group through the use of HEA as the synthetic handle, allowing the acrylate for crosslinking to be introduced in a second step through an acyl halide coupling with reagents such as acryloyl chloride. Having a hydroxy group on the side chain however, leads to a competitive reaction pathway with the other hydroxy group where chain extension with the linker molecule should occur, potentially leading to a branching effect whereby a point of further reaction is introduced (Figure 62a).

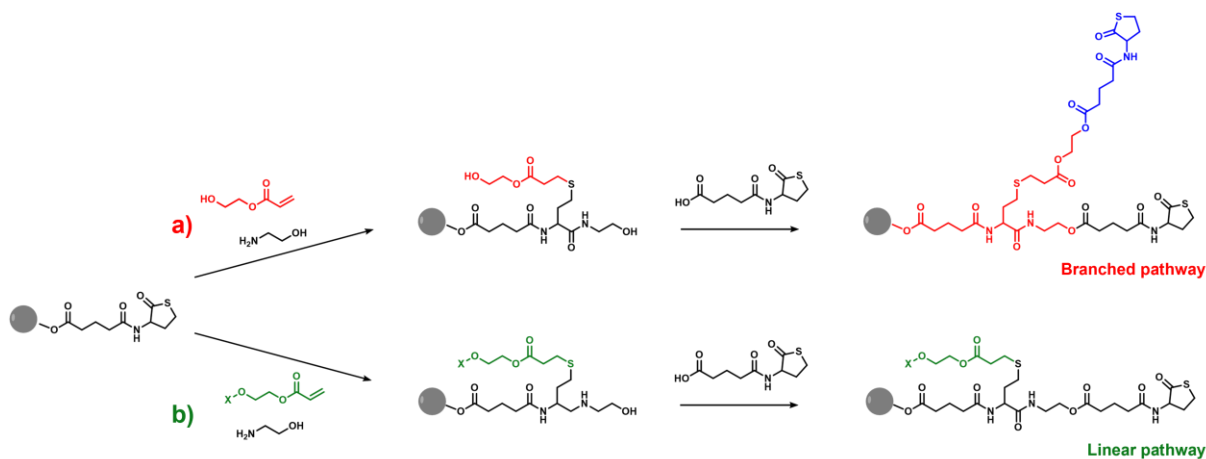


Figure 62: Reaction scheme for the potential a) branched and b) linear pathways possible for monomer addition and linker addition using a) unprotected or b) protected monomers, respectively.

The branched pathway would lead to formation of dendrimers that grow exponentially at each step, also due to the excess reagents, rather than a linear sequence-defined product. This branching has been intentionally exploited by the group of Du Prez for the synthesis of defined mikto-arm star shape macromolecules.^[127] Thus, it was necessary to protect the OH group in a way that is stable enough to remain covalently attached to the oligomer at all steps of the synthesis. Here, two silyl ether protective groups were examined: trimethylsilyl (TMS) and triisopropylsilyl (TIPS), to determine the most suitable and most stable type, considering also the ease of synthesis due to the previously mentioned requirement for a large excess of reagents. The TMS- and TIPS-protected HEA were successfully synthesised and characterised with ¹H NMR spectroscopy (Figure A3 and Figure A4, respectively). To determine the suitability as a protecting group for the specific reaction conditions, a small molecule study was performed (Figure 63).

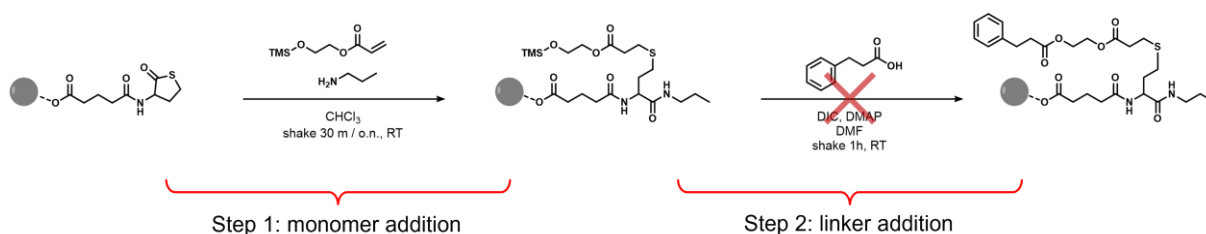


Figure 63: Reaction scheme of the small molecule study used to determine the suitability of TMS as a protecting group for the reaction conditions. Successful protection of OH with TMS would result in an unsuccessful linker addition reaction in Step 2. The red cross indicates the attempted reaction that should not take place, if the TMS protection is successful.

Herein, the monomer addition step is simulated with protected TMS-HEA, and instead of addition of ethanolamine which gives the OH handle for the chain extension step with the linker molecule, 'non-functional' propylamine is used instead, creating a 'dead' end. When simulating the second step esterification linker addition, there is now only one position where the functionalisation can occur, and this reaction can only occur if the TMS group is no longer protecting the hydroxy group. For step 2, hydrocinnamic acid was chosen to represent the linker molecule due to the easily identifiable signals of the aromatic group in ^1H NMR spectroscopy. After performing the two mock reactions, the product was cleaved from the solid resin with 1% trifluoroacetic acid (TFA) in dichloromethane (DCM) and the resulting material was analysed using ^1H NMR spectroscopy (Figure 64). From the signals that appear between 7.1 – 7.3 ppm, it is seen that the protection has been unsuccessful with these reaction conditions. The study shows that the cleavage of the product from the solid resin using the 1% TFA in DCM was however successful, allowing the product to be isolated as desired without cleaving the hydrocinnamic acid from the side chain position.

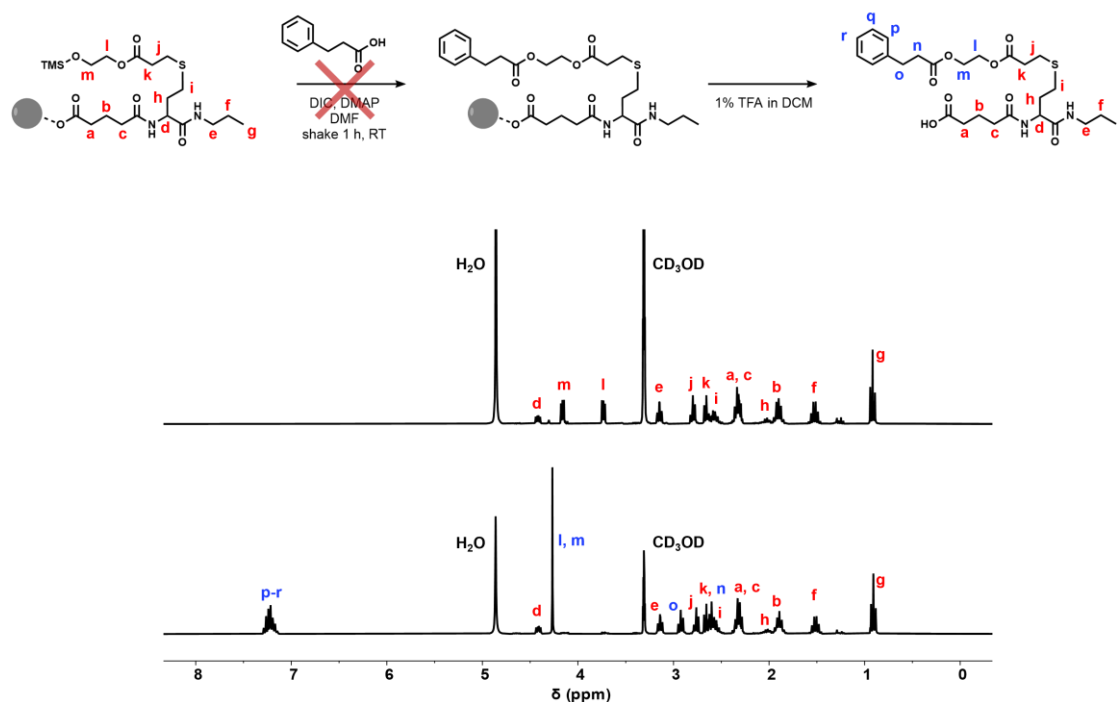


Figure 64: ^1H NMR spectra (CD_3OD , 300 MHz) of representative monomer addition small molecule study with top) TMS protected starting material after cleaving solid support, and bottom) product after introducing hydrocinnamic acid, showing the reaction was successful and thus the protection of OH with TMS was insufficient. The red cross indicates the attempted reaction that should not take place, if the TMS protection is successful.

The second protecting group studied was TIPS, which should be more stable in both acidic and basic conditions than TMS. In this case, the study was performed using the original isocyanate linker molecule, and analysis was performed using mass spectrometry (MS). After the addition of one monomer cycle containing the TIPS-HEA molecule, the first linker addition was performed, and the product was cleaved from the solid resin and analysed through MS (Figure 65).

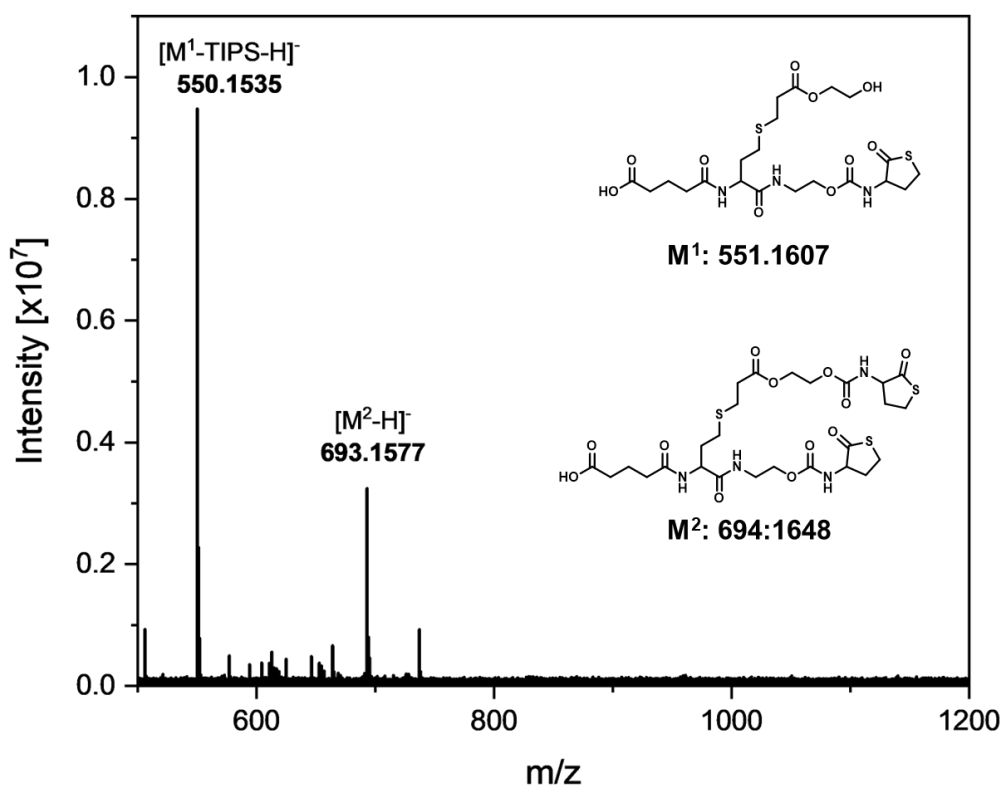


Figure 65: ESI-MS spectrum (negative mode, DCM/methanol) of the first monomer addition to TIPS protected OH oligomer, showing the undesired deprotected branching product where the linker molecule attached to the side chain.

Ideally, one of two products would be present—the single unit monomer addition with the linker extension, either with or without the TIPS group present, as the protective group may also be removed during the resin cleavage (or from ionisation during the mass spectrometry measurement). The deprotected single unit product was present (**M¹**), however the branched product was also found (**M²**). As mentioned previously, even small amounts of the branched side product would lead to exponential growth of dendritic architectures, and the product would no longer be sequence-defined. Additionally, the

synthesis of the protected TIPS-HEA product gave low yields of approximately 5% despite multiple attempts. Therefore, a new synthetic pathway was developed.

Here, a carboxylic acid was chosen as the synthetic handle for functionalisation, rather than the previously used hydroxy group. Although now the branching problem from the previous synthetic pathway is not possible, the same precaution is still necessary, i.e. the COOH group needs be protected as there is now the potential for a reaction between the COOH group from one resin and the OH group of another (Figure 66).

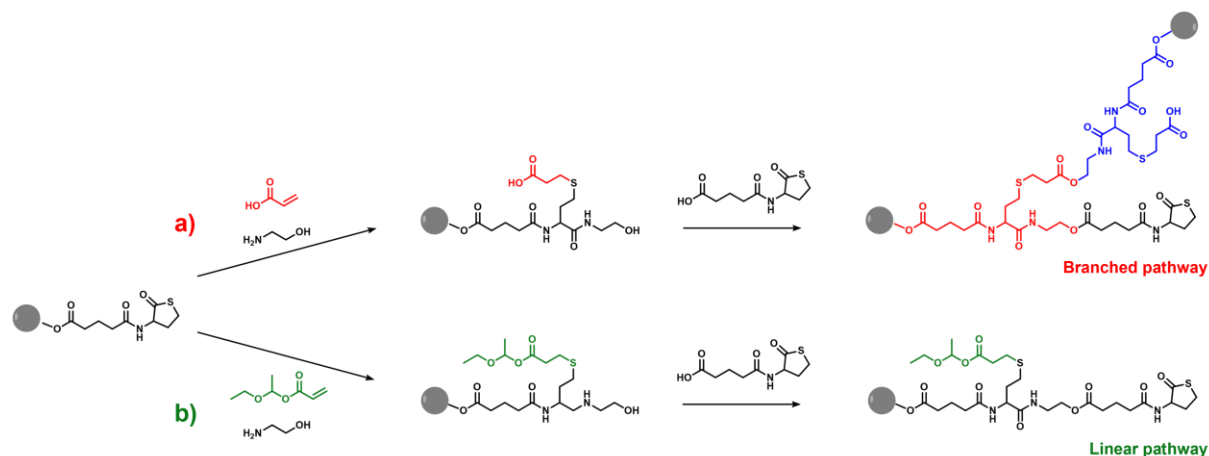


Figure 66: Schematic of potential reaction pathways for solid-supported synthesis with a) unreacted monomer, leading to branching where esterification combines the -OH of one resin with the -COOH of a second or third leading to exponential branching, and b) protected monomer giving the desired linear sequence product.

For the protection, this time a 1-ethoxyethyl acrylate (EEA) group was chosen based on previous literature.^[128] A small molecule ^1H NMR spectroscopy study was conducted again, similar to the previous study with TMS-HEA, to examine the stability of the protective group under the same conditions that would be used for the post functionalisation. The EEA-HEA was introduced as the first monomer unit, as well as a 'dead' end propylamine rather than the ethanolamine. The post functionalisation reaction as performed, using HEA as the reagent, and the product was cleaved from the solid resin with 1% TFA in DCM (Figure 67).

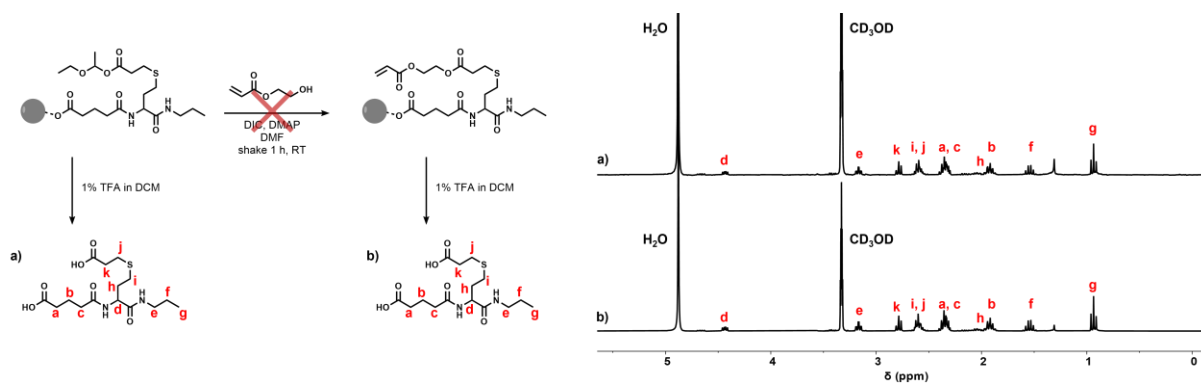


Figure 67: Small molecule study of EEA protected monomer reaction, showing the ¹H NMR spectrum (CD₃OD, 300 MHz) of a) model oligomer after one monomer addition with protected OH group, after cleavage from solid support and b) model oligomer after one monomer addition with protected OH group, followed by esterification reaction with HEA and cleavage from the solid resin.

Here, the NMR spectra show that the product a) before and b) after the model reaction, are identical. Thus, the protection was successful. It should be noted that the before and after NMR spectra both do not show signals for the EEA protective group, as it is cleaved at the same time as the product is cleaved from the resin, however as there was no reaction of the HEA at the carboxylic acid side chain it can be assumed that the protective group remains stable until this cleavage occurs. It is possible that the post functionalisation does take place, where the HEA replaces the EEA group, but that the new ester bond between HEA and the COOH is cleaved in the same way as the ester of the EEA during the cleavage step in TFA. In this small scale study, it is not possible to determine if this is the case, however, the purpose of the protection is not to prevent the post functionalisation, but rather to prevent branching with other molecules, whereby two ‘loaded’ resins would be linked together (as seen in Figure 66a). From the mass spectra, the branching was not observed, as seen by the lack of species above 3000 m/z in the mass spectrum as seen in Figure A5. With the protection deemed successful, the final optimised synthetic pathway, comprised of five steps, was as shown in Figure 68.

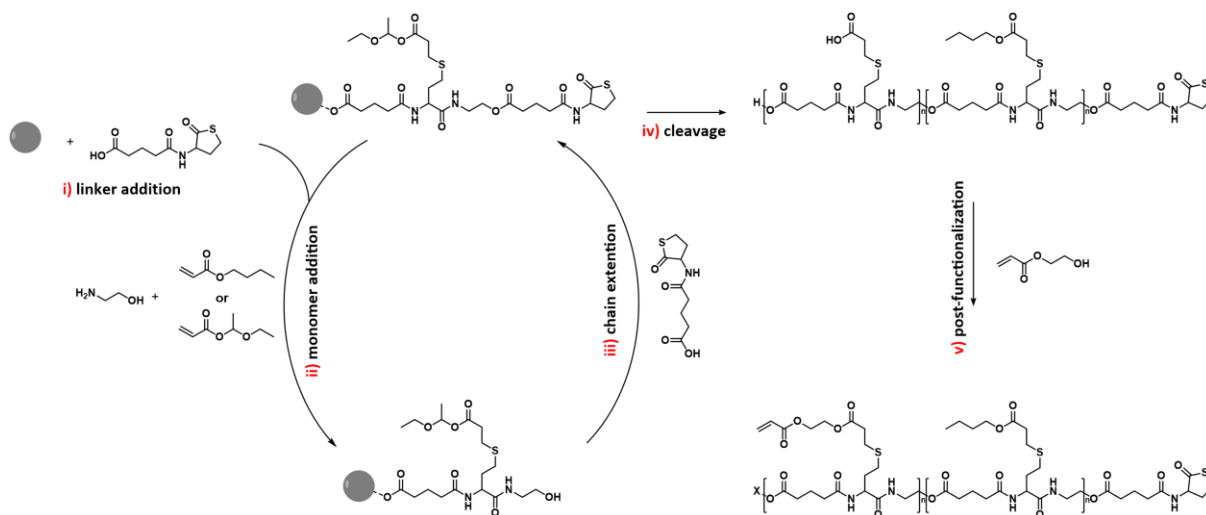


Figure 68: Complete reaction scheme showing the five steps for the synthesis of sequence-defined oligomer species i) addition of linker to the insoluble resin, iterative steps of ii) monomer addition with EEA protected functional monomer or butyl acrylate and iii) chain extension, followed by iv) cleavage of the product from the insoluble resin and v) post functionalisation to introduce the crosslinkable acrylate group.

For each oligomer, the iterative synthesis cycle was repeated until the oligomer was composed of 8 total units, adding either monomer B (butyl acrylate) or C (protected carboxylic acid) at each step, giving a total of three oligomers with either alternating, triblock, or block configuration. After cleaving the solid state resin, which consecutively cleaves the protecting group of the carboxylic acid side chain, the three products (alternating (blue), triblock (red) and block (grey)), were confirmed by matrix-assisted laser desorption/ionisation (MALDI)-MS and ^1H NMR spectrometry (Figure 69). The three oligomers are identical in mass, also aligning with the predicted isotopic pattern, and indistinguishable through ^1H -NMR spectroscopy, only varying by their sequence through the order of monomer addition.

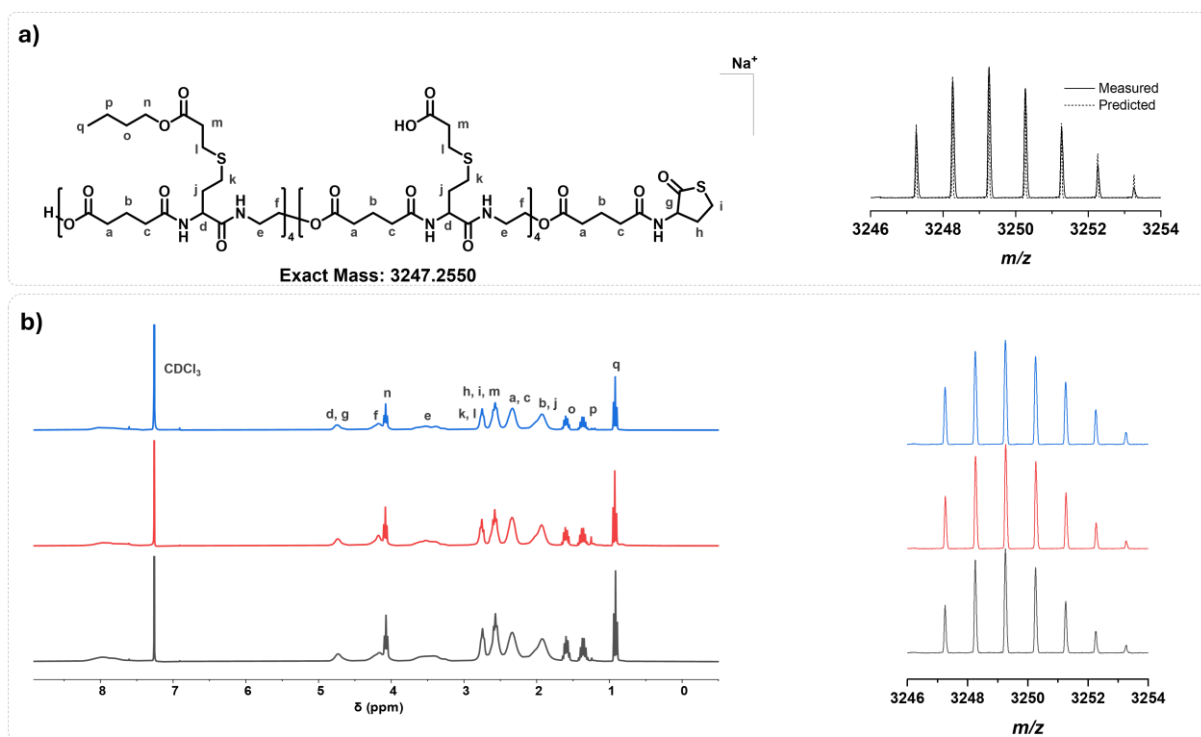


Figure 69: Characterisation of the synthesis of three sequences. a) The general structure of each sequence with identical exact mass with measured versus predicted isotopic pattern, and b) measured ¹H-NMR spectra (CDCl₃, 600 MHz) and high resolution MALDI-MS spectra of the sequences, top to bottom: alternating (blue), triblock (red), and block (grey). Adapted according to the terms and conditions of the creative commons CC BY 4.0 license.^[93] Copyright 2023, The Authors.

Subsequently, the post functionalisation reaction (Figure 70a) was performed on each oligomer to introduce the acrylate group that will be used for 2PLP. Through Steglich esterification, the acrylate group was successfully introduced to all oligomers (Figure 70b), as confirmed by ¹H NMR spectroscopy (Figure 70c).

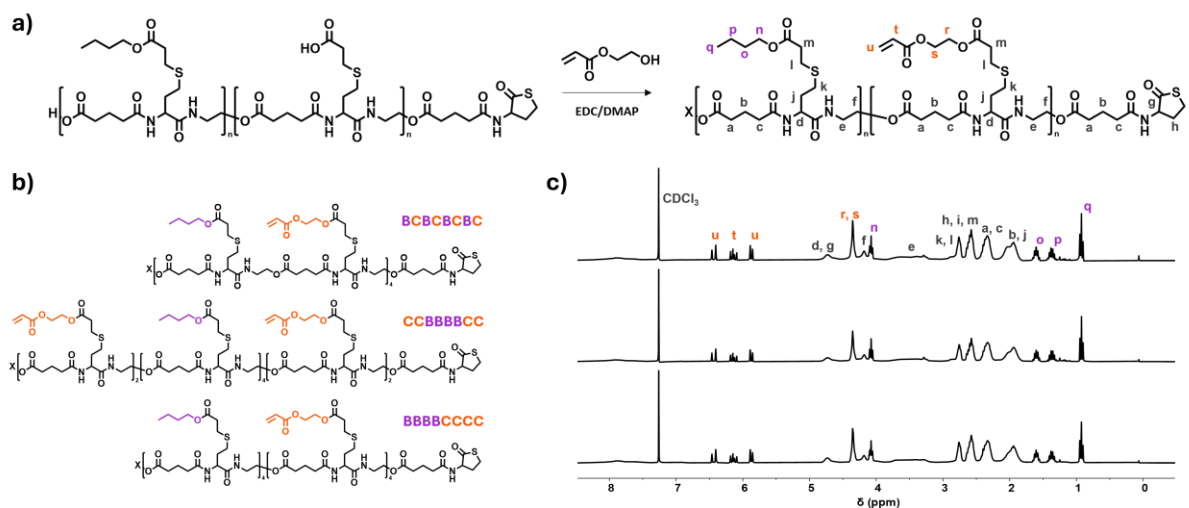


Figure 70: a) Reaction scheme for the general post functionalisation reaction between the cleaved oligomer to introduce the crosslinkable acrylate moiety for 2PLP, b) the chemical structure of the three crosslinkable oligomers: alternating, triblock and block (top to bottom), and c) $^1\text{H-NMR}$ (CDCl_3 , 300 MHz, 295 K) spectra of the three chemical structures shown in (b): alternating, triblock and block (top to bottom), confirming the successful functionalisation with acrylate ($\approx 4.3:4.0$ acrylate:butyl). Adapted according to the terms and conditions of the creative commons CC BY 4.0 license.^[93] Copyright, 2023 The Authors.

4.3 SEQUENCE-DEFINED INKS FOR 2PLP: STRUCTURE-PROPERTY RELATIONSHIPS

After the successful synthesis of three sequence-defined oligomers, the next challenge was formulation a printable ink for 2PLP. After formulating the ink and determining the window of printability, structures can be printed for characterisation of the chemical properties such as acrylate conversion, as well as mechanical properties such as reduced elastic modulus.

4.3.1 Ink formulation

For successful 2PLP of acrylates, radical species are typically generated through the addition of a suitable photoinitiator. In this case, as with the pre-polymer ink formulation DETC, was chosen. Due to the high viscosity of the oligomers, it was necessary to introduce the photoinitiator with solvent. Initially, attempts were made to use a stock solution in a low boiling point solvent (DCM), to introduce a precise mass of photoinitiator, where the solvent could then be removed before printing. However, it was found that due to the high viscosity and general 'stickiness' of the oligomers, it was not

possible to effectively and reproducibly remove the DCM. Additionally, as some solvent remained during the printing, it was notable that over the printing duration the material continued to dry as more solvent evaporated within the sample holder of the printer. As the goal is to directly compare the effect of the sequence of monomers within the oligomer, it is critical that all other parameters are identical, and therefore the lack of reproducibility would lead to inconclusive results. To solve this challenge, the solvent was switched to a high boiling point solvent that should undergo no evaporation. In this case, DMAc was chosen. The final formulation for all three materials consisted of 65 wt% oligomer, 0.25 wt% DETC, 0.1 wt% butylated hydroxytoluene (BHT) and the remainder DMAc. Printing attempts of complex 3D structures showed that when using this ink formulation it was possible to print high resolution structures with fine features and overhangs, as can be seen by SEM images (Figure 71).

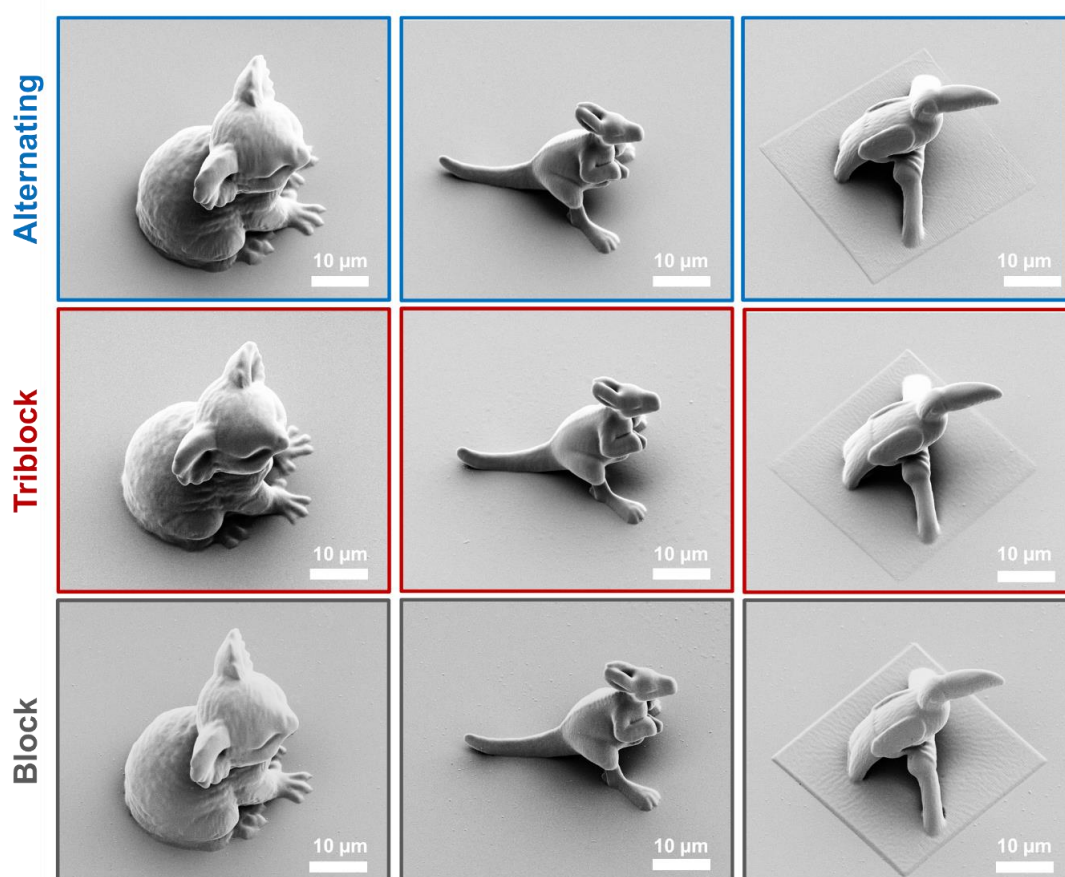


Figure 71: SEM images of structures printed using alternating, triblock, and block structures showing the high resolution and fine features with overhangs achievable with optimised ink formulation for all three oligomers. Adapted according to the terms and conditions of the creative commons CC BY 4.0 license.^[93] Copyright, 2023 The Authors.

Despite the high quality printing capacity of the ink formulation, it was realized after attempts to characterise the materials, that the photoinitiator DETC interfered with the potential for Raman spectroscopy due to its fluorescence reducing significantly the signal to noise ratio. Attempts to purify the printed material of residual photoinitiator did not resolve the problem, and therefore further experiments were conducted with another common two-photon photoinitiator: BAPO. For the formulation with BAPO, the concentration was increased to 2 wt%, however all other parameters remained constant. This formulation was used for all further testing.

4.3.2 Printability window

Using the previously optimised printing formulation, the printability of the three inks was examined. To that end, a relatively complex structure was chosen as the standard, a Buckminster C60 fullerene 'buckyball'. Using this structure, a printability window was determined by printing an array of structures with varied laser powers and scan speeds, from 10 – 40 mW and 3 – 6 mm s⁻¹, respectively. The printed buckyballs were imaged with SEM and examined (Figure 72a and Figure 72b).

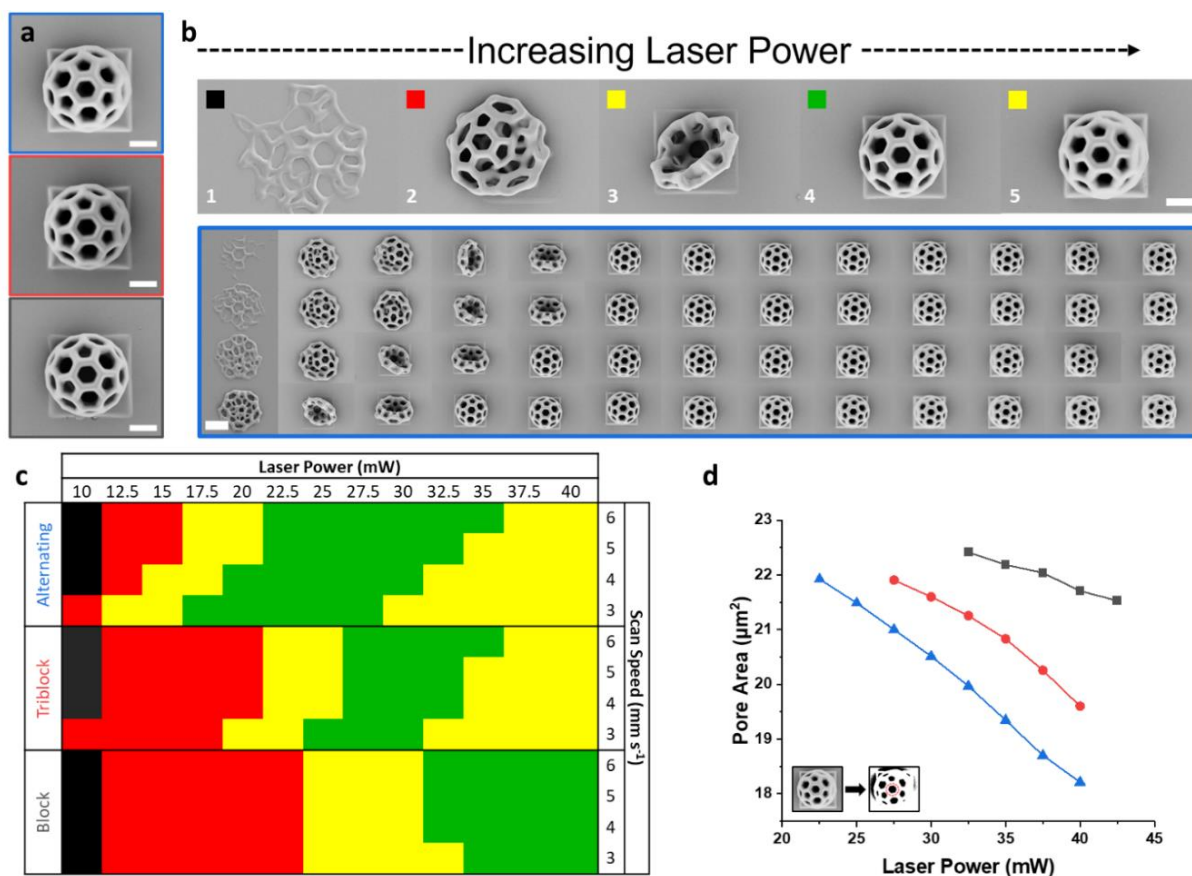


Figure 72: a) SEM images of 3D buckyball structures 2PLP printed using alternating (blue), triblock (red), and block (grey) oligomer inks (laser power = 32.5 mW, scan speed 5 mm s⁻¹), b) SEM images of the showing the printability window with increasing laser powers for alternating ink, from 10 mW to 40 mW (left to right) and scan speeds from 3 to 6 mm s⁻¹ (bottom to top). c) Schematic representation of the printability window over laser power range 10–40 mW and scan speeds of 3–6 mm s⁻¹ for the three inks. d) Decreasing area of the central pore of representative buckyball structures with increasing laser power, measured by converting the SEM images to binary. Insert of (d) shows representative SEM image (left) and binary image (right) with the analysed area highlighted in red. Scale = 8 μm. Adapted according to the terms and conditions of the creative commons CC BY 4.0 license.^[93] Copyright, 2023 The Authors.

It can be seen that there is a window whereby the parameters result in a stable and well defined structure. Below this threshold, at lower laser powers, the network formation is too low and the structures collapse under their own weight. At even lower laser powers, the structure does not fully form and much of the material is unreacted and therefore washed away during the development step. Above a certain laser power, there is another detrimental effect, referred to here as overexposure, where the fine features such as the pores of the buckyball are lost. Beyond this point, the printing process shows so called

microexplosions leading to uncontrolled polymerisation and no printed structures. The effect of the scan speed is similar across all inks, where increasing scan speed effectively reduces the laser power dosage as it reduces the contact time of the laser at each voxel, giving a step-like pattern of the printability window as seen in Figure 72c.

From this investigation, it is clear that the three oligomers have different printability due to their differing sequence. For example, the printability window was larger for the alternating sequence, beginning at a low laser power of 17.5 mW at 3 mm s⁻¹, up to 35 mW at 6 mm s⁻¹. The triblock sequence required higher intensity (25 mW at 3 mm s⁻¹) to form stable structures, and overexposure occurred at similar intensities as for the alternating sequence, leading to a narrow printing window. Interestingly, the block oligomer required a much higher laser power to form stable structures, beginning with a minimum intensity of 32.5 mW. Here, also, no pore closure was observed. Despite this, it was seen that as the laser power increased, the thickness of the printed lines also increased. The alternating sequence showed a larger range, starting at a low laser power of 17.5 mW at 3 mm/s and going up to 35 mW at 6 mm/s. In contrast, the triblock sequence needed higher power (25 mW at 3 mm/s) to achieve stable structures, and overexposure occurred at similar intensities, resulting in a narrow printing window. Notably, the block oligomer required a significantly higher laser power to form stable structures, with a minimum intensity of 32.5 mW. Additionally, no pore closure was observed in this case. However, it was noted that as the laser power increased, the thickness of the printed lines also increased.

4.3.3 Structure–property relationships

To examine what may be happening on a molecular level during the printing process, and gain more insight into how the network formation may be occurring, the degree of acrylate conversion as well as the reduced elastic modulus was measured.

Chemical conversion: Raman spectroscopy

To determine the degree of crosslinking during the printing process, the number of acrylate groups participating in the reaction, i.e. present after the printing process

compared to before, must be calculated. For this purpose, Raman spectroscopy was chosen as a quantitative method for calculating the degree of acrylate conversion (DoC). Figure 73 shows a typical Raman spectrum of the control sample in red. $40 \times 40 \times 10 \mu\text{m}^3$ cubes were printed for each parameter, an example spectrum measured of the printed structure is seen in black in Figure 73. Spectra are normalized against the carbonyl peak at 1725 cm^{-1} , showing the decreasing of the acrylate C=C bond at 1638 cm^{-1} after printing.

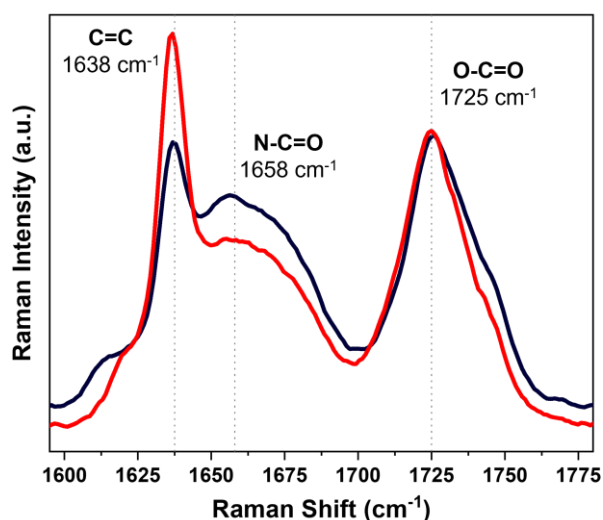


Figure 73: Exemplary Raman spectra of the unreacted oligomer ink (red) and the spectrum taken of the printed oligomer ink (black) showing a decrease in the C=C peak at approximately 1638 cm^{-1} .

Spectra of the oligomers before printing, as well as at different laser powers, were measured for all oligomers over a laser power range of 10 – 40 mW. It was observed that the scan speed did not make a large difference to the trend, and therefore a constant scan speed of 5 mm s^{-1} was used (Figure B2). For all inks, there is a clear decrease in the C=C band intensity as laser power increases (Figure B3). As discussed previously, the carbonyl peak was chosen as a control that does not participate in the reaction and therefore spectra were normalised against this peak, and peak fitting was performed on all spectra to give the integrated area of each band (Figure B4). As previously described in Chapter 3.3.3 the degree of acrylate conversion was calculated for each printing parameter using Equation 5. Here, DoC can be compared between each ink (Figure 74).

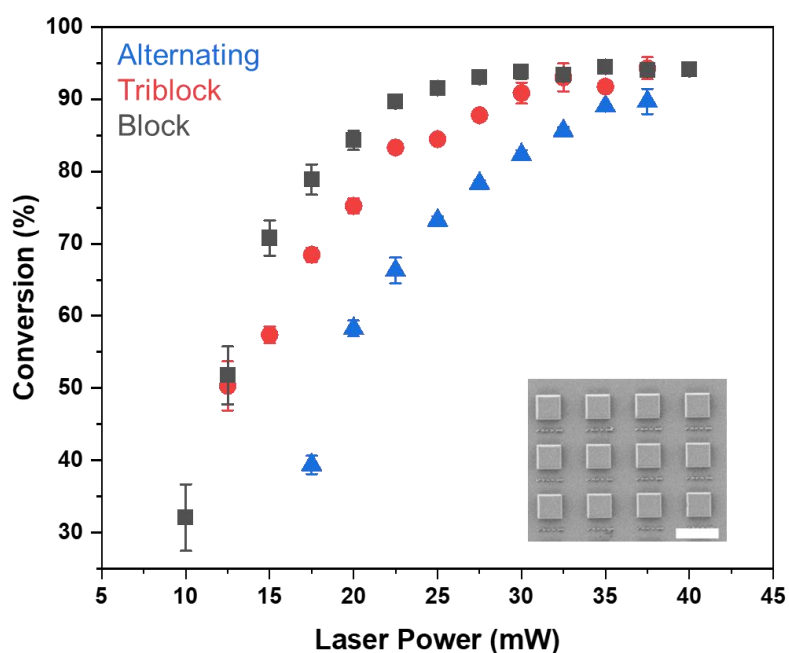


Figure 74: Degree of acrylate conversion as determined by Raman spectroscopy of structures printed with alternating (blue), triblock (red), and block (grey) oligomer inks over a range of increasing laser power. Scale bar = 50 μm , $n = 3$. Adapted according to the terms and conditions of the creative commons CC BY 4.0 license.^[93] Copyright, 2023 The Authors.

From here, the differences in each ink become clear. The block sequence DoC is higher than the other two sequences over the whole range of laser powers, increasing steeply to a plateau at approximately 30 mW, around 95%. The alternating and triblock sequence have a more gradual increase in conversion, where the alternating has the lowest conversion over the whole range, reaching about 90% DoC at the highest laser power. The triblock sequence is intermediate between the other two sequences. Overall, the alternating sequence has the lowest degree of acrylate conversion, however it has the best printability at lower laser powers, as determined previously (Figure 72c). This suggests that even with a lower conversion of crosslinkable groups, the network formation is more stable leading to stable printed structures, thus the threshold for printing is lower for the alternating sequence. When looking at the block sequence, the opposite is observed. Despite having a high acrylate conversion, the laser power required to print stable structures is much higher, at 32.5 mW. The kinetics of acrylate crosslinking, as well as the network topology formed, are complex and influenced by

many parameters, that until now has not been comprehensively investigated.^[129] In this case, as the DoC and the printability window differ between each oligomer, it is likely that the differences arise due to the sequence of the oligomer, and more specifically due to the positioning of the crosslinkable group along the backbone, potentially also their proximity to one another. In the block oligomer, the four crosslinkable units are in closest proximity to one another, potentially increasing the likelihood for intramolecular reactions while being less hindered by the non functional butyl side chain groups, which is supported by the high DoC achieved with a lower laser power compared to the other two sequences. For the alternating sequence, the crosslinkable group is more homogeneously distributed along the backbone, between the non functional groups, leading potentially to a more homogenous network. This is supported by the wide printing window, with stable structures being achieved at lower laser power with lower DoC. It follows that the triblock oligomer can form networks where the non functional monomer acts as a longer spacer between the crosslinked acrylate groups. The reaction is still capable of reaching high conversion and forming stable structures over a large printing window. The sequence of the oligomers influences not only the kinetics of acrylate conversion but also the topology of the resulting networks, as noted in the literature.^[38]

Mechanical properties: Nanoindentation

As network topology also has an influence on the properties of materials, the mechanical properties of printed microstructures were also investigated, to additionally provide insight into the relationship between the printability and DoC. For the characterisation of microscale structures, nanoindentation was chosen. Samples were created by printing arrays of pillars with a 20 μm diameter and 15 μm height, allowing for indentation using a standard Berkovich diamond tip. From calculating the slope of the tangent of the elastic unloading curve from the load–displacement curve, it was possible to determine the reduced Young’s modulus, E_r , which represents the elastic deformation in the microstructures, as well as the hardness.^[108] Figure 75 shows the reduced modulus, while the hardness of the three oligomers over a printing window of 20 – 40 mW at a scan speed of 5 mm s^{-1} . The hardness can be seen in Figure B5. For all inks, there is an increase in mechanical properties as the laser power increases, as expected. This aligns with the

increased network density with increased photon dosage, and corresponds to the trend observed in the acrylate conversion, which also increases with increased laser power for all oligomers.

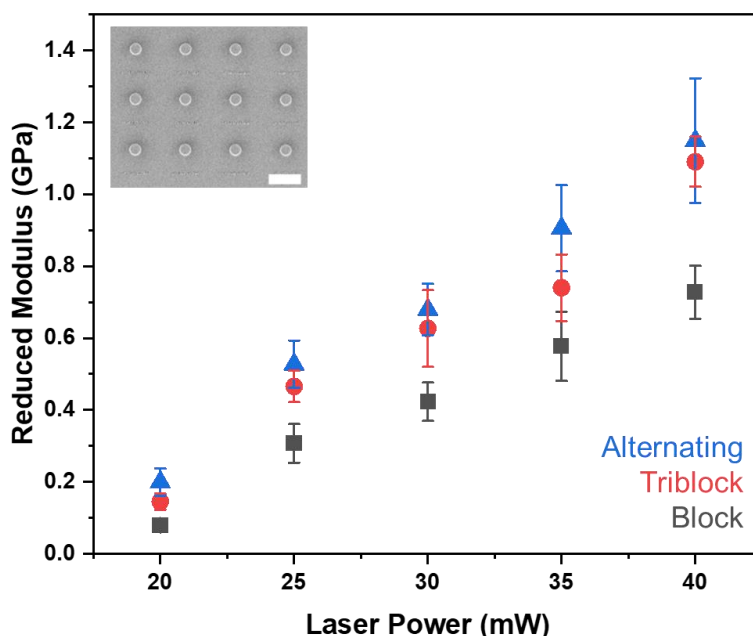


Figure 75: Nanoindentation results showing the reduced elastic modulus (E_r) and hardness measured with micropillars printed with alternating, triblock and block inks using varied laser powers. Scale bar = 50 μm . Adapted according to the terms and conditions of the creative commons CC BY 4.0 license.^[93] Copyright, 2023 The Authors.

Interestingly, when considering the E_r , it was observed that the structures printed with the alternating sequence have a higher modulus than the other two sequences, in particular the block sequence. At the maximum laser power the alternating sequence shows a E_r of 1.15 ± 0.17 GPa, despite having the lowest conversion, while the block sequence reaches 0.73 ± 0.07 GPa with the highest DC. The same trend is observed in the hardness of the structures, where the alternating has a higher hardness than the block and triblock sequence. When considering the degree of acrylate conversion, one would expect that the block sequence would have a higher modulus, due to the higher DoC, followed by the triblock. Although it has been observed that DoC is an important factor for determining the mechanical properties of printed microstructures in this case between the three different oligomers the opposite trend is observed, suggesting that

conversion is not the only factor at play influencing the mechanical properties.^[119] Indeed, it has also been shown that properties such as macromolecular structure as well as molecular network structure and topology play an undeniable role.^[38,129,130] The Young's modulus is also affected by the number of crosslinks, degree of crosslinks, and the stiffness of the chain between segments.^[129,131] For example, it has been observed that linear diacrylates separated by longer alkyl chains lead to a lower modulus than their shorter counterparts.^[131]

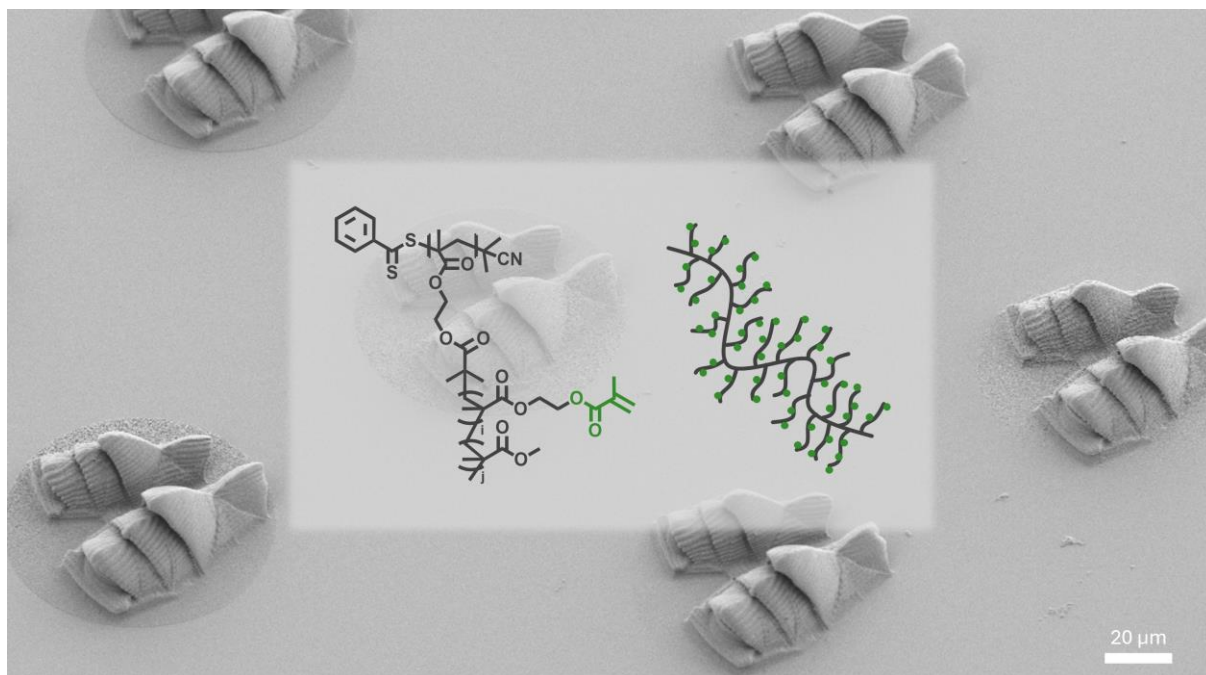
It is postulated that in this case, the sequence of the oligomers affects the network formation and topology of the printed structures. For example the alternating sequence, as mentioned above, with the homogeneous distribution of crosslinkable group, may lead to a more homogeneous network. This would support the lower DoC required to print stable structures, resulting in a large printability window, as well as the higher E_r . On the other hand, the triblock sequence has two functional acrylate ends separated by four butyl side chains that may act as spacers within the resultant network, in turn also potentially reducing the mechanical properties when compared to the alternating sequence, while maintaining reasonable printability. In the last case of the block sequence, four crosslinkable acrylate groups are directly positions adjacent to one another, followed by the four butyl side chains. Here, there is more potential for intramolecular reactions as mentioned previously. Is it proposed that the lower mechanical properties of the block sequence may be due to inhomogeneous network formation where the non functional groups act as a plasticiser, reducing the mechanical properties despite the high conversion. This is supported by the high laser powers required for stable structures i.e despite high conversion at lower laser powers, the network formation is not stable causing the structures to collapse, or in cases of insufficient crosslinking, for the material to be washed away during development. This trend has been observed in literature, where crosslinking of defined molecules with similar sequences led to networks with intramolecular loops and dangling ends, showing a similar effect on conversion and mechanical properties.^[38]

4.4 SUMMARY

In this chapter, the successful 3D microprinting of sequence-defined macromolecular inks was demonstrated for the first time. Three oligomers comprised of 8 units—four ‘functional’, and four ‘non-functional’—were synthesised using an optimised iterative solid-supported synthesis protocol. The three oligomers had identical molecular mass and varied only in the sequence of the repeat units, resulting in either alternating, triblock, or block sequences. These oligomers were then formulated into suitable inks for 2PLP. Each ink displayed the potential for printing high resolution with complex features such as overhangs and fine detail.

It was shown that the macromolecular structure, specifically the positioning of the crosslinkable groups and resulting network topology, plays a critical role in printability, degree of monomer conversion, and mechanical properties. For example, the alternating sequence required the lowest DoC for printing stable structures, but the structures displayed the highest stiffness. Alternatively, the block sequence required the highest laser powers to print stable structures, despite having a higher DoC. At the same time, despite the high DoC, the structures had lower E_r compared to both alternating and triblock inks. It is proposed that network topology, as a result of macromolecular sequence, has a significant impact on both the printability as well as the resultant chemical and mechanical properties of 2PLP structures. The alternating sequence displayed the best overall performance, with the highest mechanical properties at the lowest acrylate conversion, while also requiring the lowest laser power to print stable and precise 3D microstructures, possibly due to reaction kinetics and homogeneous network topology. However, it is seen that with the rational design of the macromolecular structure of an ink, it is possible to ‘tune’ the properties of the resultant 2PLP structures.

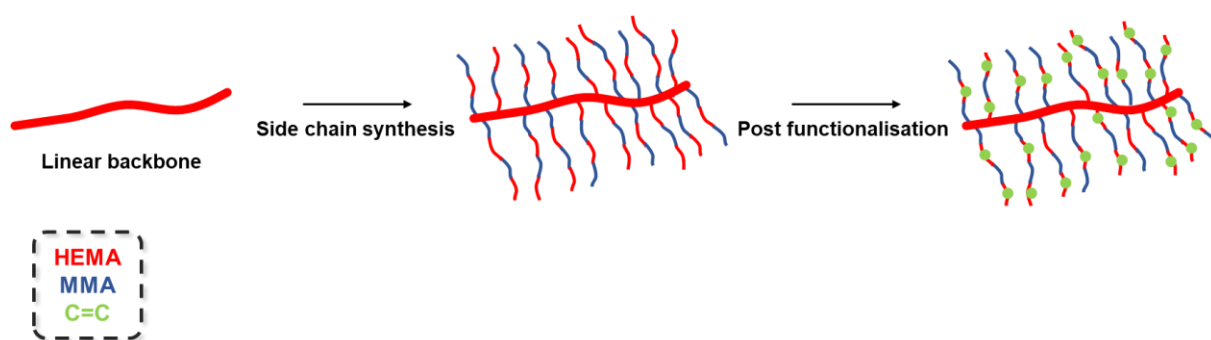
5 Molecular polymer bottlebrush architectures as novel 2PLP inks



The results described in this chapter are part of an ongoing DAAD supported collaboration with the group of Prof. Müllner in the University of Sydney, Australia.

5.1 MOTIVATION AND AIMS

Until now, most inks for 2PLP have been predominantly formulated from multifunctional small molecules, or composed of linear oligomers or polymers, such as detailed in Chapter 3 and 4. However, with advances in technology and applications new molecular architectures are becoming of increasing interest, with the potential to impart unique properties to printed structures. To that end, molecular polymer bottlebrushes (MPBs) are relatively new polymer architecture in the field of 3D printing. Despite having interesting properties afforded by their unique architecture and resultant confirmations, MPBs have been explored only in extrusion-based methods on the macroscale. The following chapter explores MPB inks as a new molecular architecture, which has yet to be explored in 2PLP. As discussed in Chapter 2.3.1, MPBs are composed of a linear polymer backbone grafted with pendant polymer side chains giving a bottlebrush-like architecture. They can be synthesised through a variety of polymerisation methods, typically RDRP-based. Herein, MPBs are synthesised in three steps, using RAFT and ATRP methods, in a grafting ‘from’ approach. First, a HEMA backbone is synthesised using RAFT polymerisation, and through the hydroxy groups, an initiation point for ATRP is introduced. Second, ATRP of comonomers MMA and HEMA generates the side chains in a grafting ‘from’ approach. Third, the resultant bottlebrushes are functionalised with methacrylate moieties, allowing for the formulation of a printable ink for 2PLP (Scheme 3).



Scheme 3: Three step protocol for the synthesis of bottlebrush p(HEMA)-g-(Acryl-co-MMA)

As a novel ink for 2PLP, the focus herein is predominantly on optimisation of the molecular macrostructure for successful printability. For example, controlled synthesis of the bottlebrush side chains and optimisation of the post functionalisation. Therefore

the side chain composition and degree of methacrylation are investigated to examine the effect on the printing.

5.2 SYNTHESIS OF MOLECULAR POLYMER BOTTLEBRUSHES

The synthetic method chosen for MPBs in this instance was grafting ‘from’, involving the preliminary synthesis of a linear backbone, followed by the secondary polymerisation of side chain polymers from initiation points along the backbone. Methacrylate groups are introduced to the brush structure, using a post functionalisation method as described in previous chapters. A summary of the synthesis strategy is shown in Figure 76, comprised of three steps.

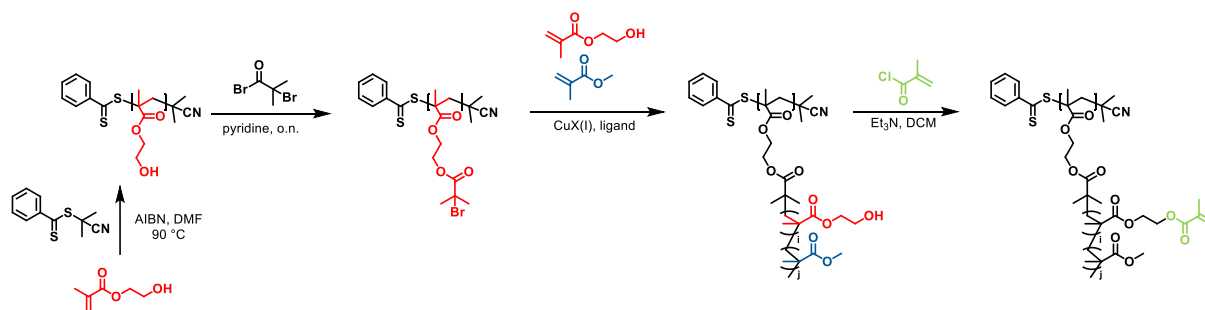


Figure 76: General synthesis procedure for MPBs employed in this chapter, comprised of backbone synthesis through RAFT polymerisation, addition of the ATRP initiation point (α -bromoisobutyryl bromide), ATRP of MMA and HEMA to generate side chains, and functionalisation with methacryloyl chloride.

First, the backbone is synthesised using controlled RAFT polymerisation of HEMA monomers to give low dispersity linear poly(2-hydroxyethyl methacrylate) (pHEMA) with hydroxy functionality. To the hydroxy groups, α -bromoisobutyryl bromide (α -BiBB) is introduced to give an initiation site for the synthesis of the side chains. The side chain polymerisation is performed from the bromine initiation site through ATRP copolymerisation of varied monomers, namely MMA and HEMA, generating a brush like molecular architecture. In the last step, hydroxy groups of the HEMA side chains are functionalised with methacryloyl chloride to be used for crosslinking during 2PLP.

5.2.1 Synthesis of MPB backbone

As mentioned previously, the conformation of bottlebrushes is highly dependent on the ratio of the length, or DP, of the backbone (N_{BB}) to the side chain (N_{SC}). For the development of an MPB ink, the targeted conformation was $N_{BB} > N_{SC}$, to simulate a linear-

polymer-like architecture. Three methods were used to approach this synthesis, summarised in Table 3. First, RAFT polymerisation using the CTA 4-cyano-4-(phenylcarbonothioylthio)pentanoic acid (CTBPA) and HEMA was performed, with the resulting product termed **pHEMA-0**. The conversion of HEMA was followed over 1.5 h, showing linear kinetics (Figure 77).

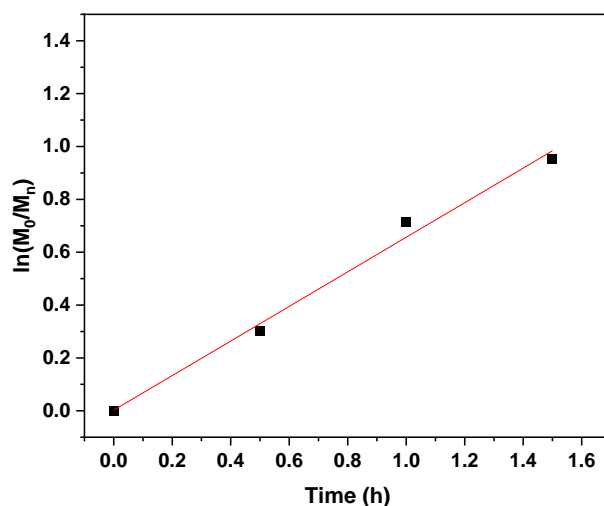


Figure 77: Graph of $\ln([M]_0/[M]_n)$ vs. time for pHEMA-0 and the corresponding linear fit of $y = 0.65x$ with $R^2_{\text{corr}} = 0.986$.

The resultant polymer pHEMA-0 had a conversion of 62% (DP = 62), M_n of approximately 15 kg mol^{-1} and a dispersity of 1.2 (Figure 78).

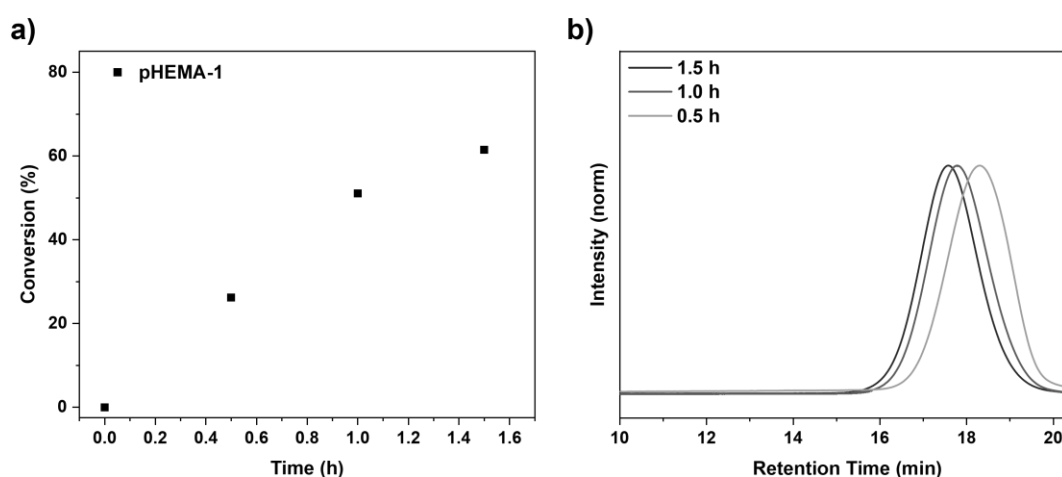


Figure 78: a) HEMA conversion over time as determined by integration of C=C protons from ^1H NMR spectra, and b) SEC traces showing monomodal dispersity and increasing molecular weight over time of pHEMA-0.

The DP was determined by monitoring the decrease of vinyl protons at approximately 5.5 – 6.5 ppm, using the solvent N,N-dimethylformamide (DMF) as an internal standard, and the final purified product was characterised by ^1H NMR spectroscopy (Figure 79).

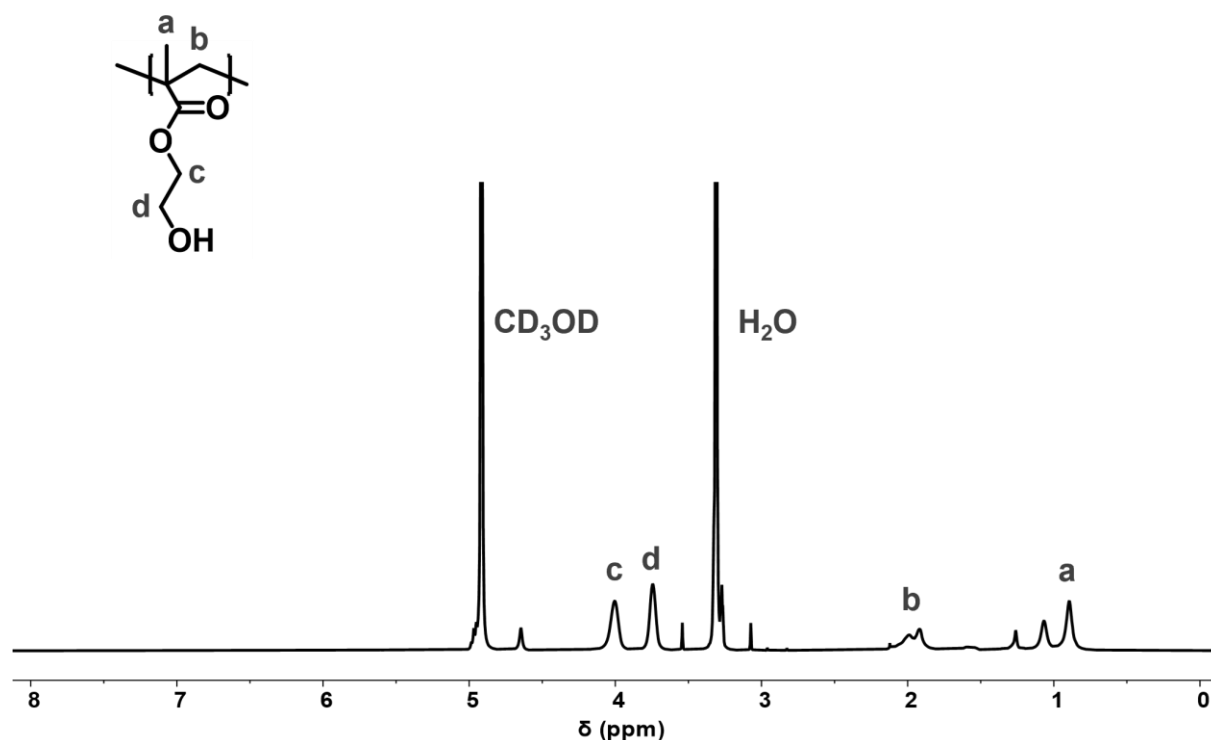


Figure 79: ^1H NMR spectrum (CD_3OD , 300 MHz) of backbone PHEMA-0.

In addition to pHEMA-0, two other backbones were synthesised and characterised: pHEMA-1 and PHEMA-2. pHEMA-1 was synthesised using ATRP (Figure A6), while pHEMA-2 was synthesised using RAFT polymerisation (Figure A7). The composition of the three HEMA polymers is summarised in Table 3, along with the characterisation after introduction of the bromine functionality for ATRP initiation of the side chains. The backbone pHEMA-1 had a DP of 65 and M_n of 24 kg mol^{-1} with a dispersity of 1.2 by SEC (Figure A8). pHEMA-2 had a DP of 72, and M_n of 16 kg mol^{-1} with a dispersity of 1.2 as seen in the SEC (Figure A9).

For the ATRP side chain reaction, first an initiation point must be present on the backbone. To that end, α -BiBB was used to functionalise the hydroxy group of the HEMA monomers, yielding poly(2-(2-bromoisobutyryloxy)ethyl methacrylate) (pBIEM). The successful esterification of the hydroxy groups was characterised with ^1H NMR

spectroscopy, where the ethylene protons are shifted downfield, and the presence of a new peak at 1.96 ppm is indicative of the new methyl protons of α -BiBB (Figure 80).

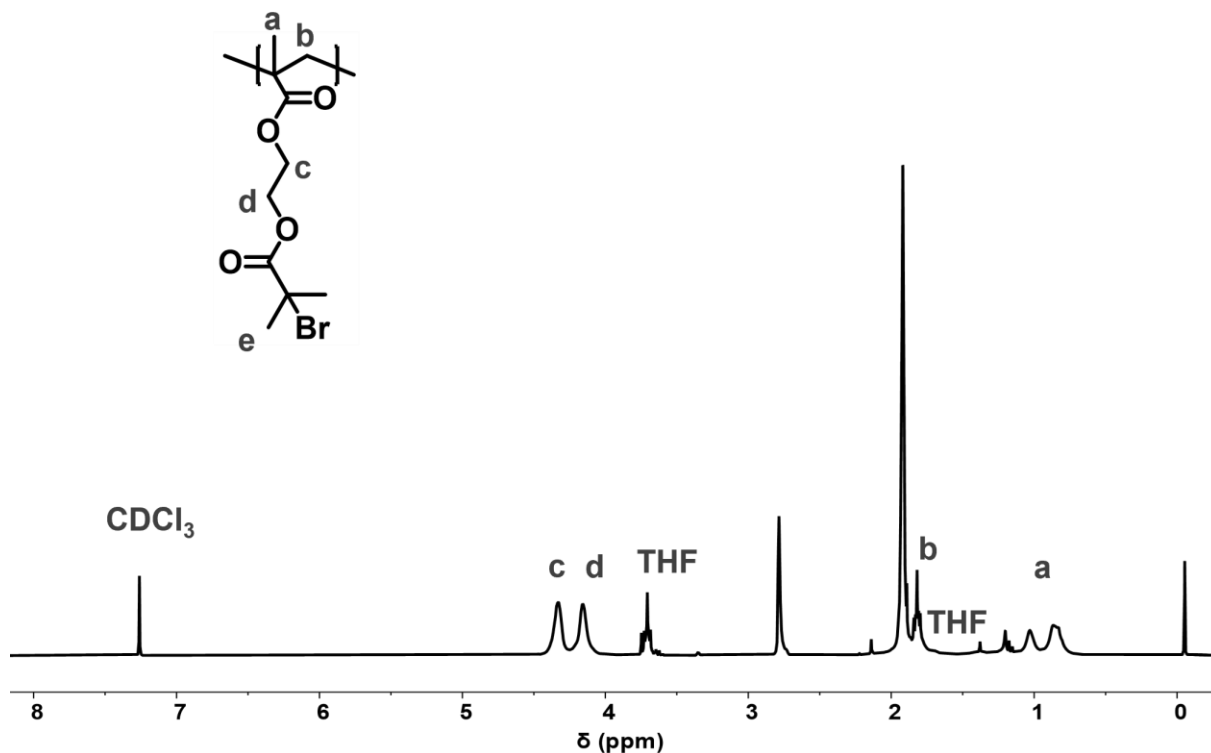


Figure 80: ^1H NMR spectrum (CDCl_3 , 300 MHz) of functionalised backbone PBIEM-0.

SEC analysis of this pBIEM-0 showed that it remained monomodal, with a slightly increased dispersity of 1.4, and a measured M_n of 12 kg mol^{-1} . Despite the increase in molecular weight due to functionalisation the SEC trace for pBIEM-0 is shifted toward higher retention times than pHEMA-0, as seen in Figure 81, indicating a smaller hydrodynamic volume.

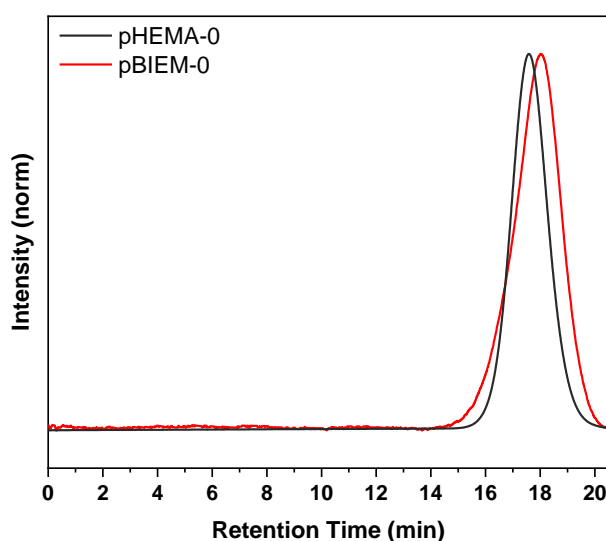


Figure 81: SEC traces (DMAc) after backbone functionalisation of pHEMA-0 to pBIEM-0 showing monomodal dispersity and slight shift in retention times.

This is likely due to the decreased polarity of the functionalised polymer, leading to a hydrophobic effect that results in lowering of the hydrodynamic volume of the polymer in the polar mobile phase, DMAc. The functionalisation of pHEMA-1 and pHEMA-2 to pBIEM-1 (Figure A8) and pBIEM-2 (Figure A9), respectively, showed the same trend. A summary of the resulting M_n and dispersity can be found in Table 3.

Table 3: Summary of synthesis and characterisation of pHEMA subsequent pBIEM characterisation.

Entry	Method (CTA)	DP	M_{nSEC} / \bar{D} (HEMA)	M_{nSEC} / \bar{D} (BIEM)
pHEMA-0 / pBIEM-0	RAFT (CPTP)	62	15 / 1.2	12 / 1.4
pHEMA-1/ pBIEM-1	ATRP	65	24 / 1.2	19 / 1.3
pHEMA-2 / pBIEM-2	RAFT (CPDB)	72	16 / 1.1	10 / 1.3

5.2.2 Side chain synthesis: ‘grafting from’

The successful introduction of the pendant bromine groups to the polymer chain provides an initiation point for side chain synthesis using controlled ATRP polymerisation in a grafting from approach (Figure 82).

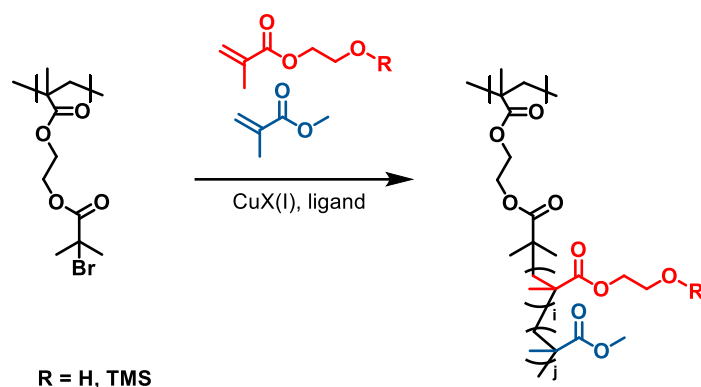


Figure 82: Reaction scheme of the general conditions used for synthesis of molecular polymer bottlebrush side chains with a grafting 'from' approach.

As the desired bottlebrush requires an additional handle for the introduction of the acrylate groups for the final application in 2PLP, the side chains were formulated as a copolymer of two monomers. Initially HEA and BA were chosen as a model system, using CuCl and PMDETA as catalyst and ligand, respectively to give the polymer pHEMA₁-g-(pHEA-co-BA), where pHEMA-1 was used as the backbone. The goal was to synthesise a brush polymer with monomodal dispersity. The polymerisation was followed through monomer conversion using ¹H NMR spectroscopy, as well as SEC. Initially, two solvents were used, either DMF or anisole, based on previous literature.^[132,133] The side chain reaction **SC1** led to a multimodal product, where initiation was also incomplete resulting in a low monomer conversion of 36.4% with visible peaks corresponding to the starting pBIEM polymer in the SEC trace (Figure 83, pHEA-BA **SC1**). When using anisole as a solvent (Table 4, **SC2**) the reaction formed a solid gel that after dissolution was not soluble and could not be characterised. Thus, the reaction was repeated in DMF (Table 4, **SC3**), reducing the concentration by half and using CuBr as a catalyst, more typically used with PMDETA than CuCl. The product, pHEA-BA **SC3** was again a multimodal product, however the remaining starting material as seen for pHEA-BA **SC1** was no longer present, while a peak at higher retention time appears, suggesting more efficient initiation (Figure 83).

Table 4: Reaction conditions and characterisation of side chain reactions SC1-3. R = ^{a)}[HEA]:[BA]:[CuCl]:[PMDETA] ^{b)}[HEA]:[BA]:[CuBr]:[PMDETA]

Entry	R	Solvent	Conditions	Conv. (%)	Product
SC1^{a)}	60:50:1:1	DMF	95 °C, 20 hr	36.4%	Multimodal
SC2^{a)}	60:50:1:1	Anisole	95 °C, 20 hr	-	Gelation
SC3^{b)}	50:50:1:1	DMF	65 °C, 4 hr	35.9%	Multimodal

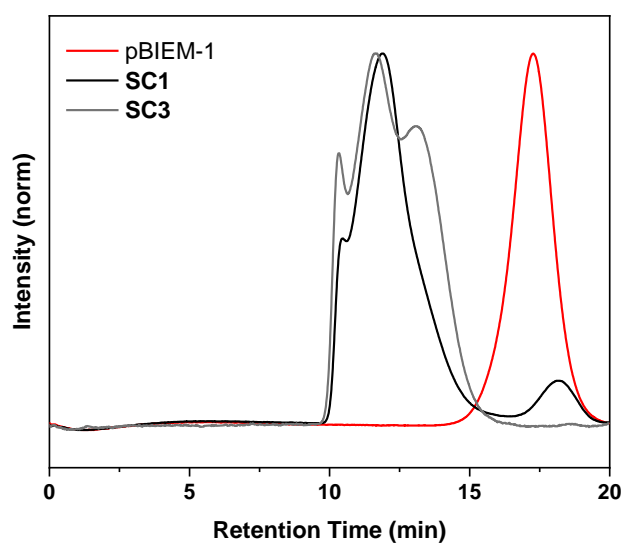


Figure 83: SEC traces (DMAc) of side chain reactions **SC1** and **SC3** (HEA-co-BA) showing multimodal dispersity.

The reaction was also repeated using HEMA rather than HEA (Table 5, **SC4**), along with a protected HEMA monomer, HEMA-TMS, to reduce the polarity compared to the comonomer BA (Table 5, **SC5**). Reaction 4 led to very low conversion below 5%, despite the SEC trace suggesting a high molecular weight product (M_n of 407 kg mol⁻¹) with a high dispersity of 2.2. A similar result was observed when using the HEMA-TMS monomer in reaction **SC5**, however, in this instance the total monomer conversion of 47.6% was calculated, with approximately 30% incorporation of HEMA-TMS. Again, the low retention time peak was seen in the SEC trace, suggesting coupling of the backbone or other side reactions (Figure 84). In reaction **SC6**, the same conditions were used, however a homopolymer of HEMA-TMS was targeted. In this case, the conversion was calculated to

be around 30%, similar to the incorporation of HEMA-TMS of the previous reaction, with a lower molecular weight peak now apparent in the SEC trace (Figure 84).

Table 5: Reaction conditions and characterisation of side chain reactions SC4-6. R = ^{a)}[HEMA]:[BA]:[CuCl]:[PMDETA] ^{b)}[HEMA-TMS]:[BA]:[CuCl]:[PMDETA] ^{c)}[HEMA-TMS]:[CuCl]:[PMDETA]

Entry	R	Solvent	Conditions	Conv. (%)	M _{nSEC} / Đ	Product
SC4 ^{a)}	50:50:1:1	DMF	95 °C, 4 hr	< 5%	407 kg mol ⁻¹ / 2.1	Multimodal, coupling
SC5 ^{b)}	50:50:1:1	DMF	95 °C, 4 hr	47.6%	-	Multimodal, coupling
SC6 ^{c)}	100:1:1	DMF	95 °C, 4 hr	29.8%	948 kg mol ⁻¹ / 2.6	Multimodal

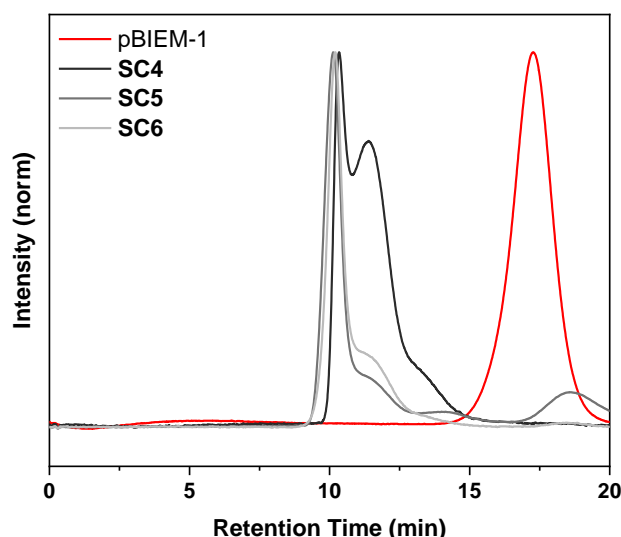


Figure 84: SEC traces (DMAc) of side chain reactions **SC4** (HEMA-co-BA), **SC5** (HEMA-TMS-co-BA), and **SC6** (HEMA-TMS) showing multimodal dispersity.

Despite the incorporation of HEMA-TMS, the side chain reaction still showed unwanted high molecular weight side products and high dispersity. For the next reactions, the comonomer was changed to methyl methacrylate, rather than butyl acrylate, to improve compatibility of the two monomers such that both are methacrylates, which have slower reaction kinetics than acrylates. Initially, anisole was used as the solvent (Table 6, **SC7**), with the prospect that the protected hydroxy group would make the reaction more stable in this solvent compared to previous attempts. In this case there reaction was more

successful than previously, with a conversion of 35.7% resulting in a polymer of $M_n = 120 \text{ kg mol}^{-1}$, however the dispersity was still quite broad at 1.3, with a higher molecular weight shoulder (Figure 85, left). For next attempts, reaction **SC8**, an alternative solvent toluene was used. Previously, all reactions were performed with a ratio of catalyst to ligand of 1:1, as per previous literature, however it has been seen that decreasing the ratio of catalyst, effectively decreasing the rate of polymerisation, can improve reaction control.^[134] This leads to lower overall conversion as well as decreased dispersity.^[135,135] Here, the ligand concentration was increased slightly from 1:1 to 1:1.1 (M:L). This resulted in a monomodal product with a slight higher molecular weight shoulder, at both 2 h (83 kg mol^{-1} , $\bar{D} = 1.2$) and 3 h (102 kg mol^{-1} , $\bar{D} = 1.1$) time points. The reaction was then repeated twice to determine reproducibility (Table 6, reaction **SC9**, **SC10**). Initially the conversion could not be determined due to the volatility compared to the previous solvent that was used as the internal standard, DMF. The reaction was repeated, including dimethyl terephthalate (DMT) as an internal standard, otherwise keeping all other parameters constant. As the distribution of **SC8** did not seem to change significantly between 2-3 hr, the further reactions were quenched at 2.5 h to reduce the overall molecular weight of the product. Despite the previously successful reaction, the product was not reproducible, leading to bimodal distributions in both reaction **SC9** and **SC10** (Figure 85, right), the conversion was calculated to be 43.8% and 46.7%, respectively.

Table 6: Reaction conditions and characterisation of side chain reactions **SC7-10**. R = [HEMA-TMS]:[MMA]:[CuCl]:[PMDTA]

Entry	R	Solvent	Conditions	Conv. (%)	M_{nSEC} / \bar{D}	Product
SC7	50:50:1:1.0	Anisole	95 °C, 3 hr	35.7	$120 \text{ kg mol}^{-1} / 1.3$	Broad
SC8	50:50:1:1.1	Toluene	95 °C, 3 hr	-	$102 \text{ kg mol}^{-1} / 1.1$	Monomodal
SC9	50:50:1:1.1	Toluene	95 °C, 2.5 hr	43.8	$130 \text{ kg mol}^{-1} / 1.3$	Bimodal
SC10	50:50:1:1.1	Toluene	95 °C, 2.5 hr	46.7	$145 \text{ kg mol}^{-1} / 1.4$	Bimodal

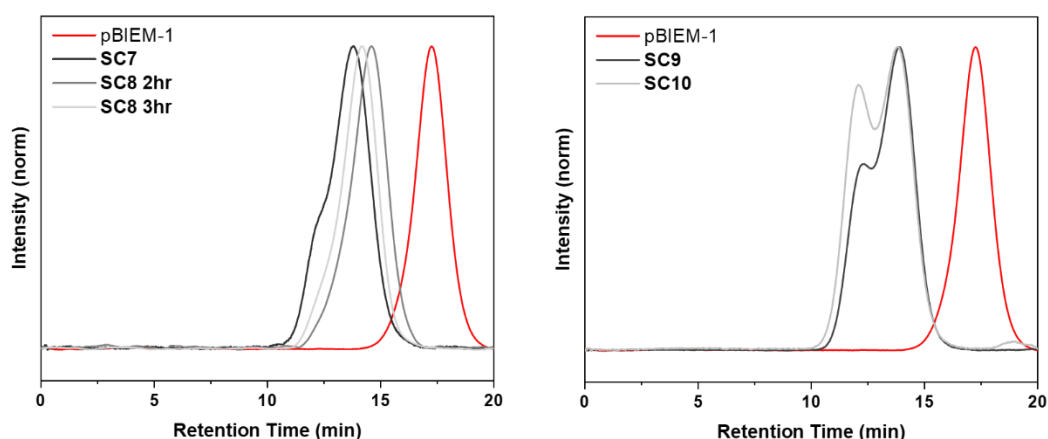


Figure 85: SEC traces (DMAc) of side chain reactions **SC7-10** showing difficulty with reproducibility of monomodal product.

It has also been seen that decreasing the reaction temperature can improve the reaction control by reducing termination reactions.^[135,136] Thus, using the same reaction conditions, the temperature was reduced from 95 °C to 80 °C (Table 7, reaction **SC11**, **SC12**). This led to a monomodal product in both cases (Figure 86, left), however the conversion and resultant molecular weight varied. The first attempt, **SC11**, showed 10.3% overall conversion, and a M_n of 54 kg mol⁻¹ with a dispersity of 1.2, while the second attempt, **SC12**, resulted in 5.0% conversion and a M_n of 29 kg mol⁻¹ with a dispersity of 1.1. However, overall, the product was suitable, with the final conformation pHEMA-*g*-(HEMA-TMS-*co*-MMA). Finally, two reactions were performed using the same conditions, switching to pBIEM-2 (**SC13** and **SC14**), while reducing the equivalents of HEMA-TMS, which as discussed in the next chapter, was chosen to reduce the number of hydroxy units available for the post functionalisation reaction. Although the initial polymerisation led to a trimodal product (**SC13**), the subsequent reaction under the same conditions led to a monomodal product with a M_n of 75 kg mol⁻¹ and a dispersity of 1.3 (**SC14**). **SC13** and **SC14** were used for further reactions.

Table 7: Reaction conditions and characterisation of side chain reactions SC11-14. R = [HEMA-TMS]:[MMA]:[CuCl]:[PMDETA]. ¹⁾ pBIEM-1 or ²⁾ pBIEM-2

Entry	R	Solvent	Conditions	Conv. (%)	$M_{nSEC} / Đ$	Product
SC11 ¹⁾	50:50:1:1.1	Toluene	80 °C, 3 hr	10.3	54 kg mol ⁻¹ / 1.2	Monomodal
SC12 ¹⁾	50:50:1:1.1	Toluene	80 °C, 3 hr	5.0	29 kg mol ⁻¹ / 1.1	Monomodal
SC13 ²⁾	25:75:1:1.1	Toluene	80 °C, 3 hr	46.2	333 kg mol ⁻¹ / 2.1	Trimodal
SC14 ²⁾	25:75:1:1.1	Toluene	80 °C, 3 hr	22.6	75 kg mol ⁻¹ / 1.3	Monomodal

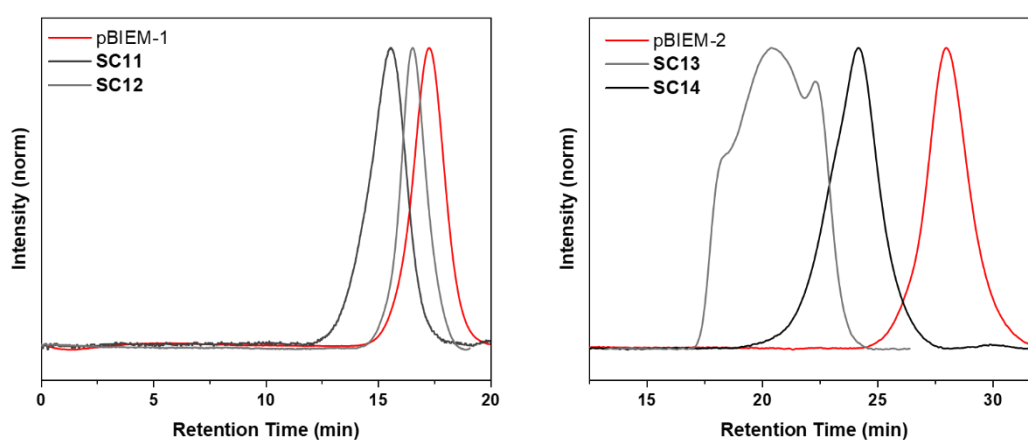


Figure 86: SEC traces (DMAc) of side chain reactions using a monomer feed ratio of left) 50:50 and right) 25:75 HEMA-TMA:MMA in duplicate.

5.2.3 Introduction of crosslinkable acrylate moiety

After the successful synthesis of monomodal bottlebrush structures pHEMA-g-(HEMA-TMS-co-MMA), the next challenge was to introduce functionality to the macromolecules for 2PLP. As discussed in the previous chapter, synthesising an ideal molecular polymer bottlebrush for 2PLP involves the introduction of a suitable crosslinkable group, however as important was designing the MPBs in a way that they were stable throughout the synthesis, purification and ink formulation prior to printing. As a large molecular architecture, MPBs can be more difficult to handle than linear polymer counterparts, and are prone to conformational changes such as aggregation, in particular this can occur irreversibly when the bottlebrushes are stored in a dry state. Thus one main challenge was maintaining solubility and keeping the brushes in solution during characterisation.

Additionally, when introducing a functional group such as (meth)acrylates, it is important to find a system that does not crosslink prematurely, which can occur even in linear polymers, thermally or bolstered by a high density of crosslinkable groups. At the same time, increased crosslinkable group density also increases the printing resolution. Thus the post functionalisation step was designed with two considerations:

1. Synthesis and characterisation without loss of solubility or unwanted crosslinking
2. Balance between meth(acrylate) density and molecular stability

To that end, methacrylates were chosen over acrylates, as used in previous chapters. This was due to the lower reactivity of methacrylates, as well as consistency within the polymer network which is otherwise composed of methacrylates in the backbone and side chains.

When determining the reaction conditions, a number of assumptions are made in this case. Firstly, due to the large size of the polymers, the end groups of the backbone or side chains are no longer visible in the spectra, thus the final composition is calculated by determining the ratio of the two monomers (HEMA-TMS and MMA) and calculating their incorporation based on the degree of polymerisation of the side chains. The example case of **SC13**, the monomer conversion of the side chains was determined to be 46.2%, assuming a grafting density of 1, i.e. every initiation point along the backbone is utilized, this results in a degree of polymerisation N_{sc} of 46. From the 1H NMR spectrum, for the three CH_3 protons of MMA, there are 2.26 $-CH_2-CH_2-$ protons of HEMA-TMS. Thus, it was determined that the ratio of MMA:HEMA-TMS was 1:0.56, i.e. for every 1 MMA unit there is 0.56 HEMA-TMS units (Figure 87).

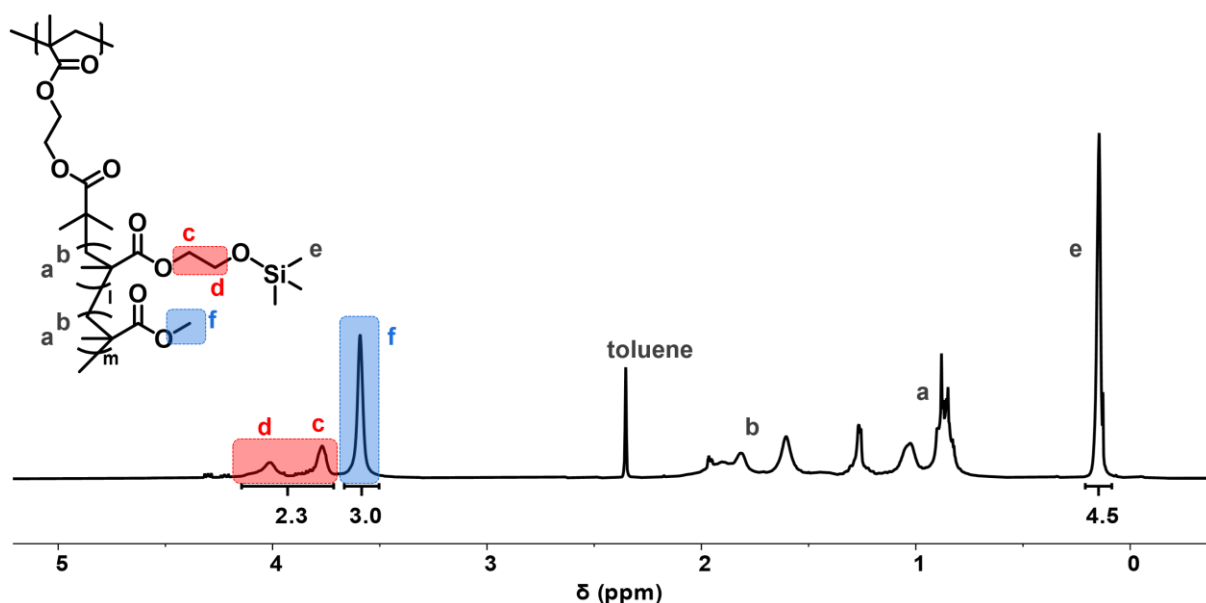


Figure 87: ¹H NMR spectra (CDCl₃, 300 MHz) of **SC13** pHEMA-g-(HEMA-TMS-co-MMA) .

With a total of 46 units, the fraction of HEMA-TMS units is therefore calculated using Equation 6:

$$\frac{HEMA-TMS}{HEMA-TMS+MMA} * DP_{SC} = N_{HEMA-TMS} \quad \text{Equation 6}$$

$$N_{HEMA-TMS} = \frac{0.56}{1.56} * 46 = 17$$

Thus, it was assumed that each side chain is comprised of 17 HEMA-TMS units and 29 MMA units. This calculation was also performed for **SC14**, which has a degree of side chain conversion, N_{SC} , of 23 and therefore a the composition of HEMA-TMS:MMA units of 4.5:18.5 , calculated from the ¹H NMR spectrum (Figure A12).

The post functionalisation reaction conditions are based additionally on another assumption, whereby the molar equivalents of methacryloyl chloride to hydroxy groups is determined based on the degree of side chain polymerisation, again assuming a grafting density of 1, as well as the molecular weight, determined through SEC. It is well known that SEC is not an accurate measure of molecular weight, particularly when considering polymers composed of alternative monomers than those used to calibrate the instrument (polystyrene or PMMA). Thus, when considering these limitations, the

determined value of N_{SC} can be thought of in relative terms but overall quantification of the molar equivalents of hydroxy groups or MMA groups through this method will not be absolute. Additionally to calculating the molar equivalents, in this case the TMS protecting group that facilitated the backbone polymerisation also needs to be deprotected giving the polymer pHEMA-*g*-(HEMA-*co*-MMA), where the product is isolated and further functionalised (Figure 88i). Alternatively, in a one pot reaction the deprotection and post functionalisation may happen concurrently (Figure 88ii). The one pot approach additionally reduces the purification steps required, minimising the likelihood of unwanted aggregation or crosslinking. Particularly due to the solvent compatibility of the protected polymer, which is soluble in DCM, compared to the more polar deprotected HEMA, which required the post functionalisation reaction to be performed in DMF, reducing the reaction efficiency and further complicating the characterisation as DMF requires harsher conditions to remove, or an additional solvent exchange step.

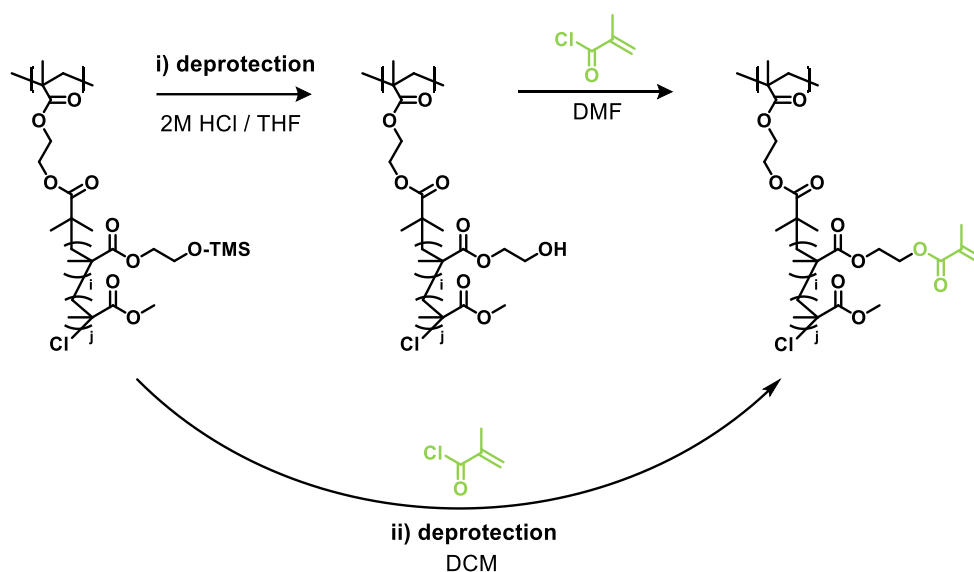


Figure 88: Reaction scheme for the two reaction paths for the introduction of methacrylate groups to the TMS-protected hydroxy functional groups of pHEMA-*g*-(HEMA-TMS-*co*-MMA) with deprotection in i) two isolated steps or ii) *in situ*.

The success of the deprotection reaction was monitored using ^1H NMR spectroscopy on a crude polymer sample using a low concentration of HCl following a literature procedure, resulting in the disappearance of the TMS signal around 0.1 ppm (Figure A15).⁴⁸ However, concurrently, the post functionalisation reaction was performed *in situ*,

using the strategy optimised in previous chapters for the esterification of hydroxy groups using an acyl halide (Figure 89).

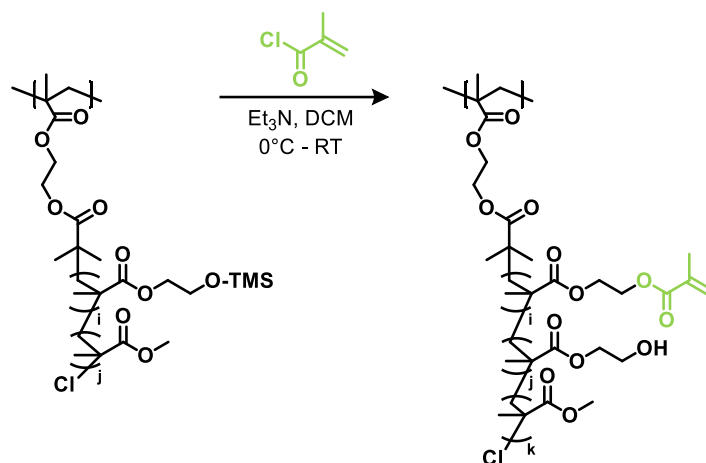


Figure 89: Reaction scheme for the introduction of methacrylate groups to the TMS protected hydroxy functional groups of pHEMA-g-(HEMA-TMS-co-MMA) with in situ deprotection.

Here it was hypothesised that deprotection of TMS followed by esterification reaction could proceed in a one pot reaction, similarly to the functionalisation of linear pHEMA-TMS with α -BiBB in a one pot reaction, as seen in literature.^[137] The purification was additionally optimised, minimising the time the products were in a dry state, through dialysis. This reaction was followed by ¹H-NMR spectroscopy where a shift in the ethylene protons of the HEMA side chain monomer was expected after the functionalisation with the methacryloyl chloride. The new shifted peak appears at approximately 4.3 ppm, and while unfunctionalised HEMA units remain as evidenced by the unshifted ethylene protons, they are fully deprotected as seen by the lack of TMS protons at 0.1 ppm. Additionally new peaks of the purified polymer appear between 5.6 and 6.1 ppm, indicative of the methacrylate group attached to the polymer side chains (Figure 90).

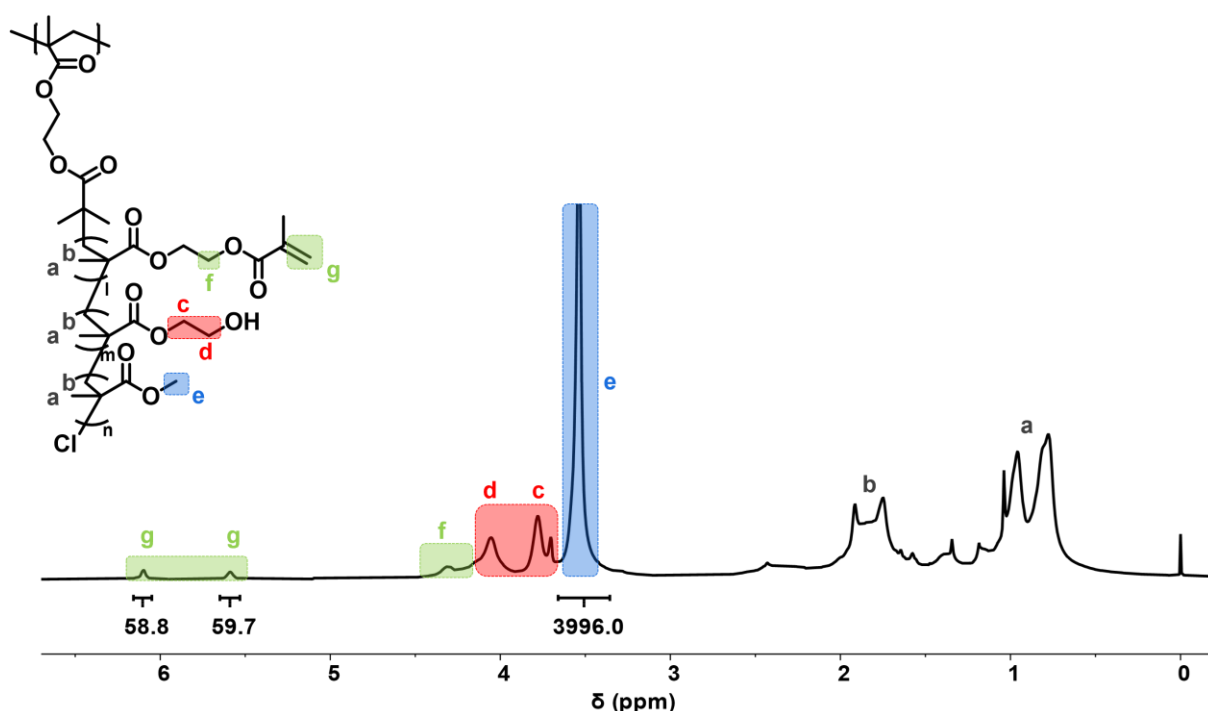


Figure 90: ^1H NMR spectrum (CDCl_3 , 300 MHz) of **PF3** pHEMA-*g*-(HEMA-*co*-MMA-*co*-methacrylate) bottlebrush.

Initially, the post functionalisation reaction was performed on a multimodal pHEMA-*g*-(pHEMA-TMS-*co*-MMA) bottlebrush **SC13** (Table 7), which has N_{SC} composition of 17:29 HEMA-TMS:MMA, giving products **PF1-2**. A third post functionalisation was performed using **SC14** giving **PF3** (Table 8). After functionalisation with methacryloyl chloride, the degree of methacrylation of the MPB was calculated from ^1H NMR spectroscopy by comparing the number of MMA protons of the side chains with the number of methacrylate groups (Figure 90). The total number of MMA units is equal to $N_{\text{BB}} * N_{\text{SC(MMA)}}$ (and accordingly the total number of HEMA units per bottlebrush molecule is equal to $N_{\text{BB}} * N_{\text{SC(HEMA)}}$), assuming a grafting density of 1. In an exemplary calculation, of the number of incorporated methacrylate groups for **PF3** was determined by ^1H NMR spectroscopy, comparing the integration of the known number of MMA protons in one brush, to the integration of the methyl acrylate protons at 5.6 and 6.1 ppm (Figure 90). The number of MMA protons can be calculated with Equation 7:

$$N_{\text{BB}} * N_{\text{SC(MMA)}} * H_{\text{CH}_3(\text{MMA})} = H_{\text{MMA}(\text{bottlebrush})} \quad \text{Equation 7}$$

$$72 * 29 * 3 = 3996 \text{ H}$$

Thus, for **PF3**, each brush contains an average of 59.3 methacrylate groups. This calculation was also performed for **PF1** (Figure A13) and **PF2** (Figure A14). A number of post functionalisation reactions were performed, optimised concurrently with printing attempts, to find a suitable degree of methacrylation that would allow for good printability while mitigating the previously discussed complications—unwanted crosslinking or irreversible aggregation. The results of three post functionalisation reactions, using either **SC13** or **SC14** are summarized in Table 8. **PF2** was upscaled to functionalise a larger batch of MPB, which resulted in an increased functionalisation degree. Finally, **PF3** was synthesised from **SC14**, which contained fewer HEMA groups per side chain and resulting in fewer methacrylate groups as expected.

Table 8: Post functionalisation reactions synthesised from ¹⁾ **SC13** or ²⁾ **SC14**

Entry	M-Acryl Cl. Eq.	M.Acryl per MPB
PF1 ¹⁾	1.75	79.5
PF2 ¹⁾	3	116.5
PF3 ²⁾	3	59.3

5.3 MOLECULAR POLYMER BOTTLEBRUSH INKS FOR 2PLP: ADVANCED ARCHITECTURES

5.3.1 Ink formulation and characterisation

For the optimisation of the ink formulation, as well as the molecular composition of the final bottlebrush structures, a few factors need to be considered: not only the degree of methacrylation but also polymer concentration, photoinitiator concentration, and the solvent. The initial tested formulation comprised 65 wt% of **PF1** with a methacrylation degree of 79.5 units per bottlebrush, with 0.5 wt% DETC as photoinitiator and 0.1 wt% BHT as inhibitor, solubilised in DMAc. In addition to the printing itself, the preparation of the ink for the printing process must also be considered. Typically, for low viscosity inks that have volatile components incorporated, the standard set up involves a PDMS well on a glass coverslip, to which the ink is deposited and sealed from above with another coverslip to prevent evaporation (Figure 91, left). Alternatively, for much higher viscosity inks or solids, the ink is deposited as a droplet in the middle of the slide and covered by a second coverslip (Figure 91, right).

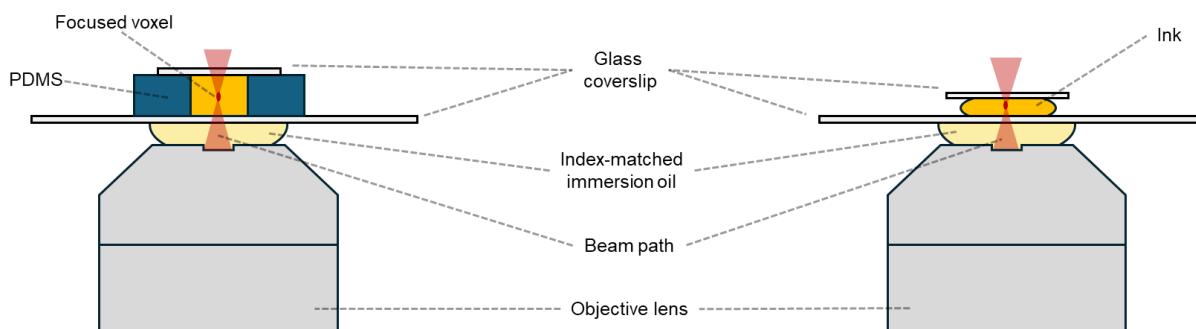


Figure 91: Schematic representation of the 2PLP set up during printing, where the ink is formulated either into a PDMS well (left) or sandwiched between two glass slides (right).

The initial formulation was chosen to contain a higher wt% of solvent, due to the likelihood of entanglement or crosslinking of the bottlebrush in the dry state, and to increase handleability, and was printed in the PDMS configuration. The initial structure chosen for printing tests was a flower, as a relatively low complexity structure that does not contain overhangs.

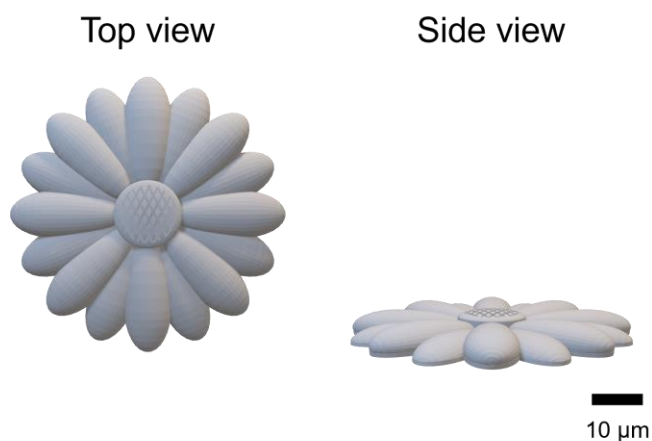


Figure 92: 3D rendering of the flower structure used for initial printing tests.

Although the ink itself was printable, after development the resulting structures were loosely crosslinked, leading to loss of resolution (Figure 93). Despite the low crosslinking density, a relatively high laser power (70 – 75 % of the maximum, or 35 – 37.5 mW) and slow scan speed (2 mm s^{-1}) was required.

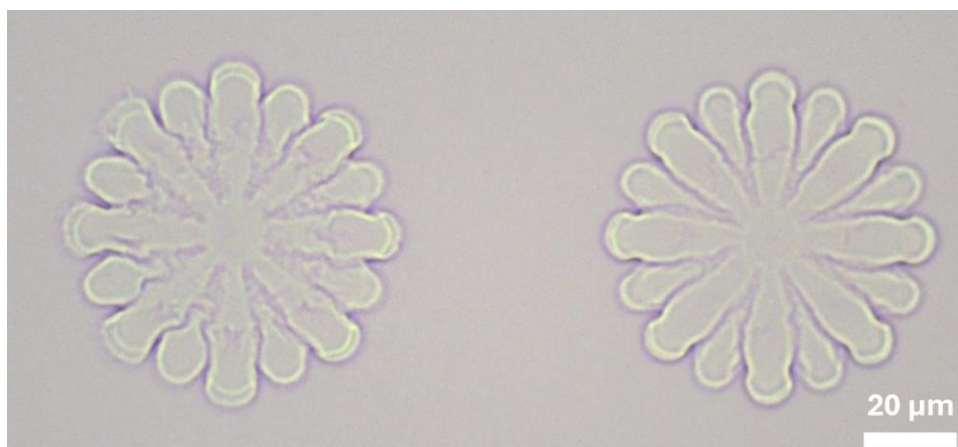


Figure 93: Microscope image of flowers printed with **PF1**, 65 wt%, 0.5 wt% DETC, and 0.1 wt% BHT in DMAc.

To improve this, either the MPB wt% could be increased, or the degree of methacrylation. When trying to increase the fraction of MPB in the ink, problems with solubility occurred, where the polymer did not dissolve homogeneously within the solvent. For **PF1**, the equivalents of methacryloyl chloride to hydroxy groups was 1.75, giving an average of 8.2 methacrylates per bottlebrush within the product. It was theorised that the potential loss of defined structure in the printing process could be due to the large molecular size of the bottlebrushes compared to linear counterparts, with potential for intramolecular crosslinking and loose network formation. **PL2**, with 116.5 methacrylates, was formulated into an ink with the same composition as previously (65 wt% MPB, 0.5 wt% DETC and 0.1 wt% BHT in DMAc). However, the printability was still poor despite the increase in methacrylate groups, appearing as though some solubility issues arise during the printing (Figure 94). Again, the resolution of the finer structures was lost. Additionally, tests where the solvent concentration was reduced resulted in premature crosslinking. **PF1-2** were formulated from bottlebrushes with a multimodal dispersity, potentially adding to the inhomogeneity observed.

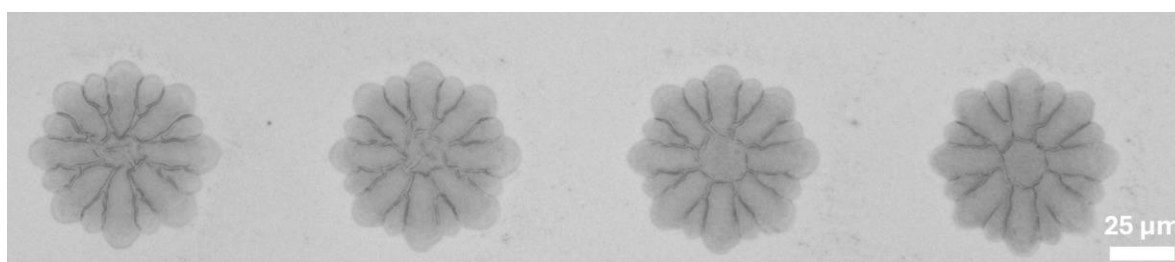


Figure 94: Microscope image of flowers printed with **PF2**, 65 wt%, 0.5 wt% DETC and 0.1 wt% BHT in DMAc.

For the next printing tests, **PF3** was used. Despite fewer calculated methacrylates per bottlebrush (59.3) than **PF1** and **PF2** the bottlebrush showed monomodal dispersity in the SEC trace. The formulation was also changed from DMAc to 1,4-dioxane in an effort to improve any solubility issues. The ink formulation here with 70 wt% MPB with 0.5 wt% DETC printed successfully (Figure 95a), however some resolution was lost when compared to the desired structure. Reducing the polymer fraction to 56 wt% resulting in overall finer resolution printing (Figure 95b). Both samples were printed with the sandwich configuration seen in Figure 91, right, and developed within an hour of loading the sample onto the slide to prevent any crosslinking of drying of the ink. The improved print quality could be due to both the change of solvent used, but also potentially the more controlled architecture due to the monomodal dispersity of the bottlebrush.

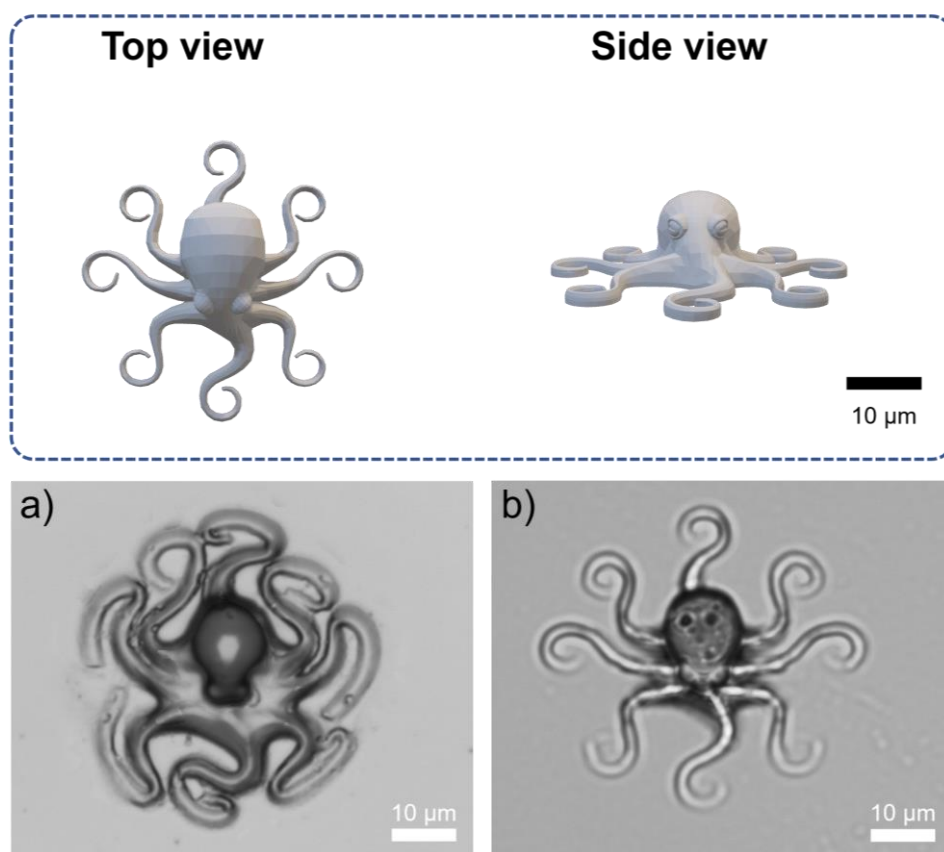


Figure 95: Rendering of the octopus structure input for 3D printing, and microscope image of octopus printed with **PF3** a) 70 wt%, 0.5 wt% DETC in 1,4-dioxane and b) 56 wt%, 0.5 wt% DETC in 1,4-dioxane.

It was hypothesised that a higher percentage of MBP in the ink would lead to better resolution, due to the increased density of methacrylates, however the opposite appears to be the case. It is also possible that the reduced concentration of bottlebrush allowed

for more flexibility and movement of the polymer backbone and side chains, leading to more intermolecular crosslinking rather than potential intramolecular crosslinking and leading to a more dense network, resulting in higher printing resolution. SEM imaging of the octopus structure of **PF3** printed at 56 wt% suggests that where the high MPB composition ink appeared more ‘swollen’ than the intended input structure, with the lower MPB composition some loss of fine detail compared to the original 3D structure design is observed (Figure 96).

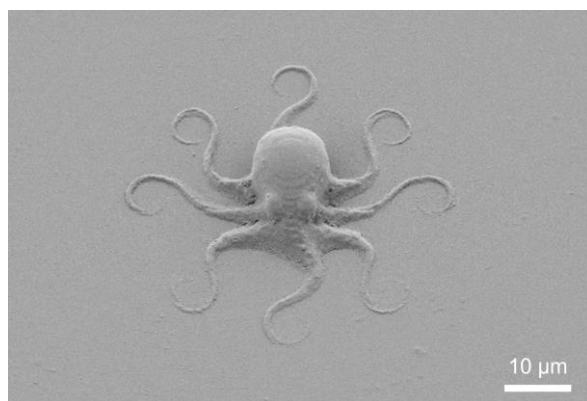


Figure 96: SEM image of octopus structure printed with **PF3**, 56 wt%, 0.5 wt% DETC in 1,4-dioxane.

This supports the 70 wt% ink forming a more loosely crosslinked network, while the lower wt% has a more densely crosslinked network, but is susceptible to shrinking. A more detailed investigation is required to determine the exact effect of the polymer bottlebrush composition not only as concentration within the ink, but also the effect of the conformation of the bottlebrush itself (backbone length, side chain length, monomer composition) on the printed network. Using the optimised formulation **PF3**, 56 wt% in 1,4-dioxane, micropillars were printed for mechanical testing using nanoindentation. Here, the reduced modulus and hardness were determined at two laser powers, either 25 mW or 40 mW. An increase in both hardness and E_r was observed with increasing laser power, as expected. The printed structures had a E_r of 2.0 – 2.6 GPa, and hardness around 150 – 200 MPa (Figure 97).

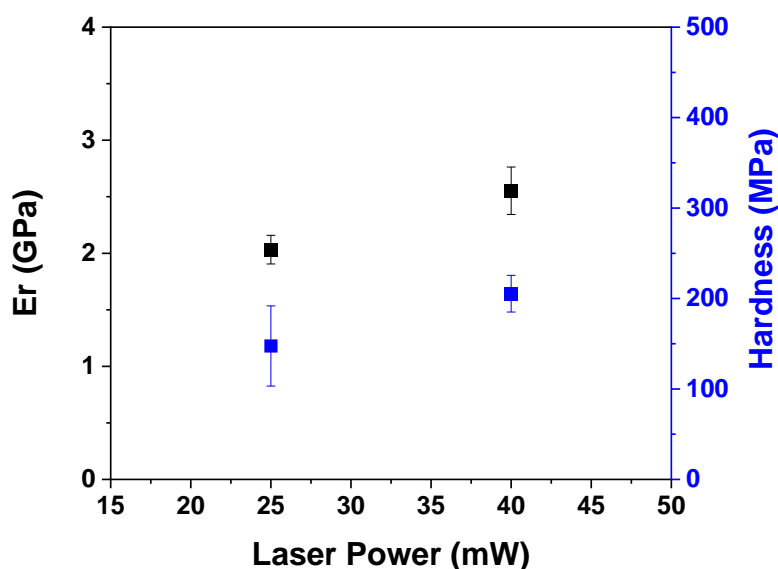


Figure 97: Nanoindentation results showing the reduced elastic modulus (E_r) and hardness measured with micropillars printed with **PF3**, 56 wt%, 0.5 wt% DETC in 1,4-dioxane, using varied laser powers.

5.4 SUMMARY

The use of MPBs as inks for 2PLP is demonstrated for the first time. Using controlled-radical polymerisations, RAFT and ATRP, HEMA backbones were synthesised. To these, a bromine initiation site was introduced for further ATRP of MMA and HEMA monomers as side chains, in a grafting ‘from’ approach. The synthesis was carefully optimised with the goal of monomodal bottlebrush architectures containing backbone and side chains of similar length. To that end, a number of reactions conditions were explored for the side chain synthesis such as temperature, solvent type, protected or unprotected hydroxy groups, monomer ratios, and metal/ligand ratios and types. An MPB with suitable backbone and compatible side chain architecture, with low dispersity and monomodal distribution, was synthesised. Due to the requirement of introduction of a crosslinkable group for 2PLP, the side chains comprised copolymers of MMA and HEMA, whereby the hydroxy group of HEMA would be used as the synthetic handle for the introduction of methacrylates. It was observed that the ATRP side chain polymerisation was more successful when the HEMA was TMS protected, and thus deprotection of the TMS group after synthesis was also necessary. This was optimised in a one step reaction with the simultaneous introduction of the crosslinkable methacrylate groups for network

formation. The printability was investigated by varying the methacrylate composition of the final bottlebrush polymer, as well as determining the most suitable solvent for solubilising the photoinitiator while retaining a handleable material, and optimising the composition of MPB by weight in the final ink. An ink composition that allowed for the successful fabrication of defined microscale structures was developed. The ink could be printed with a range of laser powers and scan speeds. Additionally, structures were fabricated for characterisation of mechanical properties with nanoindentation. The final printed bottlebrush structures demonstrated E_r in the range of 2.0 – 2.6 GPa and hardness of 150 – 200 MPa, over a laser power range of 25 to 45 mW. Overall, the use of MPBs as a printable molecular architecture using 2PLP was demonstrated for the first time.

6 Conclusion and Outlook

Herein, three distinct pathways toward new and controlled macromolecular inks 2PLP are explored. To that end, two systems were developed to examine how molecular design can influence the printing process and how this affects the resultant printed structures, as seen in '**Chapter 3: Pre-polymers as 2PLP inks**' and '**Chapter 4: Sequence-defined oligomers as 2PLP inks**'. In both instances, structure–property relationships were examined in a three-step approach. First, specific strategies were used to design and synthesise reactive (macro)molecules with controlled structure and composition. Second, each (macro)molecule was formulated into a suitable 2PLP ink, and the stable printing window was investigated. Third, these inks were used to print diverse 3D geometries, with varied parameters such as laser power and scan speed, to examine relationships between the printing window and the chemical and mechanical properties. SEM was used to determine the range of printability over the varied laser power and scan speeds. The chemical properties of printed structures were characterised with vibrational spectroscopy, either Raman or FTIR spectroscopy, to determine the degree of conversion of the reactive group during printing. Additionally, the mechanical properties i.e. reduced elastic modulus and hardness, were determined using nanoindentation. This procedure allowed for correlations to be drawn between the observed printing behaviour, and chemical and mechanical properties, with specific composition of the inks.

Chapter 3 examined three 'pre-polymers' with different composition and thus differing physical properties i.e. molecular weight, comonomer type, glass transition temperature, and number of crosslinkable groups. Three monomers were chosen, to give side chains of butyl, methyl, or isobornyl groups. Each of these monomers were polymerised with 2-hydroxyethyl acrylate (HEA), which was then functionalised with an acrylate as the reactive group to enable 2PLP. The resultant 'pre-polymers' BA-co-Acryl, MA-co-Acryl, and IBA-co-Acryl were characterised, showing varied molecular weight, glass transition temperature, and number of acrylate units. The range of laser powers and scan speeds that produced stable structures during 2PLP was examined, where IBA-co-Acryl required the lowest laser power over all scan speeds, whereas BA-co-Acryl required

the highest. When correlating the printing range to degree of acrylate conversion it became apparent that each ink was printable within a similar window of DoC. All inks displayed a lower DoC threshold of approximately 40% required to print stable structures and an upper threshold of approximately 70% before overexposure occurred. Interestingly, the laser power required to reach this threshold was different for each ink. The IBA-co-Acryl required the lowest laser power, while BA-co-Acryl required the highest. When examining the mechanical properties, it was seen that IBA-co-Acryl had the highest reduced modulus, followed by MA-co-Acryl, while BA-co-Acryl showed the lowest reduced modulus over the entire laser power range. Thus, even at similar conversion degree, the structures printed with BA-co-Acryl showed lower mechanical properties than both MA-co-Acryl and IBA-co-Acryl suggesting effects such as network topology due to comonomer type, molecular weight etc. have an influence on the properties. Overall, it was clear that the macromolecular structure plays a role in the printability and properties in 2PLP.

To further investigate these effects in greater detail and draw deeper correlations, it would be beneficial to fabricate a larger library of polymers. Factors such as increasing molecular weight within a single copolymer composition, comonomers with different glass transition temperatures, fewer or greater acrylate units, or the effect of incorporating functionality, would be interesting parameters to investigate. However, small changes in composition can have a large effect on the printed structures and it is therefore necessary to keep each varied parameter as consistent as possible. This can prove difficult when changing the physical properties of the pre-polymers. For example, increasing the molecular weight may lead to different solubility properties, in turn making it difficult to keep the ink formulation constant. Despite the potential difficulties, investigation into the effect of different ink formulations is also worthwhile. To that end, it is likely that high throughput approaches could be incorporated, however to some degree an initial level of manual investment is required when designing new inks.

As discussed earlier the second investigation, detailed in **Chapter 4**, followed a similar outline. Here, a different type of molecular control was employed. Where **Chapter 3** investigated the pre-polymer composition through different comonomers, **Chapter 4** focuses on the monomer sequence within the ink. Three oligomers were designed based

on two repeat units, either non functional (butyl side chains, B) or functional (acrylate side chains, C, as the reactive units for 2PLP). Each oligomer was eight units in length, and varied only in the sequence of the repeat units, either alternating (BCBCBCBC), triblock (CCBBBBCC) or block (BBBBCCCC). The oligomers were synthesised in a precise manner using solid phase iterative synthesis protocols, similar to that used for peptides. In this case, the three molecules displayed similar glass transition temperatures, are identical in molecular weight, and indistinguishable by NMR spectroscopy. By keeping the ink formulation constant, the only changing variable during printing was the positioning of the reactive acrylate groups. In this way, the effect of sequence on the printing and the chemical and mechanical properties could be determined. Looking at the range of laser powers required to print stable structures, it was found that the alternating sequence required the lowest laser power dose, whereas the block sequence required the highest. The triblock sequence was in the range in between the two other sequences. To correlate the printing behaviour to the chemical properties, the degree of acrylate conversion of printed structures was determined using Raman spectroscopy. The alternating sequence displayed the lowest acrylate conversion over all laser powers, whereas the block sequence had the highest, reaching almost full conversion at the highest laser power. Interestingly, the mechanical properties of the printed structures did not follow the expected trend when comparing printability and acrylate conversion. For example, despite having the highest DoC, structures printed with block sequence showed the lowest reduced elastic modulus, while the alternating sequence had the highest reduced elastic modulus despite having a lower DoC. We propose that the alternating nature of the reactive acrylate groups results in more homogeneous network formation, leading to a printable stable network even with a lower degree of acrylate conversion. On the other hand, the block sequence is more susceptible to intramolecular reactions due to the proximity of the acrylate groups along the backbone, leading to a more inhomogeneous network requiring higher DoC for stable structures. In addition, the butyl side chains may act as 'dangling ends' with a plasticising effect, leading to lower reduced elastic modulus. The triblock sequenced had intermediate properties compared to the other two sequences. Thus, it was shown that not only the properties of printed

structures, but also the optimal printing conditions, can vary significantly depending on the molecular structure of the ink.

This concept could be expanded to new tailorable materials through precise ink design. The optimised synthesis procedure would allow for the 'non functional' monomer to be replaced by any acrylate molecule, as long as no competitive functional groups were present. In this way, a host of new functionalities could be incorporated for various applications, such as site-specific cell binding moieties, molecular material data encryption, labelling, or mechanobiological investigations.

In the final investigation in **Chapter 5**, the focus was on the design of a new advanced molecular architecture as an ink for 2PLP. To that end, molecular polymer bottlebrushes were proposed due to their unique and tuneable properties. An initial system consisting of a HEMA backbone with MMA and TMS protected HEMA copolymer side chains was synthesised, with methacrylate groups introduced into the side chains for 2PLP. The resultant MPB was formulated into a printable ink through the molecular optimisation of the side chain composition and number of acrylate groups as well as optimisation of the weight percentage of MPB, photoinitiator, and solvent, as well as solvent type. The final ink contained a MPB with a HEMA backbone length of 72 and side chains containing 19:27 HEMA-TMS:MMA units, with an average of 6.3 methacrylates per bottlebrush. The ink formulation at 56 wt% as well as 70 wt% in 1,4-dioxane with 0.5 wt% DETC showed reasonable printability, where the higher fraction of MPB led to some loss of resolution in the final structure potentially due to a more loosely formed network. The reduced modulus and hardness of the initial 56 wt% ink were determined using nanoindentation, with an E_r of between 2.0 – 2.6 GPa, and hardness in the range of 150 – 200 MPa, increasing with increasing laser power.

Many investigations of MPBs as materials have exploited the super soft elastomeric properties that can be achieved with bottlebrush type polymers compared to typical linear polymers, as well as functionality such as tailorable self-assembly behaviour. Until now, these properties MPBs have been explored in the realm of 3D printing only on the macroscale, using extrusion- or vat-based methods. Thus, further investigation into exploring this attribute in microprinted structures is envisioned. It is also promising to look deeper into the influence of modifying the molecular architecture, such as the ratio

of the length of backbone to side chains. This could give insight into the influence of MPB conformation in printed structures, as well the influence on the mechanical properties. There is also potential to utilise the self-assembly behaviour of MBPs into different conformations, based on the architecture, toward 3D printed structures with hierarchical order over different length scales, i.e. from nano- to micro- and potentially even macroscale.

For the future facile design of functional and complex inks for 2PLP, careful attention to (macro)molecular structure can lead to the rational design of inks with known properties that can be tailored to the desired application. It is clear that in the design and development of new multifunctional materials, understanding the complex relationships between the macro(molecular) structure and the behaviour of 2PLP materials is vital.

7 Experimental

7.1 MATERIALS

Chemicals and solvents were supplied from either Sigma–Aldrich or Fisher Scientific unless otherwise mentioned. All materials were used as received without further purification unless indicated. Acrylate and methacrylate monomers were filtered through basic alumina prior to use.

7.2 SYNTHESIS

7.2.1 Pre-polymer library

Synthesis of polymers: MX-co-HEMA

In a typical RAFT polymerisation, MMA (1.0 g, 10.0 mmol, 50.0 eq.) and HEMA (416.5 mg, 3.2 mmol, 16.0 eq.) were combined with and 2-cyanoprop-2-yl dithiobenzoate (CPDB) (44.3 mg, 0.2 mmol, 1.0 eq.) and dissolved in 1,4-dioxane (3.5 mL). The mixture was transferred to a Schlenk tube and AIBN (3.3 mg, 0.02 mmol, 0.1 eq.) was added. The solution was degassed through freeze-pump-thaw (4 x 8 min), followed by backfilling with nitrogen. The reaction mixture was stirred at 90 °C for 30 min. The reaction was quenched by immersion in liquid nitrogen and opened to atmosphere. After dilution with DCM, the solution was precipitated into cold n-hexane. After centrifugation and decanting of the supernatant, the copolymer MX-co-HEMA was received as a pink solid.

Synthesis of polymers: X-co-HEA

For a typical RAFT polymerisation the following feed ratios of comonomers X:HEA were used: BA:HEA (6:4 eq.), IBA:HEA (10:6) and MA:HEA (8:6 eq.). Monomers were combined with and 2-cyano-2-propyl dodecyl trithiocarbonate (CPDT) (342.7 mg, 1.0 mmol, 1.0 eq.) and dissolved in toluene (8 mL). The mixture was transferred to a Schlenk tube and AIBN (8.1 mg, 0.05 mmol, 0.05 eq.) was added. The solution was degassed through freeze-pump-thaw (4 x 8 min), followed by backfilling with nitrogen. The reaction mixture was

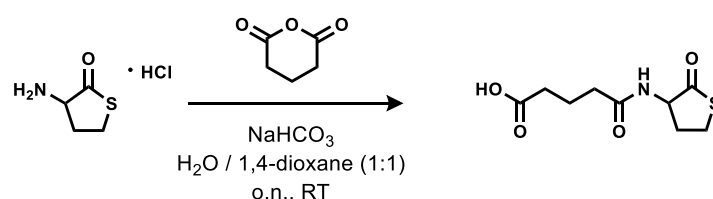
stirred at 100 °C for 35 min. The reaction was quenched by immersion in liquid nitrogen and opened to atmosphere. After dilution with DCM, the solution was precipitated into cold n-hexane. After centrifugation and decanting of the supernatant, the product was dried under high vacuum. The copolymer X-co-HEA was received as a yellow solid.

Post Functionalisation with acryloyl chloride: X-co-Acryl

For a typical post functionalisation reaction the following procedure was followed: under a nitrogen atmosphere, non-functionalised polymer (X-co-HEA, 150.0 mg, 1.0 eq. OH) was dissolved in dry DCM (20 mL). Et₃N (3.0 eq.) was added to the solution under nitrogen and stirred for a few minutes. The solution was cooled in ice and to this, acryloyl chloride (3.5 eq.) was added dropwise. The mixture was allowed to reach room temperature (RT) overnight under nitrogen atmosphere. The solvent was evaporated and the crude mixture redissolved in acetonitrile (30 mL) and 5% NaHCO₃ (30 mL). The solution was extracted with DCM (3 x 30mL). The organic fraction was dried over MgSO₄, filtered, and concentrated under reduced pressure, taking care not to heat above 40 °C. The product was then precipitated from DCM into ice cold n-hexane and centrifuged. The product dried under high vacuum and was received as a yellow solid.

7.2.2 Sequence-defined oligomers

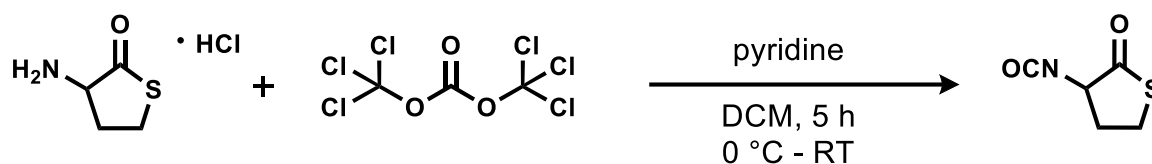
Synthesis of thiolactone carboxylic acid linker:



Synthesis of the thiolactone carboxylic acid linker (TLa-COOH) was performed according to previously reported procedures.^[126] D,L-homocysteine thiolactone hydrochloride (25.0 g, 0.16 mol, 1.0 eq.) was dissolved in a water/1,4-dioxane mixture (1:1, 400 mL). The solution was cooled to 0 °C in an ice bath. After careful addition of NaHCO₃ (68.4 g, 0.81 mol, 5.0 eq.), the mixture was stirred for 30 min. Glutaric anhydride (37.1 g, 0.33 mol, 2 eq.) was slowly added and the reaction was stirred and left to warm to room temperature overnight. 12 M HCl was added until a pH of 1 was reached. After addition of

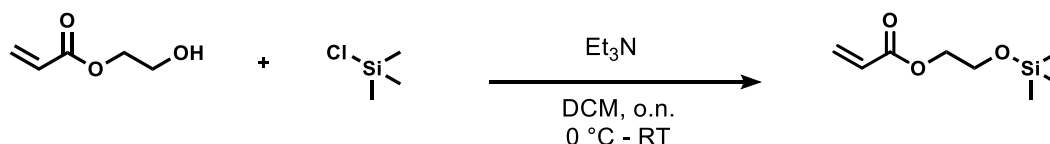
brine (150 mL), the mixture was transferred to a separating funnel and washed with ethyl acetate (3 x 150 mL). The organic fractions were combined and dried over MgSO₄. After removing the solvent the crude product was recrystallized from acetone, yielding a white, crystalline solid. (37.6 g, 82.4 %). **¹H NMR (300 MHz, DMSO-d₆):** δ (ppm) 12.05 (s, 1H), 8.18 (d, 1H), 4.67 – 4.52 (m, 1H), 3.47 – 3.21 (m, 4H), 2.41 (m, 1H), 2.29 – 1.97 (m, 5H), 1.72 (m, 2H).

Synthesis of thiolactone isocyanate linker:



Synthesis of the isocyanate carboxylic acid linker (TLa-COOH) was performed according to previously reported procedures.^[126] Triphosgene (9.2 g, 31 mmol, 0.3 eq.) was added to 100 mL ice-cooled dry DCM under a nitrogen atmosphere. A solution of 15 g D,L-homocysteine thiolactone hydrochloride (98 mmol, 1.0 eq.) in 80mL ice-cooled DCM was added. Afterwards, pyridine 26mL (25 g, 0.32 mol, 3.3 eq.) was added dropwise and the solution was stirred for 60 minutes at 0 °C. Subsequently the solution was allowed to reach room temperature and it was stirred for 4 hours. After filtration the organic phase was washed with each 100mL of a 2 M HCl solution, brine and ice water. Afterwards the solution was dried with magnesium sulphate and filtered. The solvent was removed under vacuum to yield a dark yellow oil. The product was purified via vacuum distillation (0.15 mbar, 75 °C). The product was obtained as a colourless oil (10.4 g, 72.6 mmol, 74.4%). **¹H NMR (300 MHz, CDCl₃):** δ (ppm) 4.23 (dd, 1H), 3.38 – 3.18 (m, 2H), 2.70 – 2.55 (m, 1H), 2.18 – 1.97 (m, 1H).

Synthesis of HEA-TMS (TMS-protected hydroxy monomer):



2-Hydroxyethyl acrylate (10.0 mL, 87.1 mmol, 1.0 eq.) and triethylamine (13.3 mL, 95.4 mmol, 1.1 eq.) were added to ice-cooled dry DCM (75 mL) under a nitrogen atmosphere.

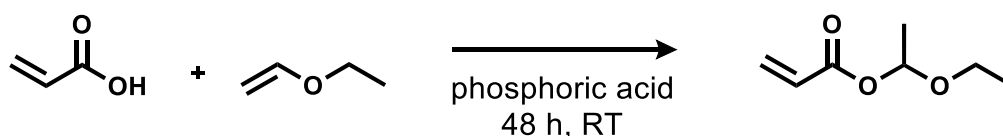
Chlorotrimethylsilane (12.1 mL, 95.4 mmol, 1.1 eq.) was dissolved in dry DCM (25 mL) and added dropwise. The reaction solution was allowed to reach room temperature while stirring overnight. The solid triethylamine hydrochloride was filtered out and the remaining solution was washed three times with a saturated sodium hydrogen carbonate solution (3 x 50 mL). Subsequently it was washed two times with 50 mL brine and dried with magnesium sulphate. After removing the solvent under vacuum, the product was obtained as colourless oil (15.8 g, 83.9 mmol, 88.0%). **¹H NMR (CDCl₃, 300 MHz) δ** (ppm): 6.41 (dd, 1 H), 6.13 (dd, 1 H), 5.81 (dd, 1 H), 4.21 (m, 2 H), 3.80 (m, 2 H), 0.11 (s, 9 H).

Synthesis of HEA-TIPS (TMS-protected hydroxy monomer):



2-Hydroxyethyl acrylate (6.0 mL, 51.9 mmol, 1.0 eq.) and triethylamine (6.0 mL, 51.9 mmol, 1.0 eq.) were added to 90 mL ice-cooled dry DCM under a nitrogen atmosphere. Triisopropylsilyl chloride (11.0 mL, 51.9 mmol, 1.0 eq.) was added dropwise. The reaction solution was allowed to reach room temperature while stirring overnight. The solution was then washed with 1 M HCl (2x 60 mL), saturated sodium hydrogen carbonate solution (60 mL) and distilled water (60 mL) and dried with magnesium sulphate. The solvent is evaporated under vacuum. The product purified by vacuum distillation (0.15 mbar, 67 °C), and obtained as a colourless oil (0.71 mg, 2.6 mmol, 5.0%). **¹H NMR (CDCl₃, 300 MHz) δ** (ppm): 6.41 (dd, 1H), 6.12 (dd, 1H), 5.81 (dd, 1H); 4.33 – 4.18 (m, 2H), 4.03 – 3.81 (m, 2H), 1.30 – 0.89 (m, 21H).

Synthesis of 1-ethoxy ethyl acrylate (EEA protected carboxylic acid monomer):



Synthesis of 1-ethoxy ethyl acrylate (monomer **C**) was performed according to previously reported procedures.^[138] Under a nitrogen atmosphere, acrylic acid (100 mL, 1.5 mol, 1.0 eq.) was added slowly to a mixture of ethyl vinyl ether (126.1 mL, 1.8 mol, 1.2 eq.) and of phosphoric acid (0.3 g, 3 mmol, 0.002 eq.) as a catalyst at 0 °C. The mixture was stirred

at room temperature for 48 h. The catalyst was then absorbed on hydrotalcite ($\text{Mg}_6\text{Al}_2(\text{OH})_{16}\text{CO}_3 \cdot 4\text{H}_2\text{O}$). After filtration the excess vinyl ether was evaporated. The product was distilled at reduced pressure (boiling point 30 °C, $3 \cdot 10^{-1}$ mbar) to obtain a colourless liquid (73.6 g, 44.1 %). **$^1\text{H NMR}$ (CDCl_3 , 300 MHz):** δ (ppm) 6.41 (dd, 1H), 6.09 (dd, 1H), 5.99 (q, 1H), 5.83 (dd, 1H), 3.77-3.46 (m, 2H), 1.41 (d, 3H), 1.18 (t, 3H).

Solid-Supported Oligomer Synthesis

The general four step procedure for the synthesis of oligomers was adapted from previous literature procedures.^[126]

Step i: Loading

The loading of the polystyrene resin was achieved through methods previously reported in literature. Briefly, 2-chlorotriethyl chloride resin (1.0 g, 1.6 mmol g^{-1} , 1.0 eq.) was swollen in anhydrous DCM (10 mL), anhydrous DMF (1 mL) and anhydrous N,N-diisopropylethylamine (DIPEA, 1.3 mL) with thiolactone carboxylic acid 1 (0.4 g, 1.9 mmol, 1.2 eq.). The reaction mixture was shaken for three hours. The reaction mixture was filtered off and the resin was washed sequentially with a mixture of chloroform, methanol, and DIPEA (17:2:1, 3 x 30 mL), DCM (3 x 30 mL), DMF (2 x 30 mL), DCM (2 x 30 mL), and diethyl ether (Et_2O) (3 x 3 mL). Subsequently, the resin was dried under vacuum for storage. 5 mg of sample was cleaved in TFA for UV-vis spectroscopy in acetonitrile. The loading was determined to be 0.705 mmol of thiolactone carboxylic acid per gram of resin, giving a loading efficiency of $0.728 \text{ mmol g}^{-1}$, 46%.

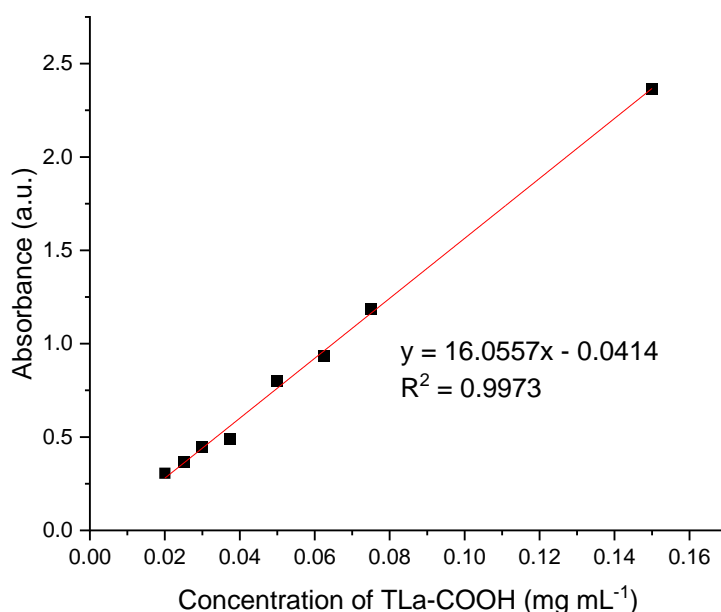


Figure 98: UV calibration curve of the thiolactone carboxylic acid linker TLa-COOH, used to determine the loading efficiency.

Step ii: General monomer addition

The resin was swollen in dry chloroform (1 mL per 100 mg of resin) for 10 minutes. The solvent was filtered off and fresh chloroform was added. Ethanolamine (15 eq.) and either monomer B or C (20 eq.) were added to the swollen resin. The mixture was shaken in a sealed reaction vessel for 30 min. The addition step was repeated, shaking for further 30 m, repeating either two times up to a 4-unit sequence and then repeating three times for further additions. The solid support was washed with DMF (x 4), methanol (x 4), chloroform (x 4) and diethyl ether (x 4).

Step iii: Chain extension with TLa-COOH

The resin was swollen in DMF (1 mL per 100 mg of resin) for 10 minutes. TLa-COOH (10 eq.) DMAP (0.5 eq.) and DIC (10 eq.) were added and the mixture was shaken in a sealed reaction vessel for 1 h. The addition step was repeated, shaking for further 1 hr, either two times up to a 4-unit sequence and then repeating three times for further additions. The solid support was washed with DMF (x 4), methanol (x 4), chloroform (x 4) and diethyl ether (x 4).

Step iv: Cleavage and Characterisation

The molecule was cleaved from the solid support by addition of a 1% TFA solution in DCM (approx. 0.1 mL per 1 mg uncleaved resin) and stirring for 5 minutes, followed by filtering of the resin and washing with DCM. The product was dried and resus was precipitated into cold diethyl ether, centrifuged, and the pellet resuspended in DCM. The product was dried under vacuum and obtained as a clear sticky resin.

Table 9: Expected and observed masses via MALDI-MS for each oligomer sequence $[M+Na]^+$

Sequence	$m/z_{(\text{theor})}$	$m/z_{(\text{exp})}$	$\Delta m/z$
1 (alternating)	3247.2556	3247.2483	0.0073
2 (triblock)	3247.2556	3247.2483	0.0073
3 (block)	3247.2556	3247.2483	0.0073

UV-Vis Spectroscopy: Spectra were recorded with a JASCO UV-Vis-NIR Photometer V-770 in acetonitrile using 1 cm glass cuvettes.

Post Functionalisation of Oligomer

Under a nitrogen atmosphere, oligomer (200.0 mg, 0.06 mmol, 1.0 eq.) was dissolved in dry DCM (30 mL). The solution was cooled in ice and DMAP (18.2 mg, 0.15 mmol, 0.6 eq.) and HEA (230.5 mg, 2.0 mmol, 8.0 eq.) were added and stirred for 30 min. To this, 1-ethyl-3-(3-dimethylaminopropyl)carbodiimide (462.3 mg, 3.0 mmol, 12.0 eq.) dissolved in dry DCM was added dropwise. The mixture was allowed to reach room temperature and stirred for 3 days under nitrogen. The product was washed with water (3 x 30 mL) and brine solution (30 mL). The organic fraction was dried over $MgSO_4$, filtered and evaporated under reduced pressure to give a clear resin-like solid (185 mg, 83 %).

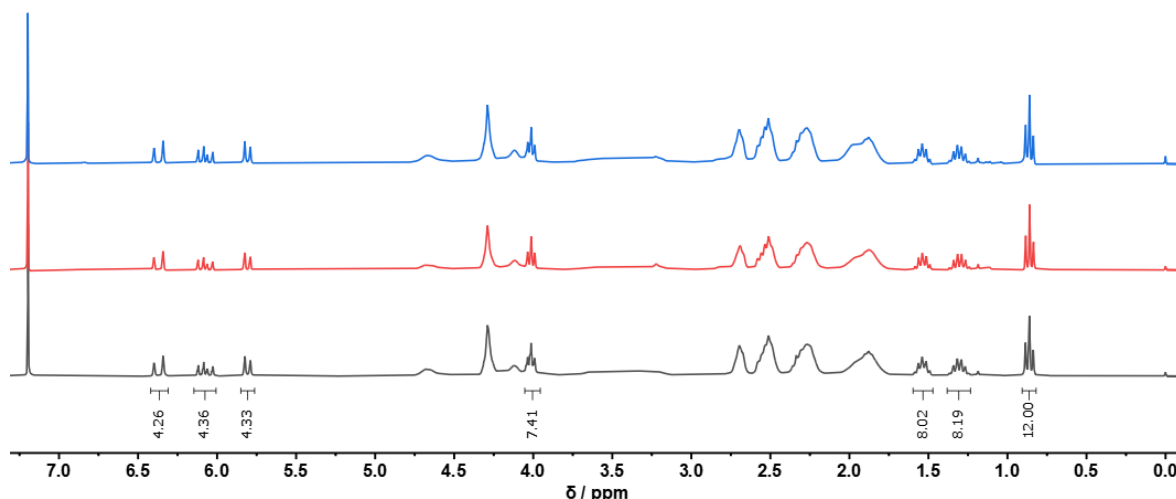


Figure 99: $^1\text{H-NMR}$ spectra (CDCl_3 , 600 MHz, 295 K) of alternating (blue), triblock (red) and block (grey) oligomers after post functionalisation with acrylate.

7.2.3 Molecular polymer bottlebrushes

Synthesis of linear backbone (RAFT): pHEMA-0 and pHEMA-1

CTBPA (40.4 mg, 0.1 mmol, 1.0 eq., pHEMA-0) or CPDB (22.1 mg, 0.1 mmol, 1.0 eq., pHEMA-1) was dissolved in DMF (3 mL), followed by addition of HEMA (1.3 g, 1.23 mL, 10.0 mmol, 100.0 eq.). To this, AIBN (1.6 mg, 0.01 mmol, 0.1 eq.) was added. The mixture was transferred to a Schlenk flask, sealed, and degassed with four and freeze-pump-thaw cycles and subsequently backfilled with N_2 . The reaction mixture was stirred at $90\text{ }^\circ\text{C}$ for 1.5 h. Subsequently, the flask was immersed in liquid nitrogen and exposed to atmosphere to quench the reaction. After dilution with DCM, the solution was precipitated into cold Et_2O . After centrifugation and decanting of the supernatant, the polymer was received as a pink solid.

Synthesis of linear backbone (ATRP): pHEMA-2

In a Schlenk flask, HEMA (4.0 g, 20.0 mmol, 100.0 eq.) was dissolved in isopropanol (11.3 mL). 1,1,4,7,10,10-Hexamethyltriethylenetetramine (HMTETA) (109 μL , 0.4 mmol, 2.0 eq.) and ethyl α -bromoisobutyrate (E-BiBB) (39.0 mg, 0.2 mmol, 1.0 eq.) were added. DMF was added as an internal standard. The tube was sealed and freeze-pump-thawed in 4 x 8 min cycles. During the last cycle, CuCl (19.8 mg, 0.1 mmol, 1.0 eq.) was added to the frozen reaction mixture under N_2 flow. The tube was resealed and evacuated. The mixture was thawed and allowed to react for 2 h under N_2 atmosphere. The reaction was

stopped by opening the flask to air. The mixture was filtered over Al_2O_3 to remove the catalyst, washing with acetone, then concentrated under reduced pressure and precipitated into cold Et_2O . The product was redissolved in 1,4-dioxane and lyophilised to give a white powder.

Functionalisation of linear backbone: pBIEM0-2

In a flask under N_2 , pHEMA (674.0 mg, 4.9 mmol, 1.0 eq. hydroxy groups) was dissolved in anhydrous pyridine (10 mL). The solution was cooled down to 0 °C and α -BiBB (3.4 g, 14.7 mmol, 3.0 eq.) was added dropwise. The reaction mixture was stirred for 18 h while warming to room temperature. The reaction mixture was then filtered through cotton, diluting with acetone. The remaining solution was concentrated under reduced pressure and precipitated twice into cold deionized water. After centrifugation, the precipitate was freeze-dried from 1,4-dioxane resulting in a pink (pBIEM0-1) or white (pBIEM-2) powder.

Side chain synthesis of bottlebrush: pHEMA-g-(pX-co-pHE(M)A)

An exemplary side chain reaction was performed according to the following: in a Schlenk flask, pBIEM (30.0 mg, 0.11 mmol of Br groups, 1.0 eq.) was dissolved in toluene (15 mL). HEMA-TMS (590 μL , 2.7 mmol, 25 eq.) and MMA (863 μL , 8.1 mmol, 75 eq.) were added, as well as PMDETA (24 μL , 0.1 mmol, 1.1 eq.). DMT (6.5 mg) was added as an internal standard. The tube was sealed and freeze-pump-thawed in 4 x 8 min cycles. During the last cycle, CuCl (10.7 mg, 0.1 mmol, 1.0 eq) was added to the frozen reaction mixture under N_2 flow. The tube was resealed and evacuated. The mixture was thawed and added to an oil bath at 80 °C under N_2 atmosphere. The reaction was stopped by opening the flask to air and cooling in liquid N_2 . The mixture was filtered over Al_2O_3 to remove the catalyst, washing with acetone, then concentrated under reduced pressure and precipitated into cold n-hexane. The product, a colourless pellet, was redissolved in DCM and kept in solution, drying partially for characterisation.

7.3 METHODS

Nuclear Magnetic Resonance Spectroscopy: Characterisation was performed with ^1H -NMR spectroscopy (Bruker Avance III 600 or Bruker Avance III 300, 128 scans, relaxation delay 0.1 s or 1 s, respectively, 295 K).

Mass Spectrometry: Measurements were performed with a Bruker AutoFlex Speed time-of-flight or Bruker timsTOF fleX for MALDI-MS, cyano-4-hydroxycinnamic acid matrix, positive mode.

Size Exclusion Chromatography (SEC): SEC measurements (THF) were performed on a Shimadzu Nexera LC-40 system (with LC-40D pump, autosampler SIL-40C, DGU-403 (degasser), CBM-40 (controlling unit), column oven CTO-40C, UV-detector SPD40, and RI-detector RID-20A). The system was equipped with 4 analytical SEC-columns (PSS): a SDV precolumn 3 μm , 2 \times SDV column 3 μm 1000 \AA , and SDV column 3 μm 10e4 \AA , with a flow rate of 1 mL min⁻¹ at a temperature of 40 °C. Chromatograms were analysed using the LabSolutions (Shimadzu) software. Calibration was performed against different PMMA standards (800 – 2 200 000 Da, PSS). For DMAc, analyses were performed using a UFLC Shimadzu Prominence SEC system equipped with PhenogelTM columns (5 μm , 10e4 \AA and 10e5 \AA) equipped with Shim-pack SEC-800DP guard column. DMAc contained butylhydroxytoluene (BHT, 0.05 % w/w) and LiBr (0.03 % w/w), set to a flow rate of 1 mL min⁻¹ at 50 °C. Apparent molecular weights were derived from a calibration curve generated by a series of monodisperse PMMA samples.

Ink preparation: Under yellow light conditions, a stock solution of DETC in 1,4-dioxane was added to dried monomer in a 2 mL Eppendorf tube to give a final composition of 0.5 wt% DETC, 66.6 wt% monomer in dioxane. The ink was centrifuged for 5 min at 150 rpm, then left shaking overnight to ensure homogeneity. The ink was used within one day of preparation.

Silanisation Procedure: Glass coverslips (Marienfeld, 170 \pm 5 μm) were washed with isopropanol and acetone and dried using pressurized N₂. Subsequently, the surface was activated for one minute by plasma treatment. The coverslips were immersed in a 4 \times 10⁻³ mol solution of 3-(trimethoxysilyl)propyl acrylate in toluene for 1.5 h. After washing twice in toluene and once in acetone then drying under N₂ flow, the acrylate-functionalised glass slides were stored under yellow light conditions.

Scanning Electron Microscopy: SEM was performed with Zeiss Ultra 55 (Carl Zeiss AG) at 3 kV in secondary electron mode. Prior to imaging, the structures were sputter-coated with a 12 nm layer of Pt/Pd (80:20).

Differential Scanning Calorimetry: DSC measurements were conducted with a Discovery DSC 250 of TA Instruments on polymer samples with 3-4 mg weight and a heating and cooling rate of 10 °C min⁻¹. Measurements were conducted on non-acrylated polymers prior to post functionalisation.

Two-Photon Laser Printing: 2PLP was performed employing a Photonic Professional GT2 (Nanoscribe GmbH) system. Microfabrication of all structures was performed in oil immersion mode with a femtosecond laser ($\lambda = 780$ nm) focused through a 63 \times oil objective lens (NA = 1.4; Zeiss). Employing Describe software (Nanoscribe) GWL files were generated from STL files of desired geometries and executed by the printer for 3D structure fabrication. Slicing was set to 300 nm and hatching to 200 nm for all microgeometries. Printing was performed with varied scan speeds (mm s⁻¹) and with laser powers up to 50 mW. To ensure stability of the samples, the ink was loaded into a PDMS mold and sealed with a coverslip during printing. Fabricated structures on glass substrates were developed by submerging in a compatible solvent, followed by drying in air. The maximum output of the instrument is 50 mW.

Fourier-Transform Infrared (FT-IR) Spectroscopy: Blocks (40 \times 40 \times 10 μm^3) were fabricated using 2PLP. Spectra were collected with an FT-IR Microscope (LUMOS-II, Bruker) in attenuated total reflectance (ATR) configuration, 64 scans, with liquid N₂ cooled detector. For all data points, n=3 samples were printed and measured for each scan speed and laser power parameter. The mean for the three spectra for each printed structure was calculated, and the average of the three structures was used for standard deviation calculations. Before averaging, each spectrum was baseline corrected and normalized against the peak of ν (C=O) (1723 cm⁻¹). The ratio of the area of ν (C=O) (1850-1655 cm⁻¹) and ν (C=C) (830-780 cm⁻¹) was determined and compared with the functionalised polymer before printing to determine the overall acrylate conversion as

per Equation 1. The functionalised polymer (ink) was measured on a JASCO FT/IR-4600 FT-IR spectrometer (128 scans).

Nanoindentation: Micropillars (z-height = 15 μm , \varnothing = 60 μm) were fabricated using 2PLP. For the measurement of the mechanical properties, nanoindentation measurements were performed with a Bruker Hysitron Triboindenter TI 980. For all measurements, a diamond Berkovich tip was used with automatic drift control. As test protocol a trapezoid loading function with a loading and unloading rate of 10 μN up to 200 μN and a plateau time of 2 s was applied. For all samples, n = 3 or n = 4 measurements were carried out on random positions and a mean value with standard deviation was calculated from the obtained results. The reduced elastic modulus and the hardness were calculated according to published work.^[108]

8 Appendices

8.1 APPENDIX A: SYNTHETIC CHARACTERISATION

8.1.1 Sequence-defined oligomers

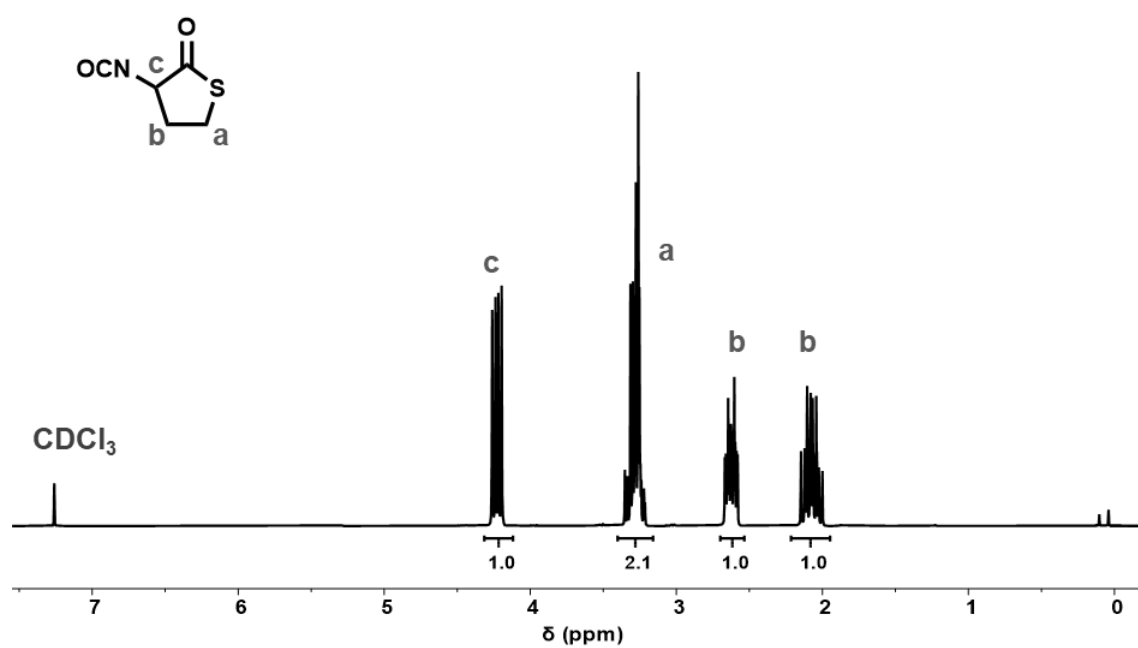


Figure A1: ^1H NMR spectrum (CDCl_3 , 300 MHz) of isocyanate-linker.

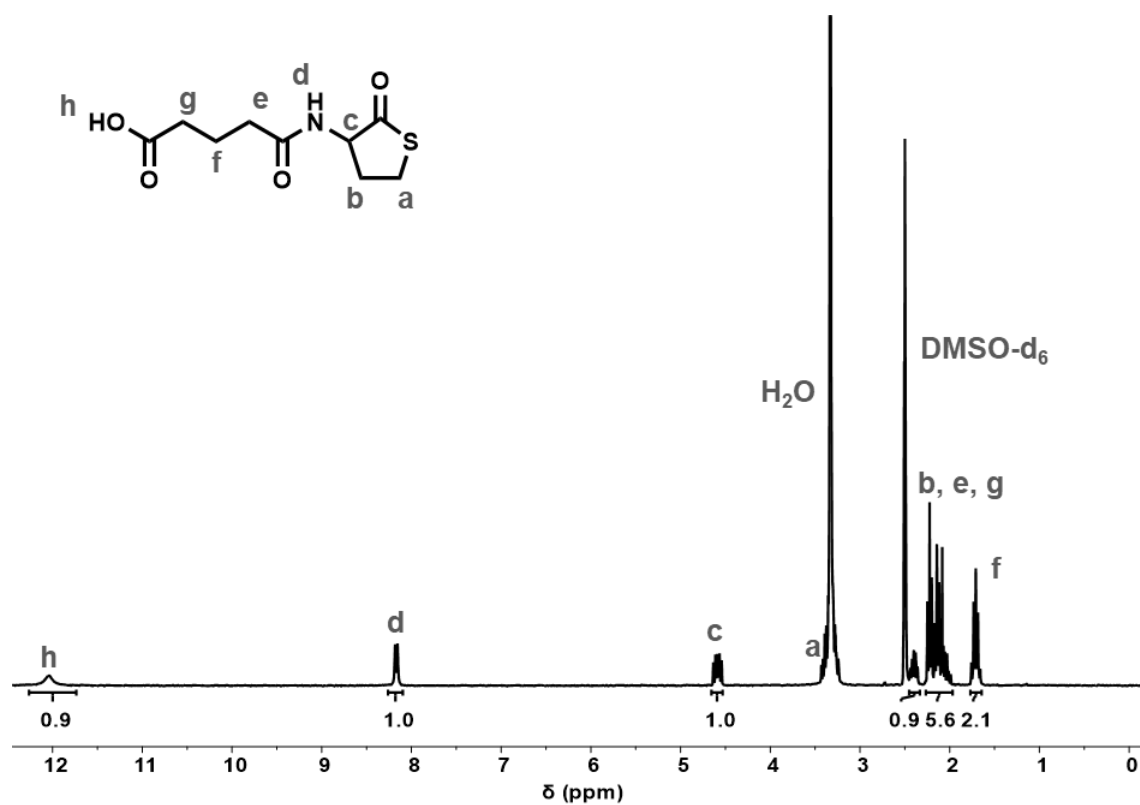


Figure A2: ¹H NMR spectrum (DMSO-d₆, 300 MHz) of COOH-linker. Protons a (-CH₂-CH₂-S-) obscured by H₂O.

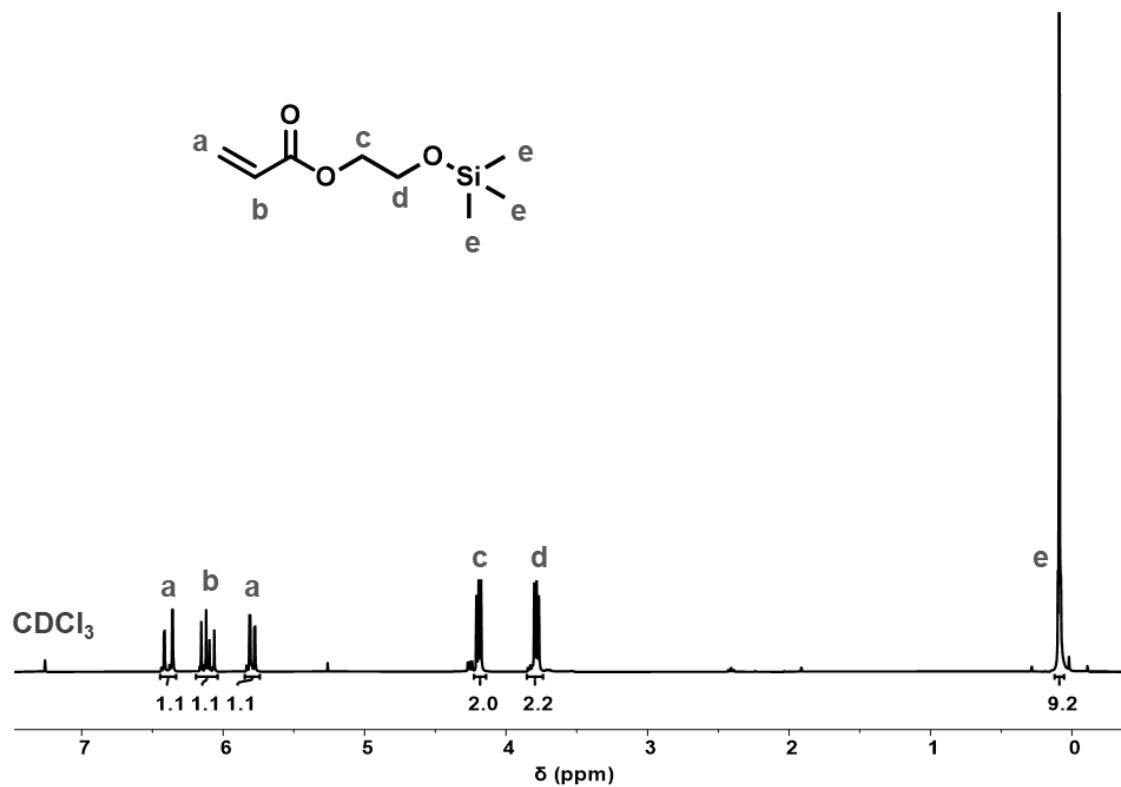


Figure A3: ¹H NMR spectrum (CDCl₃, 300 MHz) spectrum of HEA-TMS

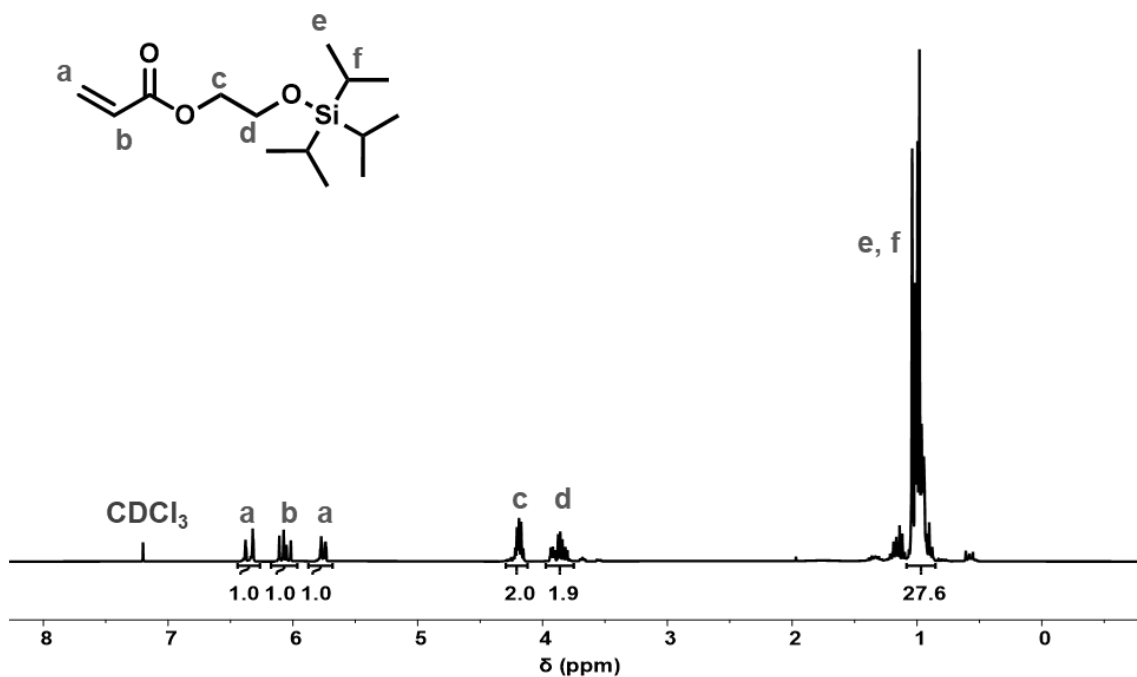


Figure A4: ^1H NMR spectrum (CDCl_3 , 300 MHz) of TIPS-HEA.

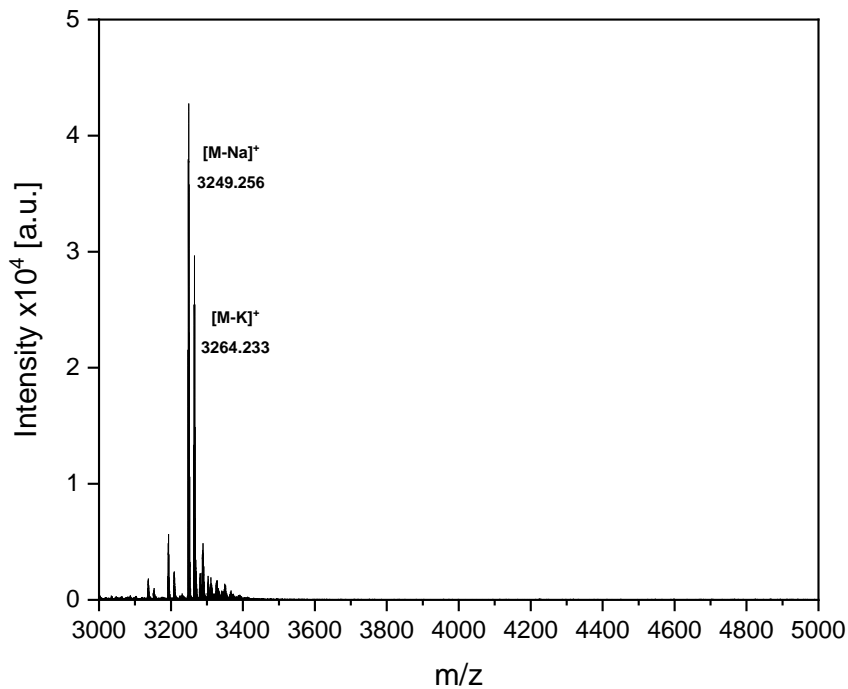


Figure A5: MALDI-MS spectrum (cyano-4-hydroxycinnamic acid matrix, positive mode) of triblock sequence prior to functionalisation.

8.1.2 Molecular polymer bottlebrushes

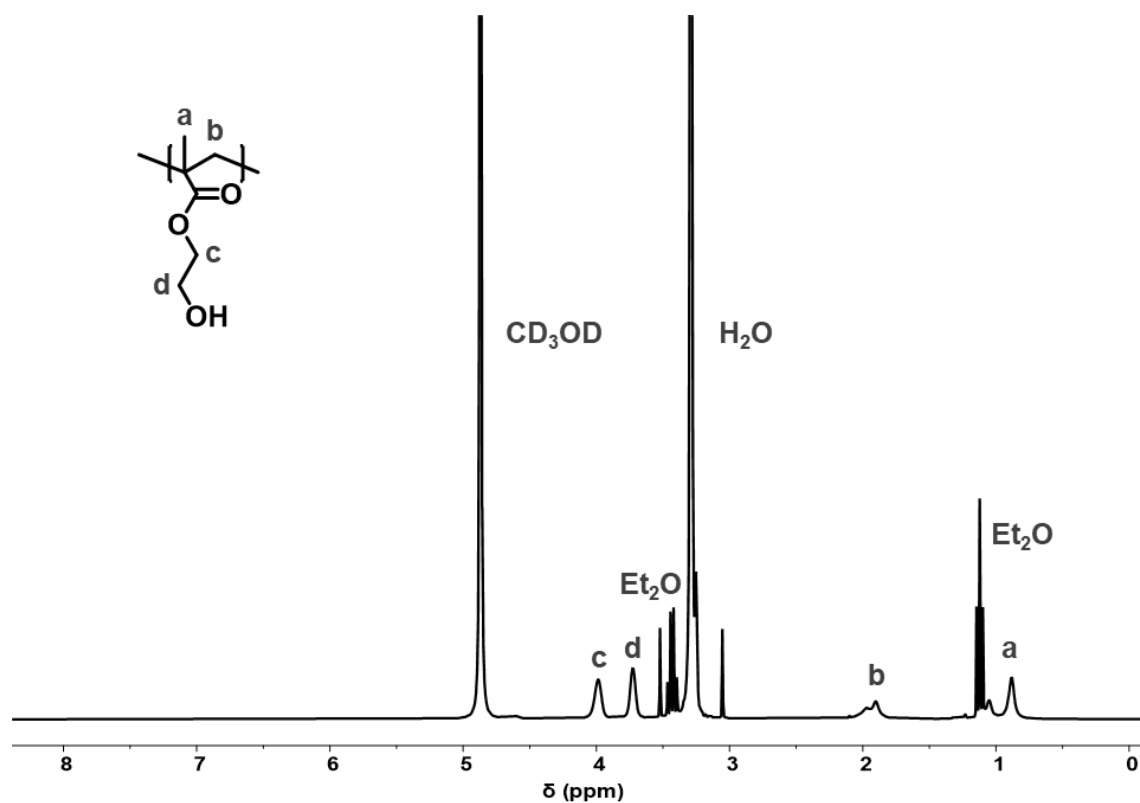


Figure A6: ^1H NMR spectrum (CD_3OD , 300 MHz) of backbone PHEMA-1.

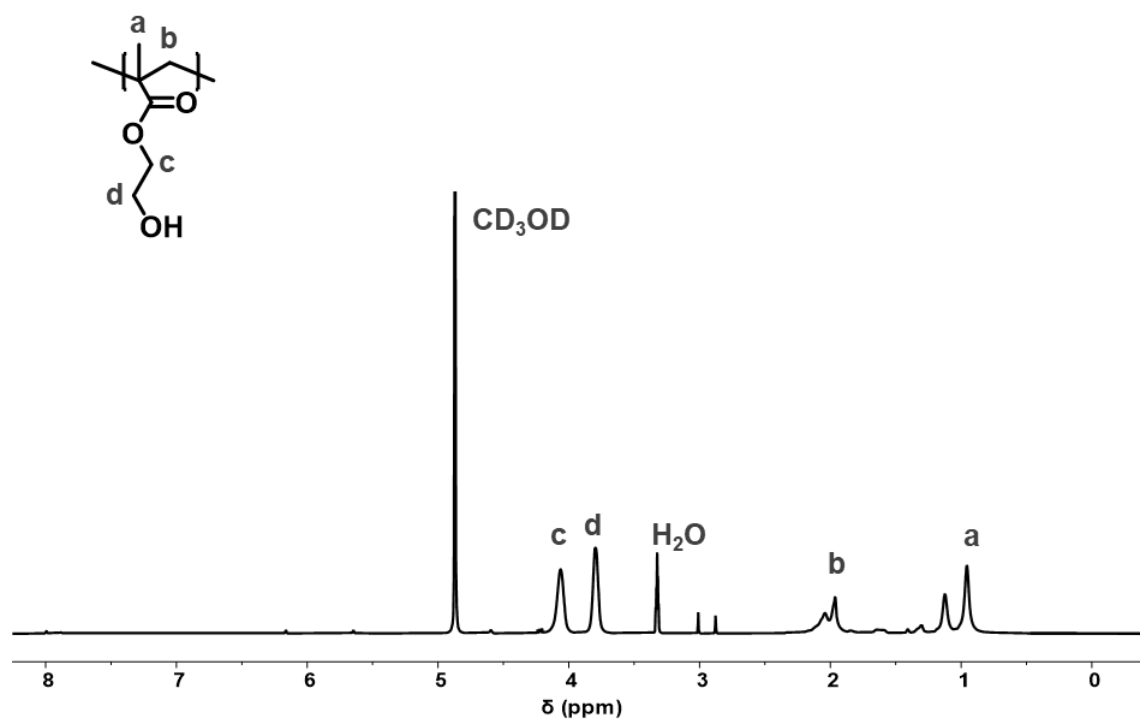


Figure A7: ^1H NMR spectrum (CD_3OD , 300 MHz) of backbone PHEMA-2.

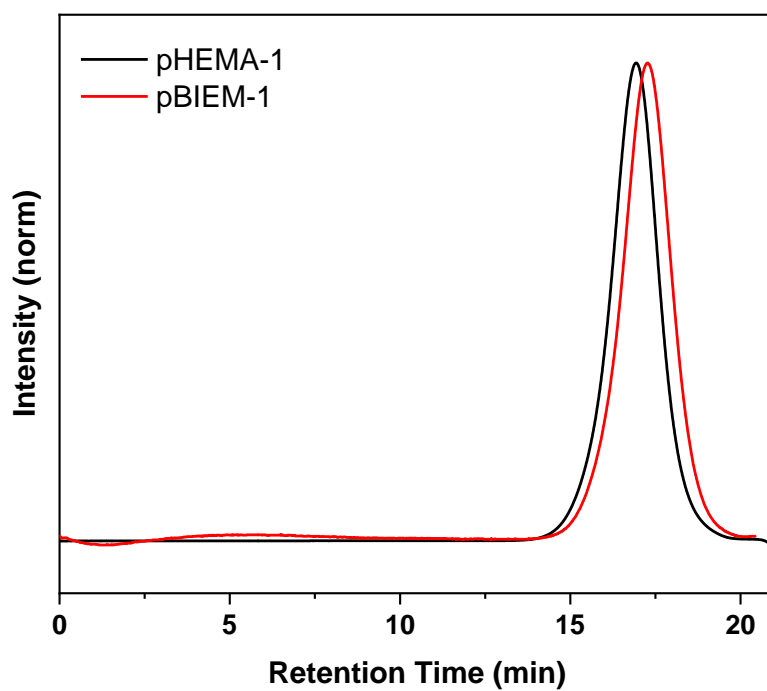


Figure A8: SEC trace (DMAc) of pHEMA-1 and pBIEM-1 showing monomodal dispersity.

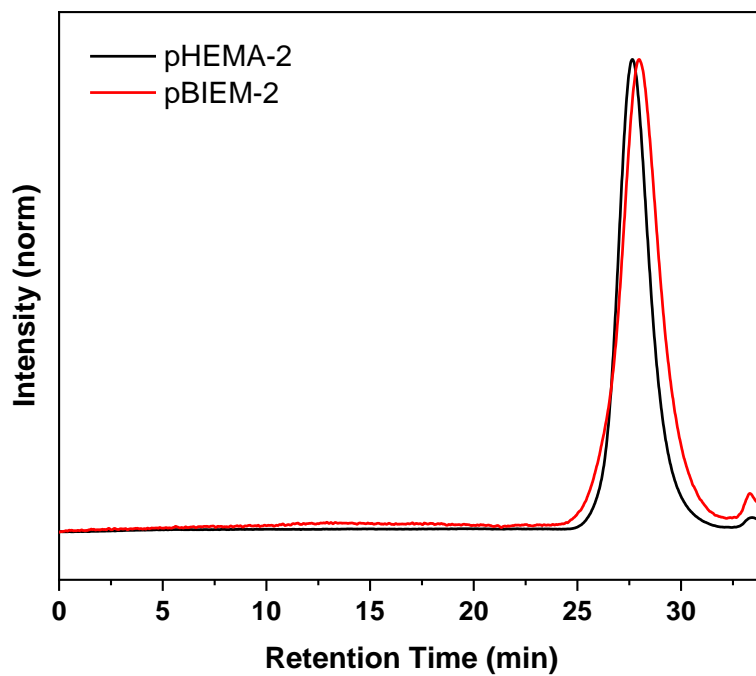


Figure A9: SEC trace (DMAc) of pHEMA-2 and pBIEM-2 showing monomodal dispersity.

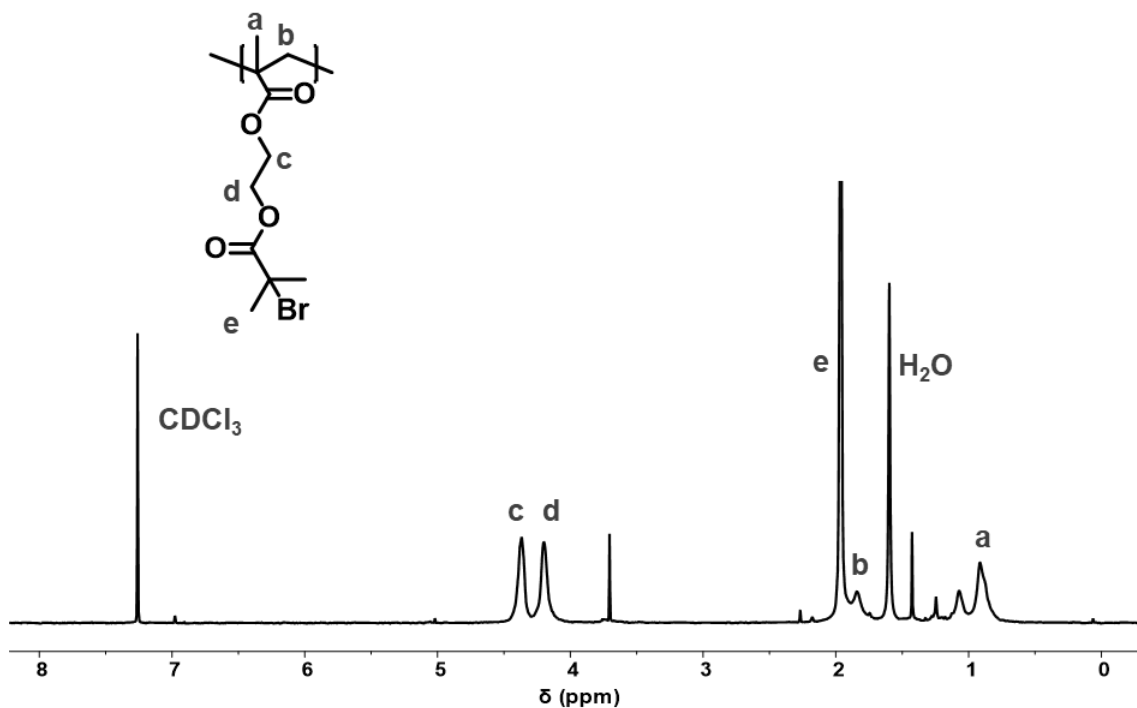


Figure A10: ¹H NMR spectrum (CDCl₃, 300 MHz) of backbone PBIEM-1.

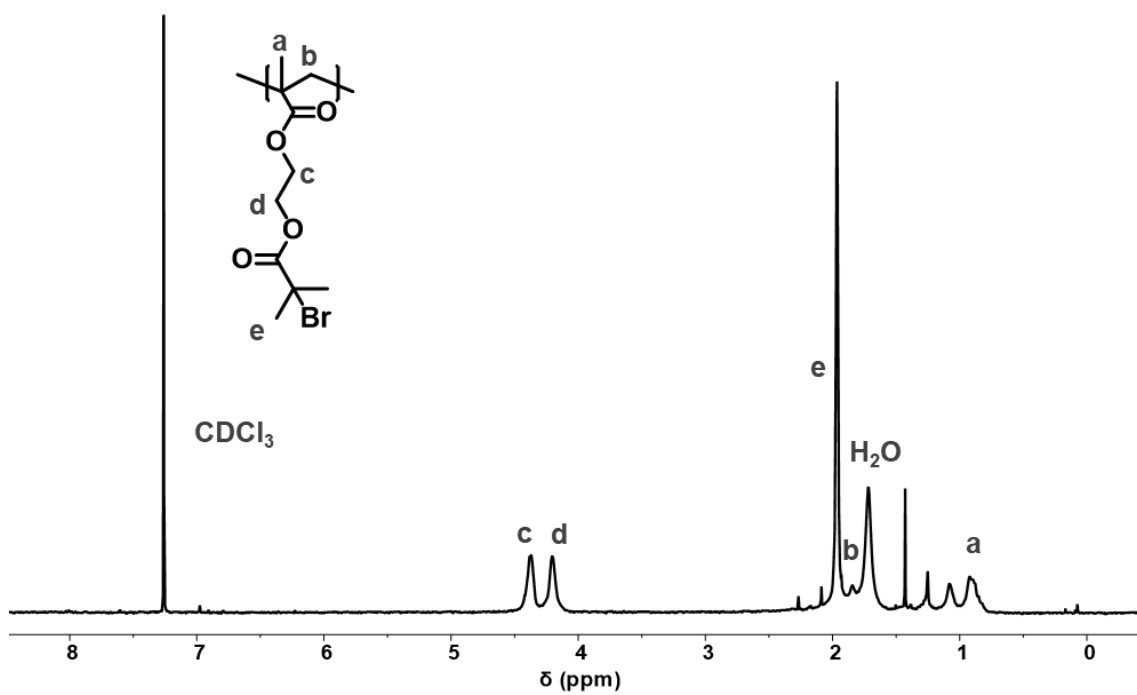


Figure A11: ¹H NMR spectrum (CDCl₃, 300 MHz) of backbone PBIEM-2.

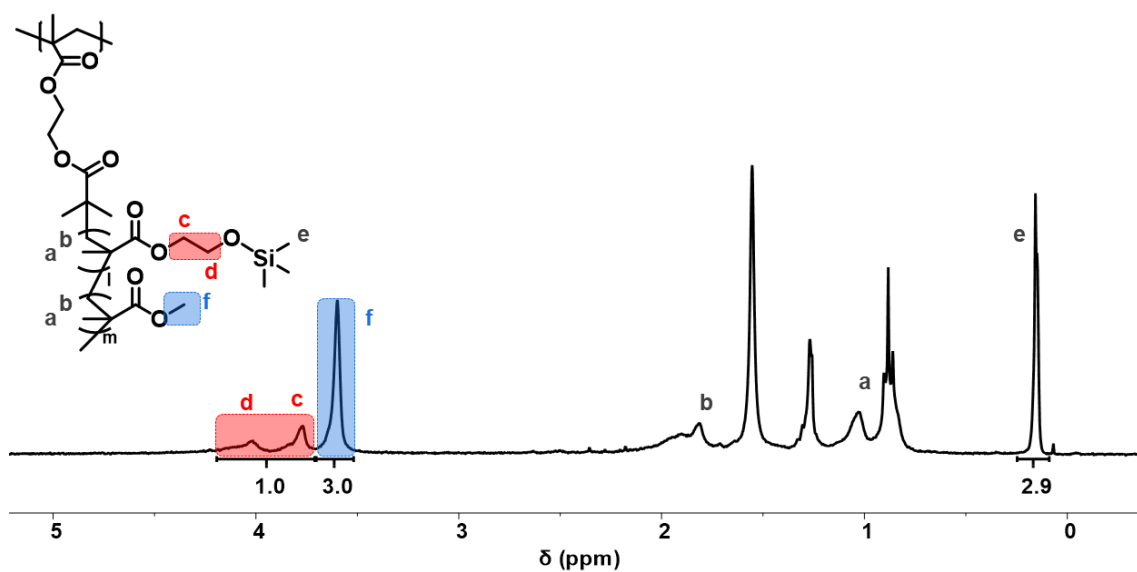


Figure A12: ^1H NMR spectra (CDCl_3 , 300 MHz) of **SC14** pHEMA-g-(HEMA-TMS-co-MMA) .

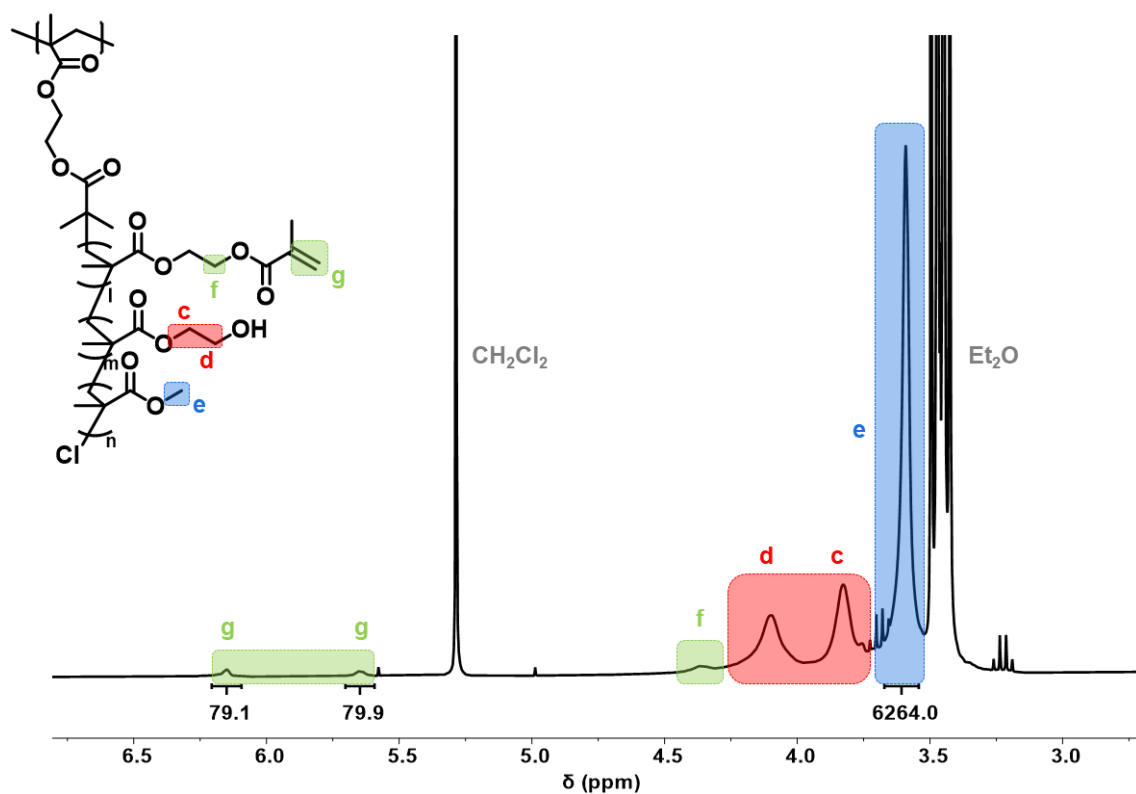


Figure A13: ^1H NMR spectrum (CDCl_3 , 300 MHz) of **PF1** pHEMA-g-(HEMA-co-MMA-co-methacrylate) bottlebrush.

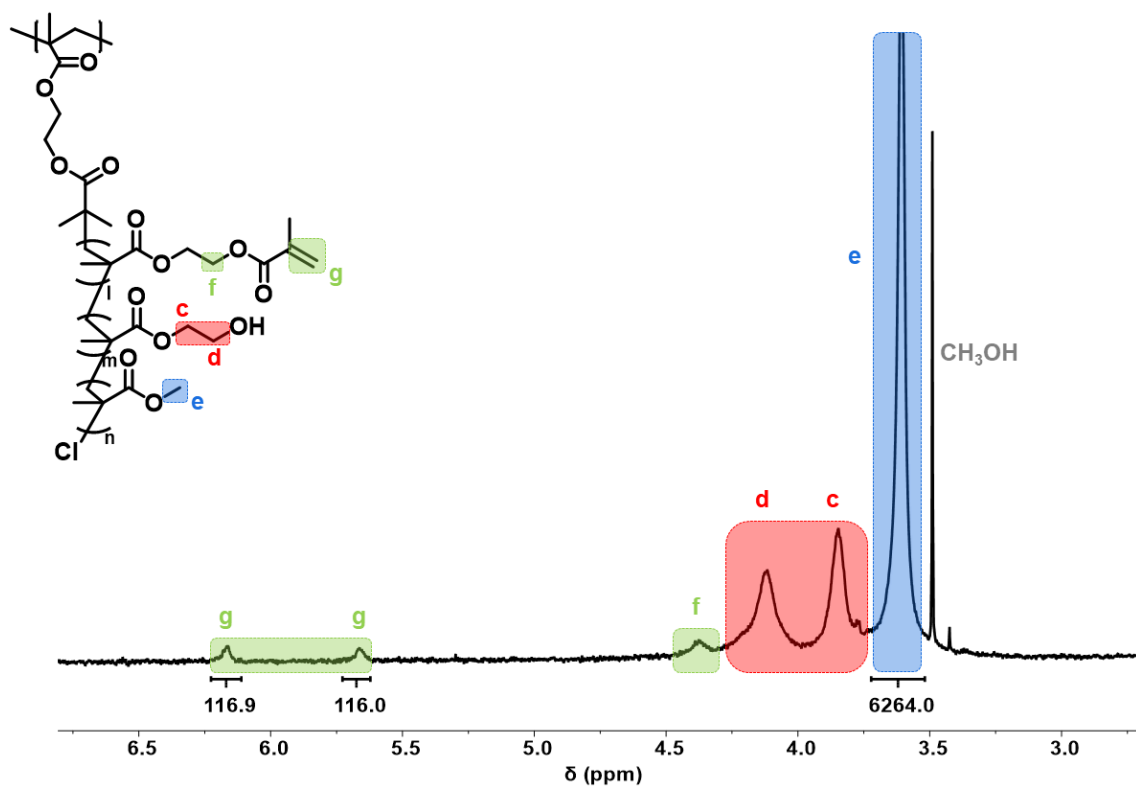


Figure A14: ^1H NMR spectrum (CDCl_3 , 300 MHz) of **PF2** pHEMA-g-(HEMA-co-MMA-co-methacrylate) bottlebrush.

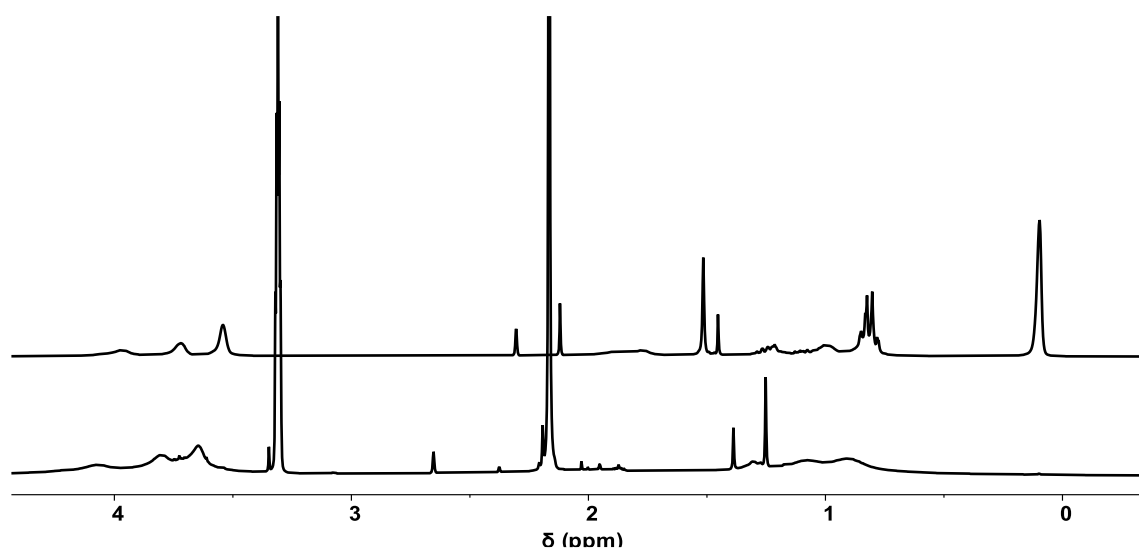


Figure A15: ^1H NMR spectrum of before (top, CDCl_3 , 300 MHz) and after (bottom, CD_3OD , 300 MHz) TMS deprotection showing the disappearance of the peak at 0.1 ppm.

8.2 APPENDIX B: MATERIAL CHARACTERISATION

8.2.1 Pre-polymer inks

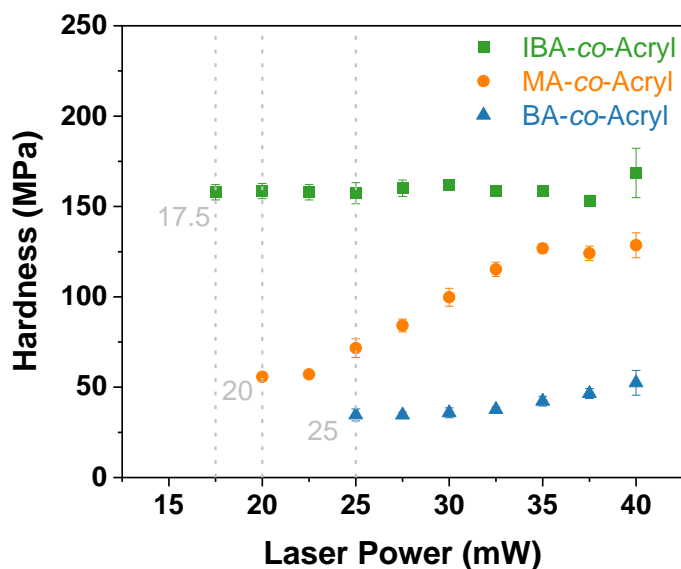


Figure B1: Hardness values for structures printed with IBA-co-Acryl, MA-co-Acryl and BA-co-Acryl inks over increasing laser powers, measured with nanoindentation.

8.2.2 Sequence-defined oligomers

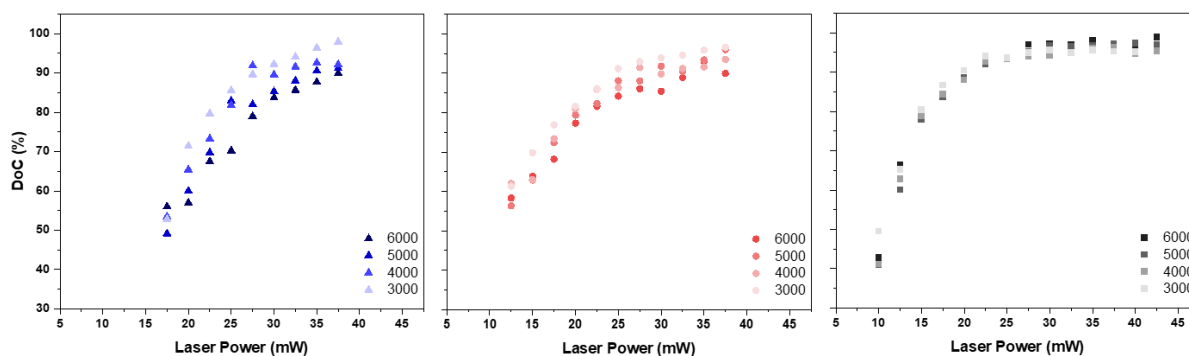


Figure B2: Calculated degree of acrylate conversion for varied scan speeds for the three oligomers: alternating (blue), triblock (red) and block (grey) from Raman spectroscopy. Structures were printed from 3000 – 6000 $\mu\text{m s}^{-1}$.

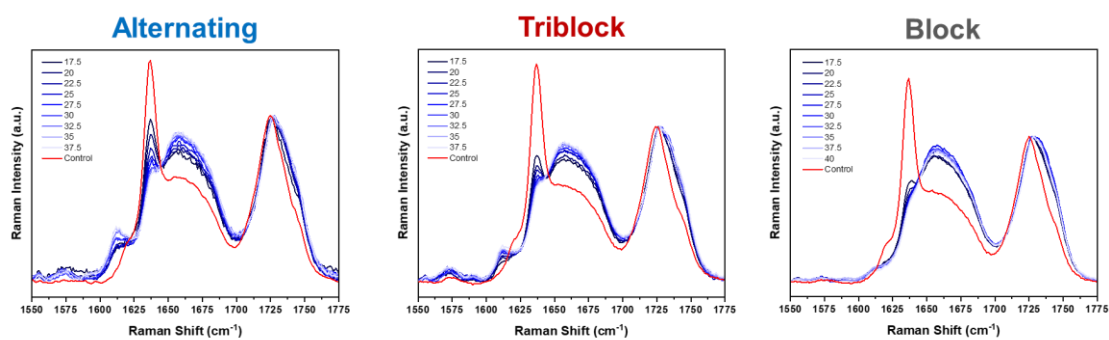


Figure B3: Raman spectra measured on structures printed with varied laser powers for the three oligomer inks, and the inks prior to printing (red), showing the decrease in the C=C double bond with increasing laser power.

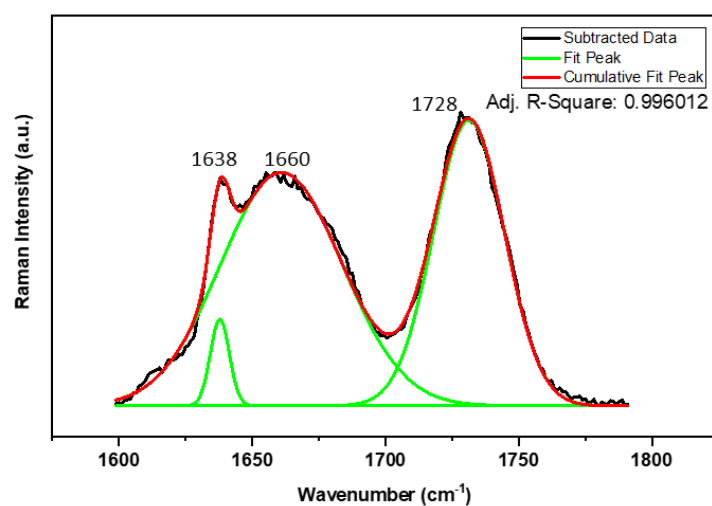


Figure B4: Exemplary Raman spectra of printed structures using sequence-defined ink showing the peak fitting of ester band O-C=O at 1728 cm^{-1} , amide band N-C=O at 1658 cm^{-1} and acrylate C=C stretching at 1638 cm^{-1} .

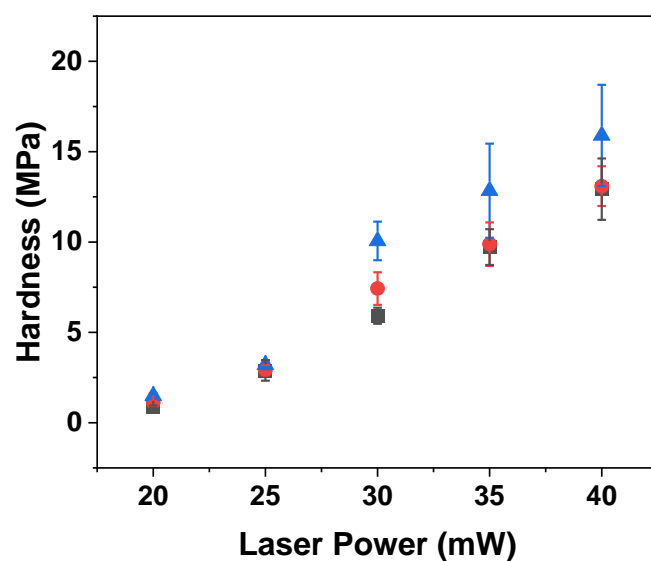


Figure B5: Hardness values for structures printed with alternating, triblock or block oligomer inks over increasing laser powers, printed with scan speed of 5 mm s^{-1} , measured with nanoindentation.

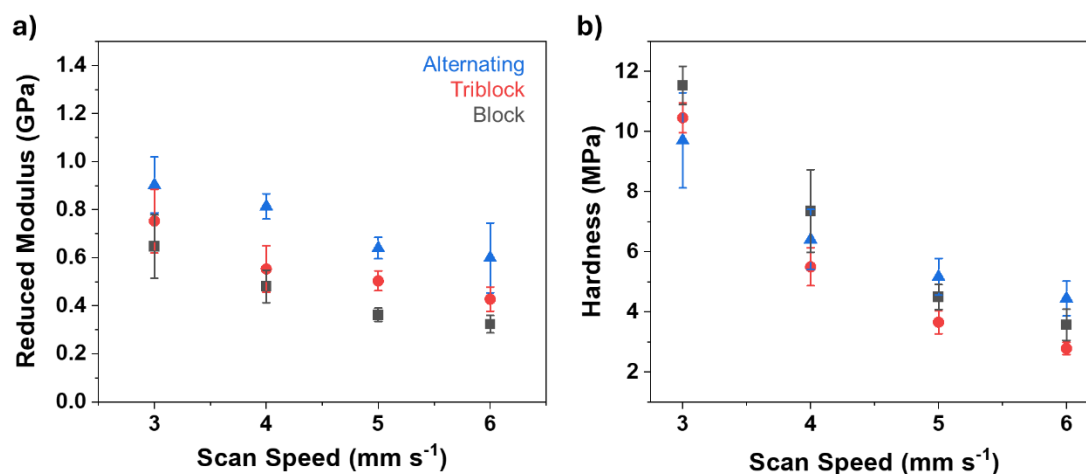


Figure B6: a) Reduced modulus and b) hardness values for structures printed with alternating, triblock or block oligomer inks over increasing scan speeds, printed with laser power 22.5 mW , measured with nanoindentation.

Bibliography

- [1] H. Staudinger, *Berichte Dtsch. Chem. Ges. B Ser.* **1920**, 53, 1073–1085.
- [2] H. Staudinger, *Berichte Dtsch. Chem. Ges. B Ser.* **1926**, 59, 3019–3043.
- [3] H. Staudinger, J. Fritsch, *Helv. Chim. Acta* **1922**, 5, 785–806.
- [4] P. C. Hiemenz, T. P. Lodge, *Polymer Chemistry*, CRC Press, Boca Raton, **2007**.
- [5] G. Odian, *Principles of Polymerization*, John Wiley & Sons, Hoboken (N.J.), **2004**.
- [6] M. Szwarc, *Nature* **1956**, 178, 1168–1169.
- [7] R. B. Grubbs, R. H. Grubbs, *Macromolecules* **2017**, 50, 6979–6997.
- [8] K. Matyjaszewski, T. P. Davis, Eds., *Handbook of Radical Polymerization*, Wiley, **2002**.
- [9] J.-S. Wang, K. Matyjaszewski, *J. Am. Chem. Soc.* **1995**, 117, 5614–5615.
- [10] N. Corrigan, K. Jung, G. Moad, C. J. Hawker, K. Matyjaszewski, C. Boyer, *Prog. Polym. Sci.* **2020**, 111, 101311.
- [11] D. Gigmes, Ed., *Nitroxide Mediated Polymerization: From Fundamentals to Applications in Materials Science*, Royal Society Of Chemistry, Cambridge, **2015**.
- [12] J. Nicolas, Y. Guillaneuf, C. Lefay, D. Bertin, D. Gigmes, B. Charleux, *Prog. Polym. Sci.* **2013**, 38, 63–235.
- [13] M. Kato, M. Kamigaito, M. Sawamoto, T. Higashimura, *Macromolecules* **1995**, 28, 1721–1723.
- [14] K. Matyjaszewski, *Macromolecules* **2012**, 45, 4015–4039.
- [15] J. Chiefari, Y. K. (Bill) Chong, F. Ercole, J. Krstina, J. Jeffery, T. P. T. Le, R. T. A. Mayadunne, G. F. Meijs, C. L. Moad, G. Moad, E. Rizzardo, S. H. Thang, *Macromolecules* **1998**, 31, 5559–5562.
- [16] D. Charmot, P. Corpart, D. Michelet, S. Z. Zard, T. Biadatti, *Method for Block Copolymer Synthesis by Controlled Radical Polymerization*, **1998**, WO9858974.
- [17] C. Barner-Kowollik, in *Handb. RAFT Polym.*, John Wiley & Sons, Ltd, **2008**, pp. 1–4.
- [18] G. Moad, E. Rizzardo, S. H. Thang, *Aust. J. Chem.* **2012**, 65, 985.
- [19] S. Perrier, *Macromolecules* **2017**, 50, 7433–7447.
- [20] N. P. Truong, G. R. Jones, K. G. E. Bradford, D. Konkolewicz, A. Anastasaki, *Nat. Rev. Chem.* **2021**, 5, 859–869.
- [21] J. de Neve, J. J. Haven, S. Harrisson, T. Junkers, *Angew. Chem. - Int. Ed.* **2019**, 58, 13869–13873.
- [22] J. Vandenberg, G. Reekmans, P. Adriaensens, T. Junkers, *Chem. Sci.* **2015**, 6, 5753–5761.
- [23] C. Fu, Z. Huang, C. J. Hawker, G. Moad, J. Xu, C. Boyer, *Polym. Chem.* **2017**, 8, 4637–4643.
- [24] J. F. Lutz, J. M. Lehn, E. W. Meijer, K. Matyjaszewski, *Nat Rev Mater* **2016**, 1, 1–14.
- [25] M. A. R. Meier, C. Barner-Kowollik, *Adv Mat* **2019**, 31, 1806027.
- [26] R. Aksakal, C. Mertens, M. Soete, N. Badi, F. Du Prez, *Adv Sci* **2021**, 8, 2004038.
- [27] S. C. Solleder, R. V. Schneider, K. S. Wetzels, A. C. Boukis, M. A. R. Meier, *Macromol. Rapid Commun.* **2017**, 38, 1–45.
- [28] Q. Shi, Z. Deng, M. Hou, X. Hu, S. Liu, *Prog. Polym. Sci.* **2023**, 141, 101677.

- [29] B. van Genabeek, B. A. G Lamers, C. J. Hawker, E. W. Meijer, W. R. Gutekunst, K J Schmidt, Bernhard V, Bernhard K J Schmidt, Correspondence V, *J Polym Sci* **2021**, 59, 373–403.
- [30] R. B. Merrifield, *Angew. Chem. Int. Ed. Engl.* **1985**, 24, 799–810.
- [31] A. J. DeStefano, R. A. Segalman, E. C. Davidson, *JACS Au* **2021**, 1, 1556–1571.
- [32] Z. Li, B. Cai, W. Yang, C. Chen, *Chem. Rev.* **2021**, 121, 14031–14087.
- [33] J. Babi, L. Zhu, A. Lin, A. Uva, H. El-Haddad, A. Pelowetse, H. Tran, *J. Polym. Sci.* **2021**, 59, 2378–2404.
- [34] H. Colquhoun, J.-F. Lutz, *Nat. Chem.* **2014**, 6, 455–456.
- [35] B. N. Norris, S. Zhang, C. M. Campbell, J. T. Auletta, P. Calvo-Marzal, G. R. Hutchison, T. Y. Meyer, *Macromolecules* **2013**, 46, 1384–1392.
- [36] R.-Z. Liu, L. Zhang, K.-K. Guo, J.-T. Xu, *Chin. J Polym Sci* **2022**, 40, 447–455.
- [37] J. J. Haven, J. de Neve, A. Castro Villavicencio, T. Junkers, *Polym. Chem.* **2019**, 10, 6540–6544.
- [38] E. A. Hoff, G. X. De Hoe, C. M. Mulvaney, M. A. Hillmyer, C. A. Alabi, *J. Am. Chem. Soc.* **2020**, 142, 6729–6736.
- [39] A. Rangamani, C. A. Alabi, *Polym Chem* **2021**, 12, 1526–1532.
- [40] Y. Tsukahara, K. Mizuno, A. Segawa, Y. Yamashita, *Macromolecules* **1989**, 22, 1546–1552.
- [41] S. S. Sheiko, B. S. Sumerlin, K. Matyjaszewski, *Prog. Polym. Sci.* **2008**, 33, 759–785.
- [42] T. Pan, M. D. Graham, Yash Kamble, B. B. Patel, M. A. Wade, S. A. Rogers, Y. Diao, C. Boucher-Jacobs, D. Guironnet, C. E. Sing, *Chem. Mater.* **2022**, DOI 10.1021/acs.chemmater.1c04030.
- [43] R. Verduzco, X. Li, S. L. Pesek, G. E. Stein, *Chem. Soc. Rev.* **2015**, 44, 2405–2420.
- [44] K. E. I. Kluthe, M. Wagner, M. Klapper, *Macromolecules* **2021**, 54, 1465–1477.
- [45] S. C. Radzinski, J. C. Foster, J. B. Matson, *Macromol. Rapid Commun.* **2016**, 37, 616–621.
- [46] R. Charvet, B. M. Novak, *Macromolecules* **2004**, 37, 8808–8811.
- [47] D. J. Walsh, D. Guironnet, *Proc. Natl. Acad. Sci.* **2019**, 116, 1538–1542.
- [48] C. Cheng, E. Khoshdel, K. L. Wooley, *Nano Lett.* **2006**, 6, 1741–1746.
- [49] D. J. Walsh, S. Dutta, C. E. Sing, D. Guironnet, *Macromolecules* **2019**, 52, 4847–4857.
- [50] M. Müllner, *Chem. Commun.* **2022**, 5683–5716.
- [51] K. L. Beers, S. G. Gaynor, K. Matyjaszewski, S. S. Sheiko, M. Möller, *Macromolecules* **1998**, 31, 9413–9415.
- [52] S. S. Sheiko, M. Da Silva, D. Shirvantiants, I. LaRue, S. Prokhorova, M. Moeller, K. Beers, K. Matyjaszewski, *J. Am. Chem. Soc.* **2003**, 125, 6725–6728.
- [53] W. F. M. Daniel, J. Burdyńska, M. Vatankhah-Varnoosfaderani, K. Matyjaszewski, J. Paturej, M. Rubinstein, A. V. Dobrynin, S. S. Sheiko, *Nat. Mater.* **2016**, 15, 183–189.
- [54] L. Cai, T. E. Kodger, R. E. Guerra, A. F. Pegoraro, M. Rubinstein, D. A. Weitz, *Adv. Mater.* **2015**, 27, 5132–5140.
- [55] E. Dashtimoghadam, F. Fahimipour, A. N. Keith, F. Vashahi, P. Popryadukhin, M. Vatankhah-Varnosfaderani, S. S. Sheiko, *Nat. Commun.* **2021**, 12, 3961.
- [56] M. B. Runge, S. Dutta, N. B. Bowden, *Macromolecules* **2006**, 39, 498–508.
- [57] M. B. Runge, C. E. Lipscomb, L. R. Ditzler, M. K. Mahanthappa, A. V. Tivanski, N. B. Bowden, *Macromolecules* **2008**, 41, 7687–7694.
- [58] M. B. Runge, N. B. Bowden, *J. Am. Chem. Soc.* **2007**, 129, 10551–10560.

- [59] B. Sun, Q. Ma, X. Wang, J. Liu, M. R. M. Rejab, *IOP Conf. Ser. Mater. Sci. Eng.* **2021**, 1078, 012007.
- [60] E. A. Guzzi, M. W. Tibbitt, *Adv. Mater.* **2020**, 32, 1901994.
- [61] W. E. Frazier, *J. Mater. Eng. Perform.* **2014**, 23, 1917–1928.
- [62] N. Tepylo, X. Huang, P. C. Patnaik, *Adv. Eng. Mater.* **2019**, 21, 1900617.
- [63] S. R. Dabbagh, M. R. Sarabi, M. T. Birtek, S. Seyfi, M. Sitti, S. Tasoglu, *Nat. Commun.* **2022**, 13, 5875.
- [64] S. C. Ligon, R. Liska, J. Stampfl, M. Gurr, R. Mülhaupt, *Chem Rev* **2017**, 117, 10212–10290.
- [65] F42 Committee, **n.d.**, DOI 10.1520/F2792-12A.
- [66] M. Ziaee, N. B. Crane, *Addit. Manuf.* **2019**, 28, 781–801.
- [67] A. Dass, A. Moridi, *Coatings* **2019**, 9, 418.
- [68] M. E. Hoque, Y. L. Chuan, I. Pashby, *Biopolymers* **2012**, 97, 83–93.
- [69] Z. Jiang, B. Diggle, M. L. Tan, J. Viktorova, C. W. Bennett, L. A. Connal, *Adv. Sci.* **2020**, 7, 2001379.
- [70] A. Elkaseer, K. J. Chen, J. C. Janhsen, O. Refle, V. Hagenmeyer, S. G. Scholz, *Addit. Manuf.* **2022**, 60, 103270.
- [71] R. Singh, A. Gupta, O. Tripathi, S. Srivastava, B. Singh, A. Awasthi, S. K. Rajput, P. Sonia, P. Singhal, K. K. Saxena, *Mater. Today Proc.* **2020**, 26, 3058–3070.
- [72] I. Gibson, D. W. Rosen, B. Stucker, in *Addit. Manuf. Technol.*, Springer US, Boston, MA, **2010**, pp. 223–252.
- [73] J. Zhang, P. Xiao, *Polym. Chem.* **2018**, 9, 1530–1540.
- [74] A. Bagheri, J. Jin, *ACS Appl. Polym. Mater.* **2019**, 1, 593–611.
- [75] M. Pagac, J. Hajnys, Q. P. Ma, L. Jancar, J. Jansa, P. Stefek, J. Mesicek, *Polymers* **2021**, 13, 1–20.
- [76] S. Maruo, O. Nakamura, S. Kawata, *Opt. Lett.* **1997**, 22, 132.
- [77] M. Göppert-Mayer, *Ann. Phys.* **2009**, 521, 466–479.
- [78] W. Kaiser, C. G. B. Garrett, *Phys. Rev. Lett.* **1961**, 7, 229–231.
- [79] T. Baldacchini, Ed. , *Three-Dimensional Microfabrication Using Two-Photon Polymerization: Fundamentals, Technology, and Applications*, Elsevier, **2016**.
- [80] P. Kiefer, V. Hahn, M. Nardi, L. Yang, E. Blasco, C. Barner-Kowollik, M. Wegener, *Adv Opt Mater* **2020**, 8, 2000895.
- [81] J. Fischer, M. Wegener, *Laser Photonics Rev.* **2013**, 7, 22–44.
- [82] P. Mainik, C. A. Spiegel, E. Blasco, *Adv. Mater.* **2024**, 36, 2310100.
- [83] M. Farsari, B. N. Chichkov, *Nat. Photonics* **2009**, 3, 450–452.
- [84] S. C. Gauci, A. Vranic, E. Blasco, S. Bräse, M. Wegener, C. Barner-Kowollik, *Adv. Mater.* **2023**, 2306468.
- [85] W. Zhou, S. M. Kuebler, K. L. Braun, T. Yu, J. K. Cammack, C. K. Ober, J. W. Perry, S. R. Marder, *Science* **2002**, 296, 1106–1109.
- [86] J. V. Crivello, *J. Polym. Sci. Part Polym. Chem.* **1999**, 37, 4241–4254.
- [87] N. Klikovits, P. Knaack, D. Bomze, I. Krossing, R. Liska, *Polym. Chem.* **2017**, 8, 4414–4421.
- [88] N. Zivic, P. K. Kuroishi, F. Dumur, D. Gigmes, A. P. Dove, H. Sardon, *Angew. Chem. Int. Ed.* **2019**, 58, 10410–10422.
- [89] L. H. Nguyen, M. Straub, M. Gu, *Adv. Funct. Mater.* **2005**, 15, 209–216.
- [90] N. S. Allen, M. C. Marin, M. Edge, D. W. Davies, J. Garrett, F. Jones, Suppiah. Navaratnam, B. J. Parsons, *J. Photochem. Photobiol. Chem.* **1999**, 126, 135–149.

- [91] J. Fischer, J. B. Mueller, A. S. Quick, J. Kaschke, C. Barner-Kowollik, M. Wegener, *Adv. Opt. Mater.* **2015**, *3*, 221–232.
- [92] A. Mauri, P. Kiefer, P. Neidinger, T. Messer, N. M. Bojanowski, L. Yang, S. Walden, A.-N. Unterreiner, C. Barner-Kowollik, M. Wegener, W. Wenzel, M. Kozłowska, *Chem. Sci.* **2024**, *15*, 12695–12709.
- [93] S. O. Catt, M. Hackner, J. P. Spatz, E. Blasco, *Small* **2023**, *19*, 2300844.
- [94] F. Pashley-Johnson, R. Munaweera, S. I. Hossain, S. C. Gauci, L. Delafresnaye, H. Frisch, M. L. O'Mara, F. E. Du Prez, C. Barner-Kowollik, *Nat. Commun.* **2024**, *15*, 6033.
- [95] B. M. Boyle, T. A. French, R. M. Pearson, B. G. McCarthy, G. M. Miyake, *ACS Nano* **2017**, *11*, 3052–3058.
- [96] B. B. Patel, D. J. Walsh, H. Kim, H. Kim, J. J. Kwok, B. Lee, D. Guironnet, Y. Diao, *Sci. Adv.* **2020**, *6*, DOI 10.1126/sciadv.aaz7202.
- [97] R. Xie, S. Mukherjee, A. E. Levi, V. G. Reynolds, H. Wang, M. L. Chabiny, C. M. Bates, *Sci. Adv.* **2020**, *6*, DOI 10.1126/sciadv.abc6900.
- [98] S. Nian, J. Zhu, Haozhe Zhang, H. Zhang, Z. Gong, G. Freychet, M. Zhernenkov, B. Xu, L. Cai, *Chem. Mater.* **2021**, *33*, 2436–2445.
- [99] V. Asadi, R. Dolleman, J. Van Der Gucht, T. E. Kodger, *Mater. Adv.* **2023**, *4*, 5535–5545.
- [100] C. Choi, Y. Okayama, Parker T. Morris, L. L. Robinson, M. Gerst, J. C. Speros, C. J. Hawker, J. R. de Alaniz, C. M. Bates, *Adv. Funct. Mater.* **2022**, 2200883.
- [101] *Electron Microscopy of Polymers*, Springer Berlin Heidelberg, Berlin, Heidelberg, **2008**.
- [102] C. LaFratta, T. Baldacchini, *Micromachines* **2017**, *8*, 101.
- [103] S. Schweiger, T. Schulze, S. Schlipf, P. Reinig, H. Schenk, *J. Opt. Microsyst.* **2022**, *2*, 033501.
- [104] K. Cicha, Z. Li, K. Stadlmann, A. Ovsianikov, R. Markut-Kohl, R. Liska, J. Stampfl, *J. Appl. Phys.* **2011**, *110*, DOI 10.1063/1.3639304.
- [105] T. Baldacchini, M. Zimmerley, C.-H. Kuo, E. O. Potma, R. Zadoyan, *J Phys Chem B* **2009**, *113*, 12663–12668.
- [106] F. Burmeister, S. Steenhusen, R. Houbertz, U. D. Zeitner, S. Nolte, A. Tünnermann, *J. Laser Appl.* **2012**, *24*, 042014.
- [107] A. V. Kazantseva, E. A. Chernykh, C. Crook, E. P. Garcia, D. A. Fishman, E. O. Potma, L. Valdevit, S. S. Kharintsev, T. Baldacchini, *J. Phys. Photonics* **2021**, *3*, 024001.
- [108] W. C. Oliver, G. M. Pharr, *J. Mater. Res.* **1992**, *7*, 1564–1583.
- [109] W. C. Oliver, G. M. Pharr, *J. Mater. Res.* **2004**, *19*, 3–20.
- [110] S. E. Arevalo, D. M. Ebenstein, L. A. Pruitt, *J. Mech. Behav. Biomed. Mater.* **2022**, *134*, 105384.
- [111] P. F. J. Van Altena, A. Accardo, *Polymers* **2023**, *15*, 1816.
- [112] K. Cicha, T. Koch, J. Torgersen, Z. Li, R. Liska, J. Stampfl, *J. Appl. Phys.* **2012**, *112*, 094906.
- [113] L. Pertoldi, V. Zega, C. Comi, R. Osellame, *J. Appl. Phys.* **2020**, *128*, 175102.
- [114] E. D. Lemma, F. Rizzi, T. Dattoma, B. Spagnolo, L. Sileo, A. Quattieri, M. de Vittorio, F. Pisanello, *IEEE Trans Nanotechnol* **2017**, *16*, 23–31.
- [115] I. S. Ladner, M. A. Cullinan, S. K. Saha, *RSC Adv.* **2019**, *9*, 28808–28813.
- [116] R. Srinivasaraghavan Govindarajan, S. Sikulskyi, Z. Ren, T. Stark, D. Kim, *Polymers* **2023**, *15*, 4377.

- [117] J. Lee, S. J. Park, S. C. Han, P. Prabhakaran, C. W. Ha, *Mater. Des.* **2023**, *235*, 112389.
- [118] L. Jiang, W. Xiong, Y. Zhou, Y. Liu, X. Huang, D. Li, T. Baldacchini, L. Jiang, Y. Lu, *Opt. Express* **2016**, *24*, 13687.
- [119] M. Diamantopoulou, N. Karathanasopoulos, D. Mohr, *Addit Manuf* **2021**, *47*, 102266.
- [120] Q. Hu, G. A. Rance, G. F. Trindade, D. Pervan, L. Jiang, A. Foerster, L. Turyanska, C. Tuck, D. J. Irvine, R. Hague, R. D. Wildman, *Addit Manuf* **2022**, *51*, 102575.
- [121] M. Belqat, X. Wu, L. P. C. Gomez, J.-P. Malval, S. Dominici, B. Leuschel, A. Spangenberg, K. Mougin, *Addit. Manuf.* **2021**, *47*, 102232.
- [122] R. Whitfield, K. Parkatzidis, N. P. Truong, T. Junkers, A. Anastasaki, *Chem* **2020**, *6*, 1340–1352.
- [123] “Thermal Transitions of Homopolymers: Glass Transition & Melting Point,” can be found under <https://www.sigmaaldrich.com/DE/en/technical-documents/technical-article/materials-science-and-engineering/polymer-synthesis/thermal-transitions-of-homopolymers>, **2024**.
- [124] S. Martens, J. van den Begin, A. Madder, F. E. Du Prez, P. Espeel, *J Am Chem Soc* **2016**, *138*, 14182–14185.
- [125] P. Espeel, F. E. Du Prez, *Eur Polym J* **2015**, *62*, 247–272.
- [126] J. O. Holloway, S. Aksakal, F. E. Du Prez, C. R. Becer, *Macromol Rapid Commun* **2017**, *38*, 1700500.
- [127] Melissa A Reith, Irene De Franceschi, M. Soete, N. Badi, R. Aksakal, F. Du Prez, *J. Am. Chem. Soc.* **2022**, DOI 10.1021/jacs.2c00145.
- [128] C. Mertens, R. Aksakal, N. Badi, F. E. Du Prez, *Polym. Chem.* **2021**, *12*, 4193–4204.
- [129] A. Torres-Knoop, I. Kryven, V. Schamboeck, P. D. Iedema, *Soft Matter* **2018**, *14*, 3404–3414.
- [130] N. Emami, K. Söderholm, *Open Dent J* **2009**, *3*, 202–207.
- [131] A. Torres-Knoop, V. Schamboeck, N. Govindarajan, P. D. Iedema, I. Kryven, *Commun. Mater.* **2021**, *2*, DOI 10.1038/s43246-021-00154-x.
- [132] K. L. Beers, S. Boo, S. G. Gaynor, K. Matyjaszewski, *Macromolecules* **1999**, *32*, 5772–5776.
- [133] P. Ramamurthi, Z. Zhao, E. Burke, N. F. Steinmetz, M. Müllner, *Adv. Healthc. Mater.* **2022**, *11*, 2200163.
- [134] A. Mühlebach, S. G. Gaynor, K. Matyjaszewski, *Macromolecules* **1998**, *31*, 6046–6052.
- [135] N. V. Tsarevsky, W. A. Braunecker, W. Tang, S. J. Brooks, K. Matyjaszewski, G. R. Weisman, E. H. Wong, *J. Mol. Catal. Chem.* **2006**, *257*, 132–140.
- [136] H. Arslan, Ç. Avcı, B. Tutkun, A. Şengül, *Polym. Bull.* **2017**, *74*, 931–948.
- [137] H. G. Börner, K. Beers, K. Matyjaszewski, S. S. Sheiko, M. Möller, *Macromolecules* **2001**, *34*, 4375–4383.
- [138] W. van Camp, F. E. Du Prez, S. A. F. Bon, *Macromolecules* **2004**, *37*, 6673–6675.



**Eidesstattliche Versicherung gemäß § 8 der Promotionsordnung für die
Naturwissenschaftlich-Mathematische Gesamtfakultät der Universität Heidelberg / Sworn
Affidavit according to § 8 of the doctoral degree regulations of the Combined Faculty of
Natural Sciences and Mathematics**

1. Bei der eingereichten Dissertation zu dem Thema / *The thesis I have submitted entitled*

handelt es sich um meine eigenständig erbrachte Leistung / *is my own work.*

2. Ich habe nur die angegebenen Quellen und Hilfsmittel benutzt und mich keiner unzulässigen Hilfe Dritter bedient. Insbesondere habe ich wörtlich oder sinngemäß aus anderen Werken übernommene Inhalte als solche kenntlich gemacht. / *I have only used the sources indicated and have not made unauthorised use of services of a third party. Where the work of others has been quoted or reproduced, the source is always given.*
3. Die Arbeit oder Teile davon habe ich wie folgt/bislang nicht¹⁾ an einer Hochschule des In- oder Auslands als Bestandteil einer Prüfungs- oder Qualifikationsleistung vorgelegt. / *I have not yet/have already¹⁾ presented this thesis or parts thereof to a university as part of an examination or degree.*

Titel der Arbeit / *Title of the thesis:*

Hochschule und Jahr / *University and year:*

Art der Prüfungs- oder Qualifikationsleistung / *Type of examination or degree:*

4. Die Richtigkeit der vorstehenden Erklärungen bestätige ich. / *I confirm that the declarations made above are correct.*
5. Die Bedeutung der eidesstattlichen Versicherung und die strafrechtlichen Folgen einer unrichtigen oder unvollständigen eidesstattlichen Versicherung sind mir bekannt. / *I am aware of the importance of a sworn affidavit and the criminal prosecution in case of a false or incomplete affidavit*

Ich versichere an Eides statt, dass ich nach bestem Wissen die reine Wahrheit erklärt und nichts verschwiegen habe. / *I affirm that the above is the absolute truth to the best of my knowledge and that I have not concealed anything.*

Ort und Datum / *Place and date*

.....
Unterschrift / *Signature*

¹⁾ Nicht Zutreffendes streichen. Bei Bejahung sind anzugeben: der Titel der andernorts vorgelegten Arbeit, die Hochschule, das Jahr der Vorlage und die Art der Prüfungs- oder Qualifikationsleistung. / *Please cross out what is not applicable. If applicable, please provide: the title of the thesis that was presented elsewhere, the name of the university, the year of presentation and the type of examination or degree.*

